

# Tracking an air target in multistatic radar networks

*Alexandre Moriya*

*Supervisor:*

*Prof. H.D Griffiths*

A thesis submitted for the degree of  
**Master of Philosophy**  
of  
**University College London**



Department of Electronic and Electrical Engineering  
University College London  
26<sup>th</sup> March 2012

I, Alexandre Moriya, confirm that the work presented in this thesis is my own and has not been submitted in any form for another degree or diploma at any university or other institute of tertiary education. Information derived from other sources has been indicated in the thesis.

Alexandre Moriya

London, March 26<sup>th</sup>, 2012.

# Abstract

The first radars used in military scenarios to detect enemies were bistatic because the technology that would allow a transmitter and a receiver to use the same antenna had not been developed. Then, with the development of monostatic radars, there was almost no interest in the bistatic radars subject. Nowadays, due to the fact that monostatic radars alone have reached its limits in terms of performance and because of the existence of new threats, the interest in bistatic and multistatic radars should last longer. Bistatic and multistatic radars are particularly interesting in military scenarios where it is important to be able to detect and track stealth targets and also to be able to operate with minimized risks of being affected by jamming attacks.

This thesis investigates how much multistatic radars can surpass stand alone monostatic radars when attempting to track a target. Simulations with different geometries and different target trajectories are performed in order to assess the tracking performance in each scenario. Tracking performance is assessed in terms of estimated position, velocity and acceleration accuracies. Different geometries include monostatic radar, netted monostatic radars, bistatic radars with target crossing and not crossing the baseline, multistatic radars with only 1 TX and many RXs, multistatic radars with many TXs and only 1 RX and multistatic radars with many TXs and RXs. Simulations are performed using real radar characteristics in order to assess whether it is possible to use navigation radars to track targets with low RCS.

The research herein presented shows that it is possible to achieve a good accuracy configuring a geometry that is suitable for the requirements of a system. Also, from the results of the simulations it is possible to understand why multistatic radars can still work with acceptable accuracy if a TXs is lost/destroyed.

To my wife and parents...

# Acknowledgements

I would like to thank my MPhil supervisor, Prof Hugh Griffiths, who has helped me throughout the whole period of my research and has given important and smart advice showing the best ways to achieve the objectives of this research and supporting me whenever it was necessary.

I would like to acknowledge, as well, all the members of the Radar Group who with I could attend interesting and important seminars and who also have contributed with interesting questions during my seminars. I would also like to mention Prof Chris Baker who has contributed with ideas in a very important moment of my research.

Likewise, I am grateful to have had the company of all my old and new friends that have made my staying in UK an unforgettable experience.

Additionally, I would like to thank the Brazilian Navy who has sponsored this research and an important and clever colleague, Commander Gelza de Moura Barbosa, who have always supported me and helped me with important technical information. From the Brazilian Navy, I am also grateful to Captain Fuad Gatti Kouri and Captain Jorge Antonio Vasconcellos dos Santos and their staff at the Office of the Brazilian Defence and Naval Attaché for all their support throughout my staying in London.

To my parents, Yoshinobu e Mitie, my special thanks for all the support they have been giving me since ever.

Finally, I would like to thank my wife, Etel, for all her love, support, advice and effort so that I could be able to concentrate on my studies and research. Without her, I would not be able to make it. I also thank our families for their unconditional support from Brazil during our period in UK.

# Contents

<b>Abstract</b> .....	<b>3</b>
<b>Acknowledgements</b> .....	<b>5</b>
<b>Contents</b> .....	<b>6</b>
<b>List of Figures</b> .....	<b>8</b>
<b>List of Tables</b> .....	<b>19</b>
<b>List of Symbols</b> .....	<b>20</b>
<b>List of Acronyms</b> .....	<b>23</b>
<b>1 Introduction</b> .....	<b>25</b>
1.1 Overview and Motivation.....	25
1.1.1 The Problem of Tracking in a Radar Network.....	29
1.2 Thesis Layout .....	34
<b>2 The Proposed Approach</b> .....	<b>36</b>
2.1 Scope and Limitations .....	37
<b>3 Bistatic / Multistatic Radar</b> .....	<b>39</b>
3.1 Advantages .....	39
3.2 Disadvantages.....	40
3.3 Bistatic Radar Properties .....	41
3.3.1 Bistatic Radar geometry.....	41
3.3.2 Bistatic Doppler .....	42
3.3.3 Bistatic Radar equation .....	44
3.3.4 Bistatic Radar Cross Section (RCS).....	46
3.4 Multistatic Radar .....	47
<b>4 Tracking algorithms</b> .....	<b>50</b>
4.1 Simple Example.....	50
4.2 Multistatic Tracking of a Target.....	52
<b>5 Review of Previous Work</b> .....	<b>54</b>
5.1 Multistatic Radar .....	54
5.2 Multistatic Tracking .....	58

5.3	Resource Management .....	63
<b>6</b>	<b>Simulations.....</b>	<b>65</b>
6.1	Setting up the Environment.....	65
6.2	Methodology.....	66
6.3	Algorithms.....	80
6.3.1	Simulated Measurements .....	80
6.3.2	Critically Damped g-h filter.....	82
6.3.3	Critically Damped g-h-k filter.....	82
6.3.4	Kalman Filter (KF).....	83
<b>7</b>	<b>Results .....</b>	<b>87</b>
7.1	Measurements Results .....	89
7.1.1	Monostatic.....	89
7.1.2	Bistatic.....	95
7.1.3	Multistatic (1 x N).....	101
7.1.4	Multistatic (M x 1) .....	103
7.1.5	Measurements Summary Table.....	106
7.2	Tracking Results.....	109
7.2.1	Target 1 (straight line).....	111
7.2.2	Target 2 (spiral-like trajectory) .....	127
7.2.3	Tracking Summary Tables .....	148
7.3	Analysis .....	151
7.4	Examples .....	155
<b>8</b>	<b>Conclusions and Further Work .....</b>	<b>160</b>
8.1	Summary.....	166
	<b>References .....</b>	<b>167</b>
	<b>Appendix A - Matlab Code.....</b>	<b>173</b>

# List of Figures

Figure 1 - Monostatic Radar .....	26
Figure 2 - Bistatic Radar .....	26
Figure 3 - Multistatic Radar .....	27
Figure 4 - Bistatic Radar being jammed .....	28
Figure 5 - Pairs of bistatic radar using different kind of transmitters .....	28
Figure 6 - Monostatic Radars working either as a monostatic or bistatic radar.....	29
Figure 7 - Centralized system .....	30
Figure 8 - Decentralized system.....	31
Figure 9 - Decentralized Data Fusion System using peer-to-peer communication links .....	32
Figure 10 - Decentralized Data Fusion System using a central network facility .....	33
Figure 11 - Hierarchical system .....	33
Figure 12 - Bistatic Radar Geometry .....	42
Figure 13 - Constant range ellipse (isorange contour) .....	42
Figure 14 - Bistatic Radar Geometry and the variables involved in the Bistatic Doppler (after [3]).....	43
Figure 15 - Radar Range Equation variables .....	46
Figure 16 – (after [18]) $\sigma_B$ and $\theta_B$ as functions of frequency (or wavelength $\lambda$ ).....	47
Figure 17 - Tracking recursive algorithm .....	51
Figure 18 - Horizontal (red) and Vertical (blue) target trajectories with different velocities and the radar located at (100,0) km. ....	67
Figure 19 – Measurement number vs $x$ -axis errors (using 150 m and 30 mrad standard deviations) .....	67
Figure 20 – Measurement number vs $y$ -axis errors (using 150 m and 30 mrad standard deviations) .....	67
Figure 21 - Measurement number vs $x$ -axis errors (using 15 m and 30 mrad standard deviations).....	68
Figure 22 - Measurement number vs $y$ -axis errors (using 15 m and 30 mrad standard deviations).....	68
Figure 23 - Measurement number vs $x$ -axis errors (using 150 m and 3 mrad standard deviations).....	68
Figure 24 - Measurement number vs $y$ -axis errors (using 150 m and 3 mrad standard deviations).....	68
Figure 25 – location of TX (black circle) and RX (black hexagram), true trajectory (red line) and measurements (green line).....	69
Figure 26 - Measurement number vs $x$ -axis errors (using 150 m and 3 mrad standard deviations).....	69
Figure 27 - Measurement number vs $y$ -axis errors (using 150 m and 3 mrad standard deviations).....	69
Figure 28 – Geometry with monostatic radar location (black circle) and target trajectory .....	71
Figure 29 - Measurement number vs $x$ -axis errors (range and azimuth standard deviations vary with distance to the radar) .....	71
Figure 30 - Measurement number vs $y$ -axis errors (range and azimuth standard deviations vary with distance to the radar) .....	71

Figure 31 – Geometry with radars location and target trajectory where black circle is TX and black hexagram is RX.....	71
Figure 32 - Measurement number vs $x$ -axis errors (range and azimuth standard deviations vary with distance to the radar) .....	72
Figure 33 - Measurement number vs $y$ -axis errors (range and azimuth standard deviations vary with distance to the radar) .....	72
Figure 34 – Geometry with radars location and target trajectory where black circle is TX and black hexagram is RX.....	73
Figure 35 – Bistatic angle along the target trajectory .....	73
Figure 36 – $x$ -position of the target vs $x$ -axis errors.....	73
Figure 37 – $x$ -position of the target vs $y$ -axis errors.....	73
Figure 38 - $x$ -position of the target vs $x$ -axis errors after tracking filter .....	74
Figure 39 - $x$ -position of the target vs $y$ -axis errors after tracking filter .....	74
Figure 40 – $x$ -position of the target vs $x$ -axis (red) and $y$ -axis (blue) estimated velocity.....	74
Figure 41 - Geometry with radars location and target trajectory (red) where green and cyan circles are monostatic radars. Green and cyan dots represent measurements from each radar respectively .....	75
Figure 42 – Individual tracks (green and cyan dots) and fused track (black line).....	75
Figure 43 – Fused measurements (yellow) and track (black line) .....	75
Figure 44 - Geometry with radar location, target trajectory (red) and measurements (green). The black circle is the monostatic radar .....	76
Figure 45 - Geometry with radars location where green, blue, red and magenta circles are monostatic radars and the same colours of lines represent their respective measurements.....	76
Figure 46 – Track when only one radar (1.5 MW) is used .....	76
Figure 47 – Fusion of tracks from each radar (4 radars of 375 kW).....	76
Figure 48 - Track when only one radar (1.5 MW) is used.....	77
Figure 49 - Fusion of tracks from each radar (4 radars of 375 kW) .....	77
Figure 50 - Geometry with radars location, target trajectory (red sinusoidal) and measurements (green/blue) from each monostatic radar (green and blue circles).....	78
Figure 51 – Tracking (black line) using a $g-h-k$ filter after doing fusion of measurements (yellow) .....	78
Figure 52 - Tracking (black line) after doing fusion of measurements (yellow) using a $g-h$ filter.....	78
Figure 53 – Estimated $y$ -velocity (blue line) using a $g-h$ filter. Black line is the true velocity. Estimated $x$ -velocity is illustrated by the red line (constant 200 m/s) .....	79
Figure 54 – Estimated $y$ -velocity (blue line) using a $g-h-k$ filter. Black line is the true velocity. Estimated $x$ -velocity is illustrated by the red line (constant 200 m/s) .....	79
Figure 55 – Estimated velocity (blue line) using a $g-h-k$ filter. Black line is the true velocity.....	79
Figure 56 – test for Equation (36), when Power is 25 kw, RCS 0.1 m <sup>2</sup> .....	85
Figure 57 – test for Equation (37), when Power is 25 kw, RCS 0.1 m <sup>2</sup> .....	85
Figure 58 – Location of TX/RX (monostatic radar with 25 kW), true trajectory (red line) and measurements (green dots).....	90
Figure 59 - $x$ -position vs $x$ -axis errors (1 radar 25 kW).....	90
Figure 60 - $x$ -position vs $y$ -axis errors (1 radar 25 kW).....	90
Figure 61 – $x$ -position vs SNR (blue line) – 1 radar 25 kW .....	90
Figure 62 – $x$ -position vs [range stddev(blue) and azimuth stddev (green)] – 1 radar 25 kW .....	90

Figure 63 - $x$ -position vs $x$ -axis errors (1 radar 6.25 kW).....	91
Figure 64 - $x$ -position vs $y$ -axis errors (1 radar 6.25 kW).....	91
Figure 65 - $x$ -position vs SNR (blue line) – 1 radar 6.25 kW .....	91
Figure 66 - $x$ -position vs [range stddev(blue) and azimuth stddev (green)] – 1 radar 6.25 kW .....	91
Figure 67 - Location of TX/RX (monostatic radar with 25 kW), true trajectory (red line) and measurements (green dots).....	91
Figure 68 - $x$ -position vs $x$ -axis errors (1 radar 25 kW).....	92
Figure 69 - $x$ -position vs $y$ -axis errors (1 radar 25 kW).....	92
Figure 70 - $x$ -position vs SNR (blue line) – 1 radar 25 kW .....	92
Figure 71 - $x$ -position vs [range stddev(blue) and azimuth stddev (green)] – 1 radar 25 kW .....	92
Figure 72 - Location of TX/RX (monostatic radar with 6.25 kW), true trajectory (red line) and measurements (green dots).....	93
Figure 73 - $x$ -position vs $x$ -axis errors (1 radar 6.25 kW).....	93
Figure 74 - $x$ -position vs $y$ -axis errors (1 radar 6.25 kW).....	93
Figure 75 - $x$ -position vs SNR (blue line) – 1 radar 6.25 kW .....	93
Figure 76 - $x$ -position vs [range stddev(blue) and azimuth stddev (green)] – 1 radar 6.25 kW .....	93
Figure 77 - Location of TX/RX (monostatic radar with 25 kW), true trajectory (red line) and measurements (green dots).....	94
Figure 78 - $x$ -position vs $x$ -axis errors (1 radar 25 kW).....	94
Figure 79 - $x$ -position vs $y$ -axis errors (1 radar 25 kW).....	94
Figure 80 - $x$ -position vs SNR (blue line) – 1 radar 25 kW .....	94
Figure 81 - $x$ -position vs [range stddev(blue) and azimuth stddev (green)] – 1 radar 25 kW .....	94
Figure 82 - Location of TX/RX (monostatic radar with 25 kW), true trajectory (red line) and measurements (green dots).....	95
Figure 83 - $x$ -position vs $x$ -axis errors (1 radar 25 kW).....	95
Figure 84 - $x$ -position vs $y$ -axis errors (1 radar 25 kW).....	95
Figure 85 - $x$ -position vs SNR (blue line) – 1 radar 25 kW .....	95
Figure 86 - $x$ -position vs [range stddev(blue) and azimuth stddev (green)] – 1 radar 25 kW .....	95
Figure 87 - Location of TX and RX (bistatic radar with TX 25 kW), true trajectory (red line) and measurements (green dots) .....	96
Figure 88 - $x$ -position vs $x$ -axis errors (1 TX 25 kW).....	96
Figure 89 - $x$ -position vs $y$ -axis errors (1 TX 25 kW).....	96
Figure 90 - $x$ -position vs [SNR (blue line) and bistatic angle (green line) – 1 TX 25 kW .....	96
Figure 91 - $x$ -position vs [range stddev(blue) and azimuth stddev (green)] – 1 TX 25 kW .....	96
Figure 92 - Location of TX and RX (bistatic radar with TX 25 kW), true trajectory (red line) and measurements (green dots) .....	97
Figure 93 - $x$ -position vs $x$ -axis errors (1 TX 25 kW).....	97
Figure 94 - $x$ -position vs $y$ -axis errors (1 TX 25 kW).....	97
Figure 95 - $x$ -position vs [SNR (blue line) and bistatic angle (green line) – 1 TX 25 kW .....	97
Figure 96 - $x$ -position vs [range stddev(blue) and azimuth stddev (green)] – 1 TX 25 kW .....	97

Figure 97 - Location of TX and RX (bistatic radar with TX 6.25 kW), true trajectory (red line) and measurements (green dots) .....	98
Figure 98 - $x$ -position vs $x$ -axis errors (1 TX 6.25 kW).....	98
Figure 99 - $x$ -position vs $y$ -axis errors (1 TX 6.25 kW).....	98
Figure 100 – $x$ -position vs [SNR (blue line) and bistatic angle (green line) – 1 TX 6.25 kW .....	98
Figure 101 – $x$ -position vs [range stddev(blue) and azimuth stddev (green)] – 1 TX 6.25 kW .....	98
Figure 102 - Location of TX and RX (bistatic radar with TX 6.25 kW), true trajectory (red line) and measurements (green dots).....	99
Figure 103 - $x$ -position vs $x$ -axis errors (1 TX 6.25 kW).....	99
Figure 104 - $x$ -position vs $y$ -axis errors (1 TX 6.25 kW).....	99
Figure 105 – $x$ -position vs [SNR (blue line) and bistatic angle (green line) – 1 TX 6.25 kW .....	99
Figure 106 – $x$ -position vs [range stddev(blue) and azimuth stddev (green)] – 1 TX 6.25 kW .....	99
Figure 107 - Location of TX and RX (bistatic radar with TX 25 kW), true trajectory (red line) and measurements (green dots) .....	100
Figure 108 - $x$ -position vs $x$ -axis errors (1 TX 25 kW).....	100
Figure 109 - $x$ -position vs $y$ -axis errors (1 TX 25 kW).....	100
Figure 110 – $x$ -position vs [SNR (blue line) and bistatic angle (green line) – 1 TX 25 kW .....	100
Figure 111 – $x$ -position vs [range stddev(blue) and azimuth stddev (green)] – 1 TX 25 kW .....	100
Figure 112 - Location of TX and RX (bistatic radar with TX 25 kW), true trajectory (red line) and measurements (green dots) .....	101
Figure 113 - $x$ -position vs $x$ -axis errors (1 TX 25 kW).....	101
Figure 114 - $x$ -position vs $y$ -axis errors (1 TX 25 kW).....	101
Figure 115 – $x$ -position vs [SNR (blue line) and bistatic angle (green line) – 1 TX 25 kW .....	101
Figure 116 – $x$ -position vs [range stddev(blue) and azimuth stddev (green)] – 1 TX 25 kW .....	101
Figure 117 - Location of 1 TX 25 kW (black circle) and 2 RXs (green and magenta hexagrams), true trajectory (red line) and measurements (green and magenta dots) .....	102
Figure 118 - $x$ -position vs $x$ -axis errors (1 TX 25 kW) – when crossing baseline... 102	102
Figure 119 - $x$ -position vs $y$ -axis errors (1 TX 25 kW) – when crossing baseline... 102	102
Figure 120 - $x$ -position vs $x$ -axis errors (1 TX 25 kW) – when parallel to baseline 102	102
Figure 121 - $x$ -position vs $y$ -axis errors (1 TX 25 kW) – when parallel to baseline 102	102
Figure 122 - $x$ -position vs $x$ -axis errors (1 TX 25 kW) – after fusion procedure .... 103	103
Figure 123 - $x$ -position vs $y$ -axis errors (1 TX 25 kW) – after fusion procedure .... 103	103
Figure 124 – $x$ -position vs SNR (for each radar) .....	103
Figure 125 – $x$ -position vs bistatic angle (for each radar).....	103
Figure 126 – $x$ -position vs Range std dev (for each radar) .....	103
Figure 127 – $x$ -position vs Azimuth std dev (for each radar) .....	103
Figure 128 - Location of 2 TXs 12.5 kW (green and magenta circles) and 1 RX (black hexagram), true trajectory (red line) and measurements (green and magenta dots).....	104
Figure 129 - $x$ -position vs $x$ -axis errors (1 TX 12.5 kW) – when crossing baseline 104	104
Figure 130 - $x$ -position vs $y$ -axis errors (1 TX 12.5 kW) – when crossing baseline 104	104

Figure 131 - $x$ -position vs $x$ -axis errors (1 TX 12.5 kW) – when parallel to baseline	104
Figure 132 - $x$ -position vs $y$ -axis errors (1 TX 12.5 kW) – when parallel to baseline	104
Figure 133 - $x$ -position vs $x$ -axis errors (2 TXs 12.5 kW) – after fusion procedure	105
Figure 134 - $x$ -position vs $y$ -axis errors (2 TXs 12.5 kW) – after fusion procedure	105
Figure 135 – $x$ -position vs SNR (for each radar)	105
Figure 136 – $x$ -position vs bistatic angle (for each radar)	105
Figure 137 – $x$ -position vs Range std dev (for each radar)	105
Figure 138 – $x$ -position vs Azimuth std dev (for each radar)	105
Figure 139 - Location of TX/RX (monostatic radar with 25 kW), true trajectory (red line) and measurements (green dots)	110
Figure 140 - $x$ -position vs SNR (blue line) – 1 radar 25 kW	110
Figure 141 - Location of TX/RX (monostatic radar with 25 kW), true trajectory (red line) and measurements (green dots)	110
Figure 142 - $x$ -position vs SNR (blue line) – 1 radar 25 kW	110
Figure 143 - $x$ -position vs [range stddev(blue) and azimuth stddev (green)] – 1 radar 25 kW	110
Figure 144 – Location of TX/RX (monostatic radar with 25 kW), true trajectory (red line) and measurements (green dots)	111
Figure 145 - Average $x$ -position error (red) after tracking. Green lines depict $\pm 1$ standard deviation	112
Figure 146 - Average $y$ -position error (blue) after tracking. Green lines depict $\pm 1$ standard deviation	112
Figure 147 - Average $x$ -velocity error (red) after tracking. Green lines depict $\pm 1$ standard deviation	112
Figure 148 - Average $y$ -velocity error (blue) after tracking. Green lines depict $\pm 1$ standard deviation	112
Figure 149 - Location of 25 kW TX (black circle) and RX (black hexagram), true trajectory (red line) and measurements (green dots)	113
Figure 150 - Average $x$ -position error (red) after tracking. Green lines depict $\pm 1$ standard deviation	113
Figure 151 - Average $y$ -position error (blue) after tracking. Green lines depict $\pm 1$ standard deviation	113
Figure 152 - Average $x$ -velocity error (red) after tracking. Green lines depict $\pm 1$ standard deviation	114
Figure 153 - Average $y$ -velocity error (blue) after tracking. Green lines depict $\pm 1$ standard deviation	114
Figure 154 - Location of 25 kW TX (black circle) and RX (black hexagram), true trajectory (red line) and measurements (green dots)	114
Figure 155 - Average $x$ -position error (red) after tracking. Green lines depict $\pm 1$ standard deviation	115
Figure 156 - Average $y$ -position error (blue) after tracking. Green lines depict $\pm 1$ standard deviation	115
Figure 157 - Average $x$ -velocity error (red) after tracking. Green lines depict $\pm 1$ standard deviation	115
Figure 158 - Average $y$ -velocity error (blue) after tracking. Green lines depict $\pm 1$ standard deviation	115
Figure 159 - Location of 25 kW TX (black circle) and RX (black hexagram), true trajectory (red line) and measurements (green dots)	116

Figure 160 - Average $x$ -position error (red) after tracking. Green lines depict $\pm 1$ standard deviation .....	116
Figure 161 - Average $y$ -position error (blue) after tracking. Green lines depict $\pm 1$ standard deviation .....	116
Figure 162 - Average $x$ -velocity error (red) after tracking. Green lines depict $\pm 1$ standard deviation .....	116
Figure 163 - Average $y$ -velocity error (blue) after tracking. Green lines depict $\pm 1$ standard deviation .....	116
Figure 164 - Geometry with four monostatic radar (6.25 kW each) where the coloured circles are the radars and the coloured dots are the measurements performed by each radar .....	117
Figure 165 - Average $x$ -position error (red) after tracking. Green lines depict $\pm 1$ standard deviation .....	117
Figure 166 - Average $y$ -position error (blue) after tracking. Green lines depict $\pm 1$ standard deviation .....	117
Figure 167 - Average $x$ -velocity error (red) after tracking. Green lines depict $\pm 1$ standard deviation .....	118
Figure 168 - Average $y$ -velocity error (blue) after tracking. Green lines depict $\pm 1$ standard deviation .....	118
Figure 169 - Geometry with 10 monostatic radar (2.5 kW each) at the same location (0,0) .....	118
Figure 170 - Average $x$ -position error (red) after tracking. Green lines depict $\pm 1$ standard deviation .....	119
Figure 171 - Average $y$ -position error (blue) after tracking. Green lines depict $\pm 1$ standard deviation .....	119
Figure 172 - Average $x$ -velocity error (red) after tracking. Green lines depict $\pm 1$ standard deviation .....	119
Figure 173 - Average $y$ -velocity error (blue) after tracking. Green lines depict $\pm 1$ standard deviation .....	119
Figure 174 - Geometry with 10 monostatic radar (2.5 kW each) on a horizontal line parallel to the trajectory – black circles are TX/RX .....	120
Figure 175 – Fused measurements (cyan dots) and track (black line) .....	120
Figure 176 - Average $x$ -position error (red) after tracking. Green lines depict $\pm 1$ standard deviation .....	120
Figure 177 - Average $y$ -position error (blue) after tracking. Green lines depict $\pm 1$ standard deviation .....	120
Figure 178 - Average $x$ -velocity error (red) after tracking. Green lines depict $\pm 1$ standard deviation .....	121
Figure 179 - Average $y$ -velocity error (blue) after tracking. Green lines depict $\pm 1$ standard deviation .....	121
Figure 180 - Geometry with one TX (black circle) and 4 RXs (coloured hexagrams). There is a TX and an RX at (-20,0) km.....	121
Figure 181 - Average $x$ -position error (red) after tracking. Green lines depict $\pm 1$ standard deviation .....	122
Figure 182 - Average $y$ -position error (blue) after tracking. Green lines depict $\pm 1$ standard deviation .....	122
Figure 183 - Average $x$ -velocity error (red) after tracking. Green lines depict $\pm 1$ standard deviation .....	122
Figure 184 - Average $y$ -velocity error (blue) after tracking. Green lines depict $\pm 1$ standard deviation .....	122

Figure 185 - Geometry with one TX (black circle) and 10 RXs (coloured hexagrams) along a horizontal line parallel to the target trajectory .....	123
Figure 186 - Average $x$ -position error (red) after tracking. Green lines depict $\pm 1$ standard deviation .....	123
Figure 187 - Average $y$ -position error (blue) after tracking. Green lines depict $\pm 1$ standard deviation .....	123
Figure 188 - Average $x$ -velocity error (red) after tracking. Green lines depict $\pm 1$ standard deviation .....	123
Figure 189 - Average $y$ -velocity error (blue) after tracking. Green lines depict $\pm 1$ standard deviation .....	123
Figure 190 - Geometry with 4 TXs 6.25 kW each (coloured circles) and 1 RX (black hexagram).....	124
Figure 191 - Average $x$ -position error (red) after tracking. Green lines depict $\pm 1$ standard deviation .....	124
Figure 192 - Average $y$ -position error (blue) after tracking. Green lines depict $\pm 1$ standard deviation .....	124
Figure 193 - Average $x$ -velocity error (red) after tracking. Green lines depict $\pm 1$ standard deviation .....	124
Figure 194 - Average $y$ -velocity error (blue) after tracking. Green lines depict $\pm 1$ standard deviation .....	124
Figure 195 - Geometry with 10 TXs 2.5 kW each (coloured circles) and 1 RX (black hexagram) along a horizontal line parallel to the target trajectory .....	125
Figure 196 - Average $x$ -position error (red) after tracking. Green lines depict $\pm 1$ standard deviation .....	125
Figure 197 - Average $y$ -position error (blue) after tracking. Green lines depict $\pm 1$ standard deviation .....	125
Figure 198 - Average $x$ -velocity error (red) after tracking. Green lines depict $\pm 1$ standard deviation .....	125
Figure 199 - Average $y$ -velocity error (blue) after tracking. Green lines depict $\pm 1$ standard deviation .....	125
Figure 200 - Geometry with 2 TXs 12.5 kW each (blue/green) and 2 RXs (red/magenta) along a horizontal line parallel to target trajectory .....	126
Figure 201 - Average $x$ -position error (red) after tracking. Green lines depict $\pm 1$ standard deviation .....	126
Figure 202 - Average $y$ -position error (blue) after tracking. Green lines depict $\pm 1$ standard deviation .....	126
Figure 203 - Average $x$ -velocity error (red) after tracking. Green lines depict $\pm 1$ standard deviation .....	126
Figure 204 - Average $y$ -velocity error (blue) after tracking. Green lines depict $\pm 1$ standard deviation .....	126
Figure 205 – The red ( $x$ -velocity) and blue ( $y$ -velocity) depict the true target velocities .....	128
Figure 206 - The red ( $x$ -acceleration) and blue ( $y$ -acceleration) depict the true target accelerations.....	128
Figure 207 – Geometry with one monostatic radar (black circle at (0,0)) and a target with spiral trajectory .....	128
Figure 208 – Average $x$ -position error (red) after tracking on each measurement. Green lines depict $\pm 1$ standard deviation .....	128
Figure 209 - Average $y$ -position error (blue) after tracking on each measurement. Green lines depict $\pm 1$ standard deviation .....	128

Figure 210 - Average $x$ -velocity error (red) after tracking on each measurement. Green lines depict $\pm 1$ standard deviation .....	129
Figure 211 - Average $y$ -velocity error (blue) after tracking on each measurement. Green lines depict $\pm 1$ standard deviation .....	129
Figure 212 - Average $x$ -acceleration error (red) after tracking on each measurement. Green lines depict $\pm 1$ standard deviation .....	129
Figure 213 - Average $y$ -acceleration error (blue) after tracking on each measurement. Green lines depict $\pm 1$ standard deviation .....	129
Figure 214 - Geometry with one bistatic radar (black circle at (0,0) is TX and black hexagram at (0,60) km is RX) and a target with spiral trajectory (target crossing baseline) .....	130
Figure 215 - Average $x$ -position error (red) after tracking on each measurement. Green lines depict $\pm 1$ standard deviation .....	130
Figure 216 - Average $y$ -position error (blue) after tracking on each measurement. Green lines depict $\pm 1$ standard deviation .....	130
Figure 217 - Average $x$ -velocity error (red) after tracking on each measurement. Green lines depict $\pm 1$ standard deviation .....	131
Figure 218 - Average $y$ -velocity error (blue) after tracking on each measurement. Green lines depict $\pm 1$ standard deviation .....	131
Figure 219 - Average $x$ -acceleration error (red) after tracking on each measurement. Green lines depict $\pm 1$ standard deviation .....	131
Figure 220 - Average $y$ -acceleration error (blue) after tracking on each measurement. Green lines depict $\pm 1$ standard deviation .....	131
Figure 221 - Geometry with one bistatic radar (black circle at (0,0) is TX and black hexagram at (-60,0) km is RX) and a target with spiral trajectory .....	132
Figure 222 - Average $x$ -position error (red) after tracking on each measurement. Green lines depict $\pm 1$ standard deviation .....	132
Figure 223 - Average $y$ -position error (blue) after tracking on each measurement. Green lines depict $\pm 1$ standard deviation .....	132
Figure 224 - Average $x$ -velocity error (red) after tracking on each measurement. Green lines depict $\pm 1$ standard deviation .....	132
Figure 225 - Average $y$ -velocity error (blue) after tracking on each measurement. Green lines depict $\pm 1$ standard deviation .....	132
Figure 226 - Average $x$ -acceleration error (red) after tracking on each measurement. Green lines depict $\pm 1$ standard deviation .....	133
Figure 227 - Average $y$ -acceleration error (blue) after tracking on each measurement. Green lines depict $\pm 1$ standard deviation .....	133
Figure 228 - Geometry with four monostatic radar (6.25 kW each) where the coloured circles are the radars and the coloured dots are the measurements performed by each radar .....	133
Figure 229 - Average $x$ -position error (red) after tracking on each measurement. Green lines depict $\pm 1$ standard deviation .....	134
Figure 230 - Average $y$ -position error (blue) after tracking on each measurement. Green lines depict $\pm 1$ standard deviation .....	134
Figure 231 - Average $x$ -velocity error (red) after tracking on each measurement. Green lines depict $\pm 1$ standard deviation .....	134
Figure 232 - Average $y$ -velocity error (blue) after tracking on each measurement. Green lines depict $\pm 1$ standard deviation .....	134
Figure 233 - Average $x$ -acceleration error (red) after tracking on each measurement. Green lines depict $\pm 1$ standard deviation .....	134

Figure 234 - Average $y$ -acceleration error (blue) after tracking on each measurement. Green lines depict $\pm 1$ standard deviation .....	134
Figure 235 - Geometry with four monostatic radar (6.25 kW each) where the coloured circles are the radars and the coloured dots are the measurements performed by each radar .....	135
Figure 236 - Average $x$ -position error (red) after tracking on each measurement. Green lines depict $\pm 1$ standard deviation .....	135
Figure 237 - Average $y$ -position error (blue) after tracking on each measurement. Green lines depict $\pm 1$ standard deviation .....	135
Figure 238 - Average $x$ -velocity error (red) after tracking on each measurement. Green lines depict $\pm 1$ standard deviation .....	135
Figure 239 - Average $y$ -velocity error (blue) after tracking on each measurement. Green lines depict $\pm 1$ standard deviation .....	135
Figure 240 - Average $x$ -acceleration error (red) after tracking on each measurement. Green lines depict $\pm 1$ standard deviation .....	136
Figure 241 - Average $y$ -acceleration error (blue) after tracking on each measurement. Green lines depict $\pm 1$ standard deviation .....	136
Figure 242 - Geometry with 10 monostatic radar (2.5 kW each) at the same location (0,0) .....	136
Figure 243 - Average $x$ -position error (red) after tracking on each measurement. Green lines depict $\pm 1$ standard deviation .....	137
Figure 244 - Average $y$ -position error (blue) after tracking on each measurement. Green lines depict $\pm 1$ standard deviation .....	137
Figure 245 - Average $x$ -velocity error (red) after tracking on each measurement. Green lines depict $\pm 1$ standard deviation .....	137
Figure 246 - Average $y$ -velocity error (blue) after tracking on each measurement. Green lines depict $\pm 1$ standard deviation .....	137
Figure 247 - Average $x$ -acceleration error (red) after tracking on each measurement. Green lines depict $\pm 1$ standard deviation .....	137
Figure 248 - Average $y$ -acceleration error (blue) after tracking on each measurement. Green lines depict $\pm 1$ standard deviation .....	137
Figure 249 - Geometry with 10 monostatic radar (2.5 kW each) on a line – black circles are TX/RX .....	138
Figure 250 - Average $x$ -position error (red) after tracking on each measurement. Green lines depict $\pm 1$ standard deviation .....	138
Figure 251 - Average $y$ -position error (blue) after tracking on each measurement. Green lines depict $\pm 1$ standard deviation .....	138
Figure 252 - Average $x$ -velocity error (red) after tracking on each measurement. Green lines depict $\pm 1$ standard deviation .....	138
Figure 253 - Average $y$ -velocity error (blue) after tracking on each measurement. Green lines depict $\pm 1$ standard deviation .....	138
Figure 254 - Average $x$ -acceleration error (red) after tracking on each measurement. Green lines depict $\pm 1$ standard deviation .....	139
Figure 255 - Average $y$ -acceleration error (blue) after tracking on each measurement. Green lines depict $\pm 1$ standard deviation .....	139
Figure 256 - Geometry with 1 TX (black circle) and 4 RXs (coloured hexagrams) and a target with spiral trajectory .....	139
Figure 257 - Average $x$ -position error (red) after tracking on each measurement. Green lines depict $\pm 1$ standard deviation .....	140

Figure 258 - Average $y$ -position error (blue) after tracking on each measurement. Green lines depict $\pm 1$ standard deviation .....	140
Figure 259 - Average $x$ -velocity error (red) after tracking on each measurement. Green lines depict $\pm 1$ standard deviation .....	140
Figure 260 - Average $y$ -velocity error (blue) after tracking on each measurement. Green lines depict $\pm 1$ standard deviation .....	140
Figure 261 - Average $x$ -acceleration error (red) after tracking on each measurement. Green lines depict $\pm 1$ standard deviation .....	141
Figure 262 - Average $y$ -acceleration error (blue) after tracking on each measurement. Green lines depict $\pm 1$ standard deviation .....	141
Figure 263 - Geometry with one TX (black circle) and 10 RXs (coloured hexagrams) along a horizontal line and a target with spiral trajectory .....	141
Figure 264 - Average $x$ -position error (red) after tracking on each measurement. Green lines depict $\pm 1$ standard deviation .....	142
Figure 265 - Average $y$ -position error (blue) after tracking on each measurement. Green lines depict $\pm 1$ standard deviation .....	142
Figure 266 - Average $x$ -velocity error (red) after tracking on each measurement. Green lines depict $\pm 1$ standard deviation .....	142
Figure 267 - Average $y$ -velocity error (blue) after tracking on each measurement. Green lines depict $\pm 1$ standard deviation .....	142
Figure 268 - Average $x$ -acceleration error (red) after tracking on each measurement. Green lines depict $\pm 1$ standard deviation .....	142
Figure 269 - Average $y$ -acceleration error (blue) after tracking on each measurement. Green lines depict $\pm 1$ standard deviation .....	142
Figure 270 - Geometry with 4 TXs 6.25 kW each (coloured circles) and 1 RX (black hexagram) and a target with spiral trajectory .....	143
Figure 271 - Average $x$ -position error (red) after tracking on each measurement. Green lines depict $\pm 1$ standard deviation .....	143
Figure 272 - Average $y$ -position error (blue) after tracking on each measurement. Green lines depict $\pm 1$ standard deviation .....	143
Figure 273 - Average $x$ -velocity error (red) after tracking on each measurement. Green lines depict $\pm 1$ standard deviation .....	144
Figure 274 - Average $y$ -velocity error (blue) after tracking on each measurement. Green lines depict $\pm 1$ standard deviation .....	144
Figure 275 - Average $x$ -acceleration error (red) after tracking on each measurement. Green lines depict $\pm 1$ standard deviation .....	144
Figure 276 - Average $y$ -acceleration error (blue) after tracking on each measurement. Green lines depict $\pm 1$ standard deviation .....	144
Figure 277 - Geometry with 10 TXs 2.5 kW each (coloured circles) and one RX (black hexagram) along a horizontal line and a target with spiral trajectory .....	145
Figure 278 - Average $x$ -position error (red) after tracking on each measurement. Green lines depict $\pm 1$ standard deviation .....	145
Figure 279 - Average $y$ -position error (blue) after tracking on each measurement. Green lines depict $\pm 1$ standard deviation .....	145
Figure 280 - Average $x$ -velocity error (red) after tracking on each measurement. Green lines depict $\pm 1$ standard deviation .....	145
Figure 281 - Average $y$ -velocity error (blue) after tracking on each measurement. Green lines depict $\pm 1$ standard deviation .....	145
Figure 282 - Average $x$ -acceleration error (red) after tracking on each measurement. Green lines depict $\pm 1$ standard deviation .....	146

Figure 283 - Average $y$ -acceleration error (blue) after tracking on each measurement. Green lines depict $\pm 1$ standard deviation .....	146
Figure 284 – Geometry with 2 TXs 12.5 kW each (blue/green) and 2 RXs (red/magenta) along a horizontal line and a target with spiral trajectory .....	146
Figure 285 - Average $x$ -position error (red) after tracking on each measurement. Green lines depict $\pm 1$ standard deviation .....	147
Figure 286 - Average $y$ -position error (blue) after tracking on each measurement. Green lines depict $\pm 1$ standard deviation .....	147
Figure 287 - Average $x$ -velocity error (red) after tracking on each measurement. Green lines depict $\pm 1$ standard deviation .....	147
Figure 288 - Average $y$ -velocity error (blue) after tracking on each measurement. Green lines depict $\pm 1$ standard deviation .....	147
Figure 289 - Average $x$ -acceleration error (red) after tracking on each measurement. Green lines depict $\pm 1$ standard deviation .....	147
Figure 290 - Average $y$ -acceleration error (blue) after tracking on each measurement. Green lines depict $\pm 1$ standard deviation .....	147
Figure 291 - Geometry with 10 TXs (black circle) at (0,0) and 4 RXs (coloured hexagrams) and a target with spiral trajectory .....	155
Figure 292 - Average $x$ -position error (red) after tracking on each measurement. Green lines depict $\pm 1$ standard deviation .....	156
Figure 293 - Average $y$ -position error (blue) after tracking on each measurement. Green lines depict $\pm 1$ standard deviation .....	156
Figure 294 - Geometry with 10 TXs (black circle) at (0,0) and 4 RXs (coloured hexagrams) and a target with spiral trajectory .....	156
Figure 295 - Average $x$ -position error (red) after tracking on each measurement. Green lines depict $\pm 1$ standard deviation .....	157
Figure 296 - Average $y$ -position error (blue) after tracking on each measurement. Green lines depict $\pm 1$ standard deviation .....	157
Figure 297 - Average $x$ -position error (red) after tracking on each measurement. Green lines depict $\pm 1$ standard deviation .....	157
Figure 298 - Average $y$ -position error (blue) after tracking on each measurement. Green lines depict $\pm 1$ standard deviation .....	157
Figure 299 Average $x$ -position error (red) after tracking on each measurement. Green lines depict $\pm 1$ standard deviation .....	158
Figure 300 - Average $y$ -position error (blue) after tracking on each measurement. Green lines depict $\pm 1$ standard deviation .....	158
Figure 301 - Geometry with 1 TX (black circle) at (0,0) and 1 RX (red hexagrams) that moves along the green line (clockwise) and a target with spiral trajectory (red line) .....	158
Figure 302 - Average $x$ -position error (red) after tracking on each measurement. Green lines depict $\pm 1$ standard deviation .....	159
Figure 303 - Average $y$ -position error (blue) after tracking on each measurement. Green lines depict $\pm 1$ standard deviation .....	159

# List of Tables

Table 1 - Different levels of complexity according to some Multistatic configuration variables (after [19]).....	48
Table 2 – Main radar parameters used in the simulations and some other related information.....	87
Table 3 – Measurements Summary for monostatic geometries – measurement errors during the trajectory of the target in different configurations, changing location and transmit power of the radar and target RCS.....	106
Table 4 - Measurements Summary for bistatic geometries – measurement errors during the trajectory of the target in different configurations, changing location and transmit power of the radar and target RCS.....	107
Table 5 - Measurements Summary for multistatic geometries – measurement errors during the trajectory of the target in 2 different configurations, one Multistatic (1 TX / 2 RXs) and the other one Multistatic (2 TXs / 1 RX).....	107
Table 6 – Maximum SNR and Best Range/Azimuth standard deviation for monostatic scenarios (target flying far from TX/RX).....	108
Table 7 - Maximum SNR and Best Range/Azimuth standard deviation for bistatic scenarios.....	108
Table 8 - Maximum SNR and Best Range/Azimuth standard deviation for multistatic scenarios.....	109
Table 9 – Tracking Results Summary – tracking position errors during the trajectory of a target that flies on a straight line with constant velocity of 250 m/s .....	148
Table 10 - Tracking Results Summary – tracking velocity errors during the trajectory of a target that flies on a straight line with constant velocity of 250 m/s .....	149
Table 11 - Tracking Results Summary – tracking position errors during the trajectory of a target that flies on a spiral trajectory with non constant velocity and acceleration. The errors are depicted at certain measurement sequence number. Each measurement is performed every 2.5 seconds.....	150
Table 12 - Tracking Results Summary – tracking velocity errors during the trajectory of a target that flies on a spiral trajectory with non constant velocity and acceleration. The errors are depicted at certain measurement sequence number. Each measurement is performed every 2.5 seconds.....	150
Table 13 - Tracking Results Summary – tracking acceleration errors during the trajectory of a target that flies on a spiral trajectory with non constant velocity and acceleration. The errors are depicted at certain measurement sequence number. Each measurement is performed every 2.5 seconds.....	151

# List of Symbols

$r_2$	Distance between target and receiver (RX) in a bistatic radar
$L$	Baseline, which is the distance between transmitter (TX) and receiver (RX) in a bistatic radar
$\Delta t$	Time interval between the reception of the transmitted signal and the target echo
$\theta_R$	Pointing angle of the receiver antenna with respect to vertical axis $y$
$r_1$	Distance between transmitter (TX) and target in a bistatic radar
$R_{TT}$	Total distance transmitter-target-receiver in a bistatic radar
$c$	Speed of propagation
$V, V_T$ and $V_R$	In a bistatic geometry, velocity magnitude for the target, transmitter and receiver, respectively
$\delta, \delta_T$ and $\delta_R$	In a bistatic geometry, aspect angles of $V, V_T$ and $V_R$
$\beta$	Bistatic angle, in a bistatic geometry
$\theta_T$	Transmitter Pointing Angle with respect to vertical axis
$\theta_R$	Receiver Pointing Angle with respect to vertical axis
$f_B$	Bistatic doppler shift caused by target motion when transmitter and receiver are stationary
$R_T$	Distance between transmitter (TX) and target in a bistatic radar
$R_R$	Distance between target and receiver (RX) in a bistatic radar
$\lambda$	Radar wavelength and is related to the transmitted frequency
$P_S$	Signal power at the receiver
$P_N$	Noise power in the receiver.
$P_t$	Transmit power at the output of the transmitter
$G_t$	Power gain of the transmit antenna

$G_r$	Power gain of the receive antenna
$\sigma$	Target Radar Cross Section (RCS)
$R$	Range from the radar to the target (monostatic)
$k$	Boltzmann's constant
$T_0$	Room temperature
$B$	Receiver bandwidth
$F_n$	Radar noise figure
$L$	Factor (greater than 1) included in order to account for all losses in the signal that can reduce the radar performance
$\sigma_B$	Bistatic Radar Cross Section
$A$	Silhouette area of a target
$r$	Radius of a sphere
$\theta_B$	Angular width of forward scatter
$d$	Linear dimension of the target in the appropriate plane
$X_{n+1}$	State of target at time $n+1$
$\phi$	Transition matrix
$X_n$	State of target at time $n$
$x_n$	Position at time $n$
$v_n$	Velocity at time $n$
$Z_n$	Measurement plus noise
$u$	Noise
$\hat{X}_n^-$	Previous prediction of state
$\hat{X}_n$	Updated state using measurement
$\hat{X}_{n+1}^-$	Prediction of state for $n+1$
$x$	Refers to $x$ -axis (Cartesian coordinates)

$y$	Refers to $y$ -axis (Cartesian coordinates)
$g, h, k$	Control parameters of $g$ - $h$ and $g$ - $h$ - $k$ filters
$\theta$	Parameter in $g$ - $h$ or $g$ - $h$ - $k$ filter to indicate how the filter is going to weigh the recent measurements against historical measurements. In the context of Kalman Filtering is the bearing angle of the receiver.
$\hat{x}_{n+1,n}^*$	Estimated velocity for step $n+1$ , using measurements until step $n$ . “*” means “estimate”.
$T$	Sampling interval
$y_n$	$n^{\text{th}}$ -measurement
$\hat{x}_{n+1,n}^*$	Estimated position for step $n+1$ , using measurements until step $n$ .
$\ddot{x}_{n+1,n}^*$	Estimated acceleration for step $n+1$ , using measurements until step $n$ .
$M$	Measurement matrix
$S_0$ and $S_1$	Covariance of prediction matrix
$I_{n \times n}$	Identity matrix $n \times n$
$Q$	Dynamic noise covariance matrix. Defined by parameters such as maximum acceleration in $x$ and $y$ axis predicted by the designer of Kalman Filter for a certain scenario
$R$	Measurement covariance vector for Cartesian coordinates. It is a function of polar-coordinates measurements and standard deviations.
$H$	Weight matrix
$X_{n,n}^*$	Update of estimation using measurements
$X_{n+1,n}^*$	Estimation for next iteration using Transition matrix $\phi$

# List of Acronyms

1D	One dimensional space
2D	Two dimensional space
3D	Three dimensional space
ARM	Anti Radiation Missile
CASA	Collaborative Adaptive Sensing of the Atmosphere
COTS	Commercial Off The Shelf
CW	Continuous Wave
ESM	Electronic Support Measures
FMCW	Frequency Modulated Continuous Wave
HRR	High Resolution Radar
IEEE	Institute of Electrical and Electronics Engineers
IMM	Interacting Multiple Model
IMM-I-UKF	Interactive Multiple Model algorithm combined with Iterated Unscented Kalman Filter
IMM-SI-EKF	Interactive Multiple Model algorithm combined with Sequential Iterated Extended Kalman Filter
I-UKF	Iterated Unscented Kalman Filter
KB	Knowledge Based
KF	Kalman Filter
LRR	Low Resolution Radar
MFR	Multi-Function Radar
MIMO	Multiple Input Multiple Output
MSTWG	Multistatic Tracking Working Group

PD	Probability of Detection
PFA	Probability of False Alarm
PRF	Pulse Repetition Frequency
RCS	Radar Cross Section
ROC	Receiver Operating Characteristic
RPM	Revolutions Per Minute
RX	Receiver
SI-EKF	Sequential Iterated Extended Kalman Filter
SMS	Sensor Management System
SNR	Signal-to-Noise Ration
TX	Transmitter
UCL	University College London

# 1 Introduction

## 1.1 Overview and Motivation

According to [1], the history of radars started in the 1930s and they were mainly bistatic being developed, almost at the same time, in many countries such as United States, the United Kingdom, Russia and Japan. Transmitters and receivers were not co-located (since, in the earlier stages, they did not have the technology to use one single antenna to transmit and receive signals) and were known as continuous wave (CW) interference detectors. Therefore, the target could be detected when it crossed the transmitter-receiver baseline by measuring the interference between the received signal and the direct signal when the target was crossing. Nevertheless, it is important to report that [2] reminds that, in 1900, Nikola Tesla came up with the idea of the possibility of employing radio waves to detect and also measure the movement of distant objects. But it was in 1904 that Christian Hülsmeier, a German engineer, applied for a patent for his “telemobiloskop” [2] which was a transmitter-receiver that used electrical waves to detect distant metallic objects. The main purpose of this system was to avoid ship collision, and although it had impressed the press and the public, naval authorities and public companies did not show any interest on it.

A radar is basically a device that transmits an electromagnetic signal and receives an echo of it after it is reflected by a target. The time to receive the echo determines the range of the target. The transmitter and the receiver can be co-located (monostatic radars) or separated (bistatic radars).

The main difference between monostatic and bistatic radars is the separation of the transmitter (TX) and receiver (RX). However, a co-located TX and RX are not considered a bistatic system, even though they do not use a common antenna. The separation between TX and RX in a radar system must be big enough if compared with a typical target range so that it can be considered a bistatic system. Figure 1 and Figure 2 show, respectively, an example of a Monostatic and a Bistatic Radar.

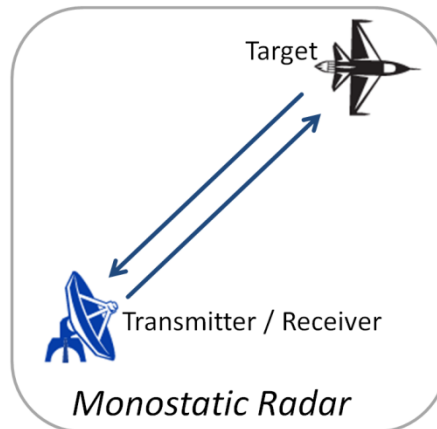


Figure 1 - Monostatic Radar

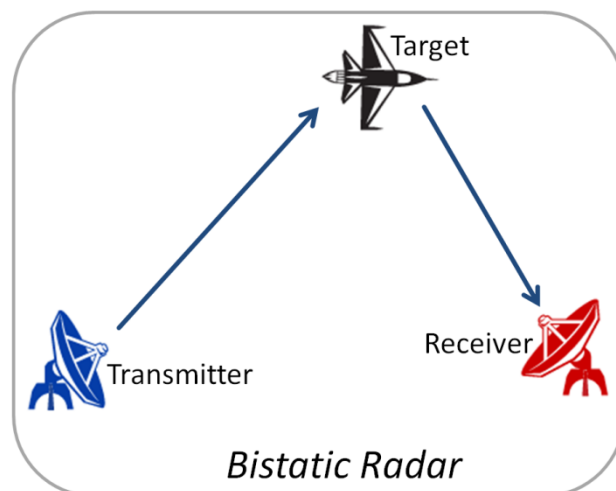


Figure 2 - Bistatic Radar

One or more transmitters and receivers working together in a coordinated and integrated way can be considered a multistatic system. Each transmitter combined with a receiver form a bistatic system and all the possible bistatic systems formed with all these transmitters and receivers form the multistatic system (see Figure 3).

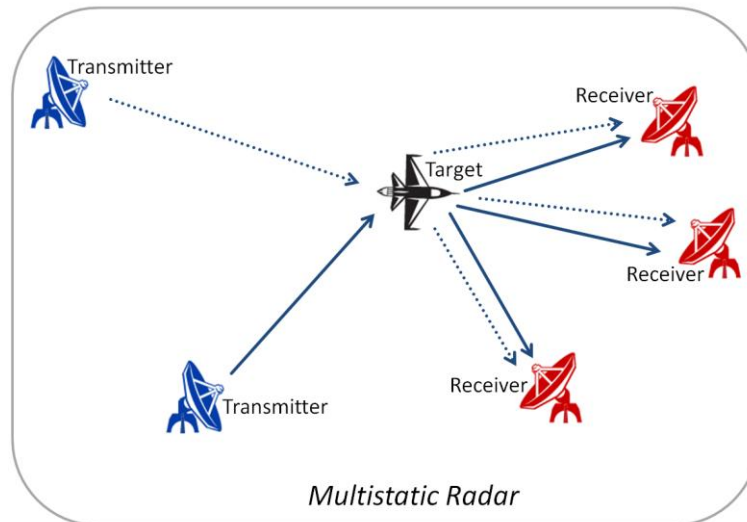


Figure 3 - Multistatic Radar

In 1936, the US Naval Research Laboratory invented the duplexer which allowed transmitting and receiving using one single antenna (monostatic radar) [3]. Because of that, there was almost no interest in bistatic radars for the next 15 years. Since then, the interest in this subject seems to be cyclic and with a period of about 15-20 years [3]. It is believed that new technologies leads to renewed interest in the subject and nowadays it seems that the interest is going to last for a longer period of time.

Nowadays, military forces have particular interest on bistatic systems due to the fact that monostatic radars can be easily detected and hence jammed or targeted by antiradiation missiles (ARM). A bistatic system with its receiver situated far (many tens or hundreds of kilometres) from the transmitter (which can be located on the ground or even on an aircraft) can offer reduced vulnerability to its threats, for example, a jammer signal directed back to the transmitter has no effect on the receiver that is potentially covert (see Figure 4).

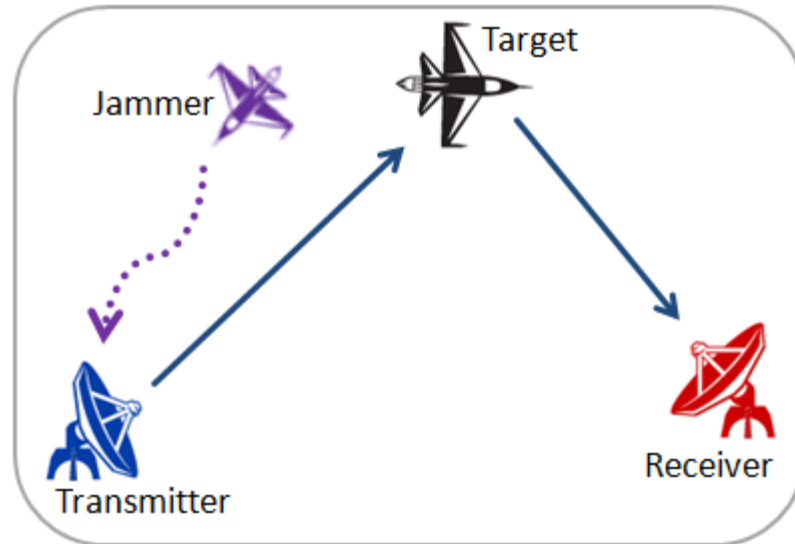


Figure 4 - Bistatic Radar being jammed

A bistatic radar may be comprised of a fully controlled transmitter that is synchronized with the receiver or a radar which is not under the control of the designer, usually named hitchhiker radar. Moreover, it can also make use of other sources (originally not for radar use) such as broadcast transmissions (see Figure 5).

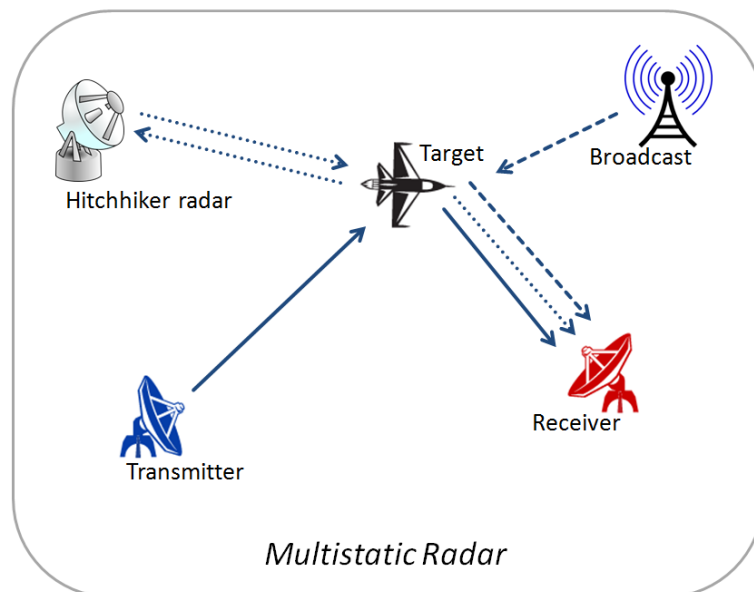


Figure 5 - Pairs of bistatic radar using different kind of transmitters

Also, monostatic radars can be used in a bistatic configuration by adding one or more receivers in the geometry. Another possibility is to use many monostatic radars working altogether in bistatic mode as well as in its original purpose, monostatic mode (see Figure 6).

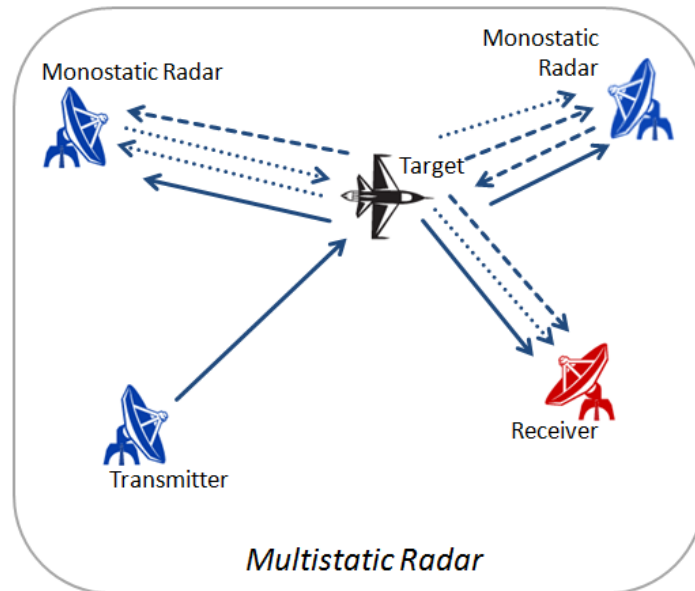


Figure 6 - Monostatic Radars working either as a monostatic or bistatic radar

### 1.1.1 The Problem of Tracking in a Radar Network

One of the most important functions of a radar surveillance system is to keep track of all targets of interest within the area covered by its sensors. Recently, many surveillance systems have been relying on multiple sensors which can work together in a coordinated and integrated way to provide more accurate and reliable estimates of targets than isolated sensors. Therefore, a network of radars working in multistatic mode could be used to detect and track targets for defence purposes. Due to the agility of electronically-steered antennas, it would be better to use this kind of antenna instead of the traditional rotating antennas in order to make it easy to coordinate the pointing direction of the transmitters and receivers antennas.

#### 1.1.1.1 Sensor Management

Nowadays, modern military or civilian systems comprise many sensors that might have different characteristics or functionalities, be located at different locations or have different dynamics [4]. These modern systems of sensors must be able to manage, co-ordinate and integrate the sensor usage to accomplish specific objectives. Sensor Management Systems are responsible for these activities and aims to optimize the performance of the whole sensor system and its objectives. The fundamental task of a Sensor Management System is to choose at a certain time the most appropriate group of sensors to execute a task.

A Sensor Management System (SMS) can be seen as a unit to the sensor data fusion unit. Therefore, the SMS design is much related to the design of the sensor data fusion unit that can be basically of three types: Centralized, Decentralized or Hierarchical.

### 1.1.1.2 Centralized Data Fusion

In this type of design, all the information collected from the different sensors is sent to a data fusion unit which is located at a central processor or node. This central node can receive raw data, detections, plots or tracks and process them depending on the applications. All decisions are made at this node, and instructions are given out to the chosen sensors (see Figure 7). This kind of approach might not be feasible or might be very expensive if the multistatic radar system is comprised of too many nodes and/or if the data is processed are at the raw level (lots of data to communicate and process).

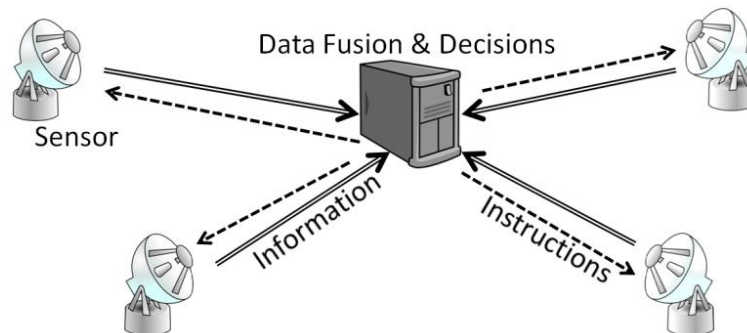


Figure 7 - Centralized system

### 1.1.1.3 Decentralized Data Fusion

In this case, the system allows its sensors more freedom to make their own decisions as data are fused locally, eventually using information from the sensors around. The co-ordination of the sensors is done through communications among them, where sensors share locally fused information. Efficient implementation of the communication network (Figure 8) is a crucial matter.

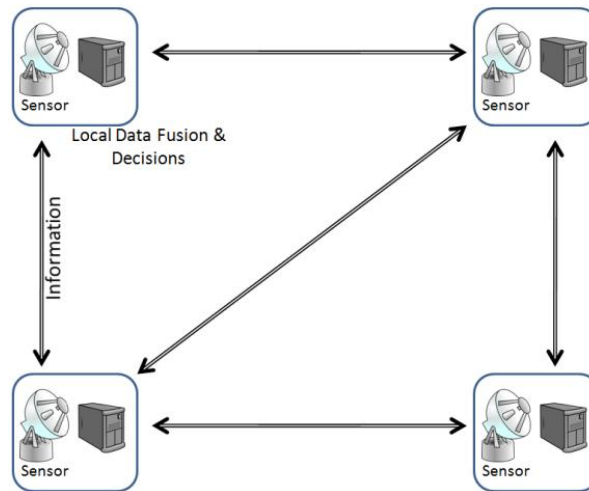


Figure 8 - Decentralized system

A decentralized data fusion system [5] consists of a set of sensor nodes (identical or not) where each sensor processes its own data and data received from neighbouring nodes. The nodes do not require any central node to send their data and also can make their own decisions based on a local data fusion. There is no node where fusion or global decisions are made. A decentralised data fusion system is characterised by three constraints:

1. There is no single central fusion node;
2. There is no common communication facility; nodes cannot broadcast results and communication must be done on a node-to-node basis (however, many systems nowadays rely on a common communication facility as seen on Figure 10); and
3. Sensor nodes do not have and should not need any global knowledge of sensor network topology.

As a consequence of the constraints mentioned above, some important characteristics (particularly in military scenarios) for decentralized data fusion systems arise:

- With no central fusion centre and no common communication facility, the system becomes scalable as there are no limits imposed by centralized computational bottlenecks or lack of communication bandwidth (scalability).
- If no node is central and no global knowledge of the sensor network topology is required, the system is more failure proof and also more flexible (and less sensitive) to changes in the network structure (survivability).

- Nodes can be designed and programmed independently of the other nodes because no global knowledge of the network is required *a priori* and all data fusion processes must take place locally at each sensor site (modularity).

The following figures show examples of topologies that can be used in decentralized data fusion systems.

Figure 9 shows a topology where the nodes maintain independent links (peer-to-peer communication) to adjacent nodes. The local algorithm in each node does not require any knowledge of network topology because the algorithm is supposed to transmit new local information to the adjacent connected nodes. These nodes receive the information and re-transmit it to their neighbours. Although this architecture brings some advantages such as survivability and scalability, there are some disadvantages related to communication complexity and delays in the information propagation through the nodes.

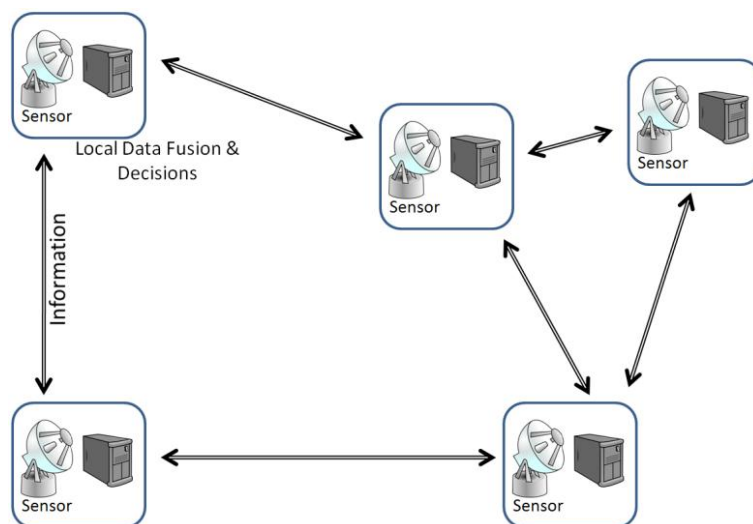


Figure 9 - Decentralized Data Fusion System using peer-to-peer communication links

Figure 10 shows a communication topology in which each node is connected to every other node in the system through a common communication facility. This topology avoids the problems of interconnection complexity and delays in information propagation but the use of a common communication medium goes against a principle of decentralised systems in avoiding any central resource. Nevertheless, the broadcast architecture is very common in many existing communication systems.

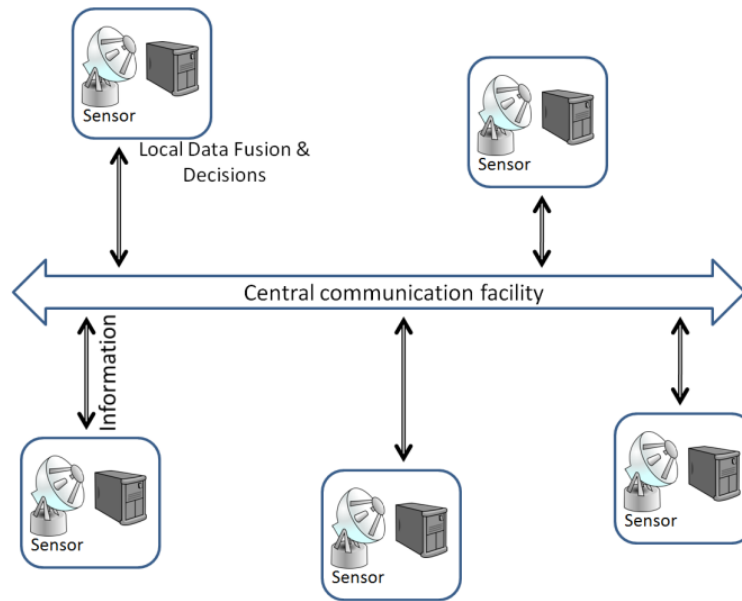


Figure 10 - Decentralized Data Fusion System using a central network facility

#### 1.1.1.4 Hierarchical Data Fusion

This design can be considered as a mix of some characteristics of the centralized and decentralized systems. In the bottom level of the hierarchy there are local fusion units responsible to fuse and control a small group of sensors. Local fusion units can group themselves and centralize their information in a higher level until they reach the top level where the information from all sensors are fused and used in a global fusion centre (see an example in Figure 11).

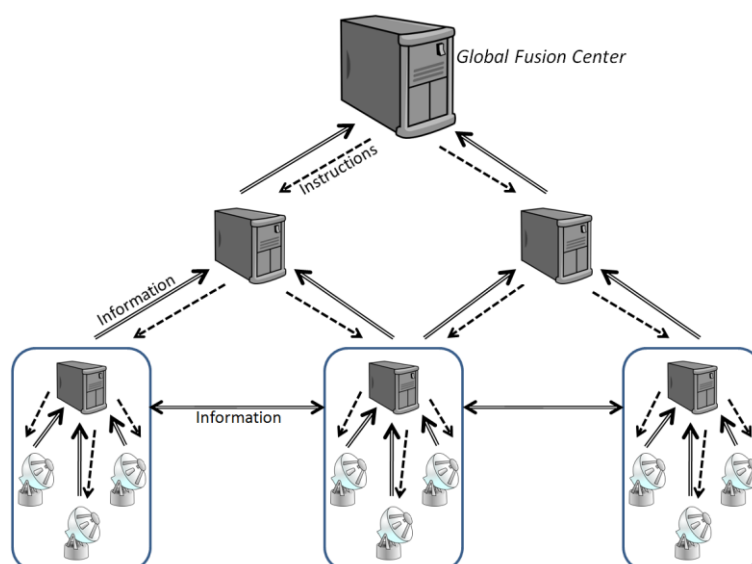


Figure 11 - Hierarchical system

## 1.2 Thesis Layout

This thesis approaches the concept of bistatic and multistatic radars that only recently has been a subject of a long-term interest due to new technologies that have emerged to help deploying such concept consistently. Also, the well known concept of stand-alone monostatic radars has reached its limits and has been facing difficulties, for example, when trying to detect and track a stealth target.

The use of a network of radars operating either monostatically or bi/multistatically will improve sensitivity, coverage, tracking accuracy and so on. It is expected that, although there are several advantages in the use of such technology, there are also some disadvantages and new challenges that must be overcome in order to make the technology operatively and financially feasible.

In this thesis, a tracking algorithm performance comparison between different configurations of networked radars and stand-alone monostatic radars is performed and analysed.

Next chapter, the objectives of this thesis are presented in more detail and the reasons to carry out this research are explained.

Chapter 3 starts with some theory about bistatic and multistatic radars and explains the basic properties of bistatic radars. In chapter 4, the idea of tracking is introduced and explained.

After that, in chapter 5, a review of the previous work produced so far about the concept of multistatic radars, multistatic tracking and resource management as well are reported.

Following this chapter, in chapter 6, the methodology and infrastructure used to perform simulations and ultimately collect data is described. The results of the simulations including a final analysis about the data gathered are presented in chapter 7.

Finally, chapter 8 presents the conclusions of this research and its contributions to the field and also suggests some improvements and possible future developments from this research.

## 2 The Proposed Approach

Nowadays, many applications rely on different kind of radars. They can be civilian or military and each of them has its own particular needs (maximum range, range resolution, bandwidth, angular resolution and so on). This thesis focuses on the class of applications related to target tracking in multistatic environments compared to monostatic ones. It does not matter whether it is for civilian or military applications although it seems that the tracking subject is likely to be more interesting for military, defence or security needs. There are many papers in the literature (for instance, [6], [7], [8], [9], [10], [11] and [12]) that are related to multistatic tracking concepts, new algorithms or comparison among algorithms. However, it has not been found so far in the literature any research or published paper that shows how different are the results when a target is tracked using several different configurations of multistatic or netted radar systems.

The main idea of this research is to prepare a simulation where one target is going to fly inside of the coverage area of a radar system. One tracking algorithm is going to be chosen based on its simplicity as the main idea is not to develop a new algorithm or to improve existing ones. The idea is to assess different configurations of radar networks and how they can improve tracking performance. So, for a chosen algorithm and same dynamics profile of the target, different configurations of radar (monostatic, netted monostatic, bistatic, multistatic with many receivers, multistatic with many transmitters and so on) are assessed and compared in terms of tracking position errors, tracking velocity errors and if necessary, tracking acceleration errors. Another configuration that is also simulated is whether the processing of the

information (measurements) is performed in a central node or performed in a decentralized way in each node and then fused on a central node. Each different configuration is going to produce a solution which is the tracking position and velocity and the solution is compared with the real position and velocity.

The simulations and the results provided by this research might help in the process of choosing a suitable multistatic geometry for a particular need. It can also help the resource management software developer to understand the consequences of moving in real-time a radar platform to another location in order to improve tracking accuracy. In addition, since all the simulations are performed using radar characteristics similar to commercial radars, an example is prepared at the end of the results section in order to show how a navigation radar aimed to track ships at distances no bigger than the horizon distance (25 km), can be used in a network of similar radars to track targets that are located further (around 70-80 km) and have smaller Radar Cross Section (RCS) such as stealth targets (which for the purpose of this research is considered to be  $RCS = 0.1 \text{ m}^2$ , although it can be found that there are stealth targets with  $RCS = 0.01\text{m}^2$  or even less).

## 2.1 Scope and Limitations

The starting scenario is comprised of a single target flying in a straight line with constant velocity. All the scenarios are simulated in a 2D environment thus only  $(x,y)$  coordinates for position and velocity are considered. From there, some other scenarios are exploited such as a target with some acceleration or a target that manoeuvres.

Also, the target RCS is considered to be constant and equivalent to a perfectly conducting sphere. The simulations are performed with RCS of  $10 \text{ m}^2$  or  $0.1 \text{ m}^2$ . RCS is also considered constant in bistatic scenarios. In addition, in bistatic scenarios, where the measurements of a bistatic radar is fused with some other radar, measurements coming from the region where the bistatic angle is between 145-180 degrees are made gradually less important and hence not considered in the fusion algorithm because simulations show that when the bistatic angle is in the aforementioned range, the location of the target is not accurate.

The measurements are simulated considering standard deviations (for range and bearing angle) and these standard deviations varies (Equations (18) and (19)) according to Signal-to-Noise Ratio (SNR), which is a function (Equation (9)) of range (distance from the target to the radar).

The research reported herein does not consider the existence of more than one target and also, the simulations consider that the radars (either TX or RX) are looking at the correct region of the space. It is considered that a proper Resource Management algorithm would be responsible for pointing the radars to the right direction at the right time given the right information from the tracking algorithm is received. Also, due to the fact that there is only one target and no clutter is considered, the measurements are assumed to be from the only existing target.

Another important thing to be mentioned is that all the measurements are schedule to be performed in fixed regular intervals.

It should also be reported that the transmission of data between nodes (radars), either for synchronization or for sending measurements/tracks is considered to be done without delays and that the processing node has all the information it needs to process the tracking or fusion algorithms.

## 3 Bistatic / Multistatic Radar

A bistatic radar according to IEEE definition [13] is “a radar using antennas for transmission and reception at sufficiently different locations that the angles or ranges to the target are significantly different” (see Figure 2). Similarly, a multistatic radar is “a radar system having two or more transmitting or receiving antennas with all antennas separated by large distances when compared to the antenna sizes” (see Figure 3). Bistatic and Multistatic radars have many advantages, especially that the receivers are passive, thus potentially undetectable (unless, for example, in the case where the bi/multistatic system comprises monostatic radars, as seen in Figure 6). Another interesting advantage is that it is easier to detect stealth targets using bi/multistatic radars because although their RCS is small to monostatic radars, it is unlikely to be small to bi/multistatic radars (see item 3.3.4). However, despite the advantages, there are some disadvantages such as the complexity of the geometry and the need to synchronize the nodes (transmitters and receivers). Below there is an extended list of advantages and disadvantages of these kind of radars.

### 3.1 Advantages

The separation of transmitter and receiver(s) in a bistatic or multistatic radar makes it difficult for an ARM to recognize the receiver since the receivers are passive and thus covered and less vulnerable to jamming.

It is expected that stealth targets are easier to detect because these targets scatters the signal to others directions instead of back to the transmitter. This kind of

configuration is highly dependent on its geometry (see Figure 12 and, for more details, item 3.3.1), so it is important to know the location of the transmitter/receiver and whether they are moving or are stationary. Some other advantages are:

- a) Graceful degradation in performance if one or more sites (transmitter or receiver) are lost
- b) Enhanced immunity to jamming. The more complex the system with multiple transmitters and receivers, the greater the immunity
- c) Potential to be used in a hostile electronic countermeasure environment (in military operations)
- d) More information is available since targets are observed from different perspectives and so, due to those many different transmitter-target-receiver paths it is unlikely that bi/multistatic radars suffer from fading like in monostatic cases. Also, with more available information, it is possible to improve detection and classification of targets.
- e) Sending data through communication channels and processing them is easier now because of the increasing processing power and capacity and reliability of the network communication links.
- f) If used in a passive configuration, the cost can be very low when avoiding the cost of expensive transmitter antennas, unless in cases where it is necessary to use expensive Electronic Array Antennas at the receiving nodes.
- g) Stealth targets whose shape is designed to scatter energy in directions away from the monostatic may be detected by bistatic radars. It is possible because of the enhancement of RCS of the target due to geometrical effects

## 3.2 Disadvantages

When designing bistatic/multistatic systems the disadvantages must be considered in order to evaluate if it is worth developing them for a given application. In some systems it would be interesting to consider a hybrid configuration comprised of monostatic nodes and also bi/multistatic nodes working either actively or even passively using illuminators of opportunity [14], [15]. This kind of configuration

makes the system very flexible because the transmitters can be located anywhere as well the receivers. The disadvantages to be considered are:

- a) Complexity of the geometry
- b) Difficulty to control and synchronize the nodes (nowadays this problem has been overcome because of the existence of high quality and high speed communication links)
- c) Difficulty to establish the exact position of the nodes (transmitters and receivers), especially if they move (can be overcome due to GPS technology)
- d) Higher costs to provide communication between sites
- e) The need of a more complex sensor/resource management system

### 3.3 Bistatic Radar Properties

In [3] and in the Chapter 23 of [16] the bistatic radar properties are described in detail. Items like bistatic geometry, bistatic doppler, bistatic radar equation, and bistatic RCS are summarized in the next sections.

#### 3.3.1 Bistatic Radar geometry

In a bistatic configuration ([3] and [15]), the receiver processor, in order to calculate the distance  $r_2$  (see Figure 12), must know the baseline  $L$  (which is the distance between the transmitter and receiver), the time interval  $\Delta t$  between the reception of the transmitted signal and the target echo, and the angle of receiver antenna  $\theta_R$ . First of all, it is necessary to calculate  $r_1+r_2$ . It is easily achieved by computing  $R_{TT} = (r_1 + r_2) = c \cdot \Delta t + L$ , where  $c$  is the speed of propagation. Now, it is possible to calculate the distance from the target to the receiver,  $r_2$ .

$$r_2 = \frac{R_{TT}^2 - L^2}{2(R_{TT} - L \sin \theta_R)} \quad (1)$$

Figure 12 depicts the scenario and the variables involved.

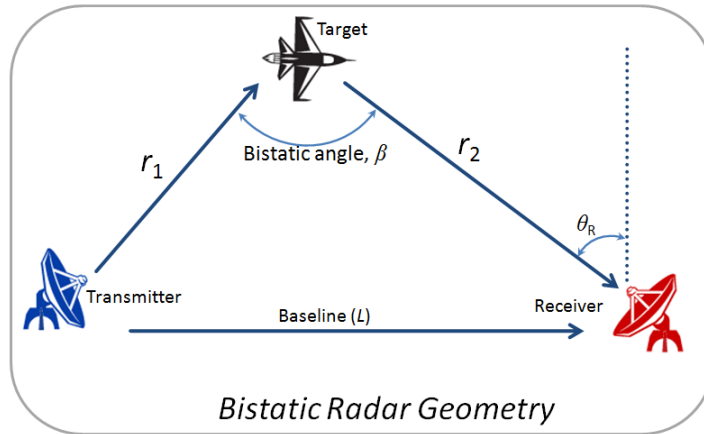


Figure 12 - Bistatic Radar Geometry

Another important concept regarding radar geometry is isorange contour. It means that for any  $R_{TT} = (r_1 + r_2)$ , regardless of the receiver look angle, the target can be in any position of an ellipse with the transmitter and receiver as the two focal points. In Figure 13, the range sum  $R_{TT}$  is the sum of  $r_1$  and  $r_2$  and with a given  $R_{TT}$ , the target can lie in any position of the “Constant range ellipse”.

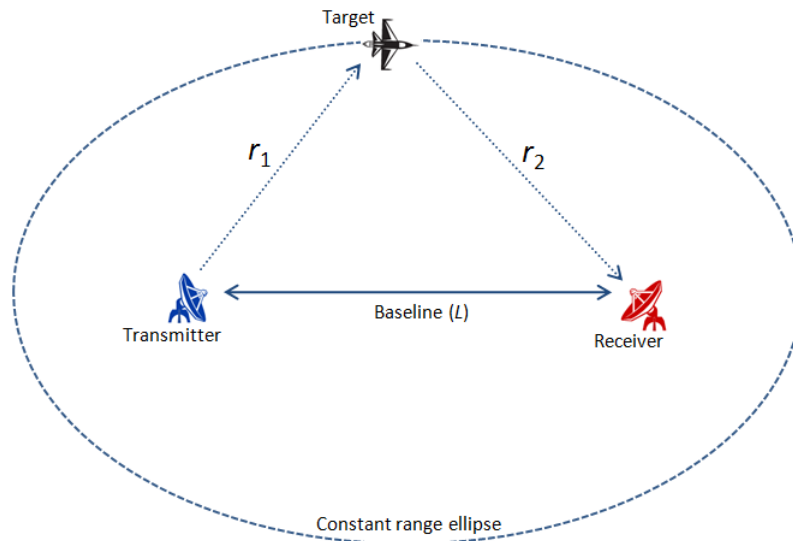


Figure 13 - Constant range ellipse (isorange contour)

### 3.3.2 Bistatic Doppler

The geometry for bistatic doppler, considering the generic case where the target, transmitter and receiver are moving, can be explained using Figure 14 [3] and is very well explained in [3] and Chapter 23 of [16].

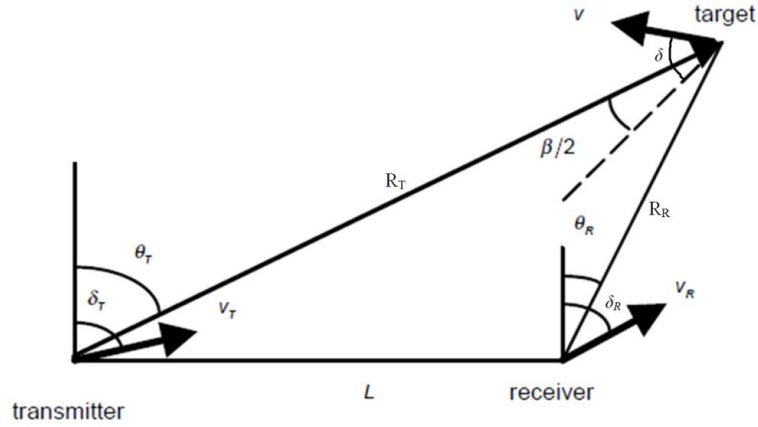


Figure 14 - Bistatic Radar Geometry and the variables involved in the Bistatic Doppler (after [3])

$V$ ,  $V_T$  and  $V_R$  are the velocity magnitude for the target, transmitter and receiver, respectively while  $\delta$ ,  $\delta_T$  and  $\delta_R$  are the aspect angles of  $V$ ,  $V_T$  and  $V_R$ .  $\beta$  is the bistatic angle and is  $\beta = \theta_T - \theta_R$  as shown below with the angles being measured in degrees.

$$(90 - \theta_T) + (90 + \theta_R) + \beta = 180 \quad \therefore \quad (2)$$

$$\beta + \theta_R - \theta_T = 0 \quad \therefore \quad (3)$$

$$\beta = \theta_T - \theta_R \quad (4)$$

Considering the simplest case, where the transmitter and receiver are not moving ( $V_T = V_R = 0$ ), the bistatic doppler at the receiver site is developed:

$$\begin{aligned} f_B &= \frac{1}{\lambda} \left[ \frac{d(R_T + R_R)}{dt} \right] \\ &= \frac{1}{\lambda} \left[ \frac{dR_T}{dt} + \frac{dR_R}{dt} \right] \end{aligned} \quad (5)$$

Where  $R_T$  is the distance between transmitter and target, and  $R_R$  is the distance between target and receiver. Moreover:

$$\frac{dR_T}{dt} = V \cos \left( \delta - \beta/2 \right) \quad (6)$$

And

$$\frac{dR_R}{dt} = V \cos\left(\delta + \beta/2\right) \quad (7)$$

Therefore:

$$f_B = \frac{V}{\lambda} \left[ \cos\left(\delta - \beta/2\right) + \cos\left(\delta + \beta/2\right) \right]$$

$$f_B = \frac{2V}{\lambda} \left[ \cos \delta \cos \beta/2 \right] \quad (8)$$

$f_B$  is the bistatic doppler shift caused by target motion when the transmitter and receiver are stationary.

### 3.3.3 Bistatic Radar equation

Similarly to the monostatic radar equation, one can develop the bistatic radar equation. In the monostatic case, the radar equation is described by:

$$\text{SNR} = \frac{P_S}{P_N} = \frac{P_t G_t G_r \lambda^2 \sigma}{(4\pi)^3 R^4 k T_0 B F_n L} \quad (9)$$

Where:

- $SNR$  is the Signal-to-Noise-Ratio
- $P_S$  is the signal power at the receiver. It is measured in watts (W)
- $P_N$  is the noise power in the receiver as well. The unit is also watt (W)
- $P_t$  is the transmit power at the output of the transmitter. The unit is watt (W)
- $G_t$  is the power gain of the transmit antenna
- $G_r$  is the power gain of the receive antenna. Usually, for monostatic radars, this is the same as the power gain of the transmit antenna.
- $\lambda$  is the radar wavelength and is related to the transmitted frequency. The unit is meter (m)
- $\sigma$  is the target RCS. Its unit is square meter (m<sup>2</sup>)

- $R$  is the range from the radar to the target. The unit is meter (m)
- $k$  is Boltzmann's constant and is equal to  $k = 1.38 \times 10^{-23}$ . The unit is  $W \times s \times K^{-1}$
- $T_0$  is the room temperature in Kelvins (K). Considering  $T_0 = 290$  K, then  $kT_0 \approx 4 \times 10^{-21}$ , with units in  $W \times s$  or  $W/Hz$ .
- $B$  is the receiver bandwidth and its unit is Hz
- $F_n$  is the radar noise figure
- $L$  is a factor (greater than 1) included in order to account for all losses in the signal that can reduce the radar performance

The equation can also be arranged in terms of SNR to find  $R$ :

$$R^4 = \frac{P_t G_t G_r \lambda^2 \sigma}{(4\pi)^3 (\text{SNR}) k T_0 B F_n L} \quad (10)$$

And  $R$  will have its maximum value when SNR is at its minimum, so:

$$R_{\max}^4 = \frac{P_t G_t G_r \lambda^2 \sigma}{(4\pi)^3 (\text{SNR})_{\min} k T_0 B F_n L} \quad (11)$$

In order to derive the bistatic radar range equation, it is necessary to split the term  $R^4$  into two different  $r^2$ , where each  $r^2$  is related to the transmitter-target and target-receiver distance respectively. Furthermore, the radar cross section (RCS)  $\sigma$  becomes the bistatic radar cross section  $\sigma_B$ . Therefore, the bistatic radar equation is:

$$(r_1 r_2)_{\max}^2 = \frac{P_t G_t G_r \lambda^2 \sigma_B}{(4\pi)^3 (\text{SNR})_{\min} k T_0 B F_n L} \quad (12)$$

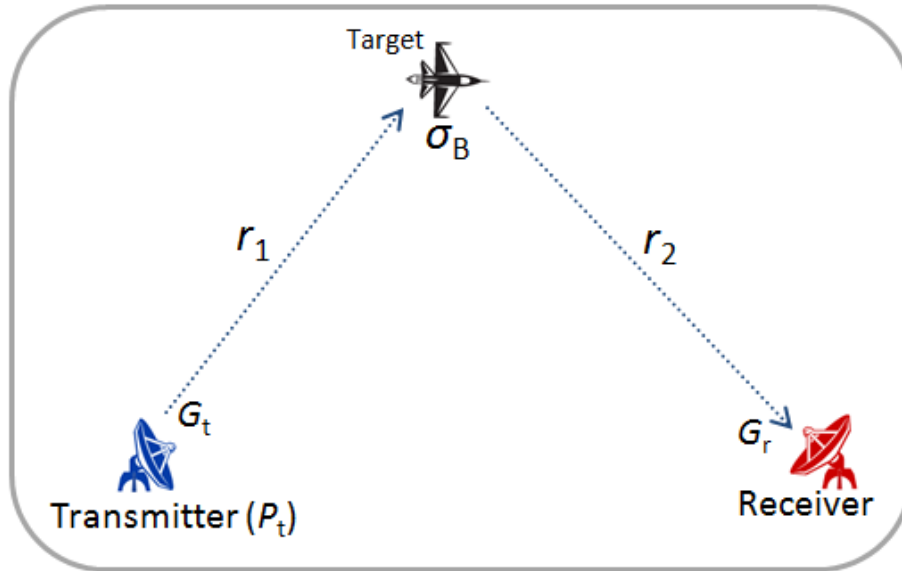


Figure 15 - Radar Range Equation variables

### 3.3.4 Bistatic Radar Cross Section (RCS)

The bistatic RCS of a target,  $\sigma_B$ , similarly to the monostatic case,  $\sigma$ , is a measure that represents how much energy is scattered from the target to the receiver. It means that, the higher the energy scattered, the more detectable the target is. Nevertheless, the similarity does not go further, because bistatic RCS are much more complex as it depends on aspect angle and bistatic angle as well as the shape of the target. There are three regions of bistatic RCS. The regions vary from  $\beta = 0^\circ$  to  $\beta = 180^\circ$  and depend primarily on target's physical characteristics. The three regions are: pseudomonostatic (small  $\beta$ ), bistatic and forward scatter ( $\beta$  near  $180^\circ$ ).

#### 3.3.4.1 Forward Scatter

The bistatic RCS of a target is improved if compared to its monostatic (backscatter) case when the bistatic angle is close to 180 degrees. For a bistatic angle  $\beta=180^\circ$ , the bistatic radar cross section  $\sigma_B$  is of the order of  $4\pi A^2/\lambda^2$  ([17] and [18]), where  $A$  is the silhouette area of the target and  $\lambda$  is the wavelength of the signal and should be small compared to the target dimensions.

As an example, for a target with monostatic RCS of  $3.14\text{m}^2$ , its silhouette area  $A$  is also  $3.14\text{m}^2$  and for a  $\lambda = 0.1\text{m}$  (3 GHz),  $\sigma_B = 3944\text{m}^2$  which corresponds to an enhancement of 31 dB. The angular width (in radians) of the forward scatter is given

by  $\theta_B = \lambda/d$ , where  $d$  is the linear dimension of the target in the appropriate plane [18]. So, for the same example above, if  $d = 20\text{m}$ , then  $\theta_B = 0.005$  radians which corresponds to 0.29 degrees.

Since the forward scatter returned from a target does not depend on its composition, bistatic radars can detect targets that were specially designed to reduce its monostatic RCS (for example, stealth aircrafts). On the other hand, if the target lies on or close the forward scatter region (or the transmitter-receiver baseline), it is not possible to extract either range or Doppler information.

For a small aircraft of  $A = 10\text{m}^2$  and  $d = 10\text{m}$ , the Figure 16 [18] depicts what happens with  $\sigma_B$  and  $\theta_B$  as the frequency of the transmitter increases.

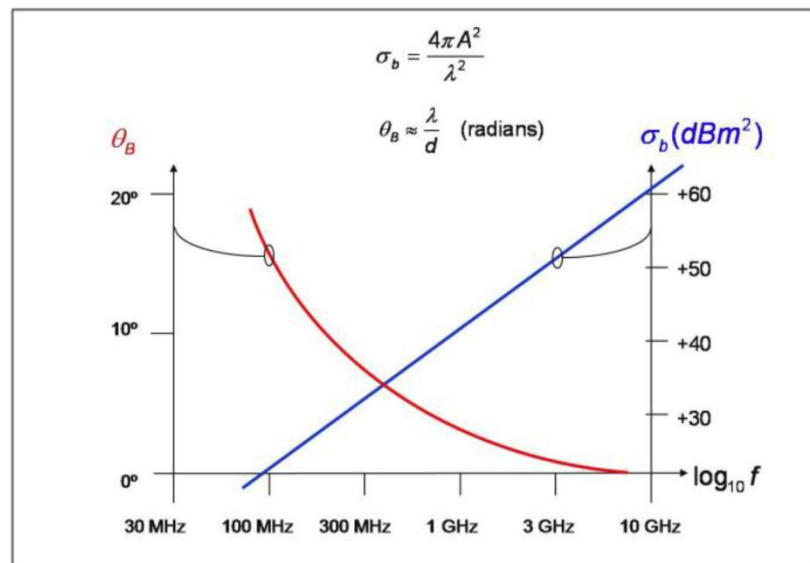


Figure 16 – (after [18])  $\sigma_B$  and  $\theta_B$  as functions of frequency (or wavelength  $\lambda$ )

It shows that, although the forward scatter RCS  $\sigma_B$  is highly improved with frequency increases, the angular width  $\theta_B$  is dramatically reduced. It is up to the designer of the system, according to the application needs, to find the best compromise between  $\sigma_B$  and  $\theta_B$ .

### 3.4 Multistatic Radar

Considering that a Multistatic Radar is “A radar system having two or more transmitting or receiving antennas with all antennas separated by large distances when compared to the antenna sizes” [13], it is a generic form of a radar network

where each pair transmitter-receiver is a bistatic radar and thus, multiple bistatic radars working and co-operating together in a unique system make a multistatic radar system. Many possible configurations for different applications can be implemented and depending on them, the complexity of the system can increase considerably. It might be important to note that the term “multistatic radar” has some similar terms used in the literature, such as multisite radar, radar networks, distributed radars, netted radars, just to mention a few of them. They are used with the same meaning but sometimes they refer to a specific type of configuration. The main idea is still that there are many sensors working co-operatively.

Table 1 [19] depicts just a few examples of configurations and their complexity according to variables such as location, operation mode and so on.

Table 1 - Different levels of complexity according to some Multistatic configuration variables (after [19])

	<b>Case 1</b>	<b>Case 2</b>	<b>Case 3</b>	<b>Case 4</b>	<b>Case 5</b>	<b>Case 6</b>
<b>Location</b>	Fixed	Fixed	Fixed	Fixed	Fixed and moving platforms	Nodes on moving platforms
<b>Data level</b>	Tracks	Tracks	Detections	Detections	Raw	Raw
<b>Coherency</b>	Incoherent	Incoherent	Incoherent	Coherent	Coherent	Coherent
<b>Operation mode</b>	N Tx, N Rx monostatic	1 Tx, N Rx multi-static	1 Tx, N Rx multi-static	M Tx, 1 Rx multi-static	M Tx, 1 Rx multi-static	M Tx, N Rx multi-static
<b>Distribution</b>	De-centralised	De-centralised	Semi De-centralised	Centralised	Centralised	Centralised
<b>Assessment</b>	Straight-forward	Multiple bistatics	Challenging	Complex	Very complex	Extremely complex

The idea of Table 1 is to illustrate what happens on the level of complexity (“Assessment” row) when some of the characteristics vary from a simple configuration to a more difficult to implement one. For example, if the locations of the platforms (nodes) are fixed (see “Location” row of Table 1), systems tend to be simpler than when platforms move. On the other hand, the system tend to be more complex when the data level vary from track level to detections and ultimately to raw

level. The last row of Table 1 shows for those 6 cases (out of a much more variety of possible combinations of characteristics) how complex is to implement each case.

In multistatic systems (or in any network radar system), differently from monostatic systems, the nodes must communicate with each other and maybe it is one of the most important differences between monostatic and multistatic/multiradar systems. Communication links might be necessary to synchronize the nodes, and they are also necessary to exchange information collected among them (e.g., measurement data) or to send the information to a central node. The synchronization of transmit and receive nodes plays an important role in the performance of the network because both kind of nodes need to be looking at the same areas or volume of interest in order to acquire or track a target. One possible solution to minimize the problem is to use omni-directional antennas (in the transmit nodes) and/or use electronically steered antennas (either in transmit or receive nodes).

## 4 Tracking algorithms

The purpose of a tracking algorithm is to track moving targets using a sequence of sensor(s) measurements (or observations). By using the measurements, it is possible to update the last estimate of a target and also estimate the next state of it (considering that the track had been formed and confirmed). The problem of tracking gets more complicated depending on the number of targets and sensors involved and also on the geometry of the system.

In [20], the author presents maybe the most famous tracking algorithm since 1960, the Kalman Filter (KF). It is an optimal recursive data processing algorithm which uses all the data available to it. Those data, also called measurements, are combined in order to estimate variables of interest. It uses the knowledge of the system and measurement device dynamics. Also it is important to use the statistical description of the system noises, measurements errors and uncertainties in the dynamic models. Finally, it uses any information provided about the initial conditions of the variables of interest. The Kalman Filter is very popular because it is convenient for online real-time processing, it is not difficult to implement and good results can be achieved in practice. It has been used so far in applications such as, tracking targets like missiles and aircraft using radars or robot localization using sensors.

### 4.1 Simple Example

For example, imagine a simple situation where an aircraft is moving horizontally in a straight line with constant velocity  $v$ . The idea is to estimate the aircraft (target)

position  $x$  and velocity  $v$ . However, the measurements performed by a sensor (e.g. monostatic radar) are corrupted by white noise, with zero mean and standard deviation  $\sigma_z$ . And also, the measurements can only be done in specific moments (discrete time). Using this very simple dynamics, the following equations model it.

$$X_{n+1} = \phi X_n = \begin{bmatrix} 1 & \Delta t \\ 0 & 1 \end{bmatrix} \begin{bmatrix} x_n \\ v_n \end{bmatrix} = \begin{bmatrix} x_n + v_n \Delta t \\ v_n \end{bmatrix} \quad (13)$$

$$Z_n = x_n + u \quad (14)$$

where the matrix  $X$  is the state of the aircraft (position, velocity),  $Z_n$  is the measurement of the position plus noise  $u$ .

After that, with measurement  $Z_n$ , and previous prediction of state  $\hat{X}_n^-$ , it is possible to update the estimate position  $\hat{X}_n$ .

$$\hat{X}_n = f(\hat{X}_n^-, Z_n) \quad (15)$$

And now, with  $\hat{X}_n$ , the state prediction  $\hat{X}_{n+1}^-$  can be updated.

$$\hat{X}_{n+1}^- = g(\hat{X}_n) \quad (16)$$

Figure 17 depicts this recursive algorithm:

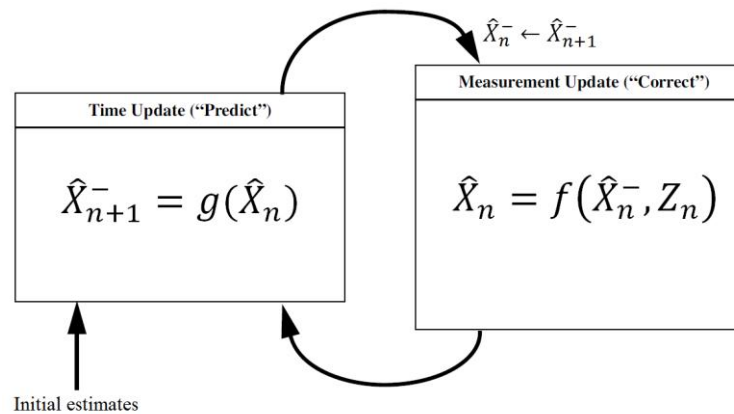


Figure 17 - Tracking recursive algorithm

In section 6.3, more details about tracking algorithms used in this thesis are presented.

## 4.2 Multistatic Tracking of a Target

As in a conventional monostatic radar tracking system, multistatic radar tracking systems might also have the objective to detect and track targets as they pass through the radar system. In this case, there are measurements being done by all the radars (receivers) of the system. A receiver performs a measurement based on information sent via the synchronization links, such as a transmitter's pointing direction and frequency being used. The main idea here is that the whole system must work in a co-ordinated and intelligent way in order to achieve the best results when detecting and tracking targets making use of all the resources available in an optimal way.

Two of the most important aspects of this problem are to:

- a) Manage the resources of the system making the transmitters and receivers work appropriately in order to acquire and track targets; and
- b) Track a target using, if necessary, measurements from all the receivers, making the best use of different perspectives.

In this present work, item "a" is considered to be performed by some software module dealing with resource management. Therefore, it can be considered that the multistatic radar system can make use of electronically-steered antennas in the receiver nodes and, if possible, in the transmitter nodes. It can smartly detect and track targets by scheduling instantaneously appropriate transmit and receive beams directions, setting the transmitter waveforms and if necessary, exploiting forward scatter (which gives high possibility of detection but no range and Doppler information).

The management of a multistatic radar system in order to detect and track targets is very similar to what happens in a Multi-Function Radar (MFR) ([21] and [22]), also known as, Phased Array Radar, where its resource management module decides if a target needs constant updating or not, considering the target's level of threat or the use of less energy. Nevertheless, for the purposes of this thesis, the updating rate of a target is considered to be fixed as if it were using a rotating antenna instead.

The second important aspect (item “b”) is related to the fusion algorithm implemented in this thesis which uses information from all receivers and with a very simple procedure, decides which information is going to be used and how it is going to be used (section 6.3).

## 5 Review of Previous Work

In the next sections, some of the important work that have been done so far and that are related to the main topic of this research are listed. The generic topic of Multistatic radar is presented in 5.1. Then, Multistatic tracking, which is directly related to this research is covered in 5.2. Then, finally in 5.3, the topic of resource management is reported as it has important connections with some future work suggested later in the thesis.

### 5.1 Multistatic Radar

As previously mentioned at the beginning of Chapter 3, IEEE defines bistatic and multistatic radar [13]. There are also some other terminology common used in the literature such as: netted radar, distributed radar, multisite radar just to mention some of them.

In [18], the author presents a review of work on multistatic, Multiple Input Multiple Output (MIMO) and networked radar. Here, some good reasons for the growing interest in this area are listed. Also the very important concept of “Forward Scatter” geometry is explained and it is shown how the detection of a target is improved although it is difficult to measure the range and/or velocity of the target from the sensor using this mechanism. Furthermore, the paper discusses some ideas ([21], [22] and [23]) that are applied to monostatic phased array radars (and other types of radar systems) and that could also be utilized in a radar network, such as intelligence and adaptability of the sensors comprising the system.

Combined position-finding accuracies of netted monostatic and netted bistatic radars are calculated in [24]. Different radar configurations are compared: single monostatic, single bistatic, netted monostatic and netted bistatic. The comparison is performed in terms of measurement error. The paper does not show many configurations but it is an important contribution given by the authors in 1983. It is shown that the results essentially depend whether the range dependence of the measurement errors are considered or not.

Monostatic radar systems have been stretched to their limits in terms of sensitivity and information by new radar applications. [25] shows that these limitations can be overcome if networks of smaller radar systems are used. For instance, networks of radar sensors can counter stealth technology at the same time that additional information for improved target classification is provided. In an overall comparison, a more efficient reception of radar scatter can be achieved by using multiple independent sensors as they are able to deliver a view of many target perspectives. The relative merits of non-coherent and coherent networks are introduced and the balance between increased performance, complexity, and cost is discussed.

The use of Bistatic and/or Multistatic radars, meaning that transmitters and receivers are not co-located, results in some great advantages over the traditional monostatic radars. Some advantages have already been mentioned in 3.1 but there are some others: a) improved tracking, location accuracy and target classification as the target is observed from different perspectives; b) spatial distribution of the nodes of the network enables the area to be tailored according to the specific application of interest; c) increased survivability and reliability is achieved because of the option of having ‘silent’ or passive operation of the receivers. These receivers can improve the location accuracy of possible jammers by fusing the information from the network nodes;

Those advantages are explored in [26] in the context of homeland security activities.

Despite the advantages, the interest on this subject has been varying periodically with peaks of interest each 15-20 years [3][27] and at the moment, the “3rd resurgence” is due.

There are some disadvantages that can explain this cyclic interest which have been mentioned in 3.2. [14] and [15], though, presents a review of bistatic radar systems with particular emphasis on Passive Coherent Location (PCL) techniques, which means using broadcast and communications signals as “illuminators of opportunity”. Additionally, [15] also explains why practical bistatic radar systems may now be developed and used and [28] presents and discusses recent developments that show that bistatic systems are becoming practical for many applications. [28] also discusses some current issues concerning, for example, passive bistatic radars.

An experimental netted radar system with four nodes was designed and developed using “Commercial Off The Shelf” (COTS) components wherever possible in order to reduce costs [29]. Some simulations were performed using that experimental system and the results were presented showing the viability of COTS components to reduce costs. [29] and [30] reports on the initial characterisation and calibration of such a low cost multistatic radar system. It is a practical contribution to the area and some improvements are being planned, such as the use of wireless synchronization and improved frequency agility.

An important aspect that has to be evaluated in netted radars is the ambiguity function. [31], [32] and [33] conclude that multistatic ambiguity function and sensitivity are dependent on the system and target geometries. [32] shows that an experimental system that was being developed at UCL ([29] and [30]) could help in determining achievable performance under realistic situations and in providing a tool for multistatic measurements.

Furthermore, [34] presents the results of processing real data acquired with the University College London (UCL) radar network ([29] and [30]) to localize a walking person using two different incoherent approaches: centralized and decentralized. Then, the results are compared with two coherent approaches. The paper does not investigate targets with much higher velocities.

In [35], the authors present an algorithm to fuse data from sensors. In this case, they are three dissimilar sensors: High Resolution Radar (HRR), Low Resolution Radar (LRR) and Electronic Support Measures (ESM). With this algorithm it was possible to jointly form a track and assign an identity flag to a target on the basis of

measurements provided by the sensors. This can be an advantage especially if the result can be displayed in one screen instead of showing it in each sensor screen.

Knowledge-Based (KB) radar signal and data processing can also be very useful in radar systems used in military operations due to the always evolving and increasing threats from military targets with small RCS, large number of targets in a scenario and so on. [36] explains how KB techniques can significantly improve performance of radar systems aiding human operators in carrying out their tasks. For example, KB techniques may have several applications in bistatic and multistatic radar systems as well as in the resource allocation of a MFR.

In [37], a sub-optimum algorithm is applied to a radar network with a double threshold for detection and it is shown that detection performance can be maintained in presence of jamming without any of the countermeasures more commonly adopted.

A multistatic radar system composed of one transmitter, a number of receivers and a central processing station is presented in [38]. Its main objective is to increase the detection probability of targets with low monostatic RCS, taking advantage of the Bistatic RCS and the low operating frequency (low UHF band). Each receiver, that makes a bistatic pair with the only transmitter, measures the targets bistatic range and range-rate information, while estimating their azimuth angle. The measurements are processed locally and after that, the resulting data are sent to a central processing station in order to perform 3D multiple target tracking. In this work, the only function of the transmitter is to emit a Frequency Modulated Continuous Wave (FMCW) signal and an appropriate synchronization beacon, while the receiver performs a totally passive function. The use of a low cost radar sensor which performs a simple operation is the main design objective, while the main system functionality is performed by the central processing station. The main objective is accomplished using relatively recent computer power.

In [39], the coverage performance of a radar network is investigated when four different forms of processing concepts are applied. The main contribution of the paper is to show that the form of the processing concept used and the number of the nodes can affect coverage performance.

Another very recent contribution is presented in [40] where the main approach is to evaluate network topologies of low power radars that improve the coverage of the lower troposphere (3 km) in the context of weather sensing. Yet in the context of weather sensing and forecasting, [41], [42], [43], [44], [45], [46], [47] and [48] show the research that has been done so far involving the Engineering Research Centre for Collaborative Adaptive Sensing of the Atmosphere (CASA) [49] which utilizes a set of radar nodes, comprised of small, low power antennas, to adaptively sense the weather including the lower part of the troposphere. Particularly, [48] is a very recent paper that reports an approach where networks of small radars can be used to support the interception of low-flying aircrafts at the same time that it can be used to detect weather hazards. This is a very interesting approach as supposedly the radar network does not need to spend much time on detecting weather hazards and the remaining idle time can be used for border security missions. However, it seems that the nodes work as monostatic radars and not bistatically or multistatically.

## 5.2 Multistatic Tracking

It is not possible to talk about tracking without mentioning [20], which is likely to be the most famous tracking algorithm since 1960. From the idea of Rudolf Emil Kalman, many other derivations of the filter emerged to tackle variations of the tracking problem (e.g., [9], [10], [11]). [50] shows in a very simple language several tracking algorithms that have been used so far.

The difficulties to implement a multiradar tracker comparing its results to the ones from a system that form monostatic radar tracks and combine them to produce a single track is reported in [51]. It is a paper that discusses three different approaches on how to use information from the radars of a multiradar system in order to track a target.

[52] describes and compares many Kalman Filter algorithms that can be used for state estimation with a multiple sensor system. Three approaches are investigated in terms of computational resources used. The idea of the work seems to be adequate in a multistatic radar scenario as well.

A multiradar tracking that utilizes position and radial velocity measurements is discussed in [6]. Although this paper is about a multiradar (many monostatic radars) and not a multistatic radar (monostatic and bistatic radars as well), it shows, through simulations, that having radial velocities measured from different perspectives improve significantly the tracking of a target compared to when radial velocity measurements are not used.

The tracking function of multistatic radar systems is analysed in [7] and a general architecture for data processing is proposed. Data compression and measurement selection methods are discussed which improve the performance of tracking filters. A tracking performance analysis based on a computer simulation is performed for a two-dimensional multistatic system with one transmitter and two receivers. A comparison between multistatic tracking systems and netted monostatic systems shows that both types of system provide similar tracking accuracy.

[8] presents a unified view of the tracking algorithms that were available for multistatic radars systems and considers the problem of deriving and evaluating the performance of those algorithms able to process data from bistatic or multistatic radar systems. In a system like that, it is mandatory that information about the nodes (transmitters and receivers) be available in order to know when and how to steer the transmitters and receivers. Also, some issues about the data flow are mentioned, considering a centralized and a distributed system. Some of the issues do not exist anymore though, as the technology in the last 25 years has evolved and has been helping to deal with them.

A complete decentralized version of the Kalman Filter is presented in [9] and [10]. Once more, these papers do not deal with a multistatic radar configuration but is able to show the importance of having, in the context of multi sensors, a decentralized filter that does not require a central processing software or centralised communications medium at all. Since there is not a node that performs a centralized computation of the filter, the system as a whole is highly resilient to loss of one or more sensing nodes. This idea of quick recovering from a difficult condition is very suitable in military applications or in systems where a failure in a node can happen without affecting so much the behaviour of them. This kind of characteristic can be

called “graceful” degradation. Also, due to the decentralized architecture of the algorithm, it is easier to add new nodes to the system making it scalable.

Despite [53] presents a fusion filter that has been designed for the tracking of airborne targets using many different sensor types at different sites, it is not a paper that deals with a multistatic radar configuration. Nonetheless, the idea seems to be appropriate in a multistatic scenario as well. Moreover, the paper assesses the performance of the algorithm in four different scenarios, although the scenarios are comprised of only one or two sensors.

The problem of tracking multiple targets in a net of passive 2D or 3D radars is presented in [54]. In this context, the authors suggest a new method to overcome problems with false detections.

[55] is an interesting paper that looks at the subject of tracking performance when comparing scenarios with one, two or three sensors. It shows for each scenario what is the accuracy in each location of the surveillance volume and also makes considerations about data fusion. It seems that information about the characteristics of the radar and waveform are missing or not very clear, although it reports the detection range and measurement rate of each sensor in each example. The paper reports an analysis method to describe tracking performance of a multistatic radar and also shows how the analysis can support decisions when comparing different system configurations. Also, the method enables the quantification of data fusion advantages.

The subject “target tracking” in a multisensor environment is presented in [56]. It presents an overview of common filtering techniques that are used for moving targets, such as Kalman Filter and its variations as well as Interacting Multiple Model (IMM) and some variations. The paper also discusses the computational demand of those algorithms and suggests some solutions to minimize such demand. The main contribution of this work is that it summarizes many aspects, characteristics and issues related to multisensor target tracking such as centralized vs decentralized tracking, sensor management, computational complexity and real time implementation.

In [57], examples of bi-/multistatic radar systems are discussed as well as their geometry dependencies with respect to measurements and their input to a tracking and fusion system. Given the configuration of the bi-/multistatic radar, four different simulated flight paths were used to evaluate three different data fusion algorithms.

One contribution that addresses multistatic tracking in the context of sonar is [58]. In addition, this paper provides a simulation-based study using centralized and decentralized tracking algorithms and identifies a trade-off between both approaches when fading detection performance data is used: the former achieves better localization accuracy, whilst the latter achieves improved Receiver Operating Characteristic (ROC) curve performance.

[59], [60], [61] and [62] are all papers related to the Multistatic Tracking Working Group (MSTWG) and several simulated multistatic sonar scenario data sets are developed and made available by this group for use in tracker evaluation by the group's participants. A common set of performance metrics is also agreed, to enable tracker algorithm comparison and evaluation. MSTWG was formed in 2005 by an international group of researchers interested in developing and improving tracking capabilities when applied to multistatic sonar and radar problems. [59] presents a brief description of the datasets and trackers developed and/or utilized by MSTWG as well as a detailed discussion of a proposed set of tracker performance metrics. Furthermore, the paper reports a number of issues associated with performance assessment for target tracking. [60] discusses an implementation of a general Bayesian tracking method and also discusses and compares the results when the algorithm is utilized with the datasets provided by MSTWG. In [61], the authors report consolidated results comparing tracking algorithms performance using the common data sets and metrics. The results are important to help in the understanding the different tracking algorithms according to the scenario and/or metric. Finally, [62] presents a tracker that overcome problems with high levels of false alarm clutter on all sonar nodes of a multistatic active sonar and presents performance results of the tracking algorithm using the simulated data sets from MSTWG.

In [12], a track fusion procedure has been implemented in a multiradar configuration in the context of homeland security and in particular on border control issues. This procedure may involve a large number of heterogeneous sensors, command and

control centres, platforms and communication networks. The sensors can be ground or ship based, 1D, 2D or 3D. The paper deals with the problem of correlation and fusion of track data related to ground and ship based radar sensors (2D and 3D) directly in the radar sites. This is another paper that deals with tracking/fusion where many (eventually different) sensors are utilized. Although the test bed presented in this paper uses monostatic radars, it seems that the use of bistatic radars would not be a problem for the algorithm.

In a recent work [11], four different filtering algorithms (Sequential Iterated Extended Kalman Filter (SI-EKF), Iterated Unscented Kalman Filter (I-UKF), Interactive Multiple Model algorithm combined with Sequential Iterated Extended Kalman Filter (IMM-SI-EKF), and Interactive Multiple Model algorithm combined with Iterated Unscented Kalman Filter (IMM-I-UKF)) are used and compared in the context of tracking a manoeuvring target passing by a given multistatic radar configuration that comprises a number of bistatic radars measuring bistatic range and bistatic range-rate. A Monte Carlo simulation is performed to demonstrate the track accuracy performance and computational complexity of each algorithm for manoeuvring targets.

In [63], from the same authors of [11], the filtering algorithm IMM-I-UKF (which was the one that performed best in [11]) is used for target tracking in a multistatic environment. The performance of the tracker is evaluated for multiple scenarios including multiple, closely-spaced, manoeuvring, with crossing track patterns targets, in dense clutter environment with non-unity Probability of Detection (PD). The tracker performed very well in all cases and also could be implemented with computer power available in 2008. Additionally, the proposed algorithm proved to be superior to some other very known and used methods. A Monte Carlo simulation is performed to demonstrate the track accuracy, probability of correct association, robustness and computational complexity for the different scenarios.

Another paper that reports the results of a tracking algorithm to track targets crossing a multistatic radar is [64]. Once more, just one scenario of multistatic radar is used to assess the algorithm. Nonetheless, the tracker is tested on a 3D multitarget scenario that includes crossing targets and targets moving in formation.

## 5.3 Resource Management

The management of radar resources in a Multi Function Radar is perhaps the most important thing to be accomplished in order to deliver the maximum potential that electronic array antennas can provide. Scheduling is an important component of radar resource management due to the correlation between how tasks should be performed into the time limits available. The same concepts of resource management used for Multi Function Radar could be applied when managing the resources of a radar network.

Controlling and managing the resources of a MFR has been the subject of study of many researchers and many papers have been published so far ([22], [65], [66], [67], [68], [69] and [70]). Using similar ideas some papers show that it is possible to overcome the challenges when managing the resources of a radar network using the concept of cognition ([23], [71], [72] and [73]).

As an example, [66] presents the issue of tracking targets using a rotating MFR in comparison with the static MFR systems and also highlights the main benefits that arise from the rotating phased array antenna. In addition to this, it outlines the existing complications in the control of the rotating MFR and presents a scheduling algorithm which deals with the complications in an efficient manner.

10 years later, [70] compares two scheduling algorithms reported in the literature so that differences between their performance could be analysed in both “underload” and “overload” conditions. This could be accomplished through a developed MFR model.

And finally, [73] reports the design and implementation of cognitive tracking radar using the same ideas published by the same author in [71]. It states that a Cognitive Radar would be comprised of 3 basic components: a) “feedback” from the receiver to the transmitter as a “facilitator of intelligence”; b) “learning” from what the radar receives from the environment and c) “information preservation” of radar returns. [71] also mentions two approaches for the cognition on a cognitive radar network: a) distributed and b) centralized. Still in the same subject, [72] develops the idea of

cognitive radar network and presents an architecture that incorporate cognitive capabilities.

## 6 Simulations

The use of computer simulations is essential for this research because of the expensive infrastructure that would be necessary to perform real experiments involving aircrafts and real navigation radars to collect the data. Computer simulations are useful when there is no budget to afford real experiments but it is also very useful when time is an important matter. Furthermore, the use of simulations makes it simpler to change parameters and observe the results bringing extra information about the behaviour of the system. However, it is important to mention that it is not an easy task (maybe impossible) to model and simulate a real scenario and thus, computer simulations might not represent exactly what would happen if real experiments were performed. For the purpose of this research simulations are used to analyse the results when a radar system (comprised of 1 or more radars) tracks a target that crosses its coverage area using a simple tracking algorithm and a simple fusion algorithm (if in a multistatic scenario).

### 6.1 Setting up the Environment

In order to perform simulations of a target crossing different kind of radar geometries (for example, one monostatic radar, a network of monostatic radars, a bistatic radar or a multistatic radar), and compare the results when looking at measurements, filtered measurements (using filters such as  $g-h$  or  $g-h-k$  [50] or Kalman Filter), fusion of measurements and filtered fused measurements, some computational resources are used.

The hardware used for the simulations is a notebook with Intel Core i7 processor and 8GB RAM memory and 1GB RAM Dedicated Video Memory. Also, it has a hard disk of 750 GB, even though, the simulations would work with hard disks with much less storage space (less than 100 GB, including the operating system). The operating system is the Windows 7 Home 64 bits. Finally, the software used for the simulation is MATLAB 7.10.0.499 (R2010a) 64 bits. In all simulations, total RAM usage is never more than 6GB RAM.

The MATLAB environment is set to save all the simulation scripts in only one folder in order to make it easy to use them in any other computer with MATLAB installed.

## 6.2 Methodology

All the simulations are performed using MATLAB scripts that make use of classes written specifically for the purposes of this thesis. All the MATLAB source code are available in Appendix A (one CD-ROM) of this thesis.

Also, the simulations consider a two-dimensional space in order to make it easier to present, understand and analyse the results.

At the beginning, one script (*script01.m* file) and one simple class named “Radar” (*Radar.m* file) are developed in order to compare true trajectories against measurements performed by a monostatic radar. The simulated measurements take into account that the range and angle measurements standard deviation are fixed and do not change according to range. Using Class “Radar”, it was possible to set different standard deviations for range and angle measurements in order to observe the effects of those changes. Since the objective of this research is related to tracking and not resource management, the simulations consider that transmitters and/or receivers are pointing and looking at the same region where the target is located. The figures below show 2 examples of measurements performed by a radar using different range and/or azimuth standard deviations. Figure 18 shows 3 horizontal target trajectories (red line) flying from left to right with velocities of 100, 200 and 300 m/s and 3 vertical target trajectories (blue line) flying from top to bottom with the same velocities. The green lines are the measurements using a radar with 150 m range standard deviation and with 30 mrad azimuth standard deviation. The radar

(green circle) is located at (100,0) km and  $x$  and  $y$  axis are in meters. In all figures related to position or position errors, the unit used is meter unless mentioned otherwise.

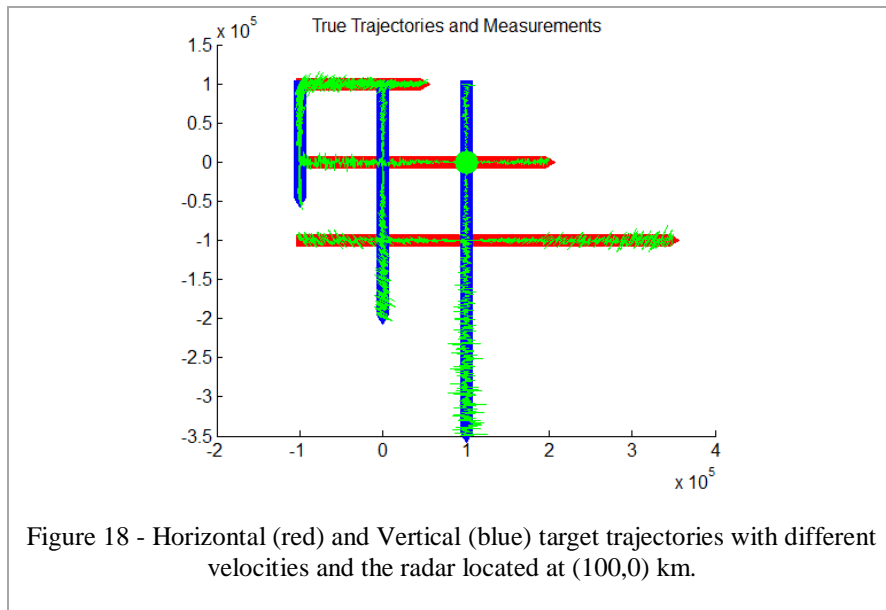


Figure 19 and Figure 20 depict the errors in  $x$ -axis and  $y$ -axis when comparing true position against measurements of the top horizontal trajectory (Figure 18) flying from (-100,100) km to (50,100) km with  $x$ -velocity of +100m/s during 1500 seconds.

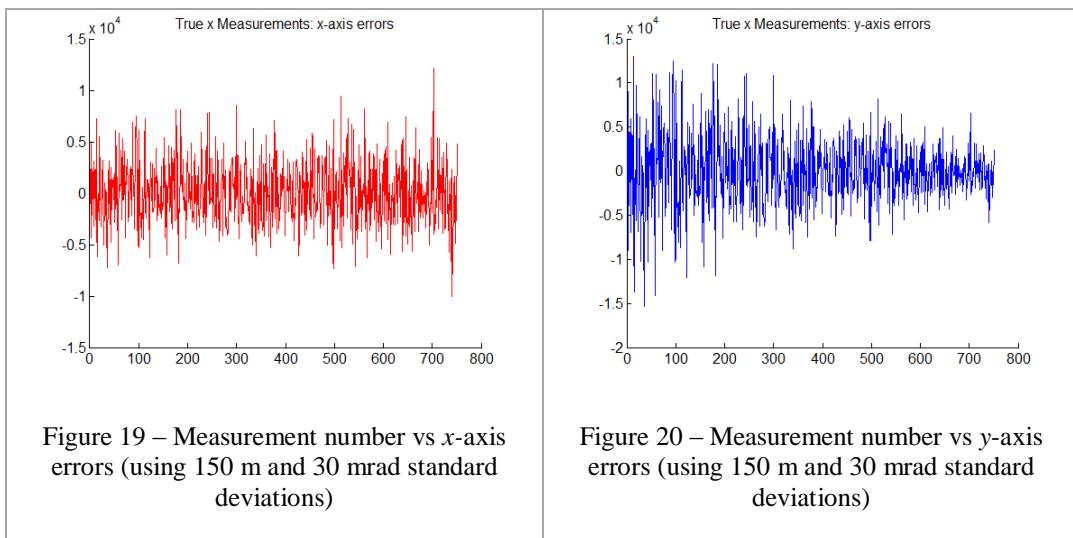
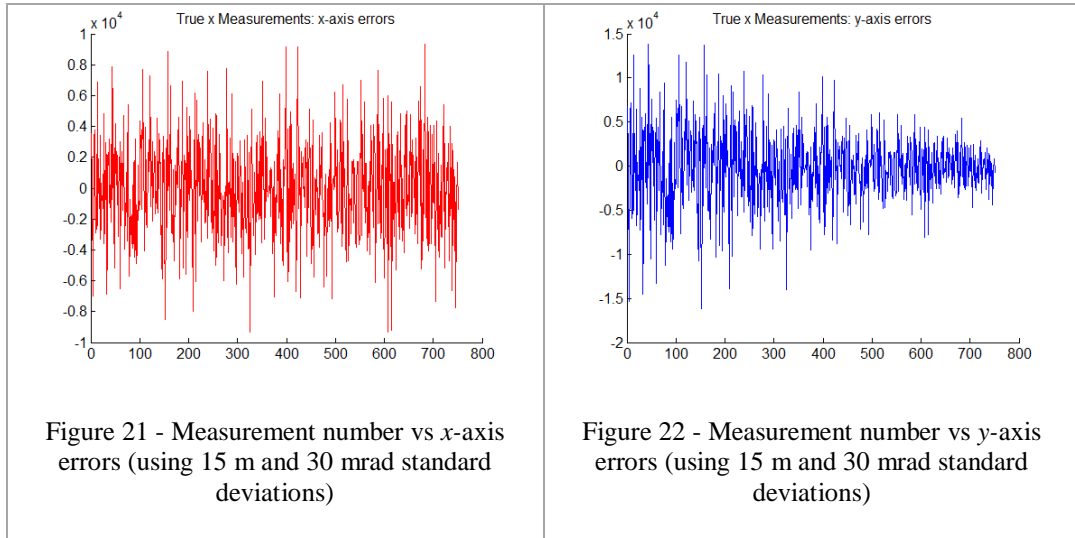
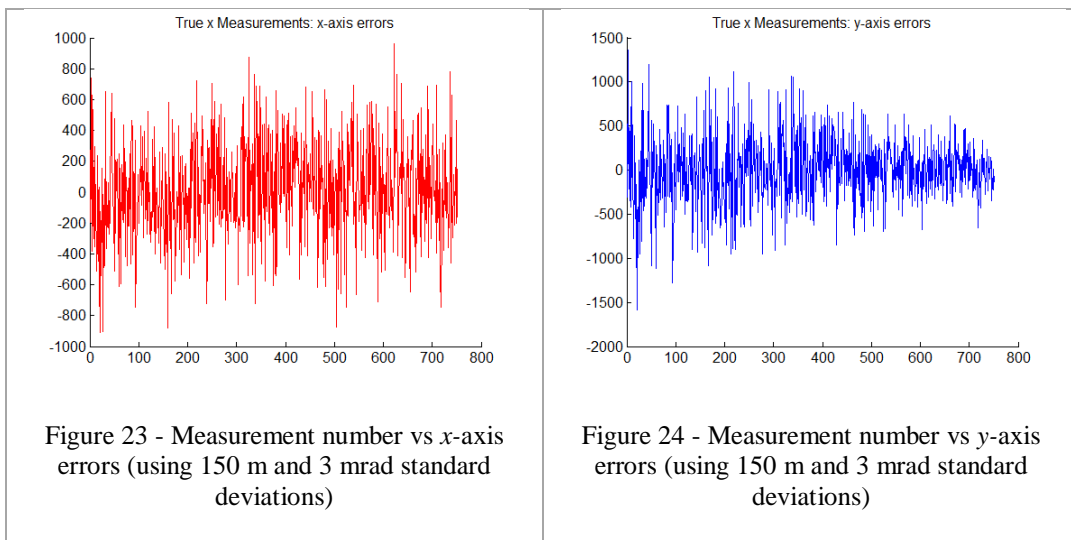


Figure 21 and Figure 22 present the same scenario but with a range standard deviation of 15 meters. In this case, it is possible to see that almost no improvement is achieved with the decreasing of range standard deviation (10 times less).



The following pictures (Figure 23 and Figure 24) depict a scenario where the range standard deviation is 150 m but the azimuth standard deviation is 3 mrad (10 times less than the previous simulations).



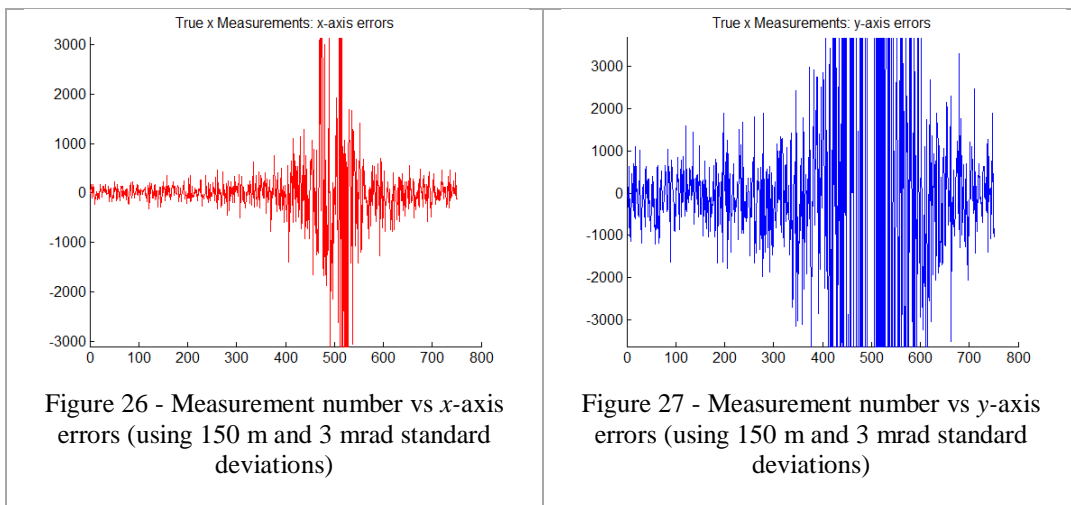
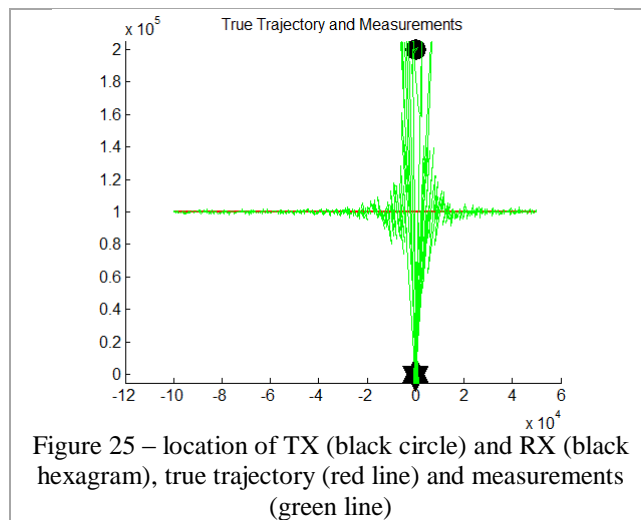
In this case, the improvement in azimuth standard deviation (10 times less) brings a great reduction in the measurement errors. The simulations above do not consider RCS or operation frequency. They are just showing how different standard deviations, which are considered to be constant regardless of range, can affect the final measurements.

The next script (*script03.m* file) also use class “Radar”, but now, 2 objects of class “Radar” are created in the script (one transmitter and one receiver), in order to simulate measurements performed by a bistatic radar. Using this script, it is possible

to simulate different geometries of bistatic radars, for example, a target crossing the bistatic line or a target going on a parallel trajectory to the baseline. To compute the range from the receiver ( $r_2$ ) to the target, equation (17) is used:

$$r_2 = \frac{R_{TT}^2 - L^2}{2(R_{TT} - L\sin\theta_R)} \quad (17)$$

An example of a scenario and measurement errors are shown in Figure 25, Figure 26 and Figure 27. The transmitter (black circle) is located at (0,200) km and the receiver (black hexagram) at (0,0) km.



It can be seen in Figure 26 and Figure 27 that when the target approaches the baseline of the bistatic radar, the measurement of the target location is much worse

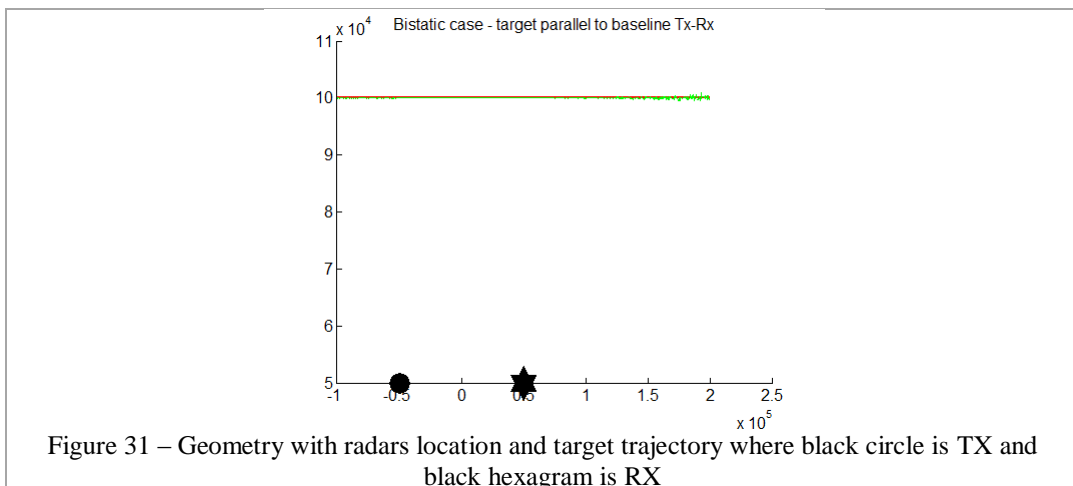
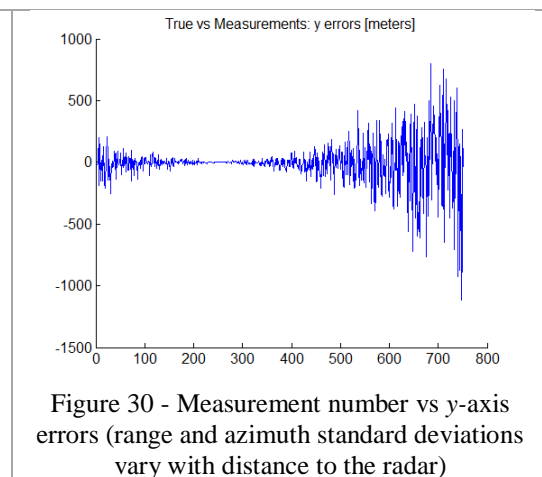
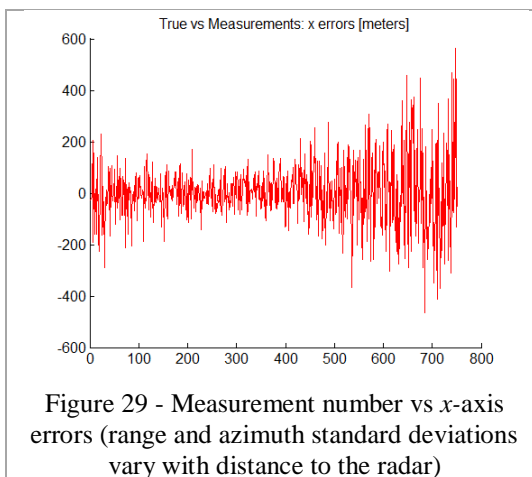
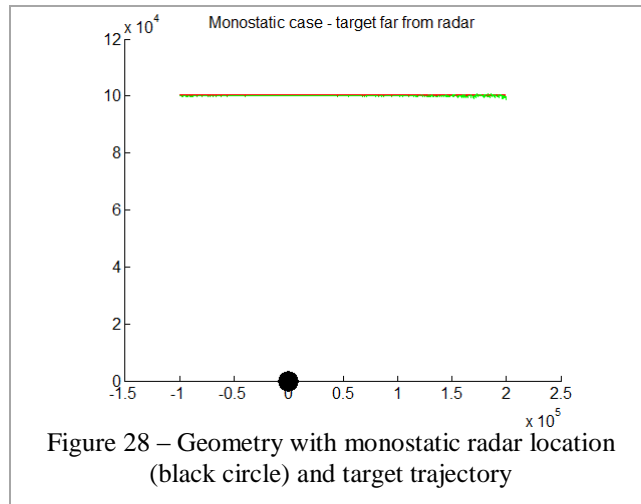
than when it is far from the baseline. For this example, a range standard deviation of 150 m and an azimuth standard deviation of 3 mrad are used.

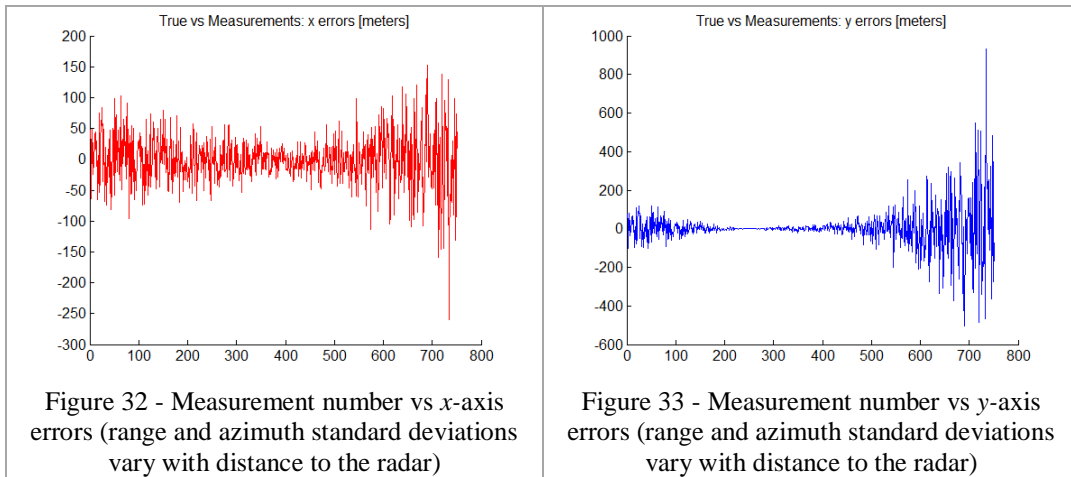
*Script04b.m* file is a script which uses new classes: “TRadar” (instead of “Radar”) and “TEnvironment” and “TTarget”. Those new classes were created to make the scripts (Matlab code) easier to read, understand and maintain. Besides, they will help to make changes to the parameters of the simulations easier. When using *Script04b.m*, it is possible to simulate different geometries of one monostatic radar or one bistatic radar. In addition, the new class “TRadar” provides the new functionality of having range and angle measurements standard deviations that vary according to SNR. It means that if the target is far from the radar, the SNR will be small and hence the standard deviation of the measurements will be bigger. Equations (18) and (19) (pages 69 and 70 of [74]) show how the standard deviations are calculated (range and azimuth standard deviations, respectively), where N is the number of pulses integrated. SNR is calculated using the radar range equation (12).

$$\sigma_R = \frac{\text{rangeResolution}}{1.81\sqrt{2} \times \text{SNR} \times N} \quad (18)$$

$$\sigma_\theta = \frac{\text{beamWidth}}{1.57\sqrt{2} \times \text{SNR} \times N} \quad (19)$$

Some examples of graphics generated from *script04b.m* are found in Figure 28, Figure 29 and Figure 30 for the monostatic case and Figure 31, Figure 32 and Figure 33 for bistatic case (when the target is parallel to the baseline).





For the examples in Figure 28 to Figure 33, the radar and target characteristics are:

- Radar Power: 1.5MW
- Frequency: 8 GHz
- PRF: 1500 Hz
- Beam width: 5 degrees
- Pulse Width: 0.7  $\mu$ s and Range Resolution: 105 meters
- Antenna rotation: 30 RPM, pulses per beam width: 27 and Sampling rate: 2 seconds (change in *TRadar.m* and *script04b.m*)
- Antennas gain: 45 dB and Noise figure: 3 dB
- target RCS is 0.1 m<sup>2</sup> and  $x$ -velocity is 200 m/s (in *TEnvironment.m*)

Following, next script (*script10.m*) uses a new class named “TghFilter” which implements a  $g$ - $h$  filter. The  $g$ - $h$  filter implemented is a version of a “Critically Damped Filter” [50] where the values of  $g$  and  $h$  are a function of  $\theta$  and  $\theta$  can be a value between 0 and 1, where values close to 0 mean that the filter trusts more on recent measurements and values close to 1 mean that the filter trusts more on historical measurements. The values of  $g$  and  $h$  are according to equation (20), once  $\theta$  is defined.

$$g = 1 - \theta^2 \text{ and } h = (1 - \theta)^2 \quad (20)$$

The simulation considers a target flying on a straight trajectory with constant velocity and the value of  $\theta$  changes during the filtering process from an initial value of 0.10 (recent measurements are more important) to a maximum value of more than 0.90 (historical measurements are more important). The values were chosen after some simulations to assess the performance of the  $g-h$  filter. The filter algorithm can be used to filter the measurements performed either by a monostatic or a by a bistatic radar. Still using *script10.m* file, it generates a series of graphs that depict, for each geometry (monostatic or different bistatic geometries), measurements, filtered measurements of position and velocity of the target and also, in the bistatic configurations, bistatic angle is presented. Below, there is an example of a simulation using bistatic geometry.

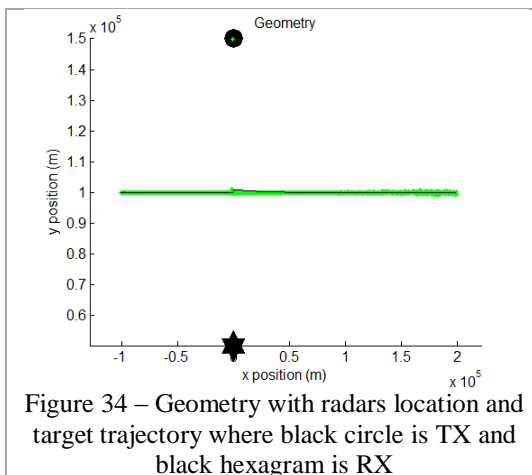


Figure 34 – Geometry with radars location and target trajectory where black circle is TX and black hexagram is RX

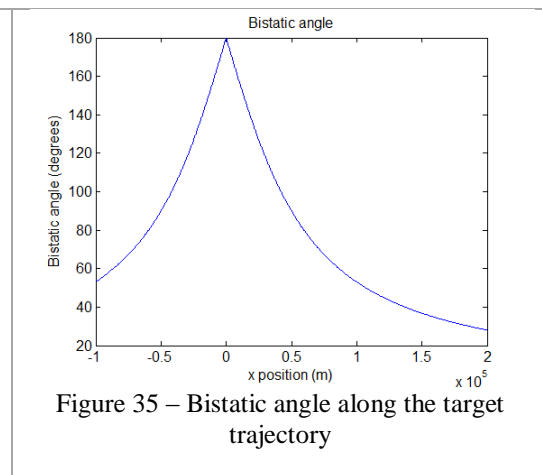


Figure 35 – Bistatic angle along the target trajectory

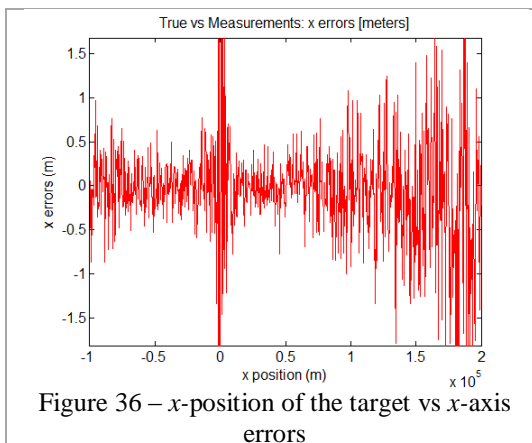


Figure 36 – x-position of the target vs x-axis errors

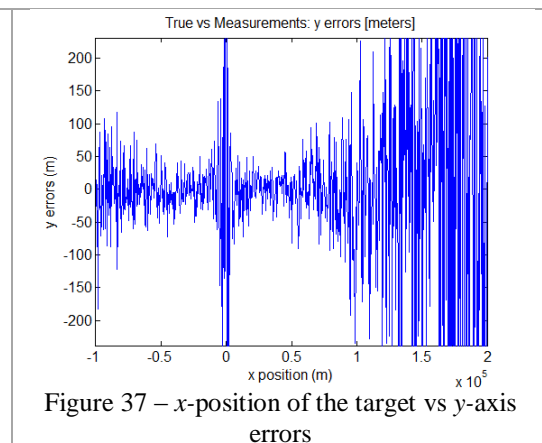


Figure 37 – x-position of the target vs y-axis errors

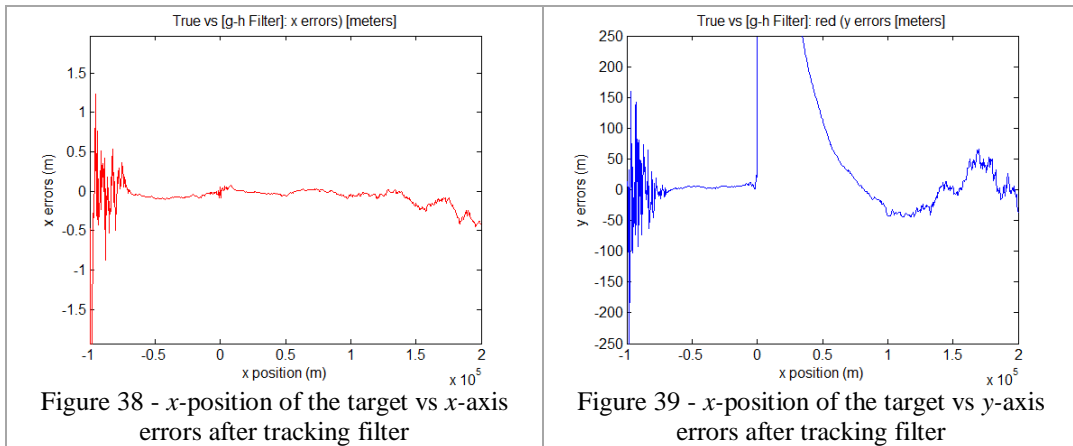


Figure 38 -  $x$ -position of the target vs  $x$ -axis errors after tracking filter

Figure 39 -  $x$ -position of the target vs  $y$ -axis errors after tracking filter

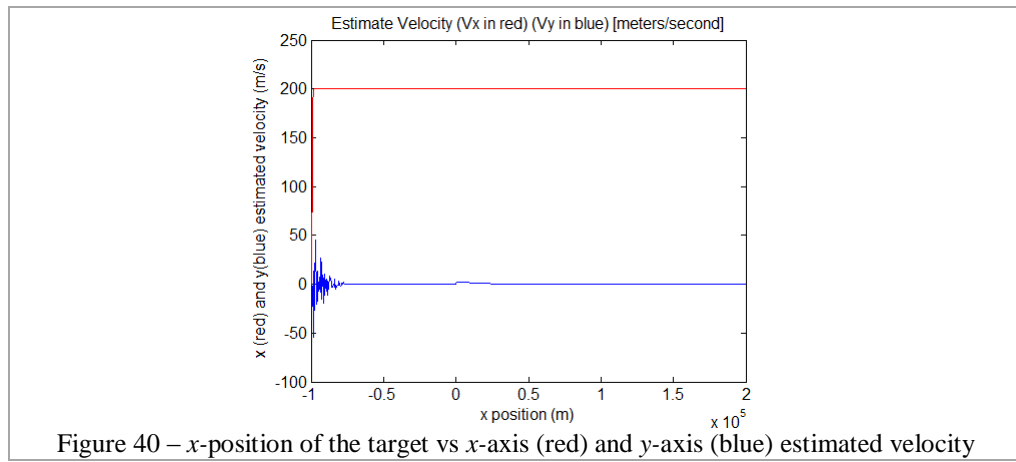


Figure 40 –  $x$ -position of the target vs  $x$ -axis (red) and  $y$ -axis (blue) estimated velocity

The main objective of *script11* file series (*script11a.m*, *script11b.m*, and so on) is to make use of data fusion in scenarios where more than one radar (monostatic or bistatic) are used in order to improve the resulting measurements or filtered measurements. The data fusion can be done, for example, in two different ways:

- a) by applying weight to the measurements according to SNR and then perform a weighted mean of the measurements or the filtered measurements to have the final result or
- b) by applying weight to the measurements according to SNR to select the best measurement or filtered measurement to be used.

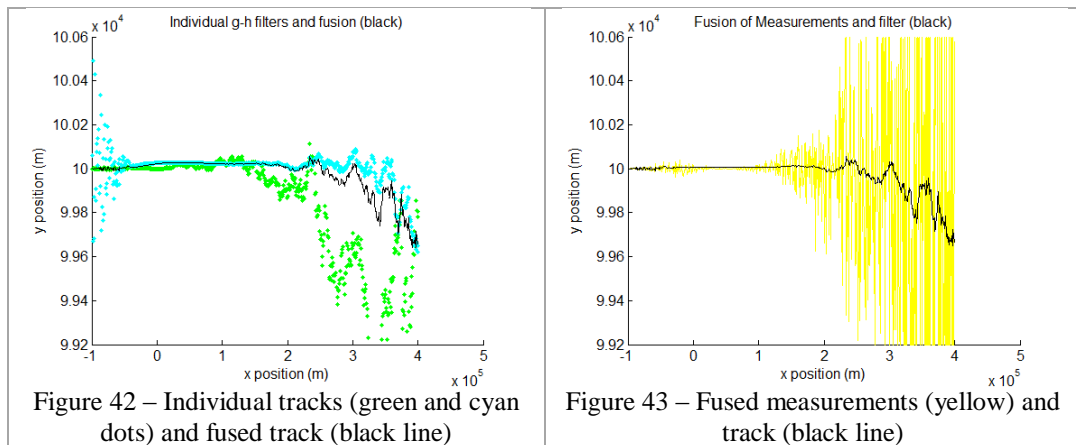
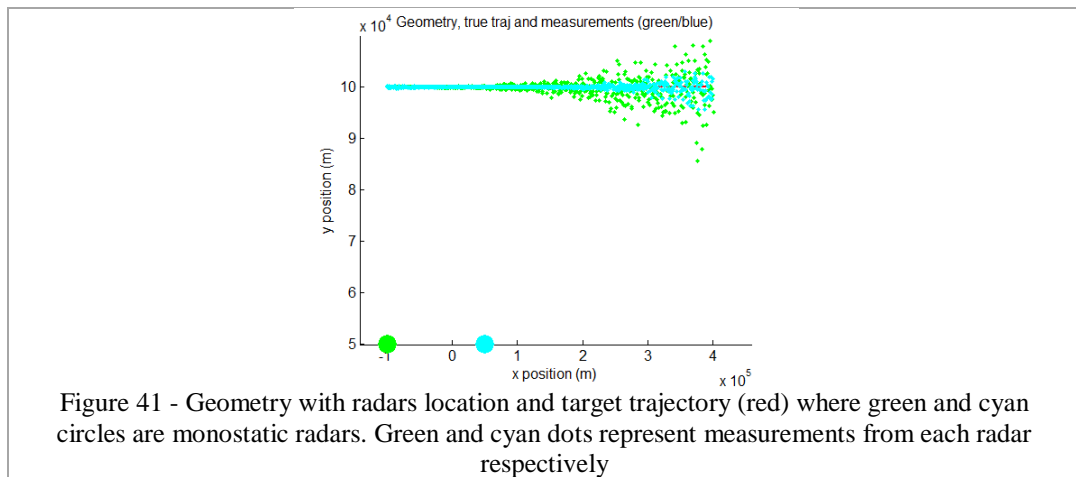
Function *wmean()* is used to perform the chosen method. In this research, method (a) is chosen for the simulations.

In all *script11* files, the sampling rate is 4 seconds and beam width is 3 degrees.

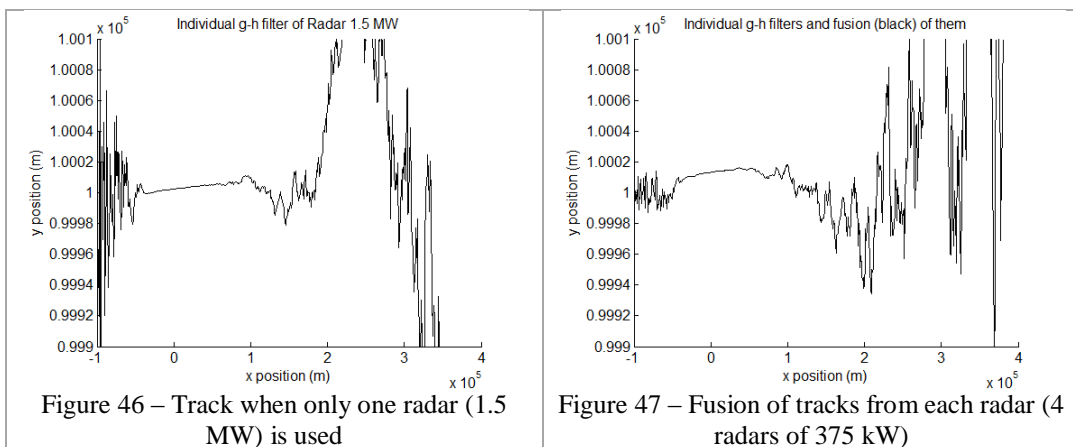
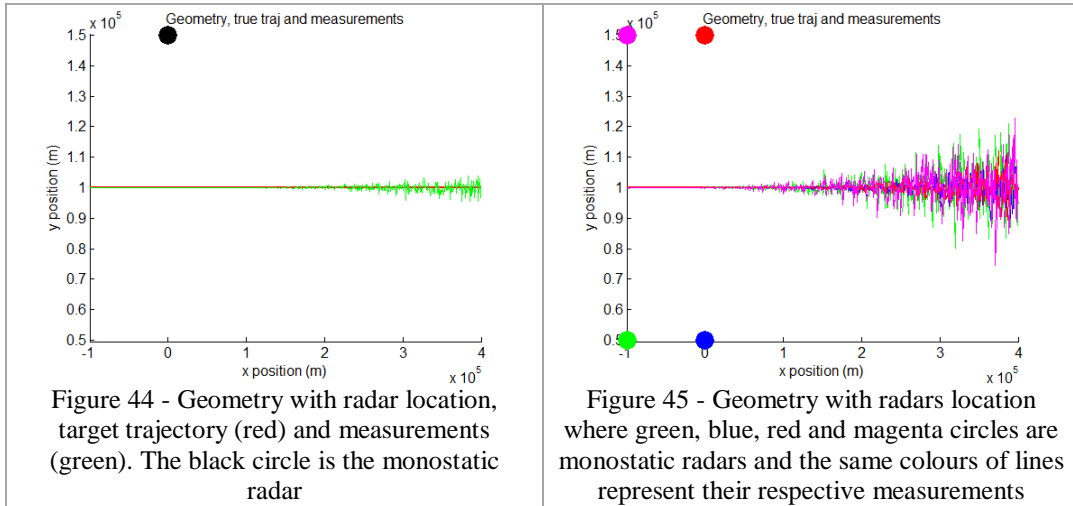
In the specific case where the SNR is high because the target is near or crossing the baseline of a bistatic radar, the weight of the measurements must be reduced when

the bistatic angle lies in the range between 145-180 degrees since the measurements in this region are not very accurate as it can be seen in Figure 36 and Figure 37.

Figure 41, Figure 42 and Figure 43, present one example of fusion of data (measurements or tracks) in a scenario with 2 monostatic radars (using *script11.m*). The resulting track is the same if comparing the algorithm that fuse the tracks (Figure 42) with the algorithm that fuse the measurements before applying the tracking filter (Figure 43).



The last script of this series, *script11z.m*, generates graphs to compare the use of one monostatic radar with power of 1.5 MW and the use of 4 monostatic radars of 375 kW on a network. The following figures depict both scenarios.

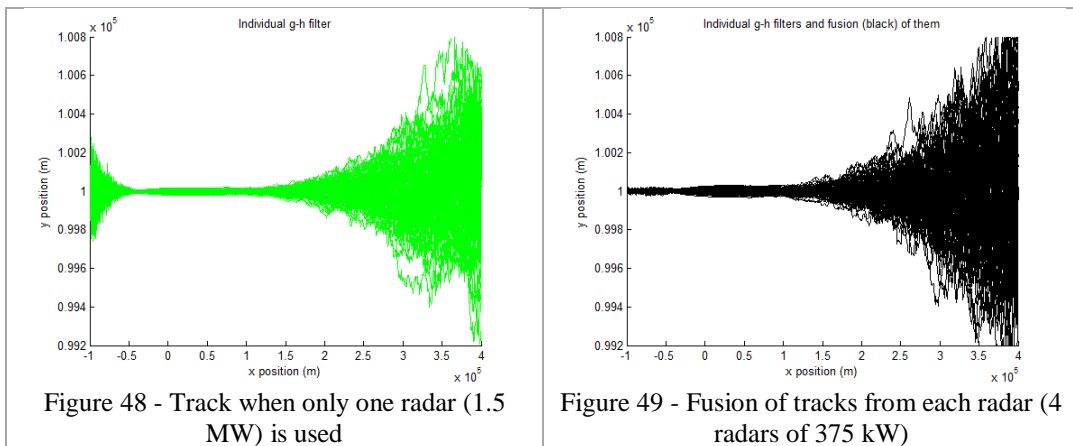


It can be observed that in Figure 46, the errors in the beginning of the trajectory are bigger than in the Figure 47. However in the geometry of Figure 46 the track is more stable until 200 km whereas in Figure 47 the track starts do diverge from 100 km.

So far, all scripts performed just one run of the simulation. The results show a rough idea about how tracking accuracy varies when geometries or radar characteristics are changed. Nevertheless, due to the random nature of the errors it is appropriate to run each simulation many times in order to see and understand the pattern of the errors.

The next series of scripts, *script12* files (*script12.m*, *script12a.m*, and so on) perform the same tasks as the *script11* series but now making use of Monte Carlo Simulation techniques. Thus, for each geometry, many Monte Carlo runs are performed before generating the graphs. For instance, for the same scenario depicted in Figure 46 and Figure 47, the results would be according to the Figure 48 and Figure 49 (with 100 simulations runs) and they show that both geometries have similar results apart from

the beginning of the trajectory where the netted monostatic geometry performs better (*script12z.m*).

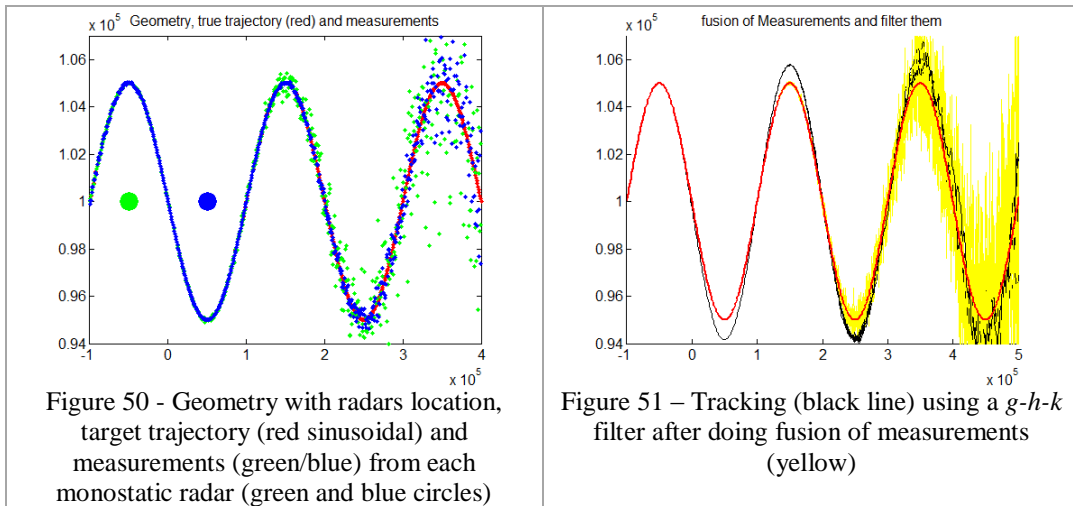


In *script13.m*, a new filter, *g-h-k* filter is programmed and assessed. It is again a version of a “Critically Damped Filter” [50] where the values of *g*, *h* and *k* are a function of  $\theta$  and  $\theta$  can be a value between 0 and 1, where values close to 0 mean that the filter should trust more on recent measurements and values close to 1 mean that the filter should trust more on historical measurements. The values of *g*, *h* and *k* are defined according to equation (21).

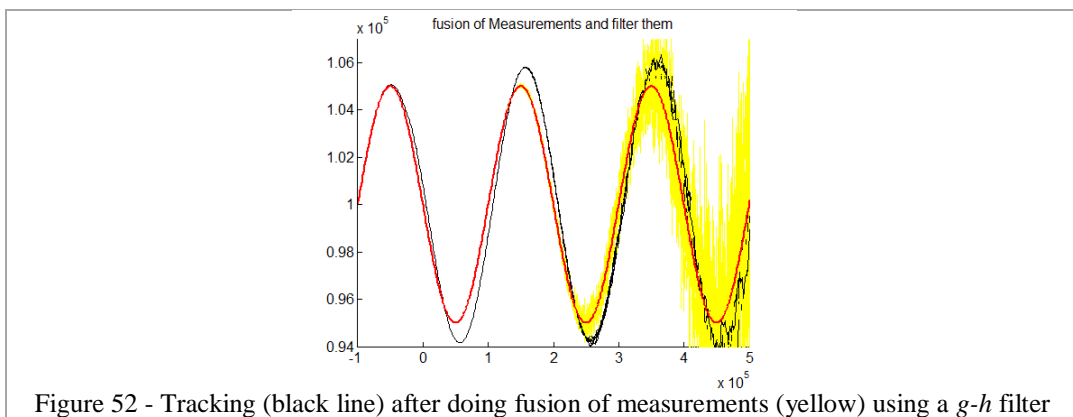
$$g = 1 - \theta^3, h = 1.5(1 - \theta^2)(1 - \theta) \text{ and} \tag{21}$$

$$k = 0.5(1 - \theta)^3$$

Similarly to the *g-h* filter, this *g-h-k* filter also starts with the value of  $\theta = 0.10$  and then increases gradually up to 0.90 or more, for example. The need of using a *g-h-k* filter comes from the idea of performing the simulations using a target that manoeuvres. A sinusoidal trajectory is used to see how the *g-h-k* filter performs. The following figures show an example of 2 monostatic radars used to track such a target.

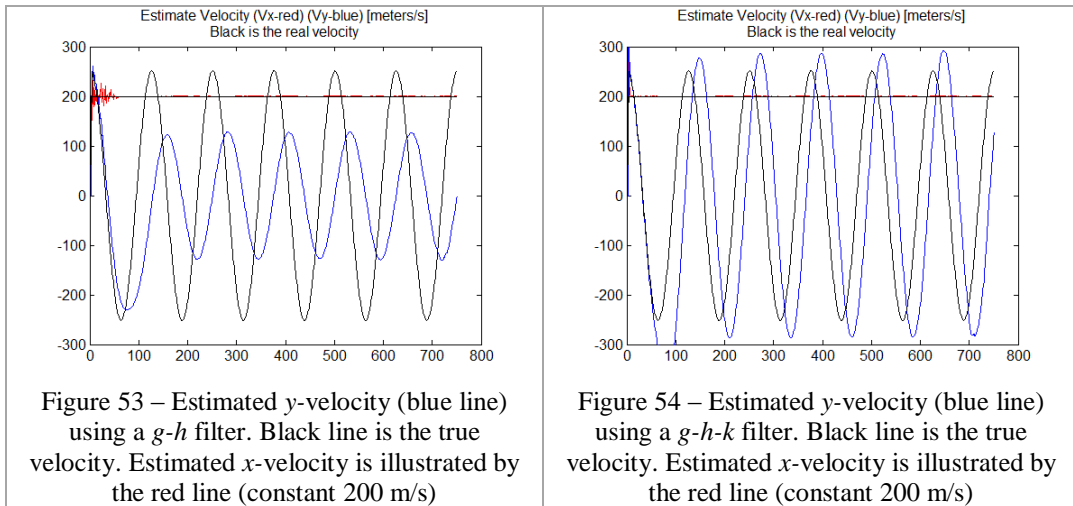


The track result from  $g-h-k$  filter (Figure 51) is better than the result from  $g-h$  filter depicted in the Figure 52.

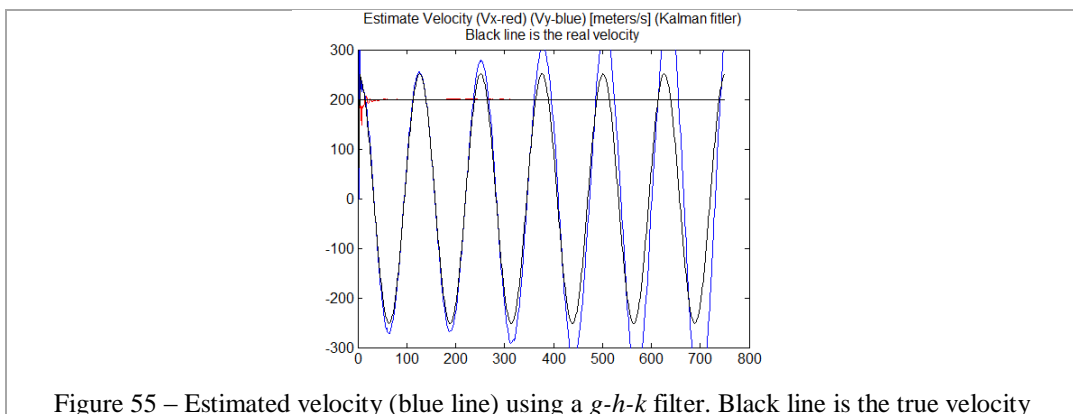


For the *script20.m*, the sampling time is changed to 2 seconds and the beam width changed to 5 degrees. The main objective of *script20.m* is to perform in the same scenarios of *scrip10.m* with a target moving on a sinusoidal trajectory to assess the  $g-h-k$  filter. The sinusoidal trajectory simulated has a constant velocity on the  $x$ -axis and a non-constant velocity and acceleration in the  $y$ -axis.

Figure 53 shows the estimate velocity using a  $g-h$  filter and Figure 54 shows the estimate velocity using a  $g-h-k$  filter. The use of  $g-h-k$  filter improved the estimation of  $y$ -velocity.



Although, so far, all the scripts to track targets uses  $g-h$  or  $g-h-k$  filters (Figure 53 and Figure 54), a Kalman Filter has been developed and the result can be seen in Figure 55.



The use of Kalman Filter brings an improvement in the estimated velocities and thus to estimated position of the target.

For the next (and last) 2 scripts (*script30.m* and *script30a.m*), only Kalman filter is considered. Kalman Filter uses more computational resources but as long as it is not a limitation for the simulations and for the current computer power available in the market and its results are considerably better, this will be the filter used for the analysis of this thesis. Therefore, the main simulations and results are performed using *script30.m* and *script30a.m*.

This section has explained the methodology and has built step-by-step the important concepts to be used by *script30.m* and *script30a.m* as the main simulations.

## 6.3 Algorithms

Choosing the right filtering algorithm to be used in the simulations depends on specific characteristics of the problem. The initial idea was to perform simulations using a target whose trajectory was linear, on a straight line and with a constant speed. In this scenario, using a  $g-h$  filter was enough to achieve acceptable results. A Critically Damped  $g-h$  filter [50] has been used, where the variable  $\theta$  was varying from some value close to 0 to some value close to 1 during the trajectory of the target.

In a scenario where some acceleration was considered (for example, when the target has a sinusoidal trajectory with constant  $x$ -velocity and some acceleration in  $y$ -axis), the use of a  $g-h-k$  filter was more appropriate. Although the filter considers a constant acceleration and the target had some non-constant acceleration, the filter performed well. Once more, the  $g-h-k$  filter that has been implemented was the Critically Damped  $g-h-k$  filter where  $\theta$  varied the same way as in the  $g-h$  version.

In a situation where computer resources are limited, the use of  $g-h-k$  filter with some tuning in the  $\theta$  variable would be enough for some target trajectories. However, nowadays, computer power is not a problem if compared to 50 years ago when the Kalman Filter was published [20]. Therefore, a Kalman Filter was implemented (3-state, position, velocity and acceleration) for the main simulations of this research and, because of that, it is possible to achieve better results when the target manoeuvres.

A brief explanation about each filter used is given in the next sections. In addition, some explanation on how the measurements are simulated is presented.

### 6.3.1 Simulated Measurements

The simulated measurements consider the real position of the target according to its trajectory (straight line, sinusoidal or spiral). From the real 2D position  $(x,y)$  of the target, a true measurement of range and bearing angle (azimuth) is calculated with respect to the radar position (receiver) using Cartesian-to-Polar conversion. Then some noise is added to the range and azimuth measurements. This noise is a white

noise, with zero mean and with variances that varies according to SNR. SNR is calculated according to the radar equation, which depends on many variables such as Transmitter Power, wavelength, antenna gains, RCS, etc. The same SNR is used by the fusion algorithm in order to measure how accurate or how good is the measurement. In bistatic measurements, this weight factor is reduced when the bistatic angle is close to 180 degrees. Therefore, the sequence below is performed in order to simulate a measurement:

- 1) In monostatic cases, from true  $x$ - $y$  position, use Cartesian-to-Polar conversion and find true range and azimuth ( $R$  and  $\theta$ );
- 2) In the case of bistatic geometries, from true  $x$ - $y$  position, the distances transmitter-target and target-receiver are calculated and then summed to find  $R_T$ .  $\theta$  in the bistatic case is the bearing angle ( $\theta_R$ ) with respect to the vertical axis (see Figure 12 and equation (1))
- 3) From the true range, calculate SNR (RCS is considered to be constant in all cases, monostatic or bistatic, regardless of aspect angle, geometry and so on) using radar range equation;
- 4) From SNR, calculate standard deviations for range and azimuth measurements [74]. See equations (18) and (19);
- 5) Calculate measurement plus noise (range plus noise and azimuth plus noise) and
- 6) Use SNR to weigh the importance of a measurement (to be used in measurement fusion procedure).

### 6.3.1.1 Fusion of measurements

SNR is used to calculate standard deviations for range and azimuth and also is the information used to weigh the measurements so that the fusion process (weighted average of measurements and variances) can give more importance to measurements with larger SNR. Nonetheless, when the target is close to the baseline of a bistatic radar which means that the bistatic angle is close to 180 degrees, its measurements can get worse and it is difficult to measure where the target is lying in or near the baseline. Therefore, the decision was to model the measurements from a bistatic

radar to be less important dividing the SNR by a factor according to equation (22) when the bistatic angle has a value between 145 and 180 degrees.

$$\text{SNR\_reduction\_factor} = 1 + 2.5^{(\text{bistaticAngle}-145)} \quad (22)$$

### 6.3.2 Critically Damped g-h filter

The Critically Damped g-h filter used in this research is a slightly different version from the one reported in [50]. In this research, it has been realized that varying the parameter  $\theta$  from small values (0.10) to higher values (more than 0.90) during the process of tracking resulted in some improvement in the tracking errors. So, the following equations are used to estimated position and velocity:

- 1) First, start with a small  $\theta$ , for example, 0.10
- 2) Calculate  $g$  and  $h$  using equation (20)
- 3) Calculate estimate position and velocity using the measurements and the following equations [50]

$$\dot{x}_{n+1,n}^* = \dot{x}_{n,n-1}^* + \frac{h}{T} (y_n - x_{n,n-1}^*), \text{ where } T \text{ is the sampling interval, } y_n \text{ is the } n^{\text{th}}\text{-measurement and } * \text{ means estimate} \quad (23)$$

$\dot{x}_{n+1,n}^*$  means the estimated velocity for step  $n+1$ , using measurements until step  $n$

$$x_{n+1,n}^* = x_{n,n-1}^* + T\dot{x}_{n+1,n}^* + g(y_n - x_{n,n-1}^*) \quad (24)$$

- 4) Increase  $\theta$  (until a maximum of about 0.90) by a small amount, for example, 0.05 and go back to step 2.

### 6.3.3 Critically Damped g-h-k filter

This filter is similar to the previous one and the steps to calculate the estimate position, velocity and acceleration are similar, except that now there is an extra parameter,  $k$ .

- 1) First, start with a small  $\theta$ , for example, 0.10

- 2) Calculate  $g$ ,  $h$  and  $k$  using equation (21)
- 3) Calculate estimate position, velocity and acceleration using the measurements and the following equations [50].

$$\ddot{x}_{n,n}^* = \ddot{x}_{n,n-1}^* + \frac{2k}{T^2}(y_n - x_{n,n-1}^*) \quad (25)$$

$$\dot{x}_{n,n}^* = \dot{x}_{n,n-1}^* + \frac{h}{T}(y_n - x_{n,n-1}^*) \quad (26)$$

$$x_{n,n}^* = x_{n,n-1}^* + g(y_n - x_{n,n-1}^*) \quad (27)$$

$$\ddot{x}_{n+1,n}^* = \ddot{x}_{n,n}^* \quad (28)$$

$$\dot{x}_{n+1,n}^* = \dot{x}_{n,n}^* + \ddot{x}_{n,n}^* T \quad (29)$$

$$x_{n+1,n}^* = x_{n,n}^* + \dot{x}_{n,n}^* T + \ddot{x}_{n,n}^* \frac{T^2}{2} \quad (30)$$

- 4) Increase  $\theta$  (until a maximum of about 0.90) by a small amount, for example, 0.05 and go back to step 2.

### 6.3.4 Kalman Filter (KF)

The KF algorithm used in this research is based on [50]. The algorithm to perform the tracking using KF is as follows:

- 1) Set  $\phi$  which is the transition matrix. It is a 2x2 matrix (for 2-state filter) or a 3x3 matrix (for 3-state filter)

$$\phi = \begin{bmatrix} 1 & T & 0 & 0 \\ 0 & 1 & 0 & 0 \\ 0 & 0 & 1 & T \\ 0 & 0 & 0 & 1 \end{bmatrix} \text{ or} \quad (31)$$

$$\phi = \begin{bmatrix} 1 & T & T^2/2 & 0 & 0 & 0 \\ 0 & 1 & T & 0 & 0 & 0 \\ 0 & 0 & 1 & 0 & 0 & 0 \\ 0 & 0 & 0 & 1 & T & T^2/2 \\ 0 & 0 & 0 & 0 & 1 & T \\ 0 & 0 & 0 & 0 & 0 & 1 \end{bmatrix}$$

- 2) Set  $M$ , the measurement matrix, which is 2(measurements)x4 for a 2-state filter or 2(measurements)x6 for a 3-state filter

$$M = \begin{bmatrix} 1 & 0 & 0 & 0 \\ 0 & 0 & 1 & 0 \end{bmatrix} \text{ or } M = \begin{bmatrix} 1 & 0 & 0 & 0 & 0 & 0 \\ 0 & 0 & 0 & 1 & 0 & 0 \end{bmatrix} \quad (32)$$

- 3) Set  $S_0$ , the covariance of prediction matrix (4x4 for 2-state filter or 6x6 matrix for 3-state filter). The number  $10^8$  was chosen to be very large in order to make the filter, at the beginning, to trust more on measurements and not on predictions

$$S_0 = I_{4 \times 4} * 10^8 \text{ or } S_0 = I_{6 \times 6} * 10^8 \quad (33)$$

- 4) Set  $Q$ , the dynamic noise covariance matrix

$$Q = U_X' * U_X + U_Y' * U_Y, \text{ where } U_X \text{ and } U_Y \text{ are}$$

$$U_X = [0 \quad 0 \quad \sigma_{U_X} \quad 0 \quad 0 \quad 0] \text{ and}$$

$$U_Y = [0 \quad 0 \quad 0 \quad 0 \quad 0 \quad \sigma_{U_Y}], \text{ where}$$

(34)

$$\sigma_{U_X} = T * \text{maxAccel}_X / B \text{ and } \sigma_{U_Y} = T * \text{maxAccel}_Y / B$$

maxAccelX, maxAccelY and B are set according to page 66 of

[50]

- 5) With the measurement, calculate  $R$ , the measurement covariance vector (see page 179 of [74])

$$R = \begin{bmatrix} r_{11} & r_{12} \\ r_{21} & r_{22} \end{bmatrix}, \text{ where}$$

$$r_{11} = \sigma_R^2 \cos^2 \theta + \sigma_\theta^2 R^2 \sin^2 \theta, \quad r_{22} = \sigma_R^2 \sin^2 \theta + \quad (35)$$

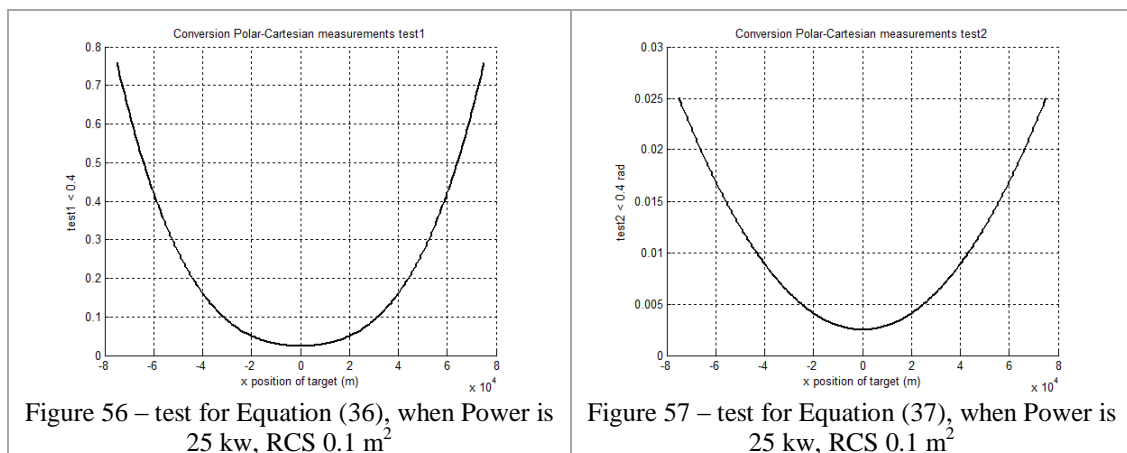
$$\sigma_\theta^2 R^2 \cos^2 \theta \text{ and } r_{12 \text{ or } 21} = \frac{1}{2} \sin 2\theta [\sigma_R^2 - R^2 \sigma_\theta^2], \text{ where}$$

$(R, \theta)$  are the measurements and  $(\sigma_R, \sigma_\theta)$  are the standard deviations of the measurements

- 6) According to page 180 [74] the use of equations (35) and converting the measurements from Polar to Cartesian coordinates can lead to bias on the measurements and equations (35) are usually valid if equations (36) and (37) are valid. Figure 56 and Figure 57 show what happens with the values of equations (36) and (37) in a scenario simulated in this thesis (section 7.2) where the transmitter power is 25 KW, RCS 0.1 m<sup>2</sup> and starting maximum distance is 80 km (section 7.2.1.1). As can be seen, the equation (36) is only valid from x-position 60 km. However, the tracking results are good and it converges well in the beginning of the tracking (Figure 145 and Figure 146).

$$\frac{R\sigma_\theta^2}{\sigma_R} < 0.4 \quad (36)$$

$$\sigma_\theta < 0.4 \text{ rad} \quad (37)$$



- 7) Calculate  $S_1$ , the predictor covariance matrix

$$S_1 = \phi S_0 \phi' + Q \quad (38)$$

- 8) Calculate  $H$ , the Weight matrix

$$H = S_1 M' (R + M S_1 M')^{-1} \quad (39)$$

- 9) Update the estimation  $X_{n,n}^*$

$$X_{n,n}^* = X_{n,n-1}^* + H_n (Y_n - M X_{n,n-1}^*), \text{ where the first} \quad (40)$$

prediction  $X_{n,n-1}^*$  is based on the first measurement  $Y_1$

10) Update  $S_0$

$$S_0 = (I - HM) * S_1 \quad (41)$$

11) Calculate the new prediction  $X_{n+1,n}^*$

$$X_{n+1,n}^* = \phi X_{n,n}^* \quad (42)$$

12) Go back to step 5

## 7 Results

When all the scripts are run, some assumptions about the radar parameters have to be made. First of all, it is a two-dimensional space where radars and target have their positions established in Cartesian coordinates ( $x$  and  $y$  coordinates). The measurements are in Polar coordinates (range or total range, and bearing angle) and the sampling rate of the measurements is 2.5 seconds (unless mentioned differently for a specific simulation), considering an antenna rotation of 24 RPM (*TRadar.m*). The measurements are then transformed to Cartesian coordinates in order to be filtered by the Kalman Filter. The target flies in a straight line with a constant velocity or for the complex scenarios, the target flies in a spiral-like trajectory. The standard deviations of range and bearing angle measurements are functions of the range to the target. SNR is calculated using the Radar Equation (or Bistatic Radar Equation). Table 2 shows a summary of the radar parameters.

Table 2 – Main radar parameters used in the simulations and some other related information

<b>Coordinates</b>	Two-dimensional
<b>Measurements</b>	Polar coordinates (range, bearing angle)
<b>Tracking</b>	Cartesian Coordinates ( $x,y$ )
<b>Antenna Rotation</b>	24 RPM, hence sampling rate 2.5 sec
<b>Tracking Filter</b>	Kalman Filter (KF)
<b>Target trajectory</b>	Straight line with constant velocity or spiral with non-constant $x$ and $y$ velocity and acceleration

<b>Probability of Detection (PD)</b>	100%
<b>Probability of False Alarm (PFA)</b>	0%
<b>Range and azimuth standard deviation</b>	Function of Range, hence SNR
<b>SNR</b>	Calculated with Radar Equation
<b>Transmitter Power</b>	25 kW (or a fraction, according to the geometry)
<b>Antenna Gain (TX and RX)</b>	45 dB
<b>Radar Frequency</b>	9.41 GHz, hence $\lambda=3.19$ cm
<b>Radar Cross Section (perfectly conducting sphere)</b>	10 m <sup>2</sup> or 0.1 m <sup>2</sup> , hence sphere radius of 1.78m or 17.8 cm
<b>Pulse width</b>	0.7 micro seconds, hence range resolution = 105m
<b>Bandwidth (B) = <math>\frac{1}{pulse\_width}</math></b>	1.4 MHz
<b>Noise figure</b>	3 dB
<b>Losses (L in Equation (9))</b>	0 dB
<b>Beam width</b>	2 degrees
<b>Pulse Repetition Frequency (PRF)</b>	1 KHz
<b>Unambiguous range</b>	150 km
<b>Pulses per beam width</b> $\left(\frac{PRF}{(RPM * 6)}\right) * beamwidth$	13
<b>Horizon (considering H1, height of antenna 10 meters and H2</b> $d = 1.22(\sqrt{H1}\sqrt{H2})$ , where d is in nautical miles and H1 and H2 are in feet	25 km, if H2=10 meters (ship) 422 km, if H2=10 km (aircraft)

Different geometries and scenarios are exploited as measurements and filtering are performed in each case. The main idea is to make comparisons of the true trajectory against measurements and filtered measurements when the target crosses different geometries of radar (monostatic, netted monostatic, bistatic or multistatic). In more sophisticated scenarios where more than one radar is working cooperatively on a network (netted monostatic radars or multiple bistatic pairs comprising a multistatic

radar), a data fusion algorithm is used in order to combine the measurements (or filtered measurements).

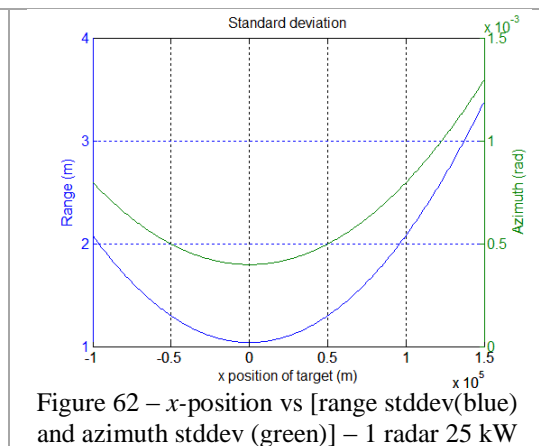
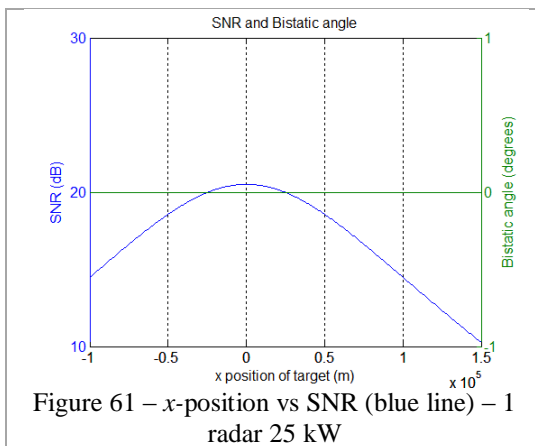
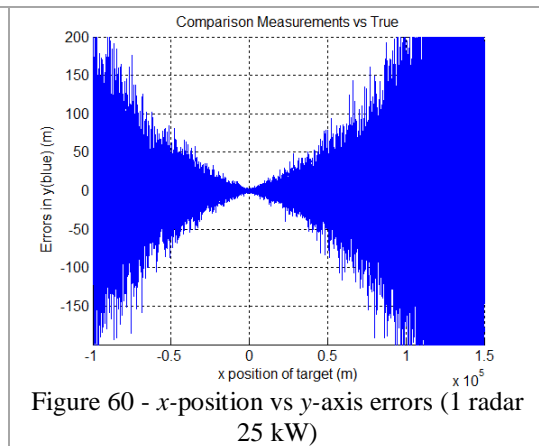
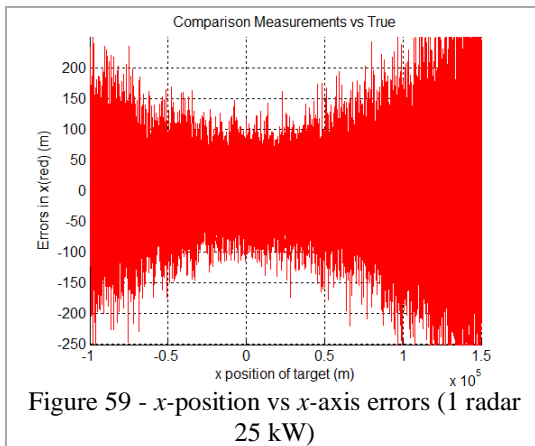
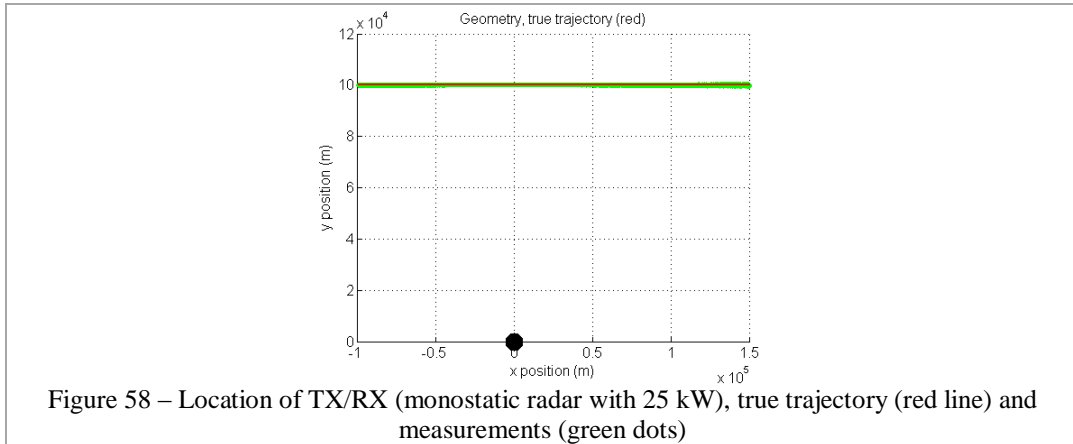
## 7.1 Measurements Results

In these simulations, *script30.m* is used and, for each scenario, two different target Radar Cross Section is used,  $10 \text{ m}^2$  and  $0.1 \text{ m}^2$  (change in *TEnvironment.m*).

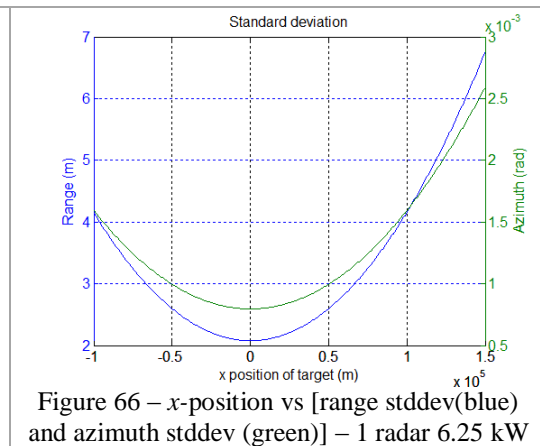
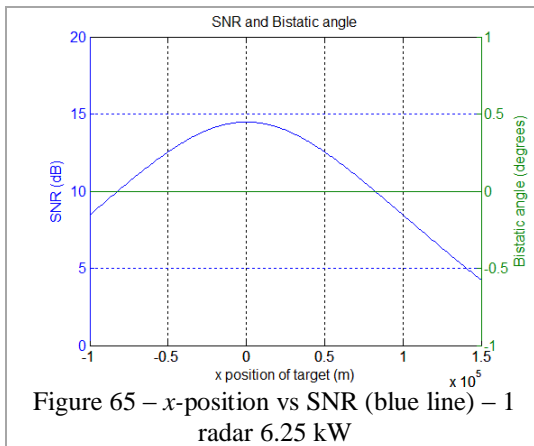
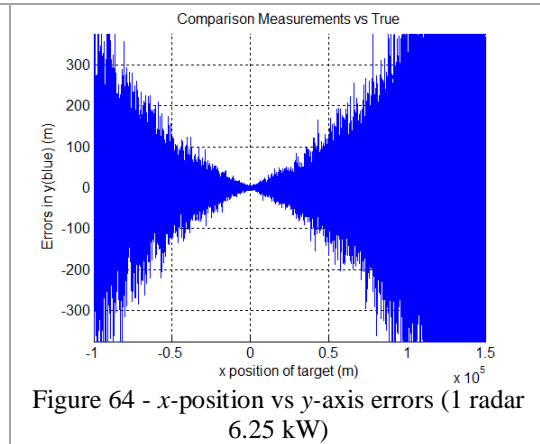
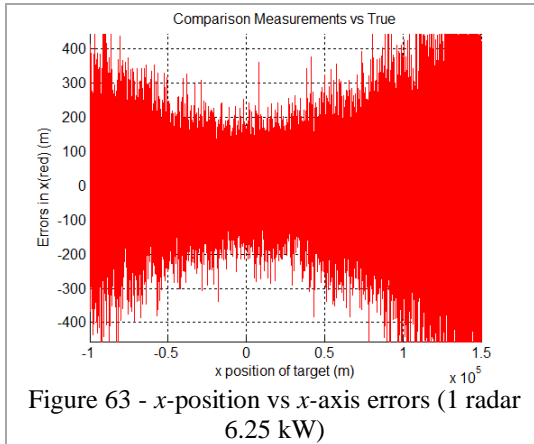
### 7.1.1 Monostatic

#### 7.1.1.1 Target RCS $10 \text{ m}^2$

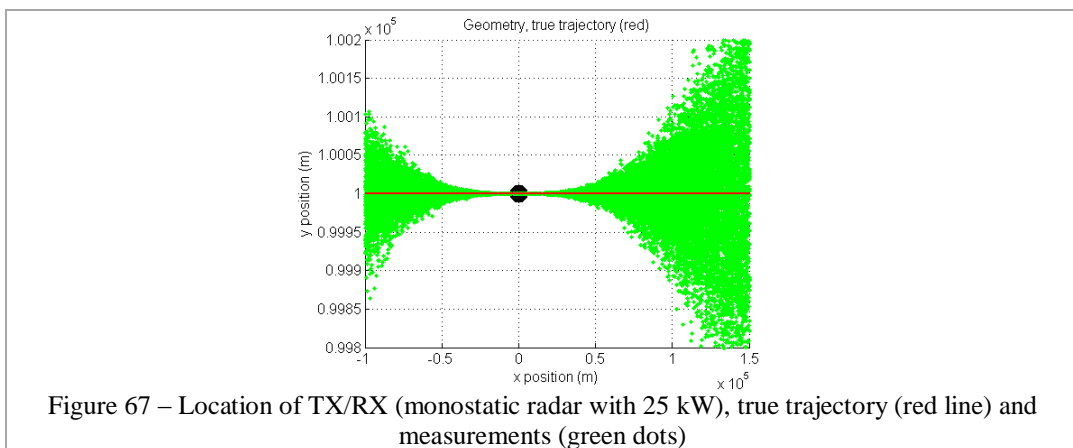
In this first simulation, only one monostatic radar of 25 kW is being used to perform the measurements on the target. The radar is located at position (0,0) and the target is flying from (-100,100) km with an  $x$ -velocity of 250 m/s (*TEnvironment.m*). The measurements are performed during 1000 seconds every 2.5 seconds (antenna rotation is 24 RPM). Figure 58 shows the geometry where a black circle represents the monostatic radar, the green dots are the measurements and the red line is the true trajectory. Figure 59 and Figure 60 depict the measurements errors in  $x$  and  $y$ -axis respectively. Figure 61 denotes how SNR and bistatic angle (on a bistatic configuration) changes with  $x$ -position of the target. And finally, Figure 62 shows the range (blue) and azimuth (green) measurements standard deviations. In this scenario, note that the errors in  $y$ -axis (Figure 60) become very good (less than  $\pm 50\text{m}$ ) between  $x$ -target locations -50 km and 50 km. This is due to the fact that range measurement standard deviation is around 1m. The  $x$ -position errors do not improve so much even though the azimuth measurement standard deviation is also small (about 0.5 mrad). This is because at a distance of 100 km, even a small error in the measurement of the bearing angle (0.5 mrad) can affect the results and the location of the target is less accurate.

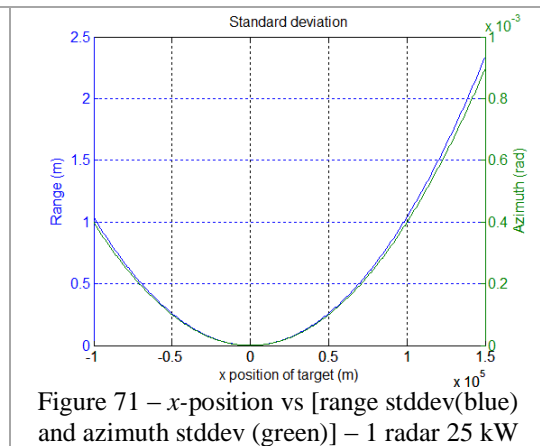
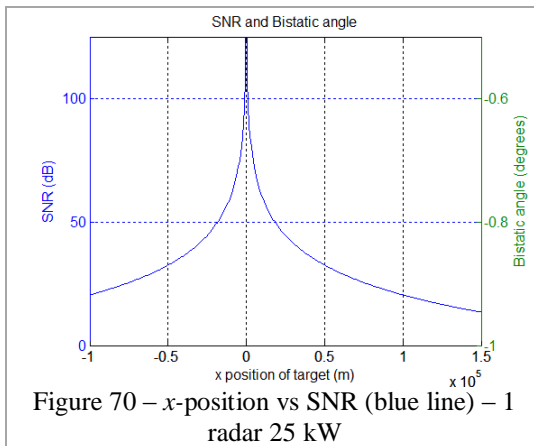
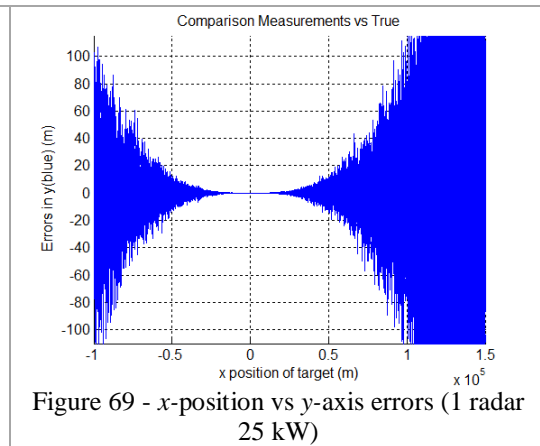
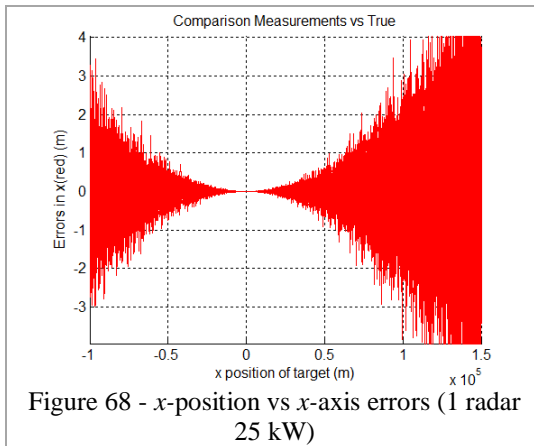


The same geometry is used in the following figures, but using a radar with 4 times less power, 6.25 kW. As it was expected the errors are larger as SNR decreases and standard deviations get worse.

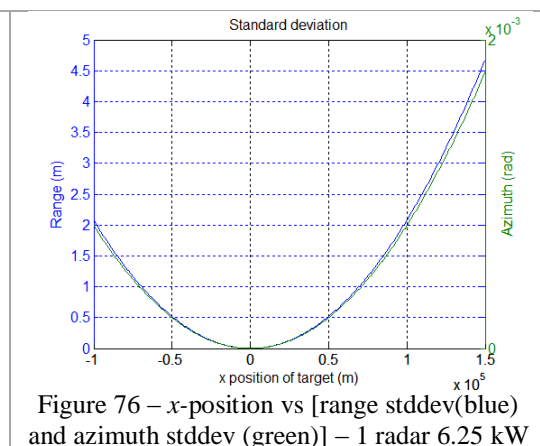
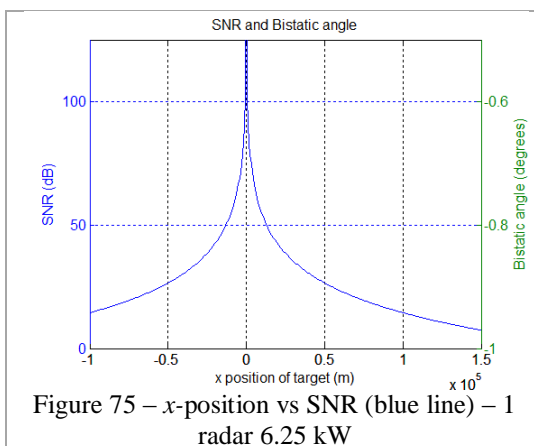
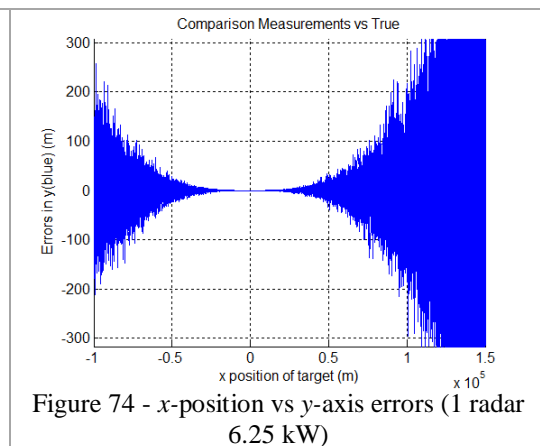
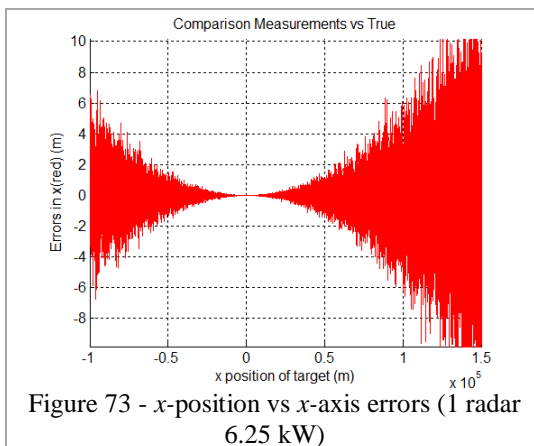
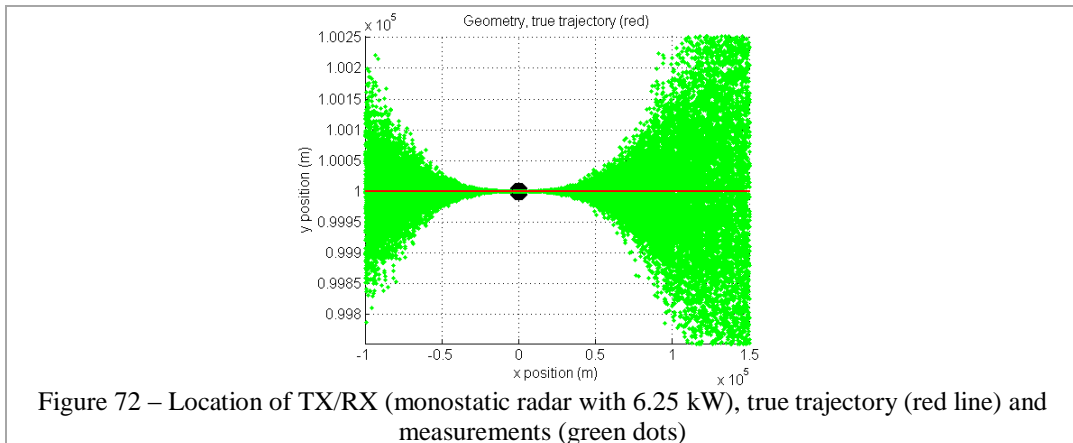


In following scenario, the radar is located on the way of the target at (0,100) km. Now, it is possible to see  $x$ -position errors are much better than  $y$ -position errors, again due to the fact that at a location 100 km from the radar, even such a small azimuth measurement standard deviation (0.4 mrad) can bring an error of about  $\pm 80$ m when the target is initiating its trajectory at (-100,100) km.





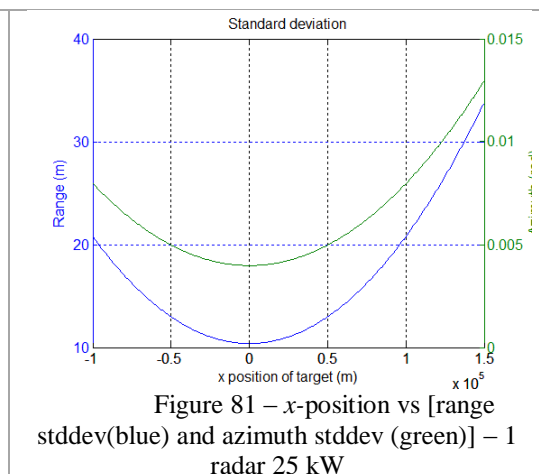
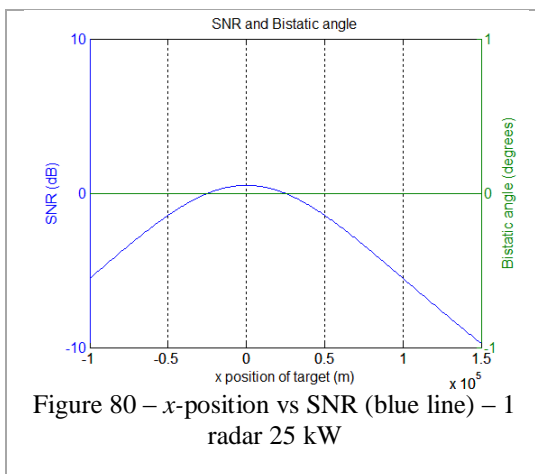
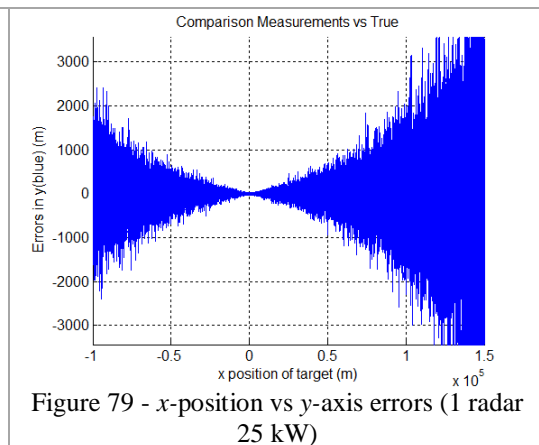
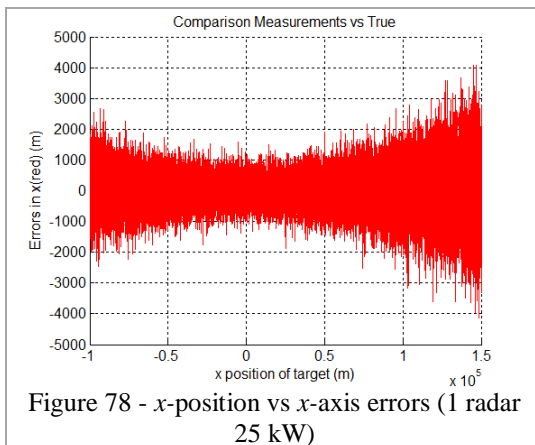
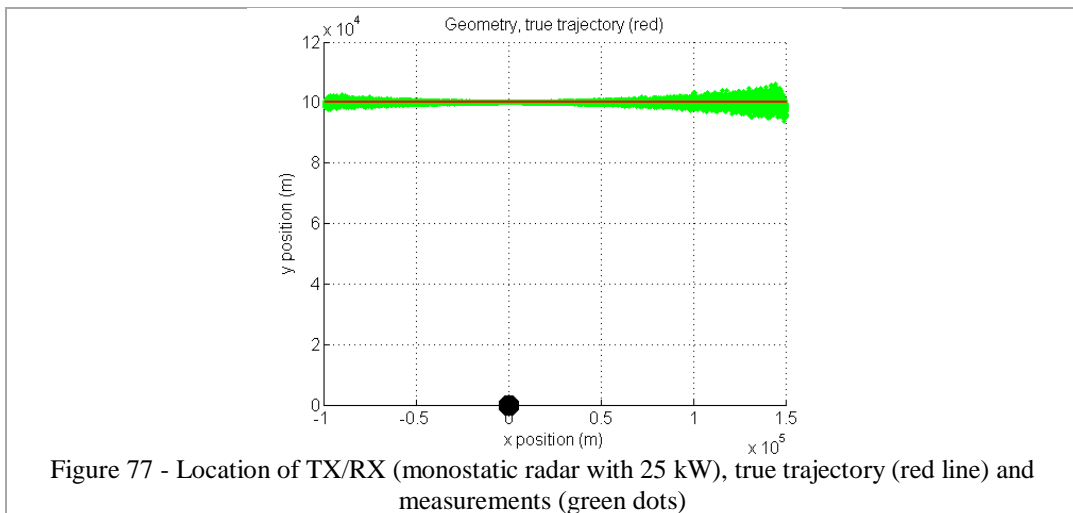
The figures below depict the same scenario with 4 times less transmitter power (6.25 kW). As shown earlier, the errors are larger because of the resulting smaller SNR and worse standard deviations. As expected, the errors are 2 times larger with the reduction on power of 4 times. This happens, because SNR reduces 4 times (due to radar equation (9)) and as a consequence, because of the square root factor of equations (18) and (19), standard deviations (range and azimuth) increase by a factor of 2.



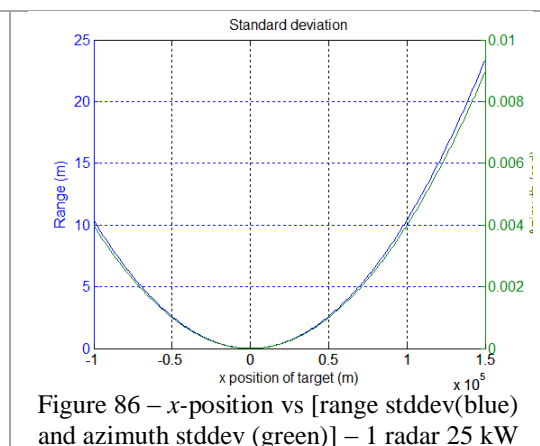
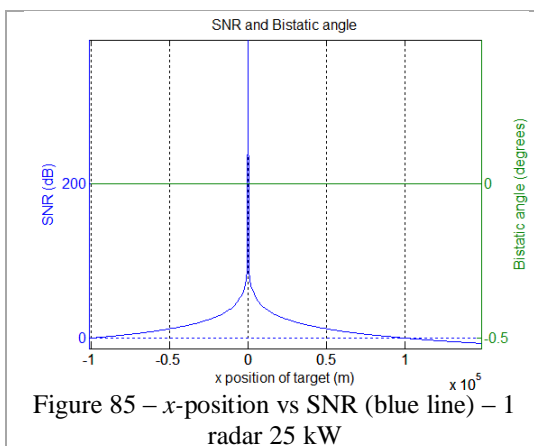
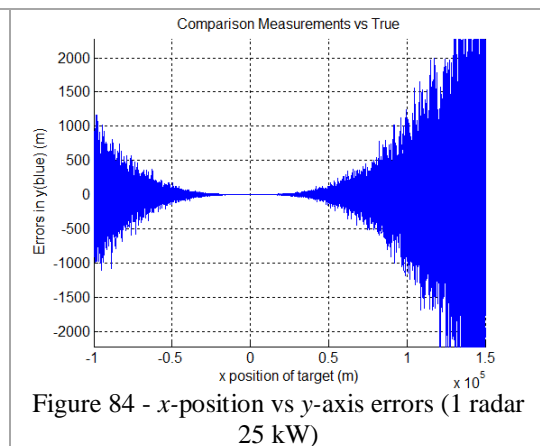
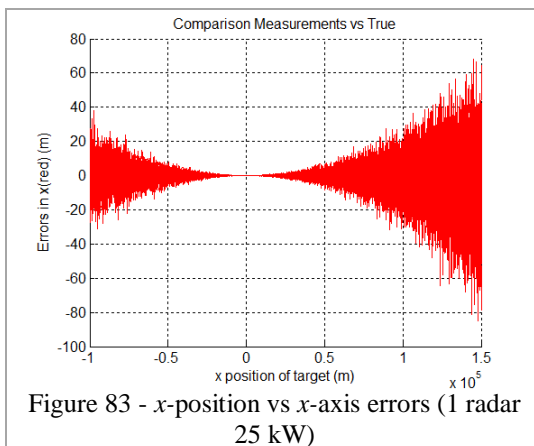
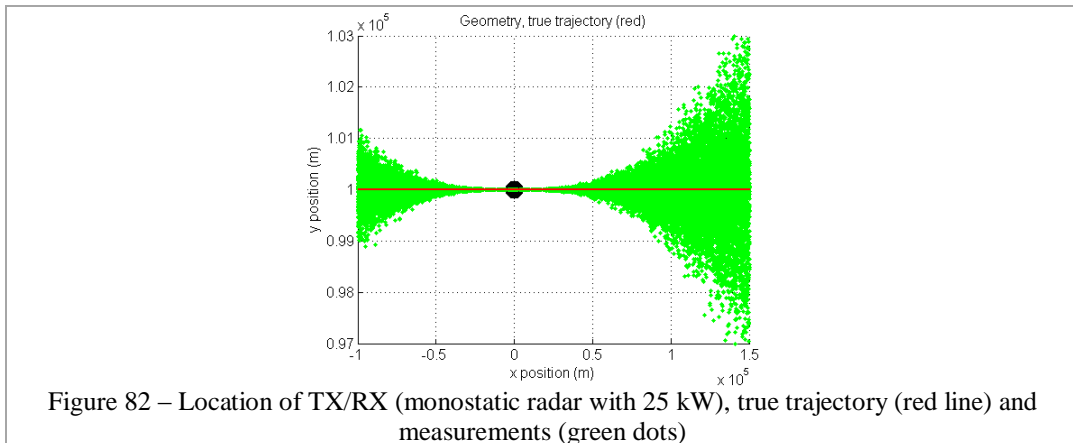
### 7.1.1.2 Target RCS 0.1 m<sup>2</sup>

Now, the same trajectory crossing the same geometries as in section 7.1.1.1, but the target has RCS of 0.1 m<sup>2</sup> (*TEnvironment.m*). It can be seen in all figures in this section, that comparing to the figures in the previous section, the reduction on RCS from 10 m<sup>2</sup> to 0.1 m<sup>2</sup>, made the errors to increase 10 times. The reduction on RCS by a factor of 100 (20 dB), makes SNR to reduce 100 times as well, and due to the

square root factor of equations (18) and (19), standard deviations increase by a factor of 10.



In the next scenario, Figure 82 to Figure 86 are equivalent to Figure 67 to Figure 71, with the target having an RCS of  $0.1 \text{ m}^2$ .

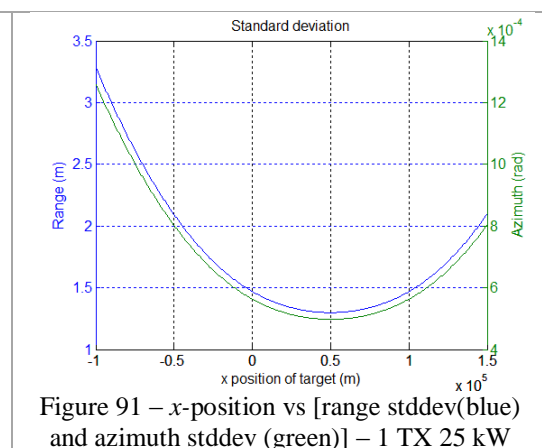
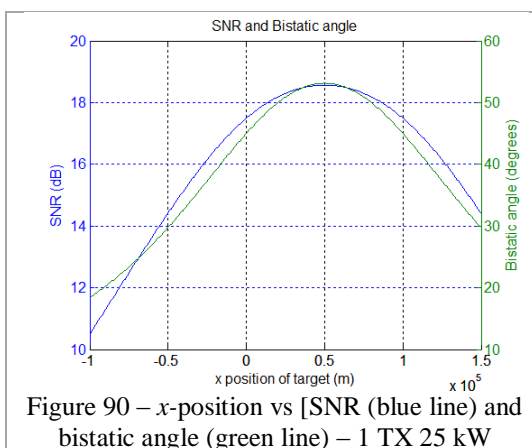
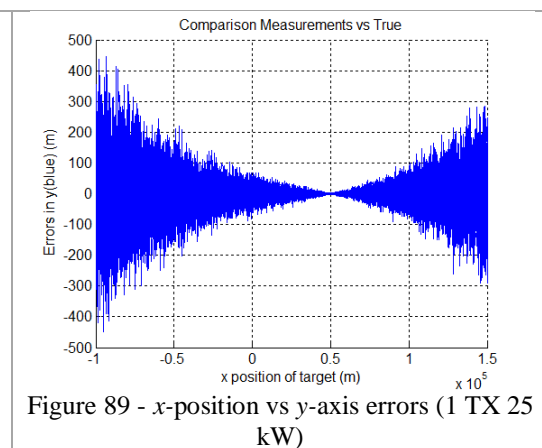
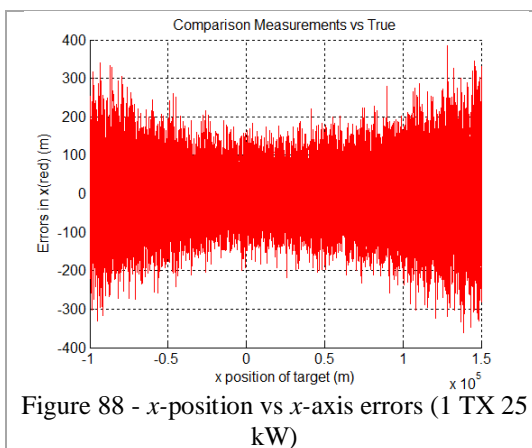
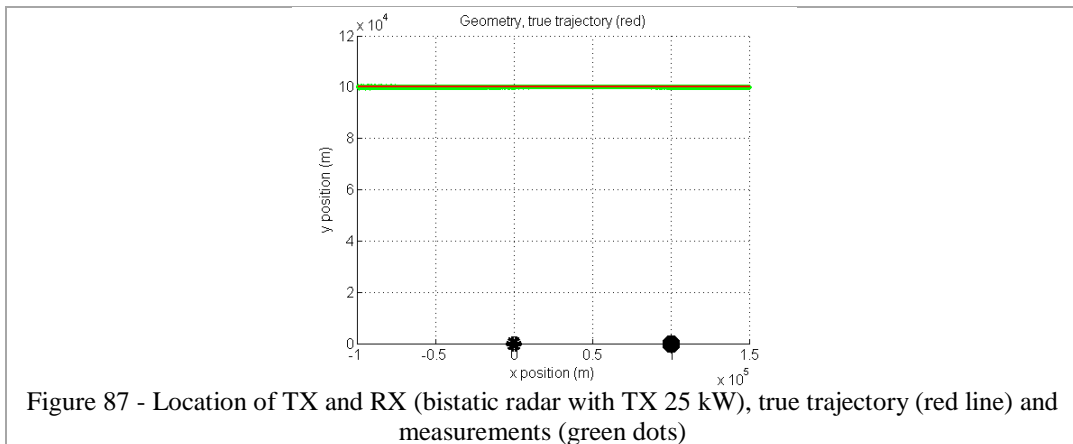


### 7.1.2 Bistatic

In the bistatic scenarios depicted in the next sections, bistatic radars are represented by a TX (black circle) and a RX (black hexagram). The target has an  $x$ -velocity of 250 m/s and the measurements are performed during 1000 seconds every 2.5 seconds.

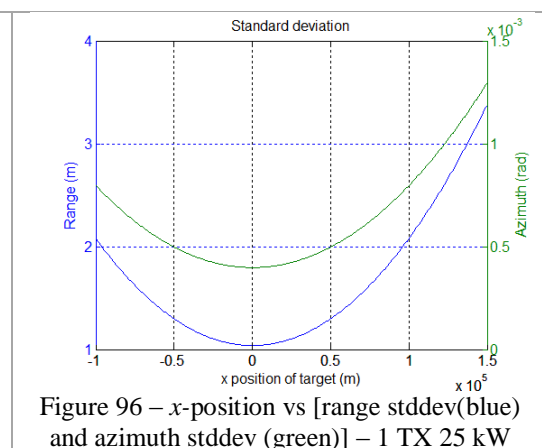
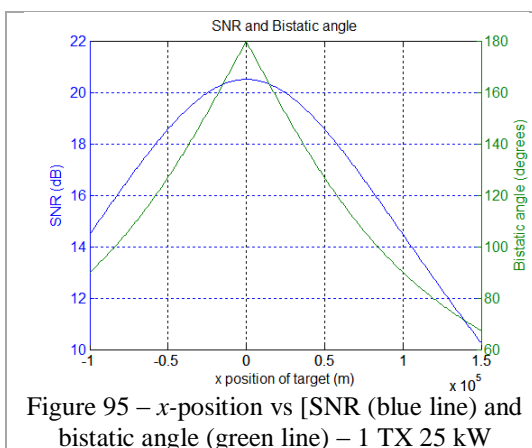
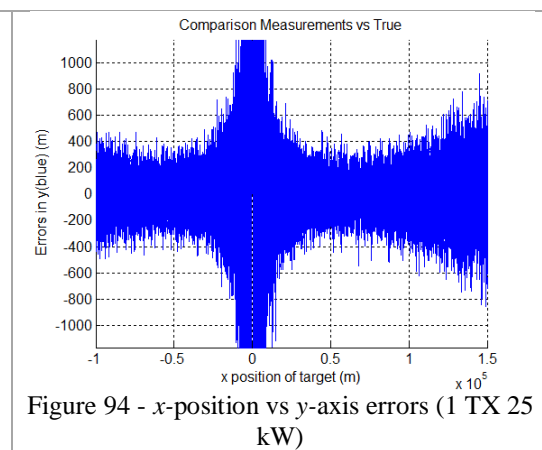
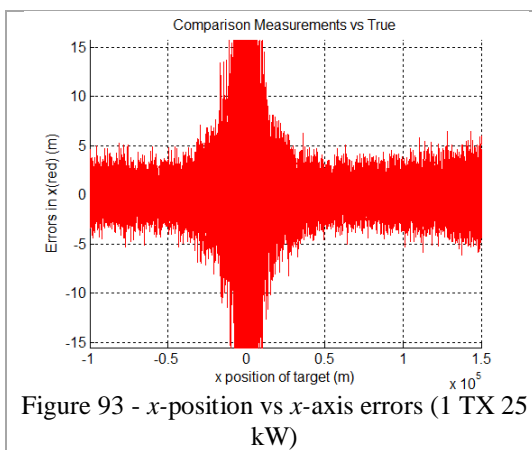
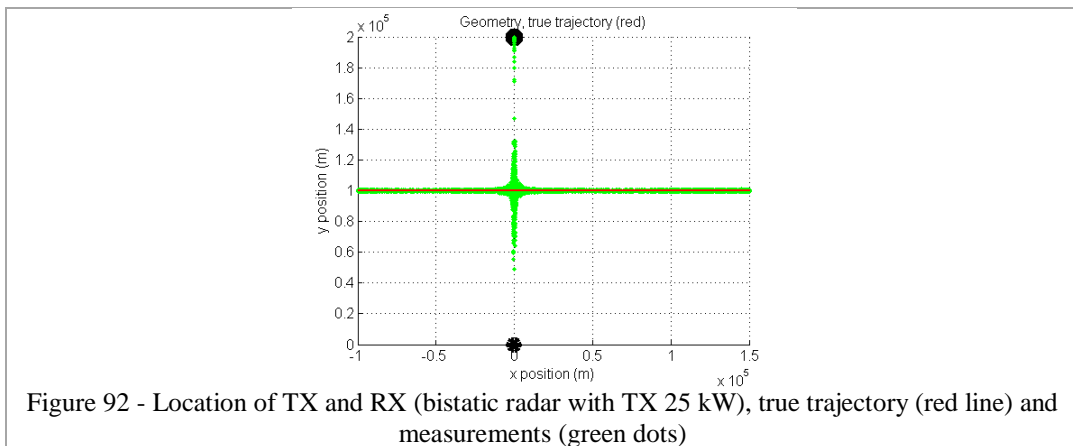
### 7.1.2.1 Target RCS 10 m<sup>2</sup>

Figure 87 shows the geometry with TX and RX separated by 100 km which is the baseline. The target is moving horizontally and parallel to the baseline.

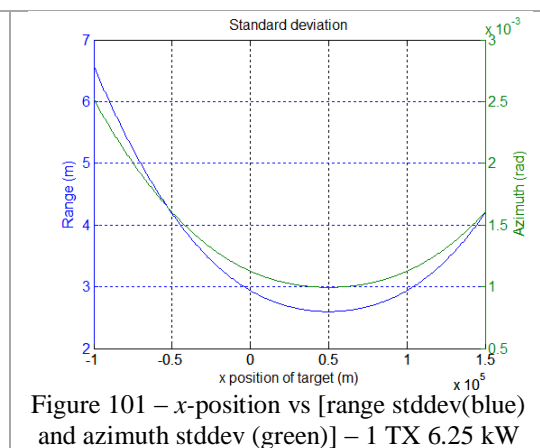
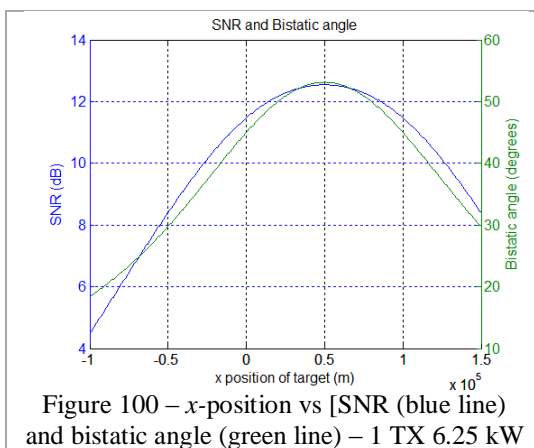
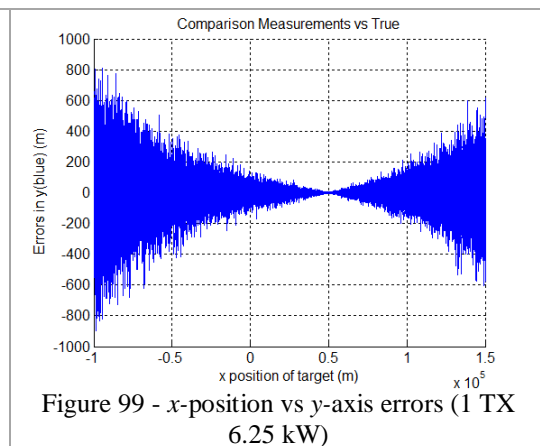
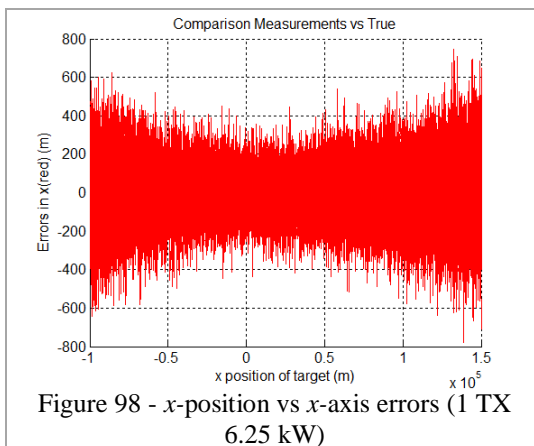
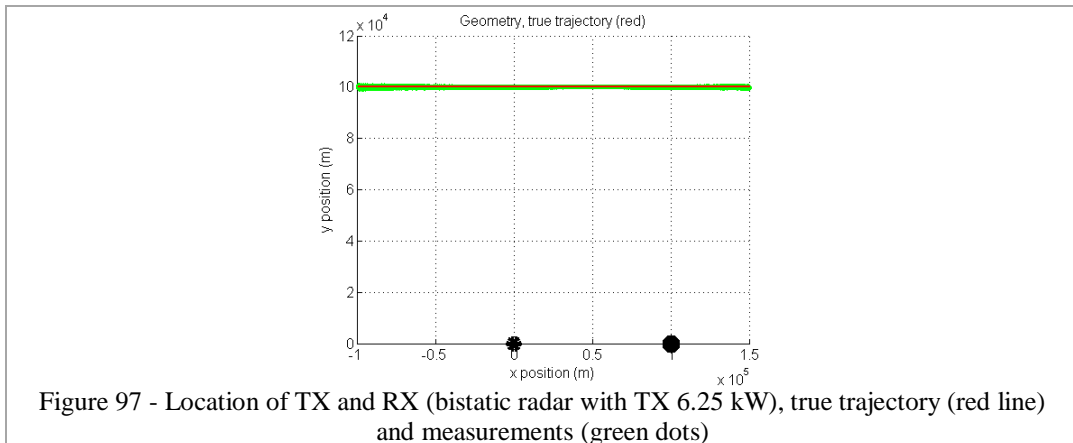


In the example below, the TX still have 25 kW power but the baseline is 200 km and is perpendicular to the target trajectory which crosses the baseline. Observing Figure 93, Figure 94 and Figure 95 it can be seen that when bistatic angle gets close to 180

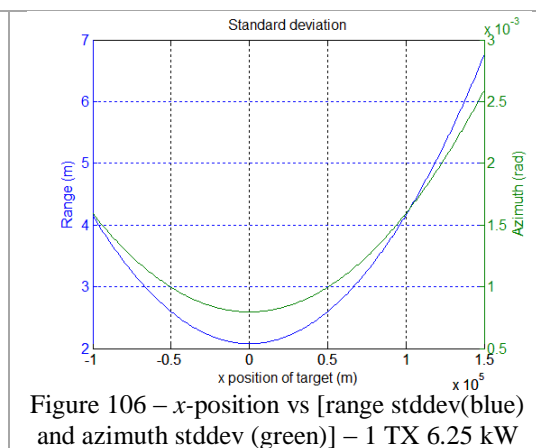
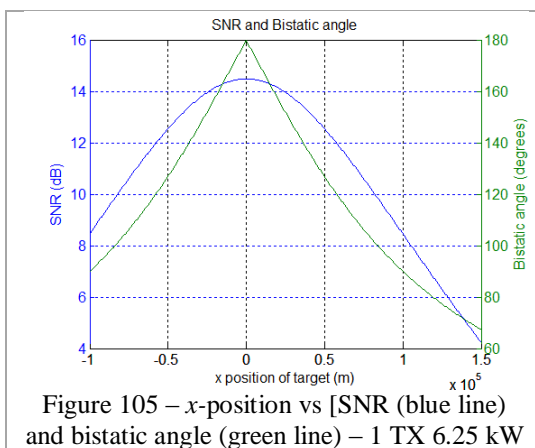
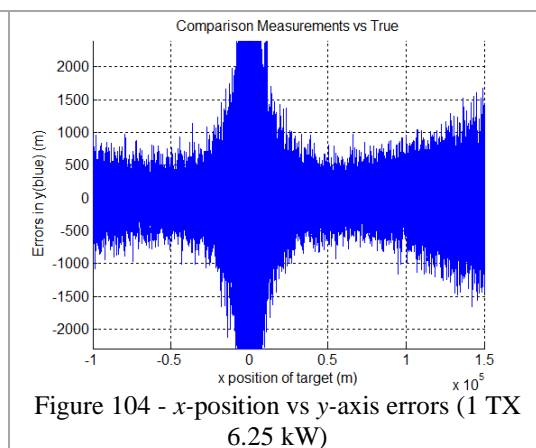
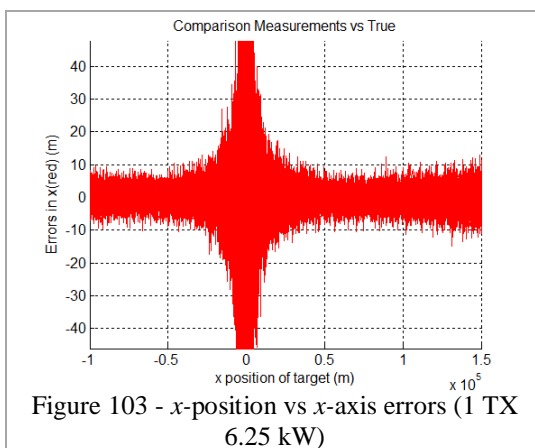
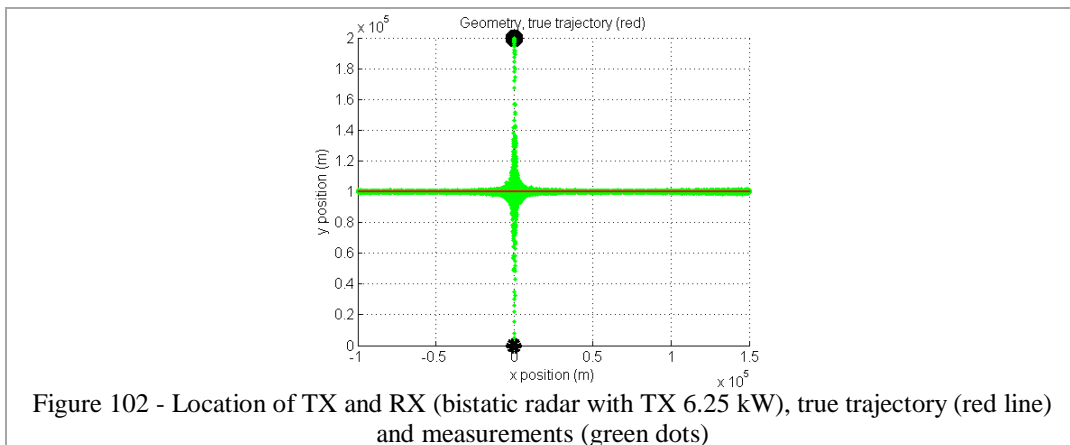
degrees, the measurements errors get much worse, although SNR is higher (Figure 95) in this region. This is due to equation (1).



The next 2 scenarios show what happens with the measurements errors when the power of TX is reduced by a factor of 4.



Note, again, that a reduction in power of a factor of 4 has the same (expected) effect on measurement errors either when the target is parallel to the baseline or crossing it.



### 7.1.2.2 Target RCS 0.1 m<sup>2</sup>

Now, the same trajectory crossing the same bistatic geometries as in section 7.1.2.1, but the target has RCS of 0.1 m<sup>2</sup>. It can be seen in all figures in this section, that comparing to the figures in the previous section, the reduction on RCS from 10 m<sup>2</sup> to 0.1 m<sup>2</sup>, made the errors to increase 10 times. The reduction on RCS by a factor of

100 (20 dB), makes SNR to reduce 100 times as well, and due to the square root factor of equations (18) and (19), standard deviations increase by a factor of 10.

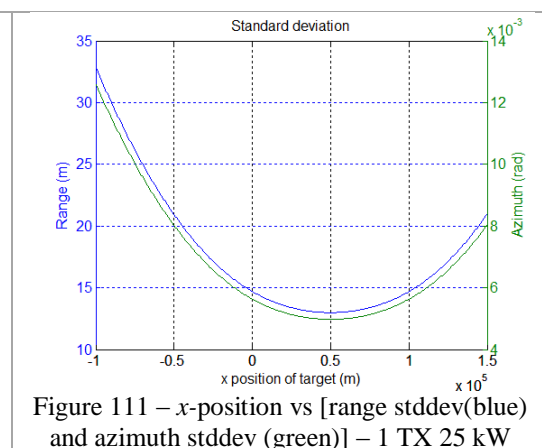
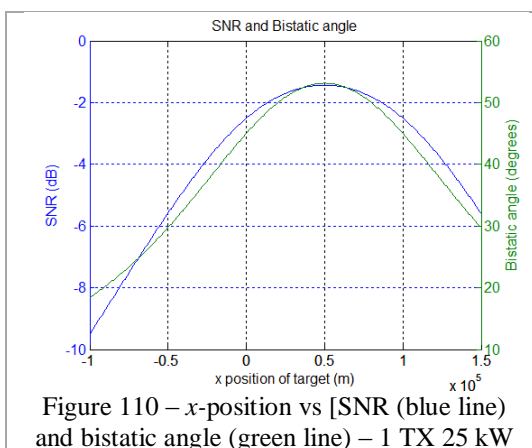
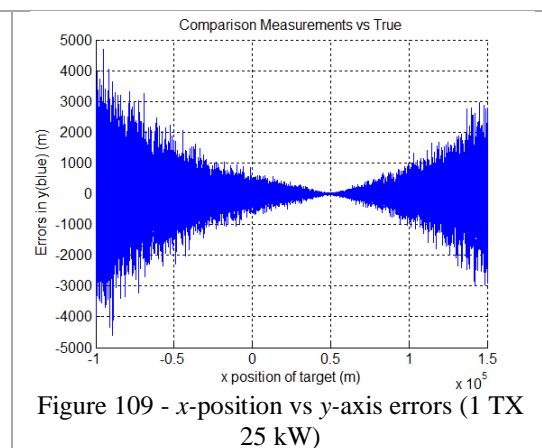
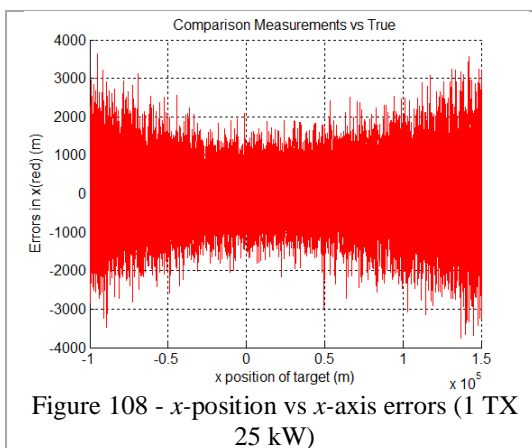
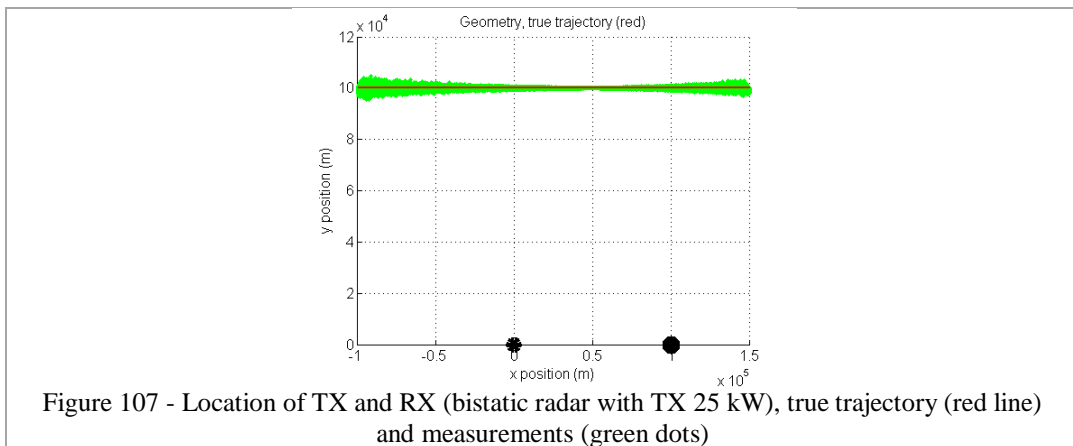
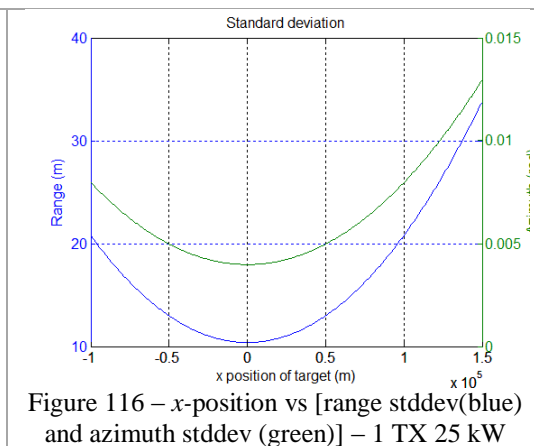
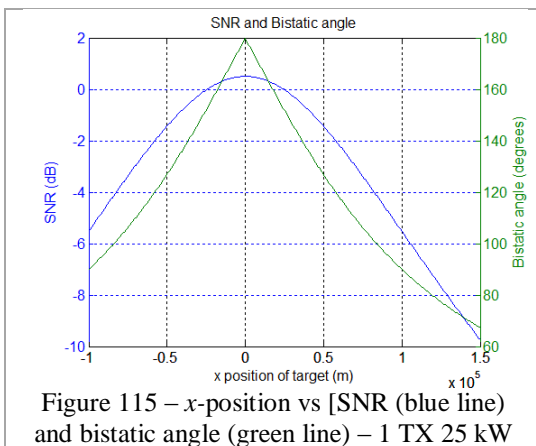
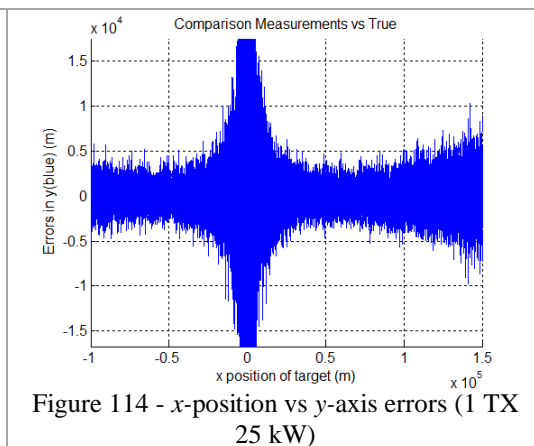
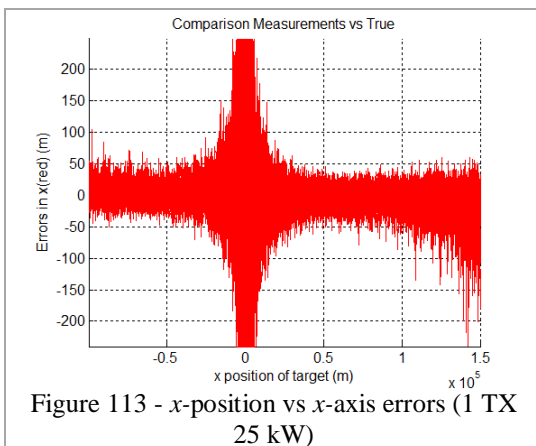
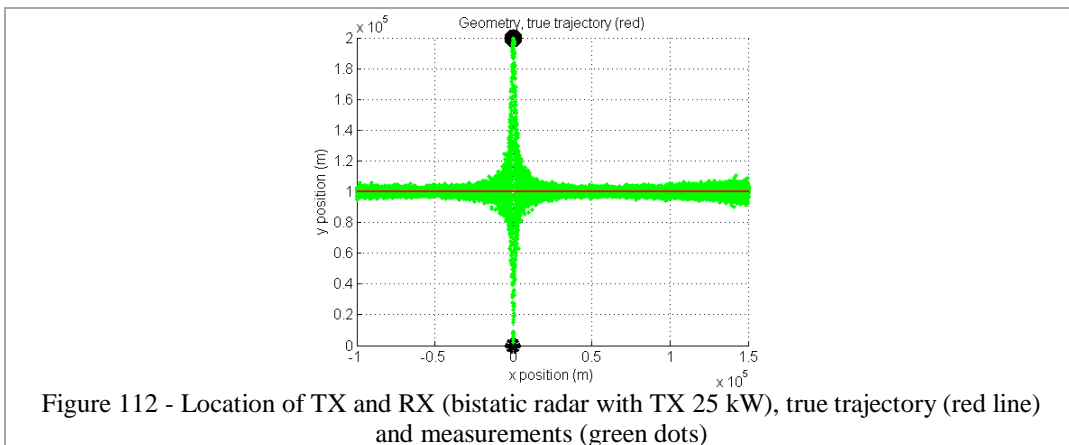


Figure 112 to Figure 116 present the scenario where the target crosses the baseline of the bistatic radar.



### 7.1.3 Multistatic (1 x N)

In the multistatic scenarios depicted below, the main purpose is to show the results from the fusion algorithm when performed using measurements from 2 radars (for example, 2 bistatic radars). For multistatic scenarios, only targets with  $RCS=0.1 \text{ m}^2$  are considered as it is the main focus of this research.

Figure 117 to Figure 127 show a geometry where there is only 1 TX (25 kW) and 2 RXs, and the target has  $RCS=0.1 \text{ m}^2$ . The black circle is the TX and the green and magenta hexagrams are RXs. Thus, the target is crossing the baseline of a bistatic radar (black/green pair) and going on a parallel line of another bistatic radar (black/magenta pair).

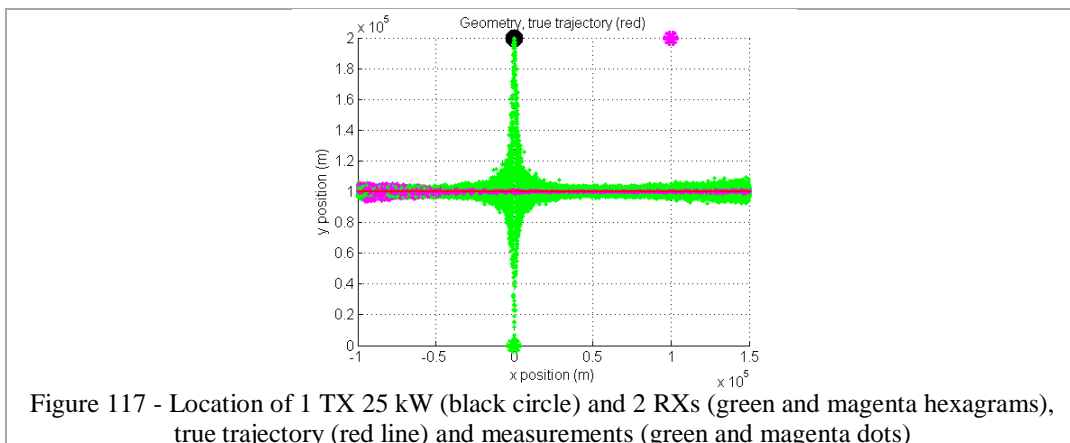


Figure 117 - Location of 1 TX 25 kW (black circle) and 2 RXs (green and magenta hexagrams), true trajectory (red line) and measurements (green and magenta dots)

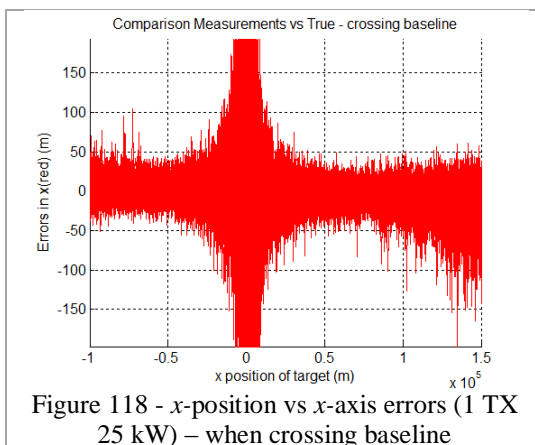


Figure 118 - x-position vs x-axis errors (1 TX 25 kW) – when crossing baseline

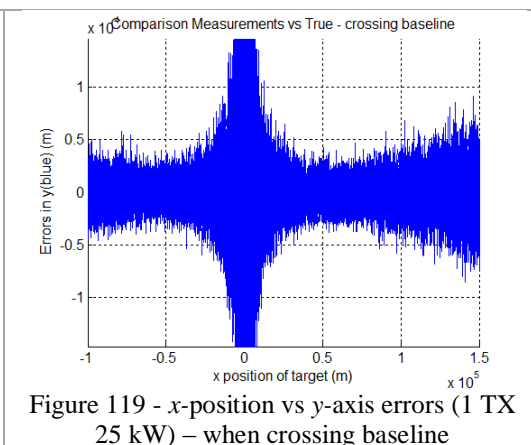


Figure 119 - x-position vs y-axis errors (1 TX 25 kW) – when crossing baseline

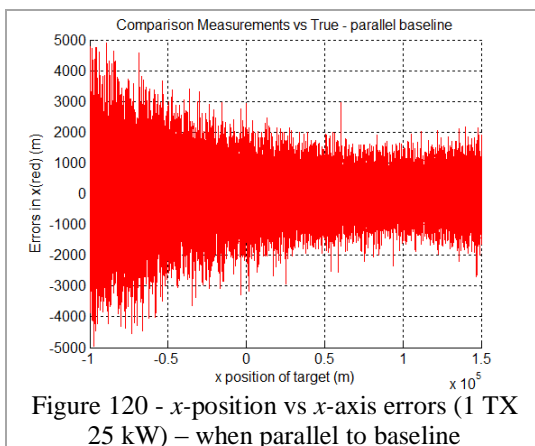


Figure 120 - x-position vs x-axis errors (1 TX 25 kW) – when parallel to baseline

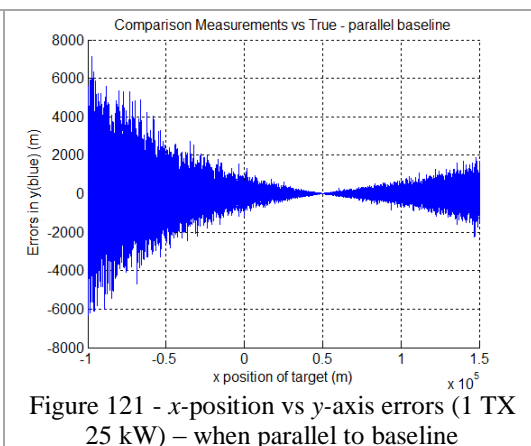
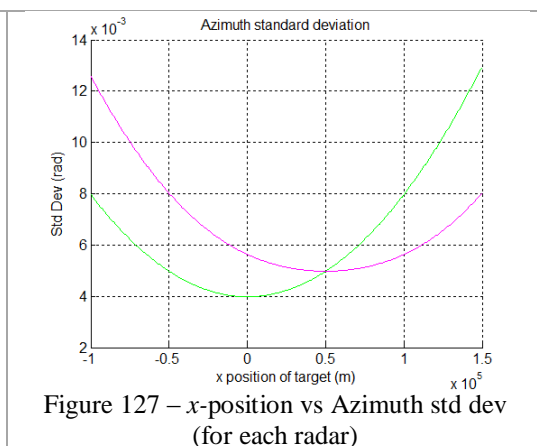
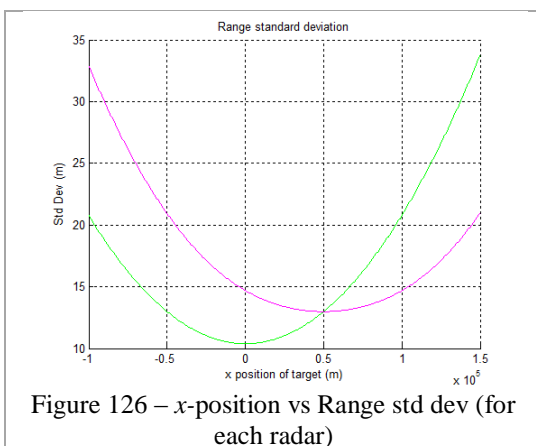
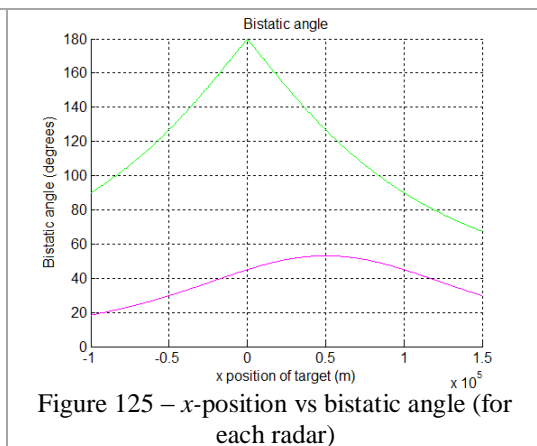
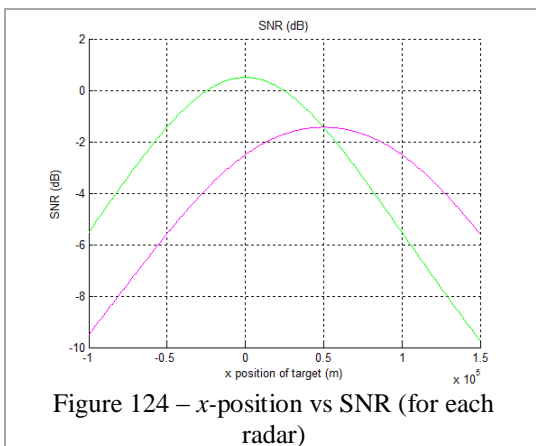
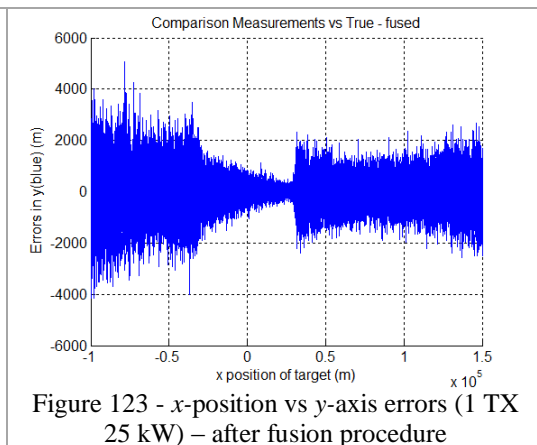
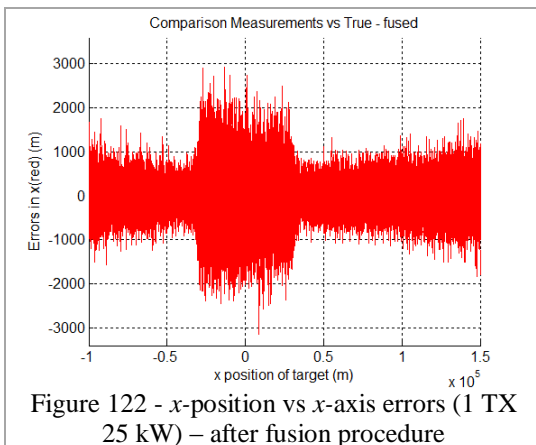
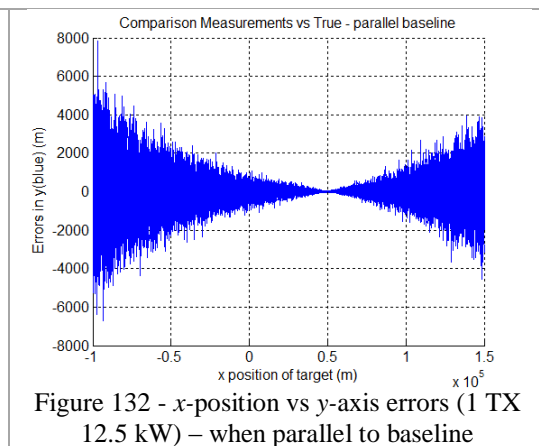
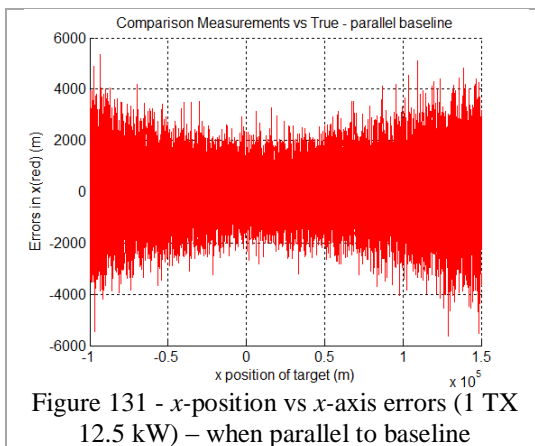
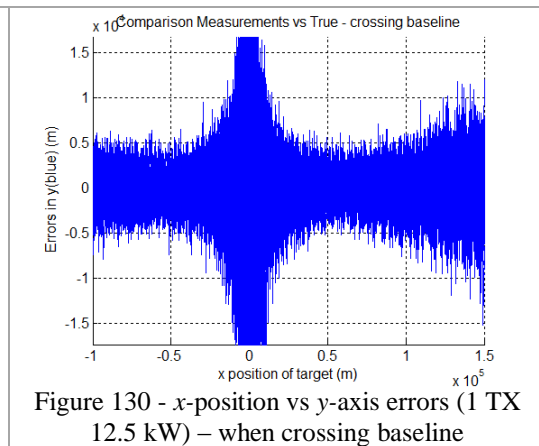
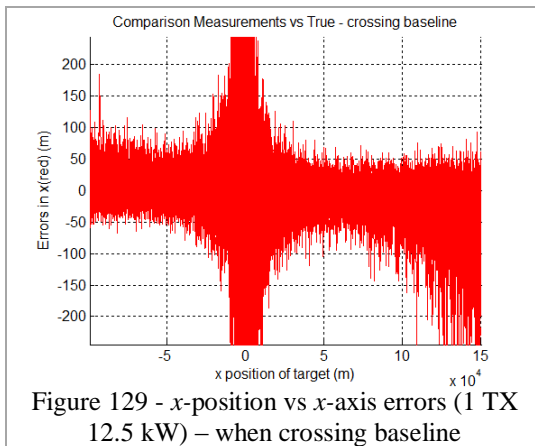
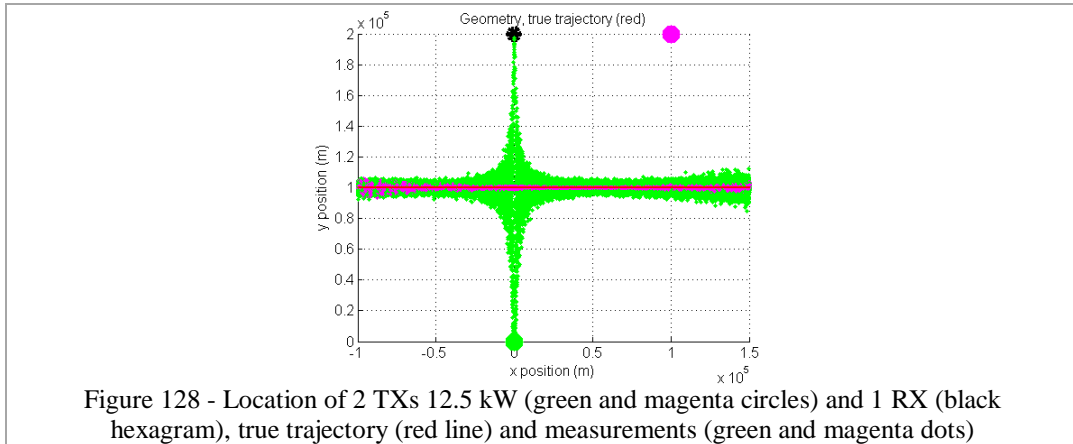


Figure 121 - x-position vs y-axis errors (1 TX 25 kW) – when parallel to baseline



### 7.1.4 Multistatic ( $M \times 1$ )

Figure 128 to Figure 138 depict a geometry where there is only 1 RX and 2 TXs (of 12.5 kW each). The black hexagram is the RX and the green and magenta circles are the TXs, like the previous scenario. Thus, the target is crossing the baseline of a bistatic radar (black/green pair) and going on a parallel line of another bistatic radar (black/magenta pair).



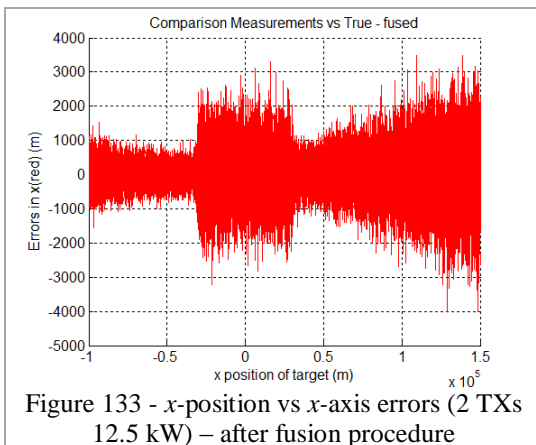


Figure 133 -  $x$ -position vs  $x$ -axis errors (2 TXs 12.5 kW) – after fusion procedure

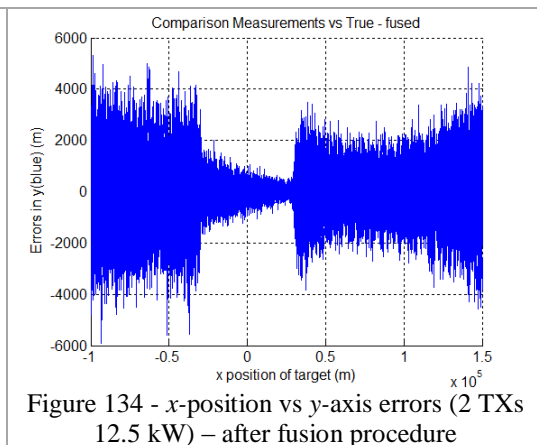


Figure 134 -  $x$ -position vs  $y$ -axis errors (2 TXs 12.5 kW) – after fusion procedure

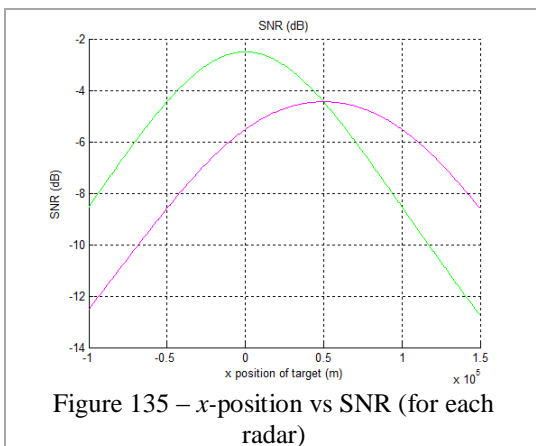


Figure 135 –  $x$ -position vs SNR (for each radar)

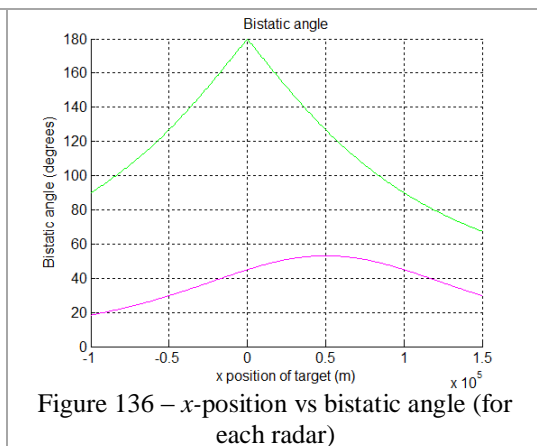


Figure 136 –  $x$ -position vs bistatic angle (for each radar)

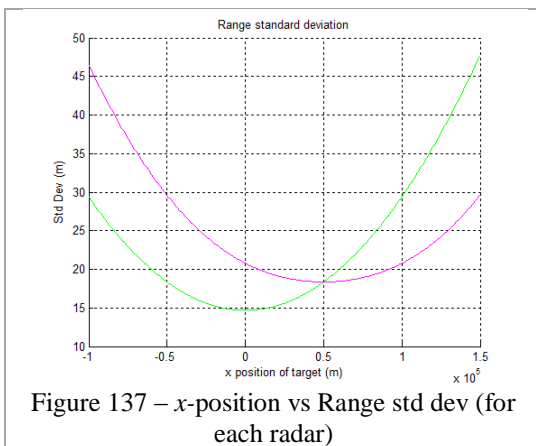


Figure 137 –  $x$ -position vs Range std dev (for each radar)

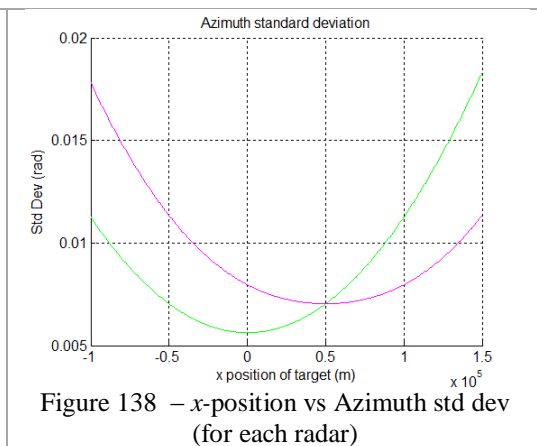


Figure 138 –  $x$ -position vs Azimuth std dev (for each radar)

In this scenario, there are 2 TXs of half of the power of the scenario where there was 1 TX (section 7.1.3). So, instead of having 2 pairs of bistatic radars with a 25 kW TX, there are 2 pairs of bistatic radars with 12.5 kW TXs. But, because of the square root factor in equations (18) and (19), the errors increased about 1.4 times if compared to the scenario in 7.1.3.

Therefore, although it seems to be better to use a configuration with 1 TX (25 kW) and 1 RX instead of 2 TXs (12.5 kW) and 1 RX, there is an advantage when using

the latter that, if one TX is lost (in military scenarios, it is more likely that a TX is located and thus destroyed) the whole system can still work (with some loss in performance).

### 7.1.5 Measurements Summary Table

Section 7.1 presents a series of simulations performing measurements in different scenarios, including monostatic, bistatic and multistatic ones. Table 3 presents a summary from the measurements simulations in monostatic geometries. This is to illustrate how different parameters on the geometry or target can affect the measurements errors.

Table 3 – Measurements Summary for monostatic geometries – measurement errors during the trajectory of the target in different configurations, changing location and transmit power of the radar and target RCS

Geometry	Errors in x-axis measurement (m)				Errors in y-axis measurement (m)			
	$x=-50$ km	$x=0$ km	$x=50$ km	$x=100$ km	$x=-50$ km	$x=0$ km	$x=50$ km	$x=100$ km
(1) Monostatic (25 kW) far	150	100	150	200	75	5	75	200
(2) Monostatic (6.25 kW) far	300	200	300	400	150	10	150	400
(3) Monostatic (25 kW)	0.75	0	0.75	3	10	0	10	100
(4) Monostatic (6.25 kW)	1.5	0	1.5	6	20	0	20	200
(5) Monostatic (25 kW) far RCS=0.1 m <sup>2</sup>	1500	1000	1500	2000	750	50	750	2000
(6) Monostatic (25 kW) RCS=0.1 m <sup>2</sup>	7.5	0	7.5	30	100	0	100	1000

From line (1) to line (2), TX power is reduced from 25 kW to 6.25kW and it results in an increase on errors by a factor of 2. The same happens from line (3) to line (4) but, in those lines, TX is on the target trajectory and thus the errors are significantly smaller. Line (5) is compared to line (1), where in line (5) RCS of the target is reduced by a factor of 100 (from 10 m<sup>2</sup> to 0.1 m<sup>2</sup>) which results in increasing of the errors by a factor of 10. The same situation occurs when comparing line (6) to line (3).

Next table, Table 4, depicts a summary from the measurements simulations in bistatic geometries and its purpose is to demonstrate that the same assumptions for the errors are valid.

Table 4 - Measurements Summary for bistatic geometries – measurement errors during the trajectory of the target in different configurations, changing location and transmit power of the radar and target RCS

Geometry	Errors in x-axis measurement (m)				Errors in y-axis measurement (m)			
	x=-50 km	x=0 km	x=50 km	x=100 km	x=-50 km	x=0 km	x=50 km	x=100 km
(1) Bistatic (25 kW)	200	125	175	225	150	50	0	100
(2) Bistatic (25 kW) crossing	4		4	4	300		300	400
(3) Bistatic (6.25 kW)	400	250	350	450	300	100	0	200
(4) Bistatic (6.25 kW) crossing	8		8	8	600		600	800
(5) Bistatic (25 kW) RCS=0.1 m <sup>2</sup>	2000	1250	1750	2250	1500	500	0	1000
(6) Bistatic (25 kW) RCS=0.1 m <sup>2</sup> crossing	40		40	40	3000		3000	4000

As an example, from Table 4, line (1) compared with line (3) has an increase in the errors by a factor of 2 due to the decrease in the power by a factor of 4. The same happens between lines (2) and (4). And if RCS is decreased by a factor of 100, the errors increase by a factor of 10 as can be seen observing lines (1) and (5) and also lines (2) and (6).

For multistatic scenarios, Table 5 summarizes what is simulated in 7.1.3 and 7.1.4 when the radar networks are comprised by 1 TX (25 kW) and 2 RXs or 2 TXs (12.5 kW each) and 1 RX. Lines (1) and (4) depict the results from the bistatic pair whose baseline the target is crossing and lines (2) and (5) show the results from the pair whose baseline is parallel to the target trajectory. Lines (3) and (6) depict the results after performing the fusion of the measurements from both pairs of bistatic radars.

Table 5 - Measurements Summary for multistatic geometries – measurement errors during the trajectory of the target in 2 different configurations, one Multistatic (1 TX / 2 RXs) and the other one Multistatic (2 TXs / 1 RX)

Geometry  RCS=0.1 m <sup>2</sup>	Errors in x-axis measurement (m)				Errors in y-axis measurement (m)			
	x=-50 km	x=0 km	x=50 km	x=100 km	x=-50 km	x=0 km	x=50 km	x=100 km
1 TX (25 kW) and 2 RXs								
(1) Crossing pair	40		40	50	3000		3000	4000
(2) Parallel pair	2500	2000	1500	1200	2000	1000	0	500
(3) Fused	800	1750	800	1000	2000	1000	1500	1500
2 TXs (12.5 kW each) and 1 RX								
(4) Crossing pair	50		50	70	4000		4000	5000
(5) Parallel pair	3000	2000	2000	3000	2000	1000	0	1500
(6) Fused	800	2000	1000	2000	3000	1000	2000	2000

Table 6 shows, for monostatic scenarios, how different is the maximum SNR which affects how good measurement standard deviations are. Only scenarios where the target is far from the monostatic radar are depicted.

Table 6 – Maximum SNR and Best Range/Azimuth standard deviation for monostatic scenarios (target flying far from TX/RX)

Geometry	Maximum SNR (dB)	Best Range standard deviation (meters)	Best Azimuth standard deviation (mrad)
(1) Far Monostatic (25 kW) RCS=10 m <sup>2</sup>	20.5 at x=0	1	0.4
(2) Far Monostatic (6.25 kW) RCS=10 m <sup>2</sup>	14.5 at x=0	2	0.8
(3) Far Monostatic (25 kW) RCS=0.1 m <sup>2</sup>	0.5 at x=0	10	4

From line (1) to line (2), the total power is reduced by a factor of 4 and thus SNR is also reduced by a factor of 4 (or 6 dB). Standard deviations are increased by a factor of 2. From line (1) to line (3), the total power is still the same, but target RCS is decreased by a factor of 100 (20 dB) and thus SNR is decreased by the same factor. Standard deviations are increased by a factor of 10.

Table 7 depicts, for bistatic scenarios, the maximum SNR and their respective best range and azimuth standard deviations. Again, the same conclusions from Table 6 are valid for Table 7 when comparing lines (1), (3) and (5) (target not crossing the baseline) and then comparing lines (2), (4) and (6) (target that cross the baseline).

Table 7 - Maximum SNR and Best Range/Azimuth standard deviation for bistatic scenarios

Geometry	Maximum SNR (dB)	Best Range standard deviation (meters)	Best Azimuth standard deviation (mrad)
(1) Far Bistatic (25 kW) RCS=10 m <sup>2</sup>	18.5 at x=50 km	1.3	0.5
(2) Crossing Bistatic (25 kW) RCS=10 m <sup>2</sup>	20.5 at x=0 km	1	0.4
(3) Far Bistatic (6.25 kW) RCS=10 m <sup>2</sup>	12.5 at x=50 km	2.6	1
(4) Crossing Bistatic (6.25 kW) RCS=10 m <sup>2</sup>	14.5 at x=0 km	2	0.8
(5) Far Bistatic (25 kW) RCS=0.1 m <sup>2</sup>	-1.5 at x=50 km	13	5
(6) Crossing Bistatic (25 kW) RCS=0.1 m <sup>2</sup>	0.5 at x=0 km	10	4

Finally, Table 8 presents Maximum SNR and standard deviations for multistatic scenarios.

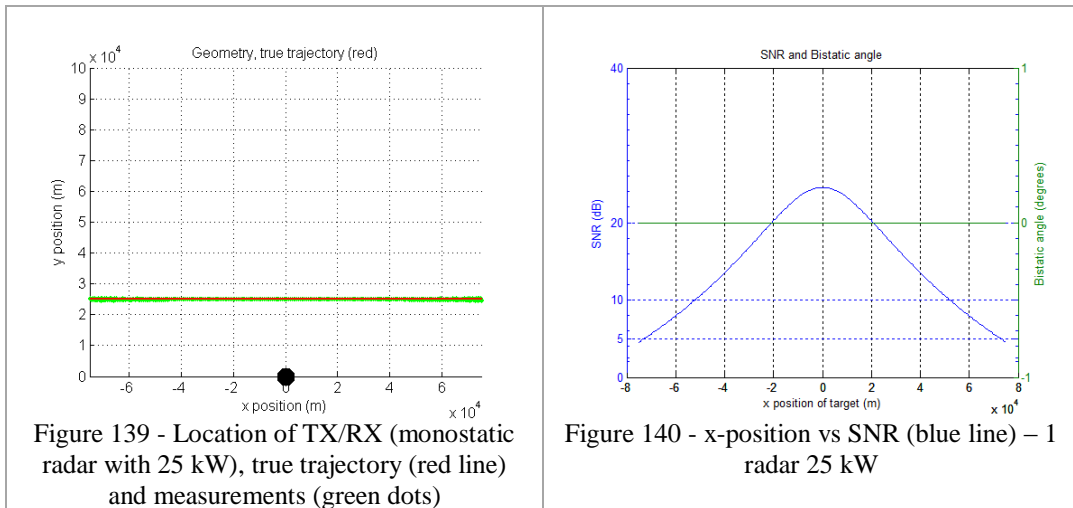
Table 8 - Maximum SNR and Best Range/Azimuth standard deviation for multistatic scenarios

Geometry	Maximum SNR (dB)	Best Range standard deviation (meters)	Best Azimuth standard deviation (mrad)
<b>Multistatic 1 x N (1 TX 25 kW and 2 RXs), RCS=0.1 m<sup>2</sup> : 2 pairs of 25 kW bistatic radars</b>			
Crossing pair	0.5 at x=0	10	4
Parallel pair	-1.5 at x=0	13	5
<b>Multistatic N x 1 (2 TXs 12.5 kW and 1 RX), RCS=0.1 m<sup>2</sup> : 2 pairs of 12.5 kW bistatic radars</b>			
Crossing pair	-2.5 at x=0	15	5.5
Parallel pair	-4.5 at x=0	18	7

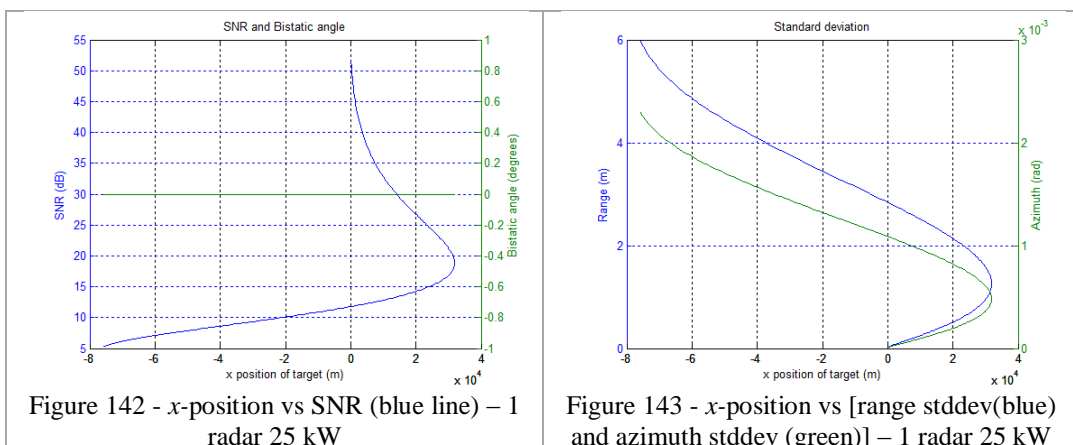
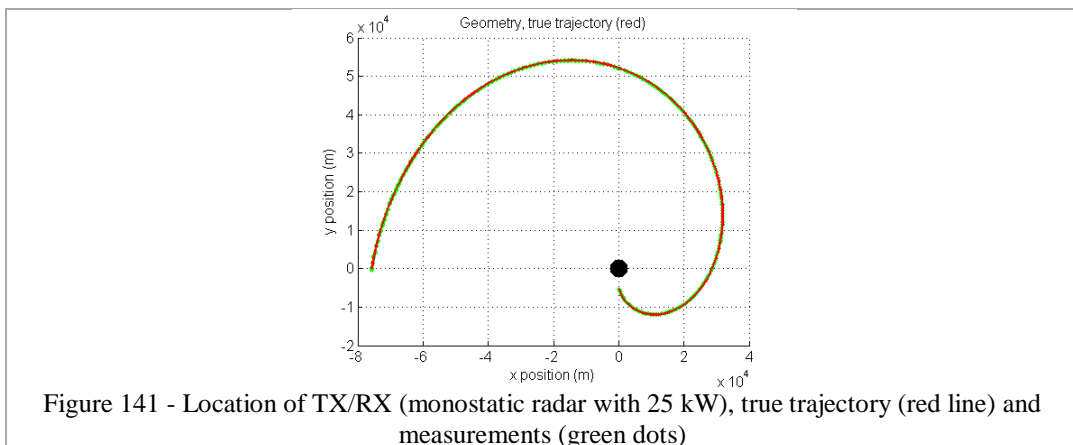
The tables in this section present some quantitative values at certain points of the trajectory and illustrate the influence of transmitter power and RCS in the results. However, the graphics in previous sections depict a more thorough idea on how the measurements behave along the whole trajectory for different geometries.

## 7.2 Tracking Results

As can be seen in Section 7.1, there are some scenarios where SNR have negative values (in dB). In this section, it is assumed, for the purpose of this research, that the minimum SNR in order to detect the target is 5 dB, which is a ratio of about 3.1. So, for more realistic results, the radar nodes are positioned closer to the target, like shown in Figure 139 and Figure 140 where the target starts to be tracked when it is about 80 Km far from the radar and at this location the measurement have an SNR of about 5 dB.



The same is applied for spiral-like trajectories and Figure 141 to Figure 143 show the trajectory, SNR and standard deviations according to  $x$ -position.



Therefore, in this section, several geometries are presented with a target (target 1) crossing with a horizontal constant speed of 250 m/s, during 600 seconds and then a target (target 2) with a spiral trajectory with no constant velocity or acceleration

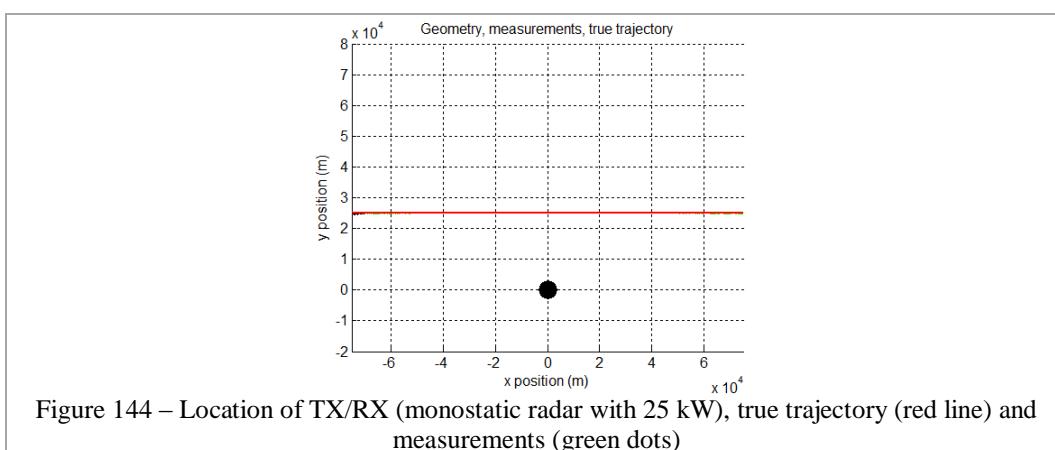
during 1000 seconds. For all scenarios in this section, target RCS is  $0.1 \text{ m}^2$ . Now, *script30a.m* is run for each scenario and *TEnvironment.m* must be adapted in order to use the correct target trajectories (comment some lines of code and uncomment some others related to horizontal trajectories).

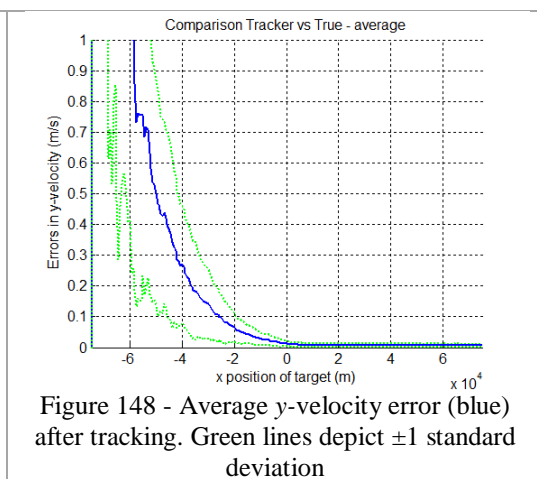
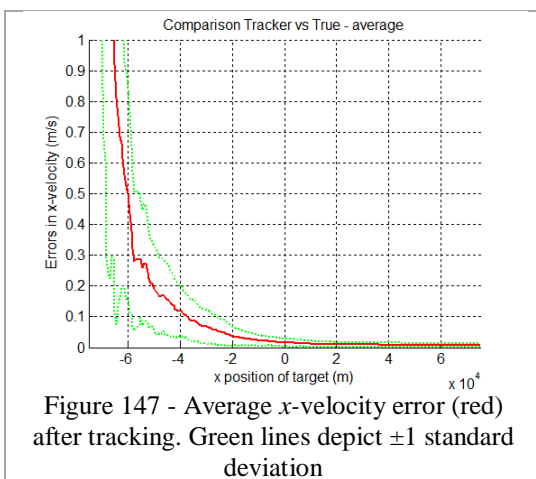
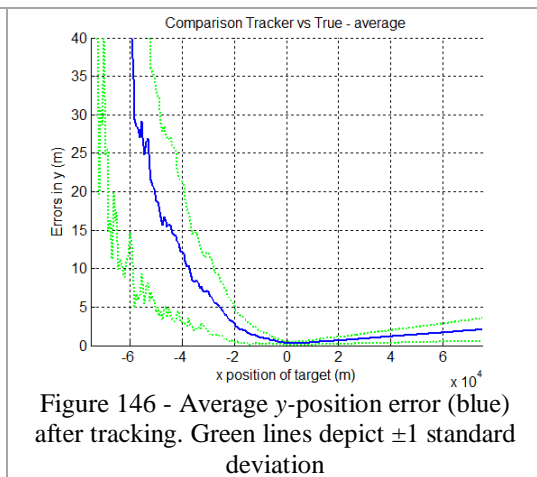
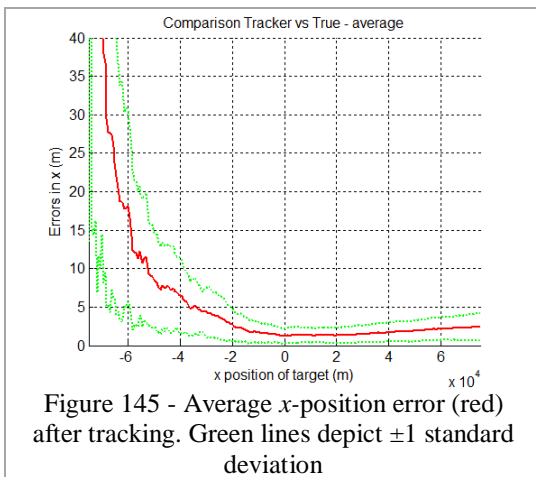
## 7.2.1 Target 1 (straight line)

In the next scenarios the target starts at  $(-75,25) \text{ km}$ , flies on a straight line and for each scenario, 100 simulation runs are performed in order to calculate the average and standard deviation of the results.

### 7.2.1.1 Monostatic

This scenario represents a monostatic geometry where in Figure 144, the black circle is the monostatic radar (TX/RX) with 25 kW, the red line is the true trajectory and the green dots are the measurements. The following 2 figures (Figure 145 and Figure 146) represent the average position errors (red for  $x$ -axis and blue for  $y$ -axis) and  $\pm 1$  standard deviation (green dotted line) after filtering. Finally, the last two figures of this scenario (Figure 147 and Figure 148) show the average velocity errors (red for  $x$ -axis and blue for  $y$ -axis) and  $\pm 1$  standard deviation (green dotted line). Note that the position errors in both axis are smaller than 20 meters after position  $x = -50 \text{ km}$  and velocity errors are smaller than  $0.5 \text{ m/s}$  from the same position.

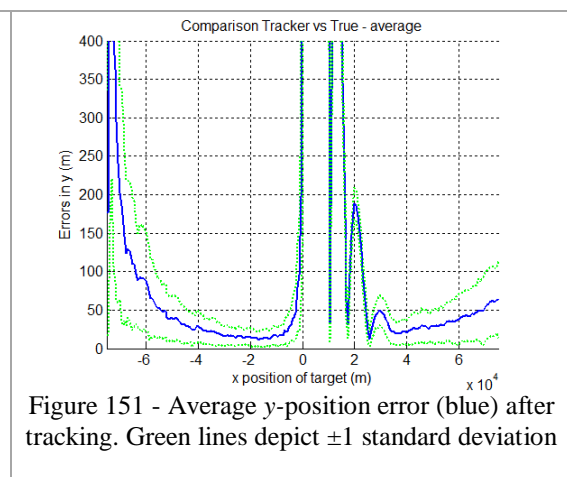
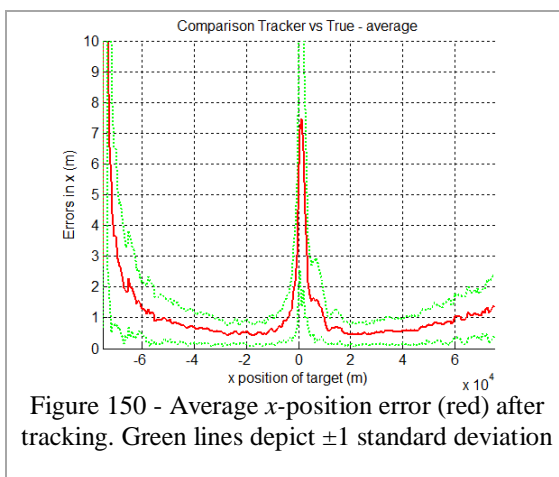
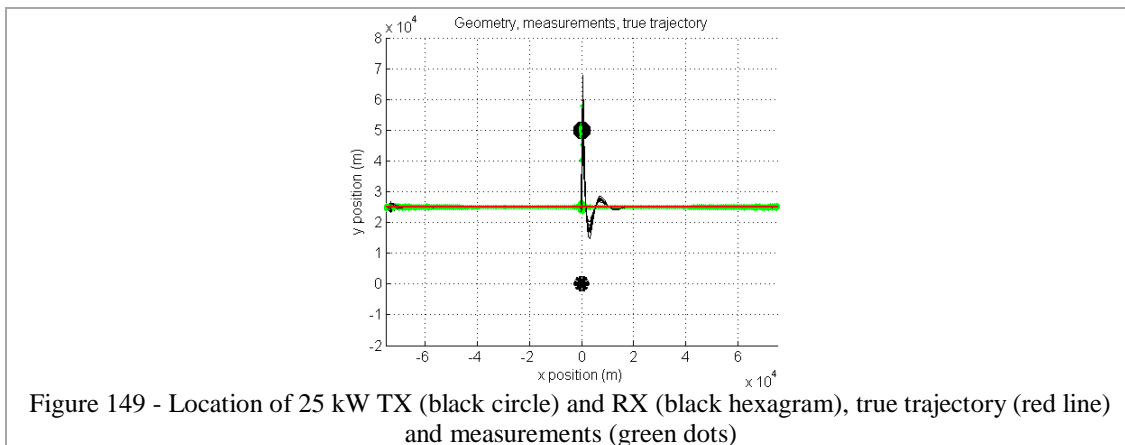




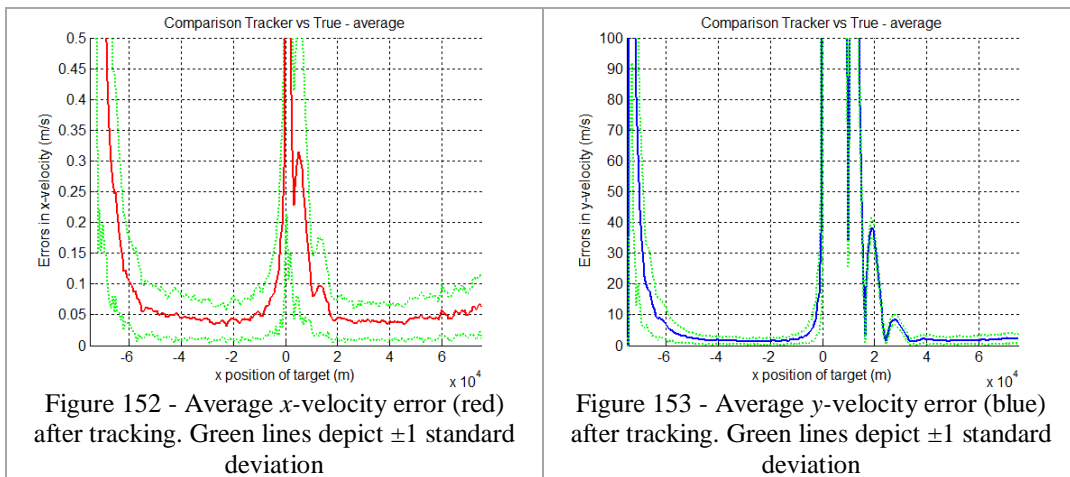
## 7.2.1.2 Bistatic

### 7.2.1.2.1 Bistatic (crossing baseline)

This scenario represents a bistatic geometry where in the Figure 149, the black circle at (0,50) km is the TX with 25 kW, the black hexagram at (0,0) km is the RX, the red line is the true trajectory and the green dots are the measurements. Black line depicts the filtered trajectory. The following figures (Figure 149 to Figure 153) represent the same type information as in Figure 144 to Figure 148.

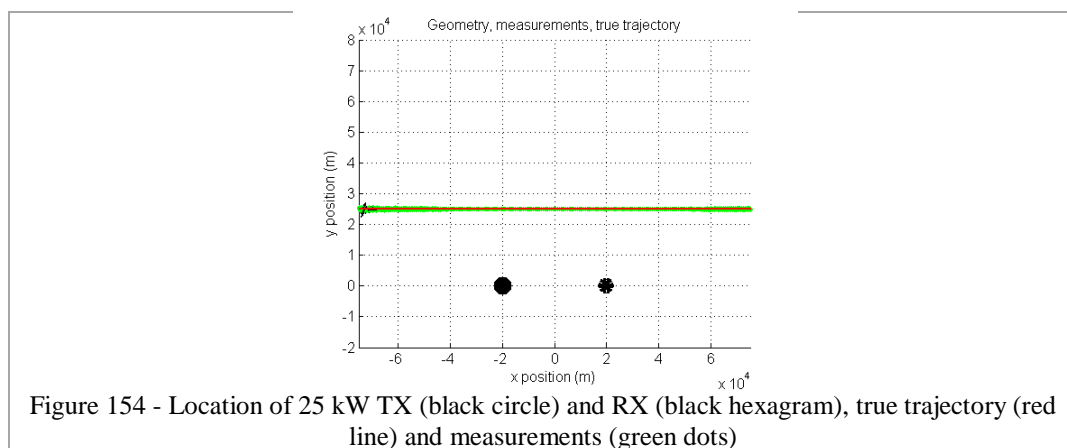


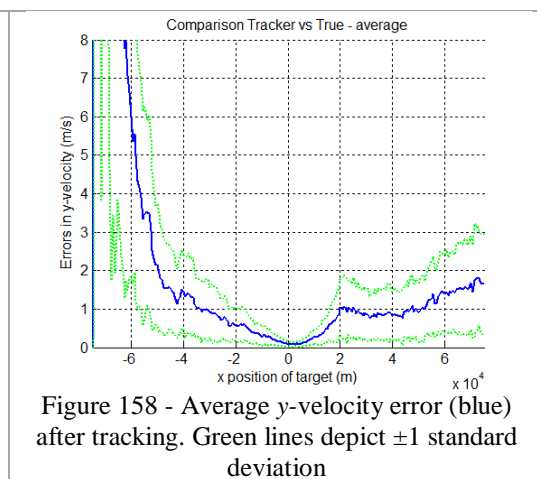
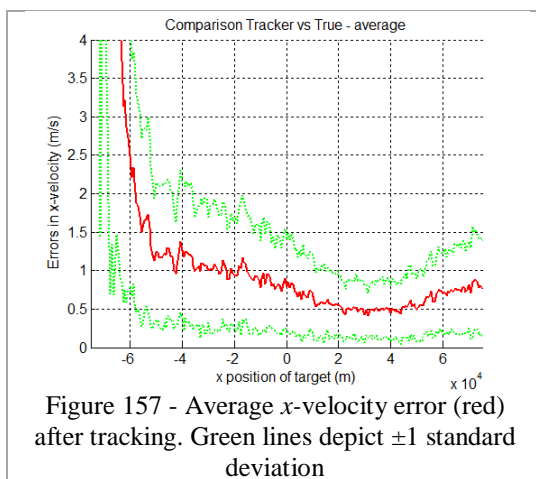
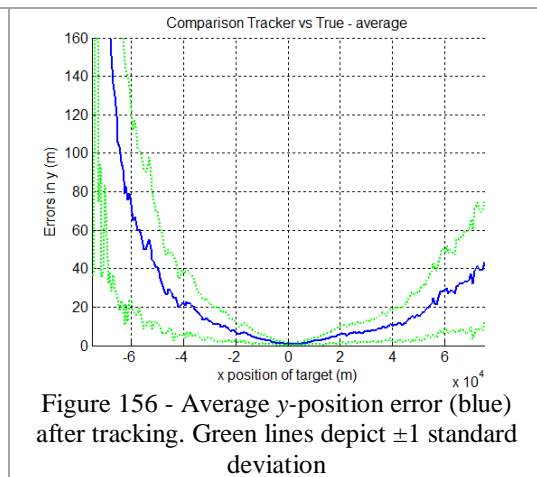
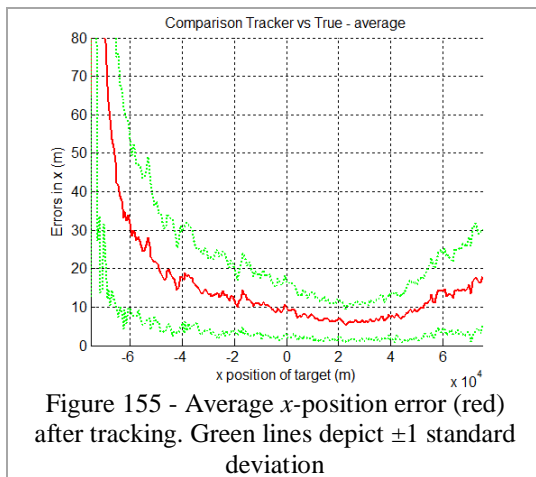
Note that, in this geometry, the tracking errors (for y-position and y-velocity) are very large in the region close to the baseline and overall the same tracking errors (for x-axis) are larger than the previous (monostatic) case. Nevertheless, the x-position and x-velocity, except when it is close to the baseline (somewhere from  $x=-10$  and  $x=10$  km) are much better than in monostatic cases. After the baseline, it takes some time in order to the tracking filter to adjust and be accurate again (at around  $x=10$  km for x-axis and  $x=25$  km for y-axis). In this scenario, the y-axis (position or velocity) tracking results are bad, because the measurements are very inaccurate in this axis, as this axis lie in the baseline or parallel to it.



**7.2.1.2.2 Bistatic (parallel to baseline TX-RX)**

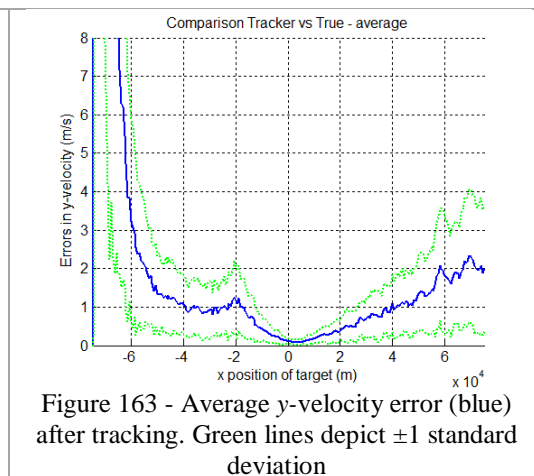
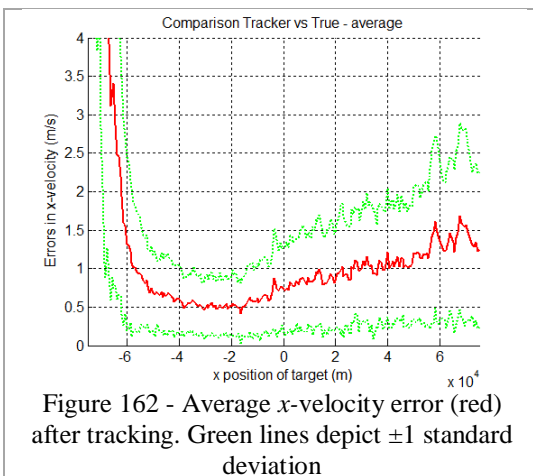
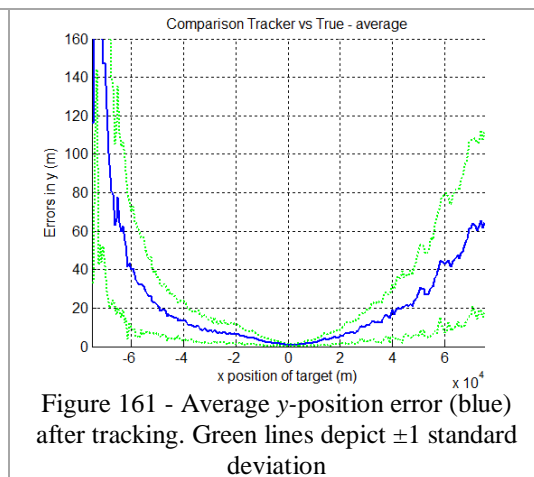
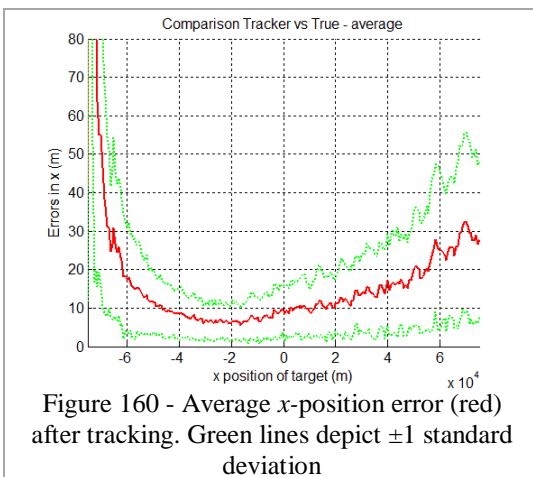
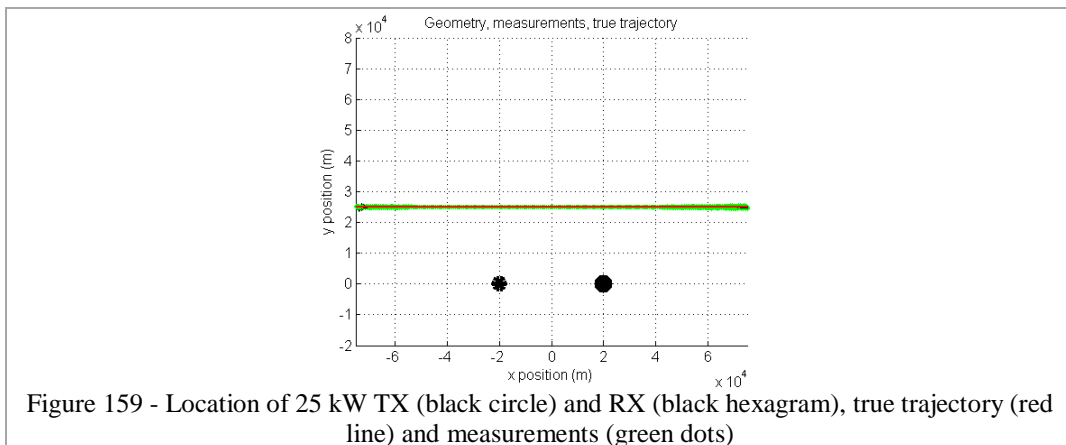
This is another bistatic example but now, the target is flying on a parallel line to the baseline of the bistatic radar. From Figure 155 and Figure 156, it is possible to see that, with this geometry, the errors in  $y$ -axis are worse than the errors in  $x$ -axis, except in the region where  $x$ -position is between -20 and 20 km.





**7.2.1.2.3 Bistatic (parallel to baseline RX-TX)**

Similarly to previous scenario, this scenario simulates a target that flies on a parallel line to the baseline of a bistatic radar. However, instead of a pair TX-RX, it is a pair RX-TX where the target passes first by RX and then by TX. It is possible to see that the accuracy close to RX is slightly better in both cases.

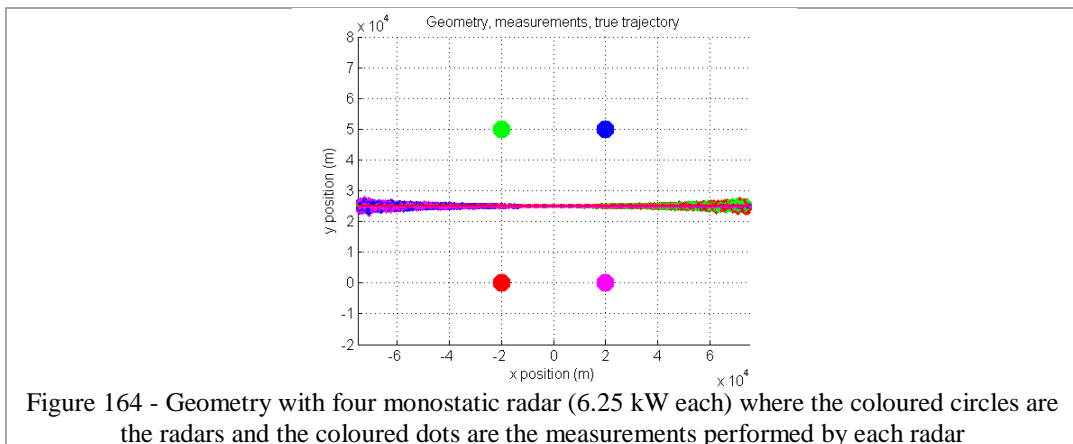


### 7.2.1.3 Netted Monostatic

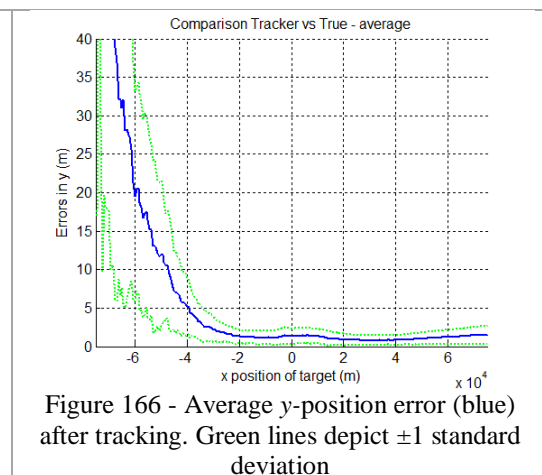
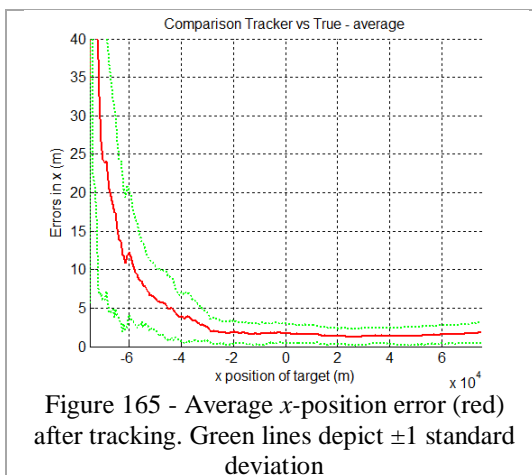
#### 7.2.1.3.1 4 monostatic (6.25 kW each)

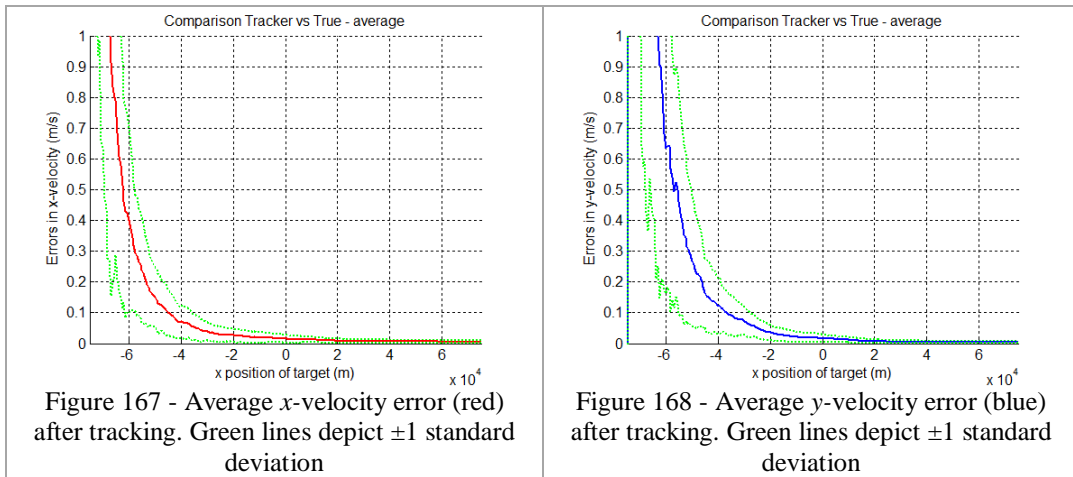
This scenario represents a netted monostatic geometry where there are 4 monostatic radars and each radar has 4 times less power than the monostatic one in 7.2.1.1. Total

power is still 25 kW though. In Figure 164, the circles (green, blue, red and magenta) are the radars (TX/RX) with 6.25 kW each.



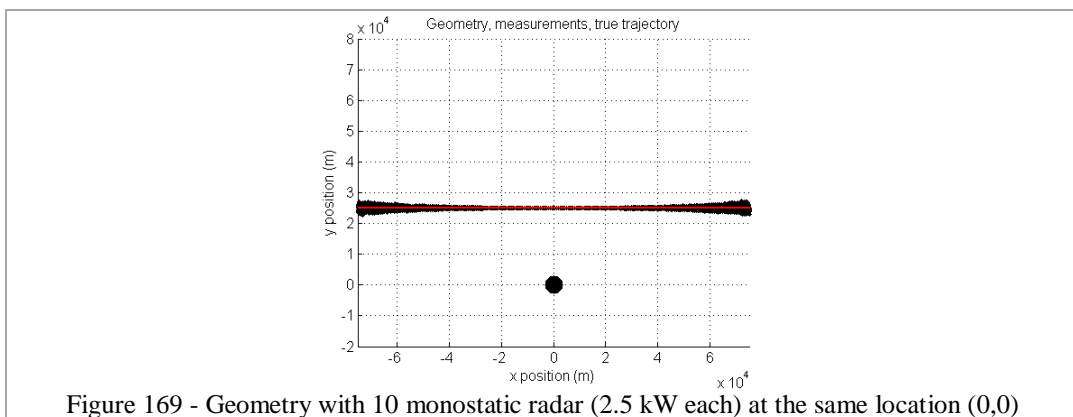
Comparing the following figures with the figures in Monostatic case where only one radar of 25 kW is used, the accuracies are very similar. Therefore, with the same total power, it is possible to achieve very similar results. However now, the system as whole is much more resilient to electronic counter measures.

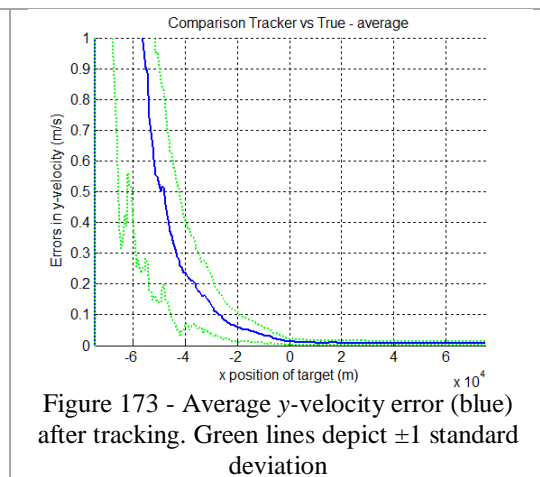
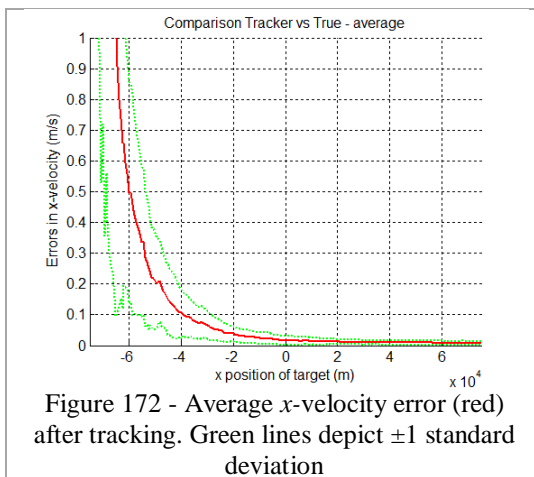
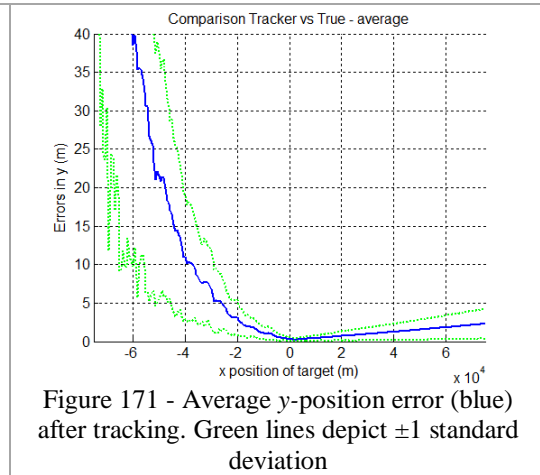
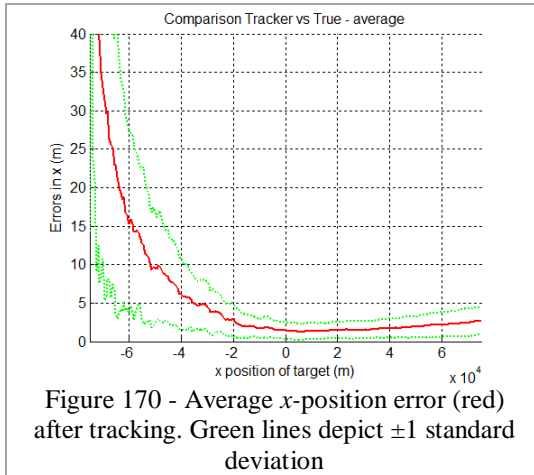




**7.2.1.3.2 10 monostatic (2.5 kW) in the same location**

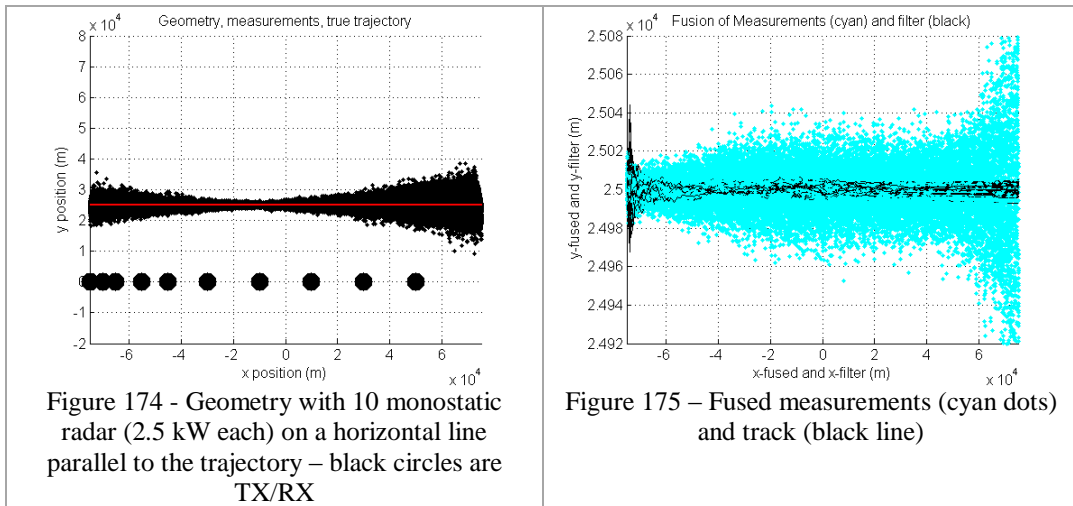
This scenario shows again a netted monostatic geometry, but in this one, there are 10 Monostatic radars (2.5 kW) at the same location, which is the same location of the only radar in the monostatic case in 7.2.1.1. Therefore, both scenarios are compared. And, as expected, both scenarios have identical results. It means that, on a situation where it is not possible to have one radar with a huge power transmitter, the solution is to deploy as many low power radars as necessary to achieve the desired total power.



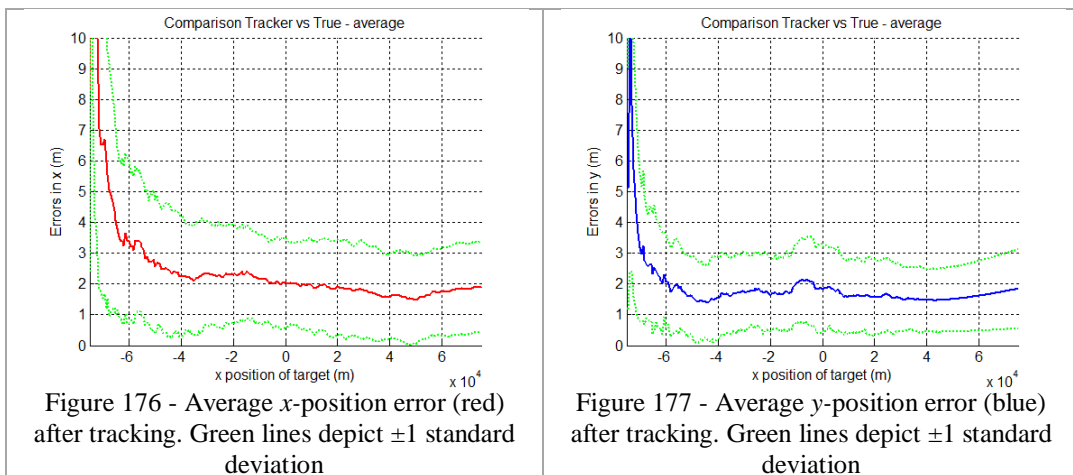


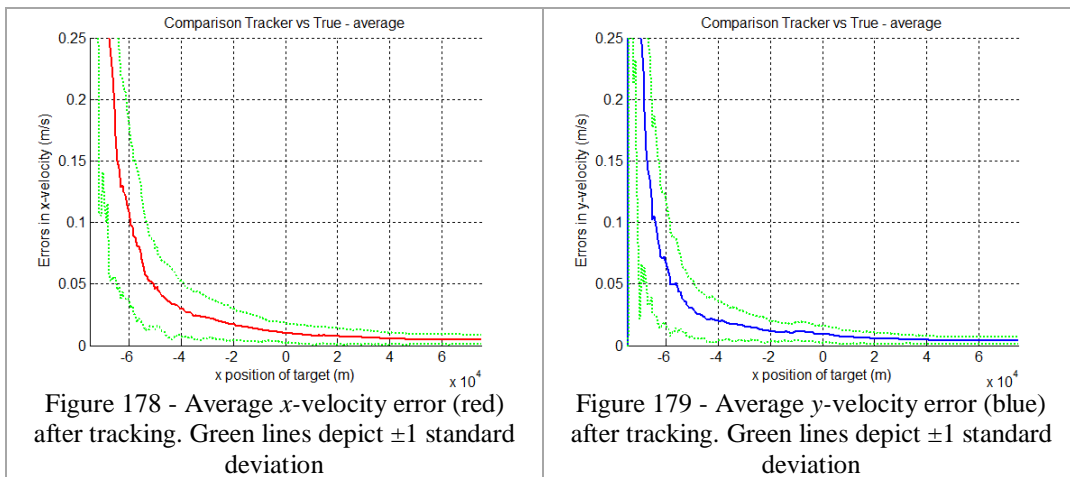
**7.2.1.3.3 10 monostatic (2.5 kW) on a parallel line to target**

Next scenario also uses a network of monostatic radars but now they are positioned along a horizontal line parallel to the target trajectory. In the beginning of the trajectory the radars are close to each other but the distance between them increases along the horizontal line. In Figure 174, the black circles are the monostatic (TX/RX) radars with 2.5 kW power each. Figure 175 presents the fused measurements (cyan dots) and the track like (black line). Note that the fused measurements have better accuracy than the view with all the radars measurements on Figure 174.



The difference here, is that this scenario makes the tracker to converge slightly faster to  $x$  or  $y$ -position errors that are less than 5 meters and to  $x$  or  $y$ -velocity errors that are less than 0.1 m/s. This is because in the beginning of the trajectory there are more radars close to the target. However, in this scenario, after converging to a certain point the tracker is not able to be more accurate than in the monostatic case. For example,  $y$ -position error here has its best value around  $x=-50$  km and the error is about 1.5 meters (Figure 177). In the monostatic case,  $y$ -position error has its best value at  $x=0$  and the error is less than 1 meter (Figure 146).

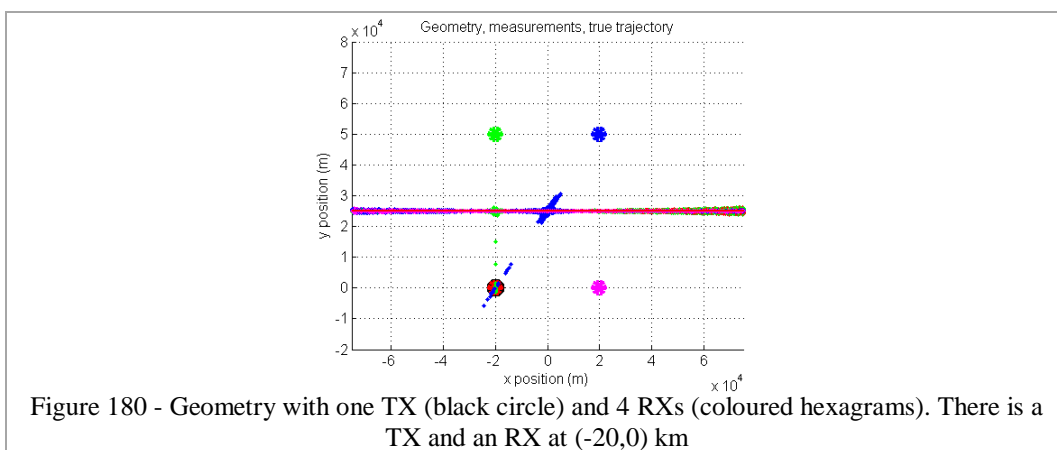




### 7.2.1.4 Multistatic (1 x N)

#### 7.2.1.4.1 1 TX (25 kW) and 4 RXs

This scenario comprises 1 TX and 4 RXs, where TX is the black circle and RXs are the coloured hexagrams. Note that there is a RX (red hexagram) at (-20,0) km with a TX as well.



Note that, adding 3 RXs to the geometry, but keeping the total power transmitted (25 kW) the tracking result in position and velocity are not very different from the monostatic case. However, it must be noted that the target crosses 2 baselines which, due to the way the fusion is made, make the results be worse than expected. On the other hand, having a system with more nodes, makes it more resilient in the case of one or more nodes are lost.

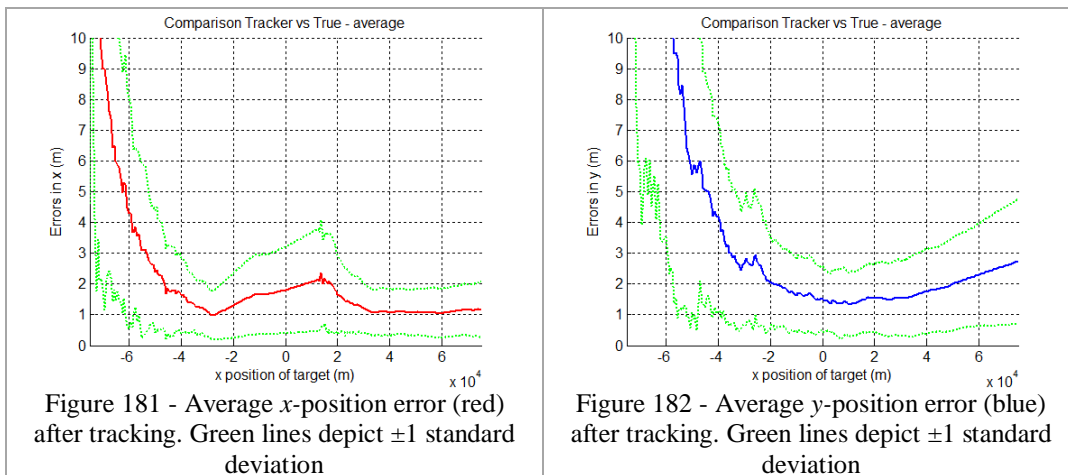


Figure 181 - Average  $x$ -position error (red) after tracking. Green lines depict  $\pm 1$  standard deviation

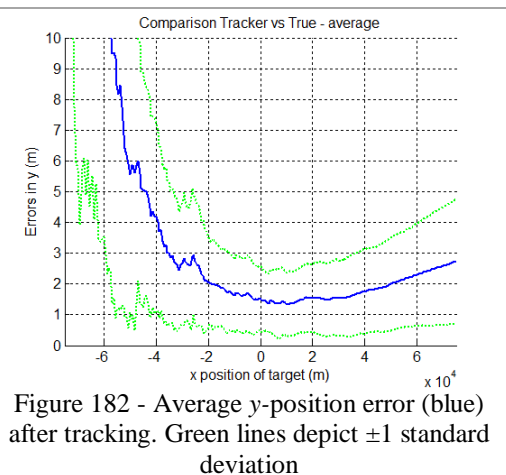


Figure 182 - Average  $y$ -position error (blue) after tracking. Green lines depict  $\pm 1$  standard deviation

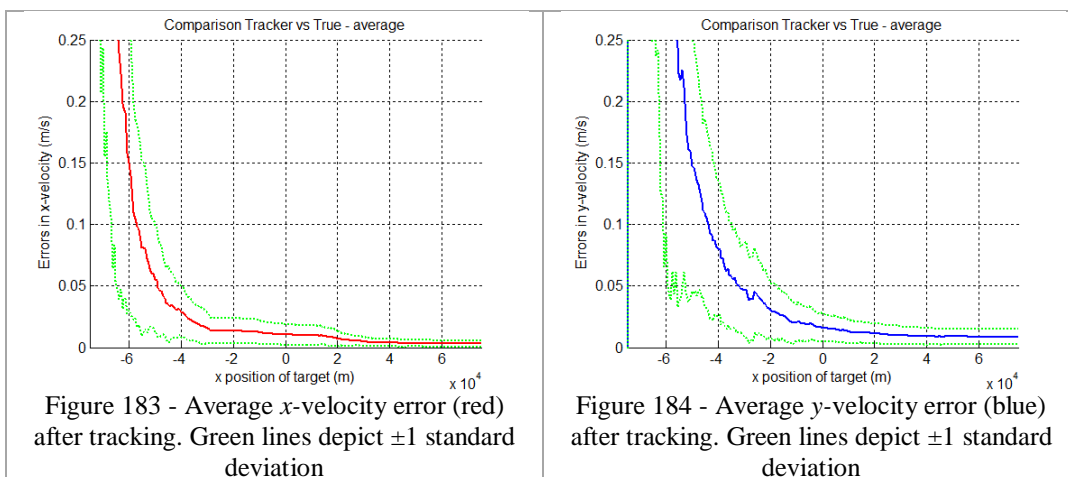


Figure 183 - Average  $x$ -velocity error (red) after tracking. Green lines depict  $\pm 1$  standard deviation

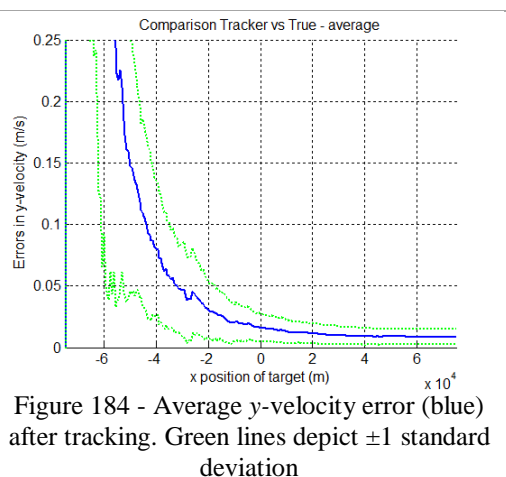
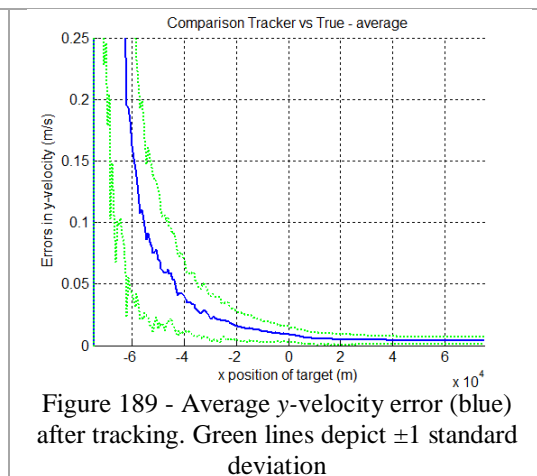
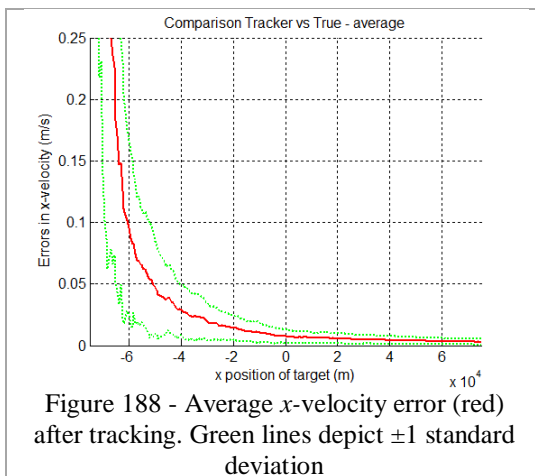
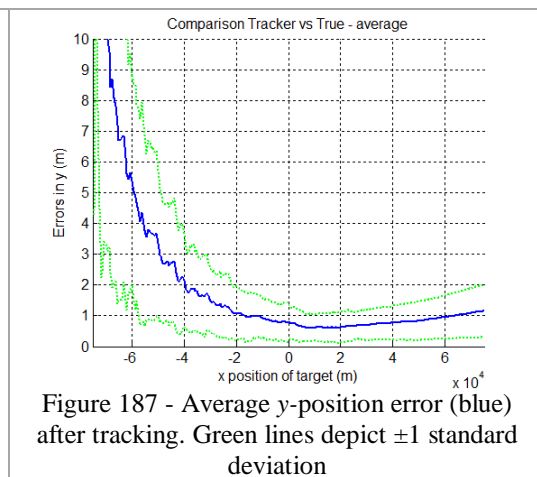
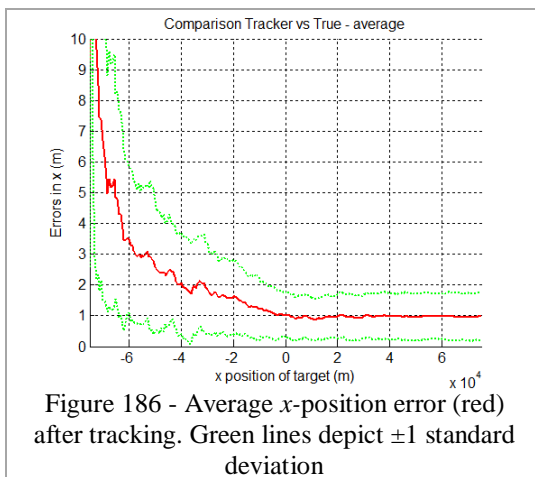
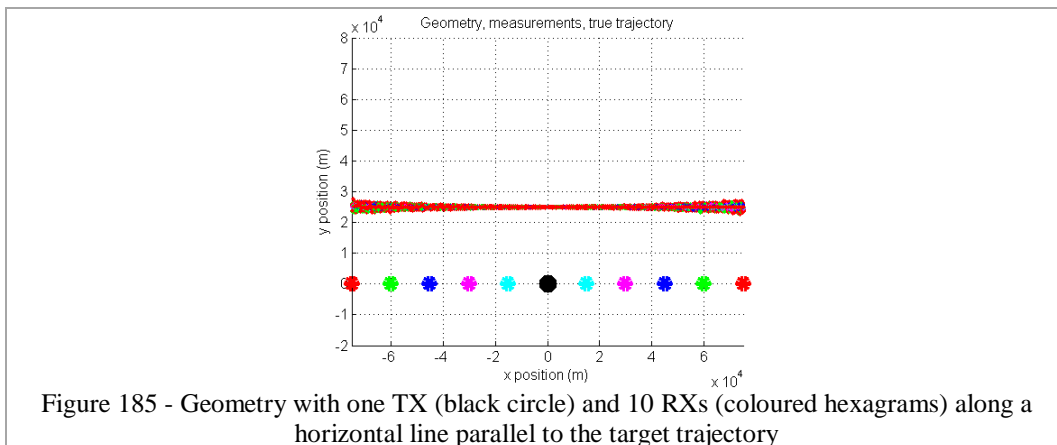


Figure 184 - Average  $y$ -velocity error (blue) after tracking. Green lines depict  $\pm 1$  standard deviation

#### 7.2.1.4.2 1 TX (25 kW) and 10 RXs (on a parallel line to target)

Once more, keeping the same total power, using only 1 TX (25 kW) and 10 RXs on a horizontal line parallel to the target trajectory, this geometry must be compared with the previous scenario. Although this scenario has 6 more RXs than the previous one, the results are not as good. It is still good and better than the previous scenario, but not as good as expected. This must be because of the location of the radars. On the other hand, this geometry has the great advantage of using just one TX and from it, it is possible to deploy a radar network comprised of 10 bistatic pairs of 25 kW power each. Therefore, it is just a matter to reposition all 10 RXs according to the requirements of the system.



### 7.2.1.5 Multistatic (M x 1)

#### 7.2.1.5.1 4 TXs (6.25 kW each) and 1 RX

In the next scenario, 4 transmitters of 6.25 kW each are used making bistatic pairs with one receiver. If compared with the one on 7.2.1.4, it is clear that this one is worse because, here, the geometry comprises 4 pairs of bistatic radars with a 6.25

kW TX instead of 4 pairs of 25 kW. The advantage of this scenario is that it is comprised of 4 TXs instead of just 1 TX. It makes this system more resilient since transmitters are more vulnerable to physical attacks.

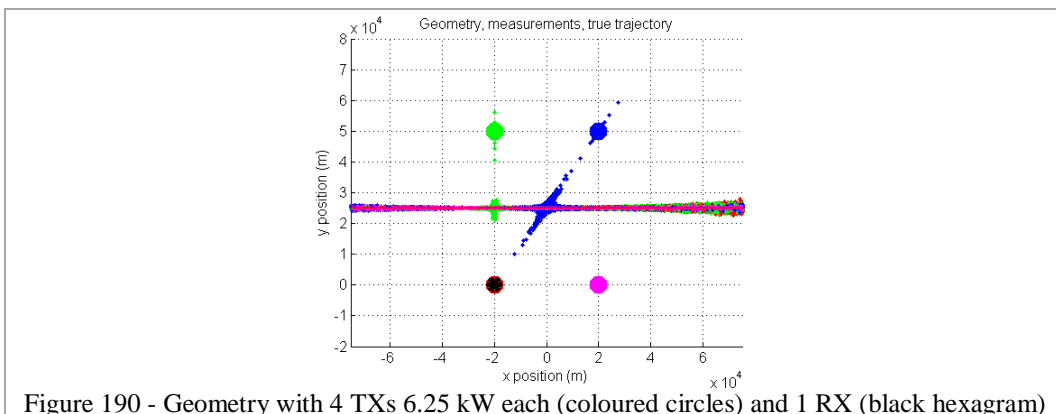


Figure 190 - Geometry with 4 TXs 6.25 kW each (coloured circles) and 1 RX (black hexagram)

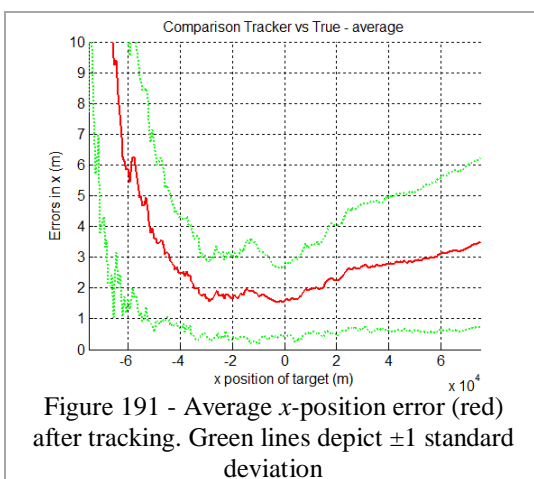


Figure 191 - Average x-position error (red) after tracking. Green lines depict  $\pm 1$  standard deviation

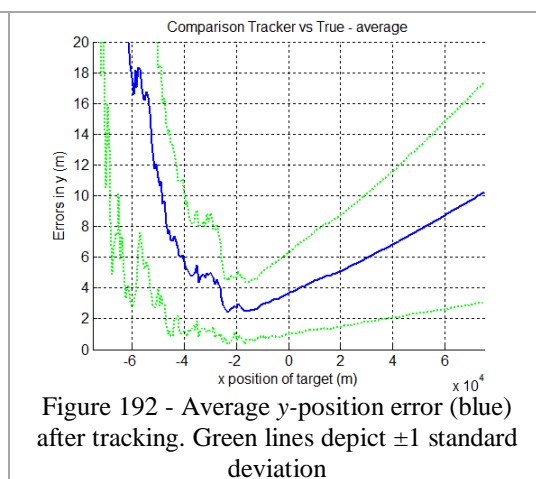


Figure 192 - Average y-position error (blue) after tracking. Green lines depict  $\pm 1$  standard deviation

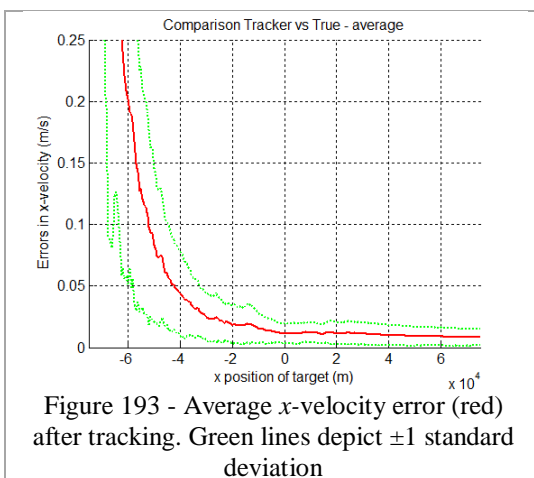


Figure 193 - Average x-velocity error (red) after tracking. Green lines depict  $\pm 1$  standard deviation

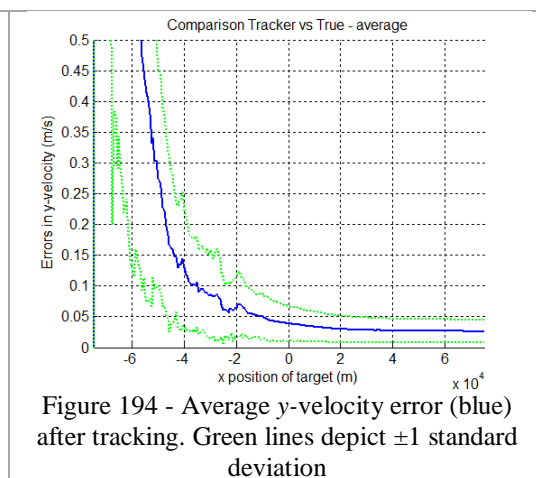
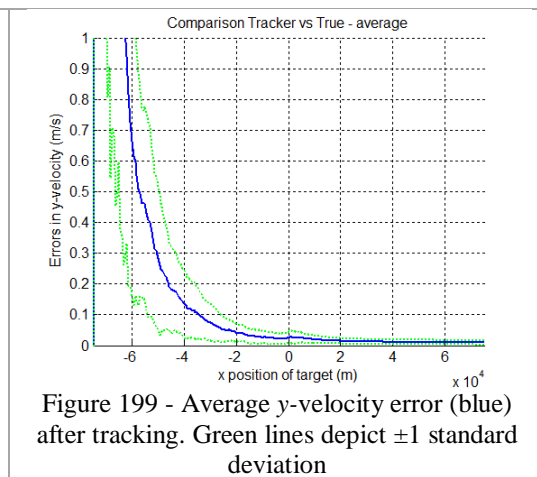
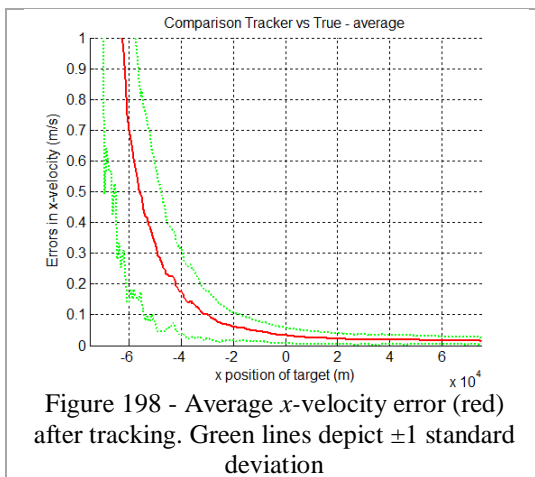
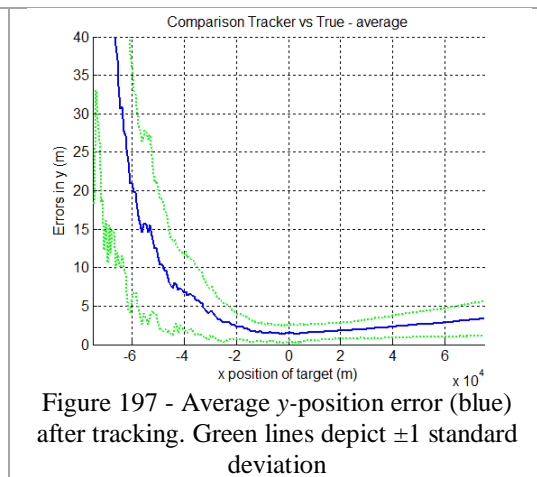
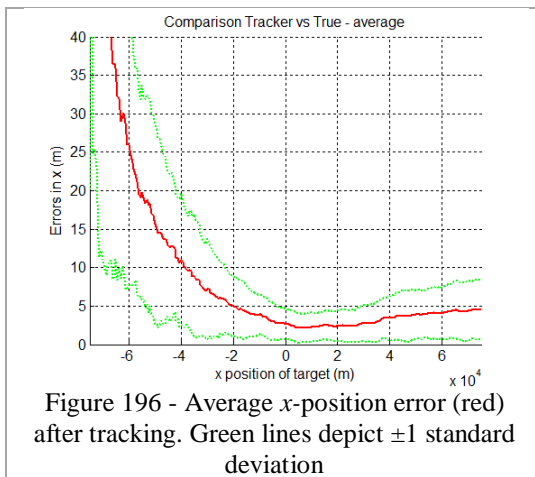
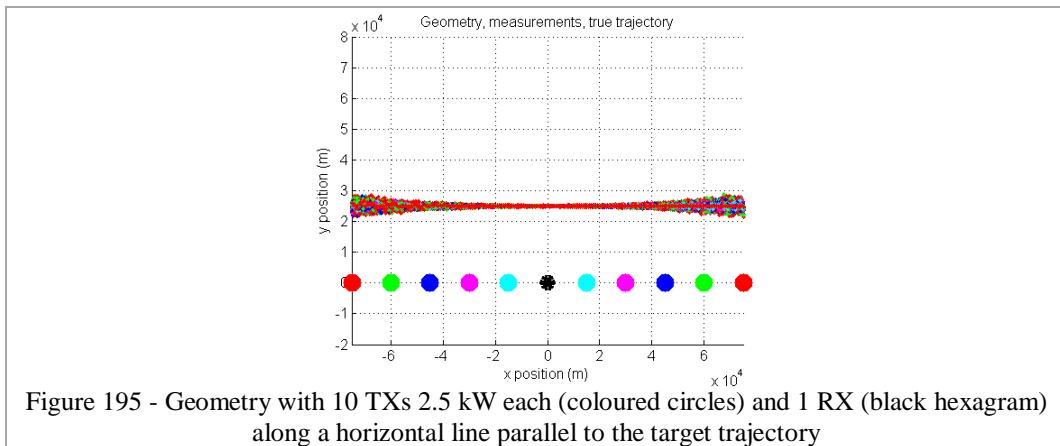


Figure 194 - Average y-velocity error (blue) after tracking. Green lines depict  $\pm 1$  standard deviation

### 7.2.1.5.2 10 TXs (2.5 kW each) and 1 RX (on a parallel line to target)

Now, the geometry (Figure 195) includes 10 TXs with 2.5 kW and just 1 RX. RX is the black hexagram and coloured circles denote the transmitters along a line parallel

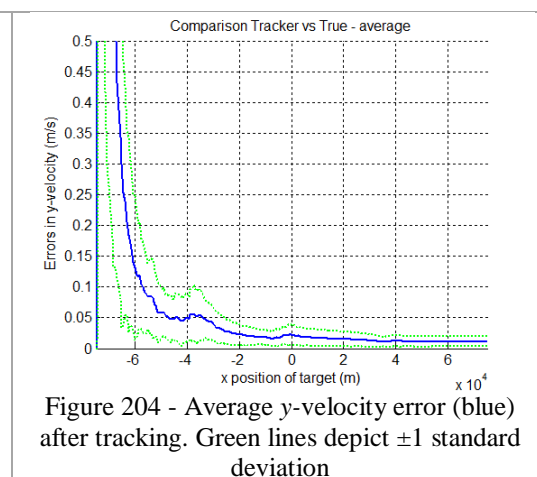
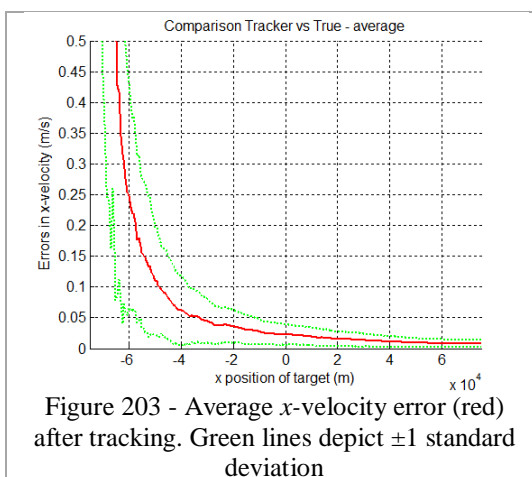
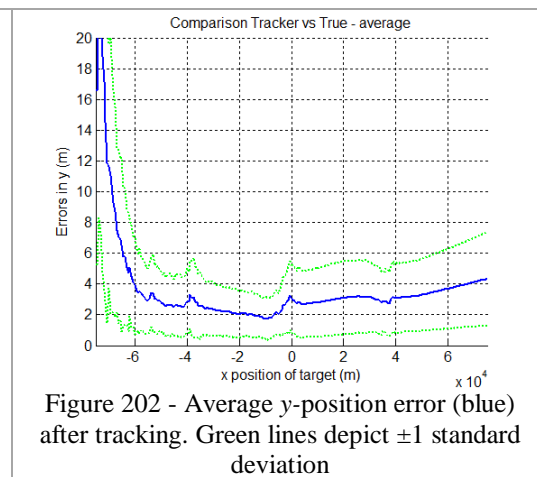
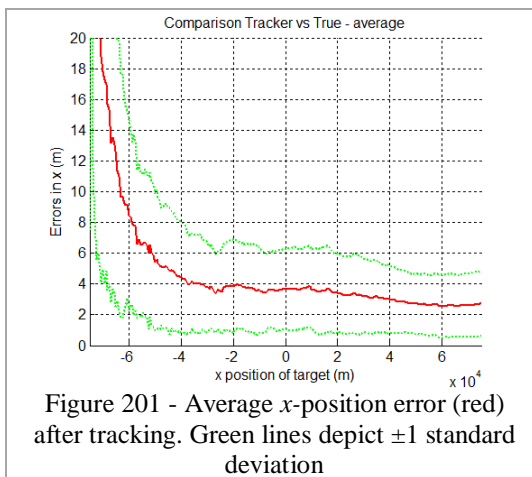
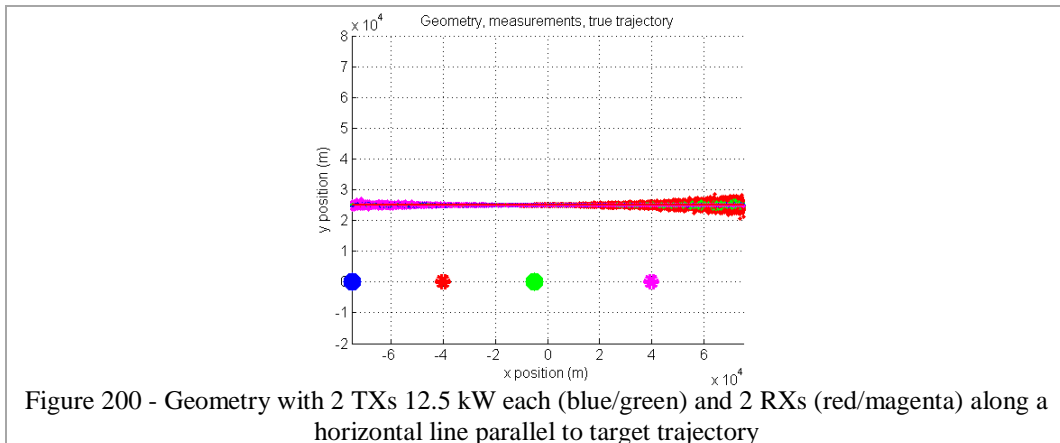
to the target trajectory. Again, as expected, this scenario, if compared with the one in 7.2.1.4, has worse results because the geometry is comprised of 10 pairs of 2.5 kW bistatic radars instead of 10 pairs of 25 kW bistatic radars.



Although the results here are worse than in the [1 TX / 10 RXs], it is not so bad and, on the other hand, there is the advantage of multiple transmitters which, make the system more resilient in the case of loss of one or more transmitters.

### 7.2.1.6 Multistatic (2 TXs and 2 RXs)

In this scenario, 2 TXs (12.5 kW) and 2 RXs results in 4 pairs of 12.5 kW bistatic radars. Comparing, this geometry with the previous one [10 TXs and 1 RX], this one is better and one could choose this geometry instead of the previous one if it were to reduce deployment costs or to minimize synchronization problems.



This scenario, if compared with the [1 TX and 10 RXs] geometry is worse, but instead has one more transmitter which might be good depending on how the radar is intended to be used.

## 7.2.2 Target 2 (*spiral-like trajectory*)

In the following scenarios, the target starts at about (-76,0) km and flies on a spiral trajectory towards one transmitter of the network during 1000 seconds. In this section, in all the figures except the one that shows the geometry, the  $x$ -axis represents the measurement sequence number. For each scenario, 100 simulation runs are performed in order to calculate the average and standard deviation of the results.

In a spiral trajectory, the target changes direction in either  $x$ -axis or  $y$ -axis a couple of times. In all scenarios in this section, the first change of direction occurs at around measurement number 110 where  $v_y$  is zero and the target is at the top of the spiral. The next change of direction occurs at around measurement number 230 where  $v_x$  is zero and the target is on the right of the spiral. The last change of direction of this trajectory occurs at around measurement number 330, where  $v_y$  is zero and the target is at the bottom of the spiral, very close to the aimed transmitter. The simulation finishes at measurement number 400, thus 70 measurements after the last change of direction and it means 175 seconds later. The trajectory finishes 5 km far from the transmitter at position (0,-5) km.

### 7.2.2.1 Monostatic

As can be seen in Figure 205 and Figure 206, the velocity and acceleration varies during the whole trajectory of the target. In both figures, red lines depict the  $x$ -axis true values and blue lines depict the  $y$ -axis true values for velocity and acceleration. Note that the maximum absolute velocity in either axis is about 350 m/s and the maximum absolute acceleration is about 1.6 m/s<sup>2</sup>. Figure 207 depicts the target trajectory and radar location (black circle).

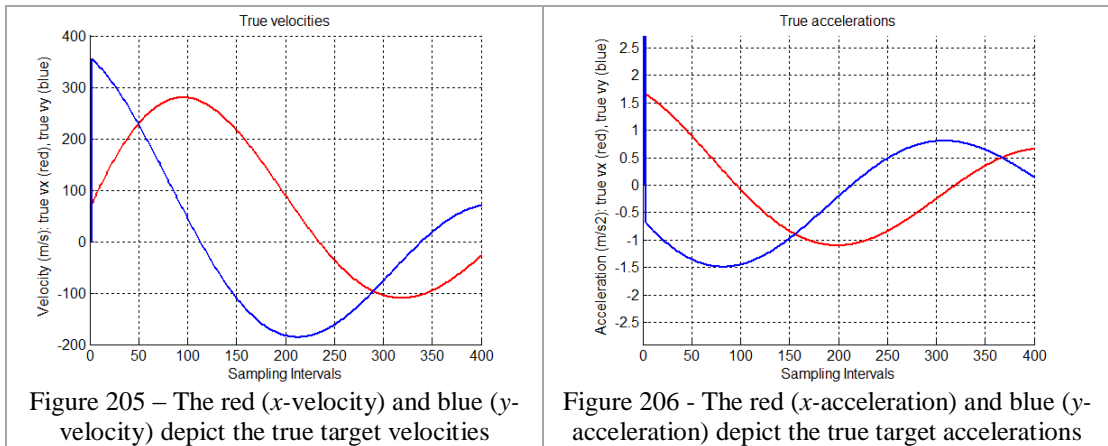


Figure 205 – The red ( $x$ -velocity) and blue ( $y$ -velocity) depict the true target velocities

Figure 206 - The red ( $x$ -acceleration) and blue ( $y$ -acceleration) depict the true target accelerations

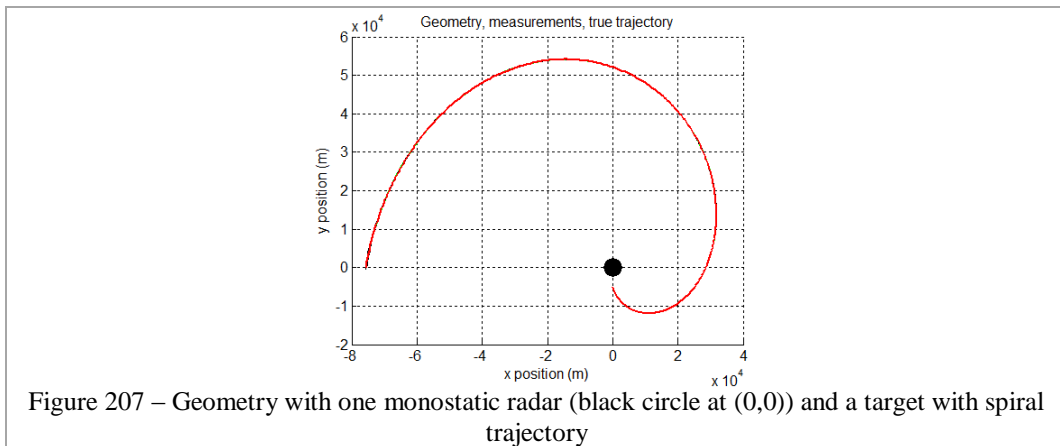


Figure 207 – Geometry with one monostatic radar (black circle at (0,0)) and a target with spiral trajectory

Figure 208 and Figure 209 depict the average position errors in  $x$  and  $y$ -axis after tracking.

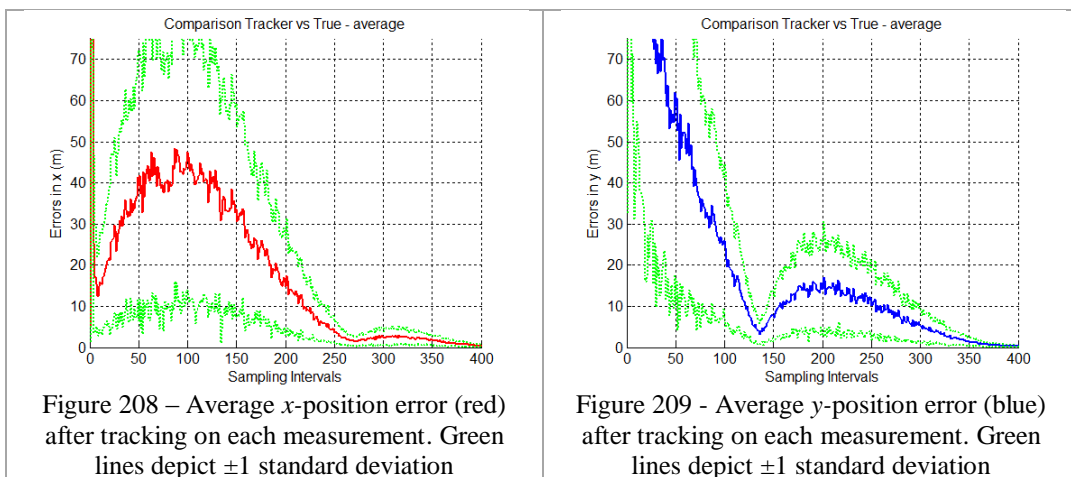


Figure 208 – Average  $x$ -position error (red) after tracking on each measurement. Green lines depict  $\pm 1$  standard deviation

Figure 209 - Average  $y$ -position error (blue) after tracking on each measurement. Green lines depict  $\pm 1$  standard deviation

Figure 210 and Figure 211 show the average velocity errors in  $x$  and  $y$ -axis after tracking.

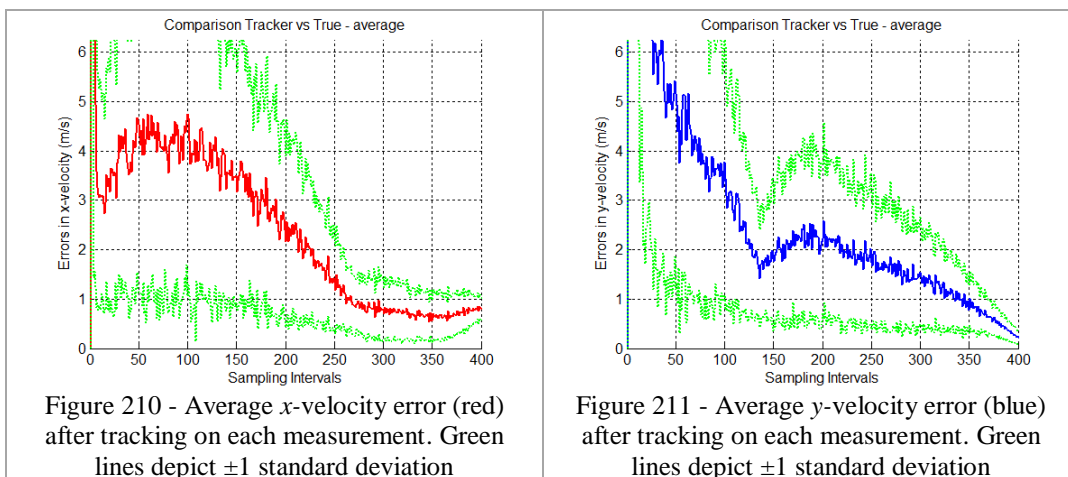
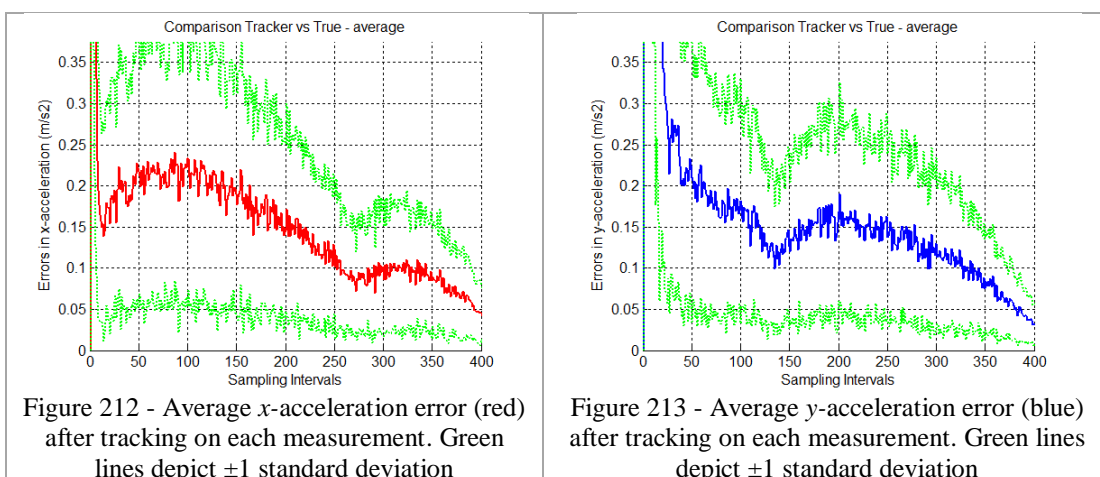


Figure 212 and Figure 213 present the average acceleration errors in  $x$  and  $y$ -axis after tracking.



## 7.2.2.2 Bistatic

This section shows 2 geometries for a bistatic radar: one where the target crosses the baseline of the radar and another one where it does not cross the baseline.

### 7.2.2.2.1 Bistatic (crossing baseline)

This scenario represents a bistatic geometry where in Figure 214, the black circle at (0,0) km is the TX with 25 kW, the black hexagram at (0,60) km is the RX, the red line is the true trajectory and the green dots are the measurements. Black line depicts the filtered trajectory. The following figures (Figure 214 to Figure 220) represent the same type information as in Figure 207 to Figure 213.

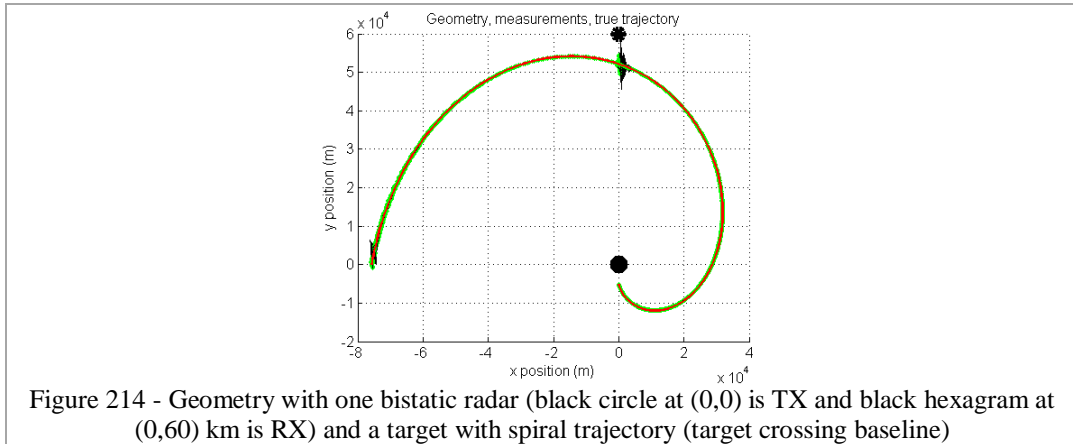


Figure 214 - Geometry with one bistatic radar (black circle at (0,0) is TX and black hexagram at (0,60) km is RX) and a target with spiral trajectory (target crossing baseline)

Overall, it can be seen that this configuration is worse than the previous one (monostatic case), especially the states (position, velocity and acceleration) in  $y$ -axis. In the  $x$ -axis, this scenario is better at the beginning of the trajectory but not so good at the end of it. Note that there are peaks in the tracking results when the target is crossing the baseline. The inaccuracy is much more evident on  $y$ -axis which is the axis parallel to baseline. It is shown in Figure 93 and Figure 94 that the measurements are much more inaccurate in the  $y$ -axis as well.

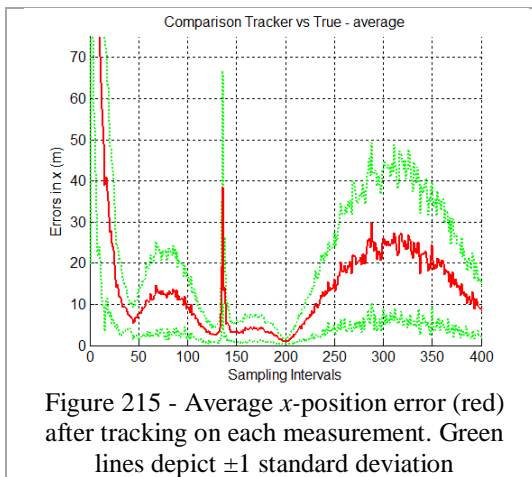


Figure 215 - Average  $x$ -position error (red) after tracking on each measurement. Green lines depict  $\pm 1$  standard deviation

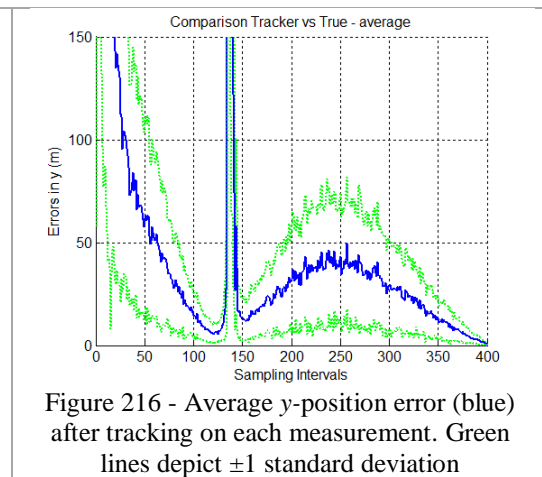
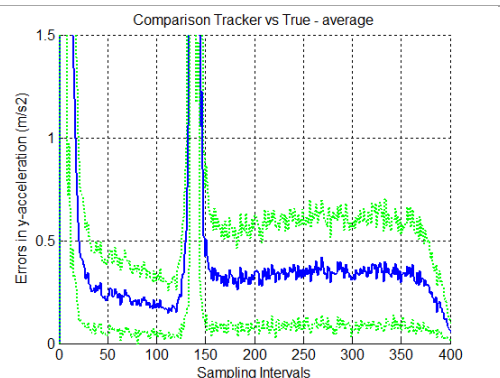
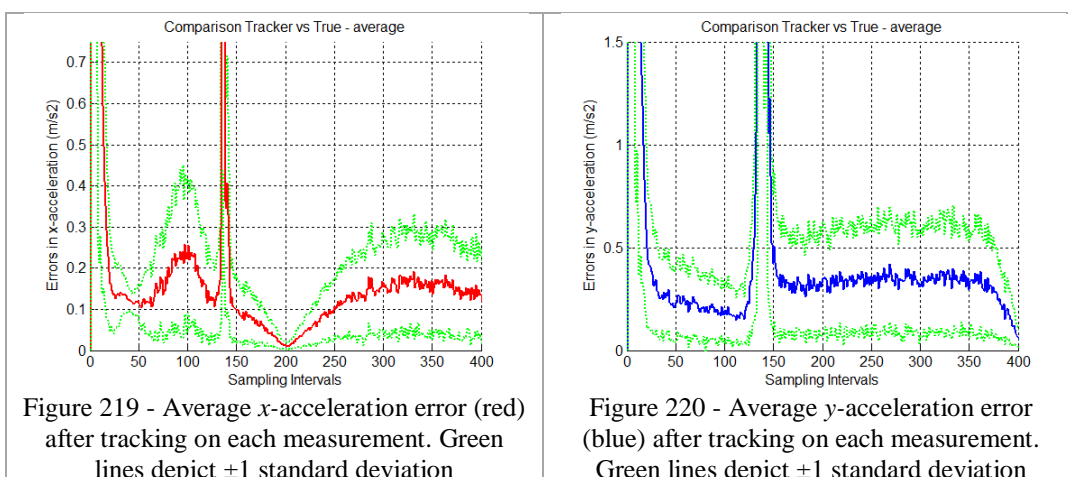
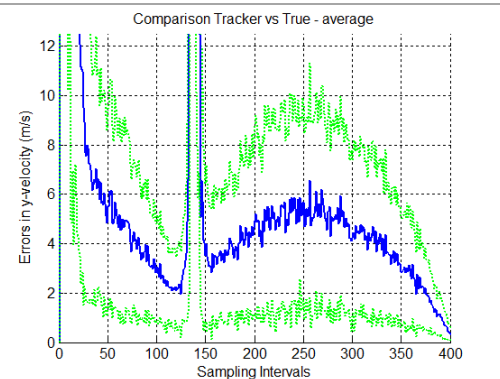
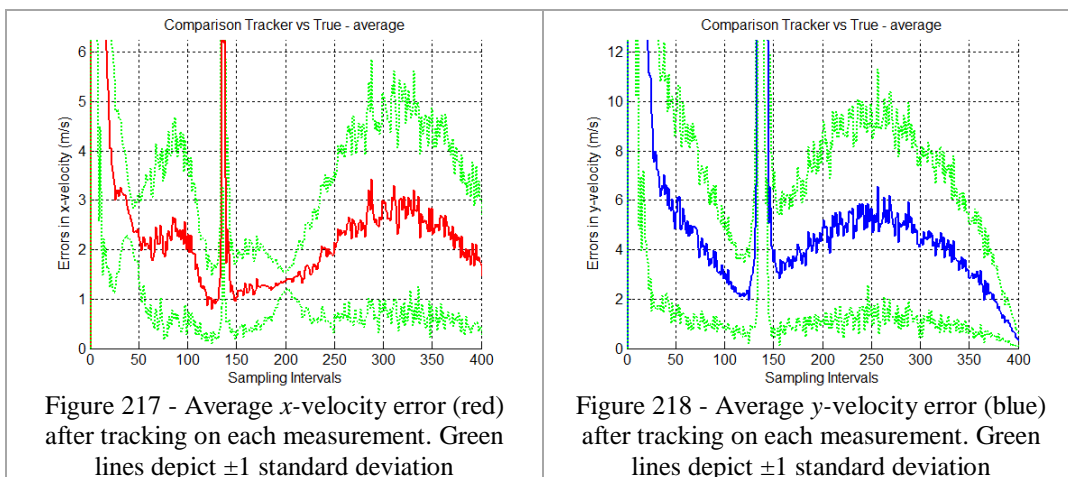
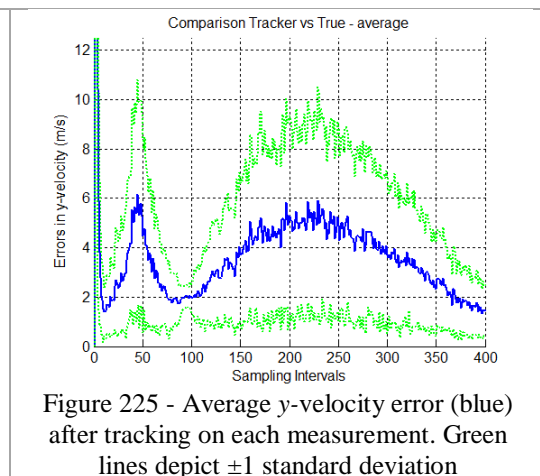
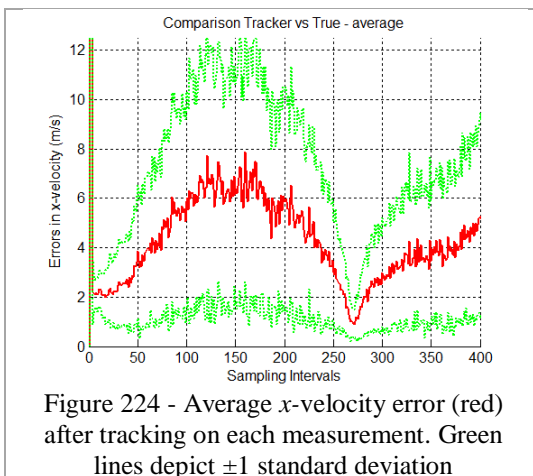
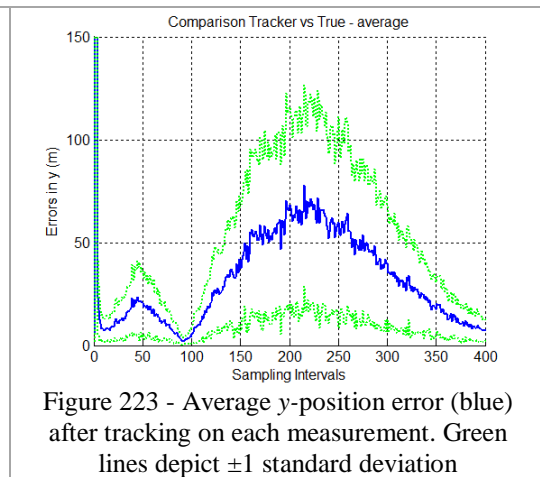
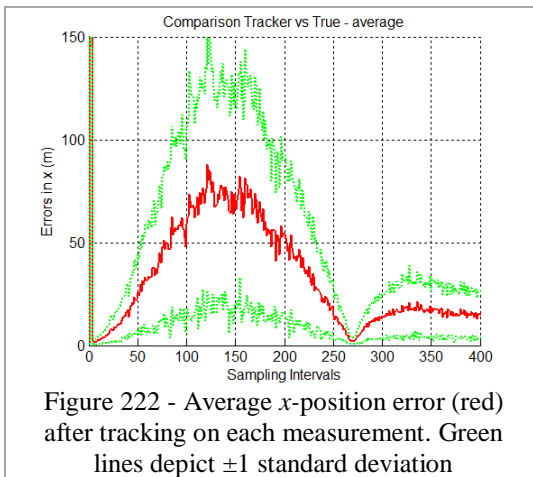
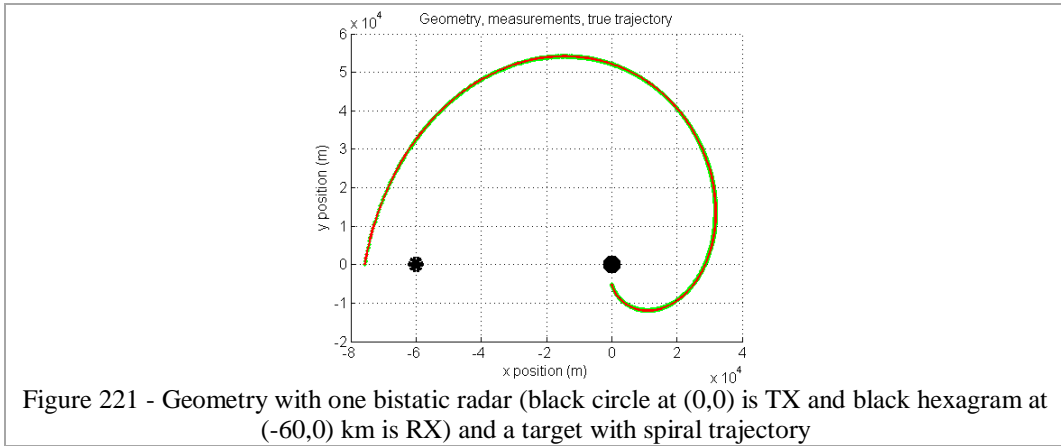


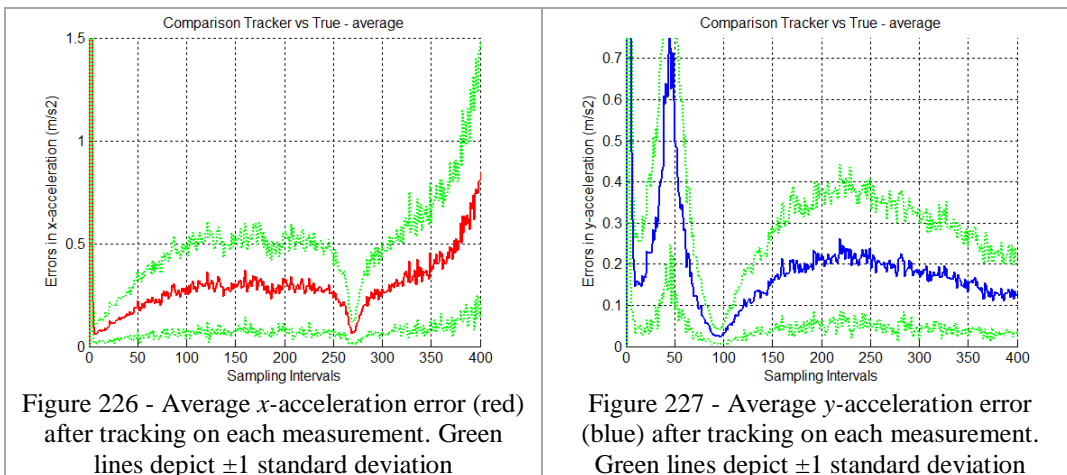
Figure 216 - Average  $y$ -position error (blue) after tracking on each measurement. Green lines depict  $\pm 1$  standard deviation



### 7.2.2.2 Bistatic (without crossing baseline)

This scenario represents a bistatic geometry where the target does not cross the baseline (Figure 221). The total power is still 25 kW. Figure 221 to Figure 227 represent the same type of information as in figures in the previous scenario. In this scenario, the position errors are big when the target is far from the radar, as expected, in the region between the top of spiral and the right of it. Overall this geometry, if compared with the monostatic case, is better at the beginning of the trajectory but worse elsewhere. This is correct, according to the model, since at the beginning of the trajectory the transmitted signal does not have to travel back to the monostatic TX/RX because the RX is very close to the beginning of trajectory.



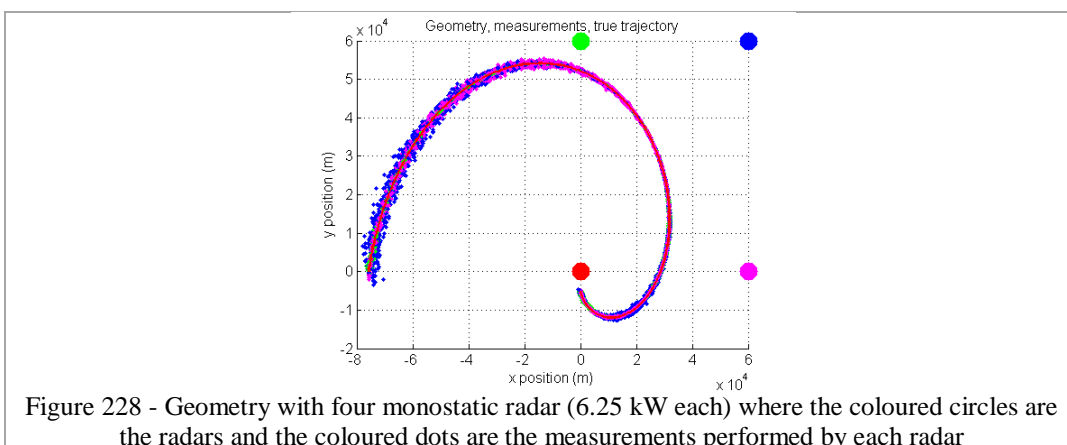


### 7.2.2.3 Netted Monostatic

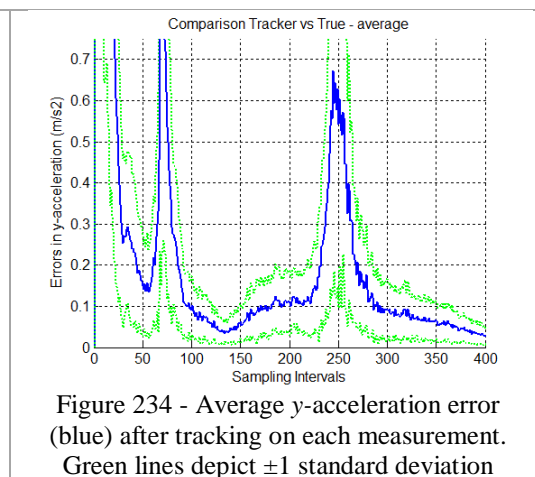
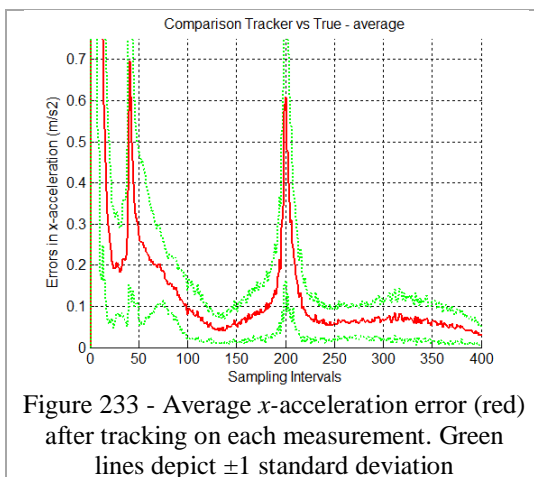
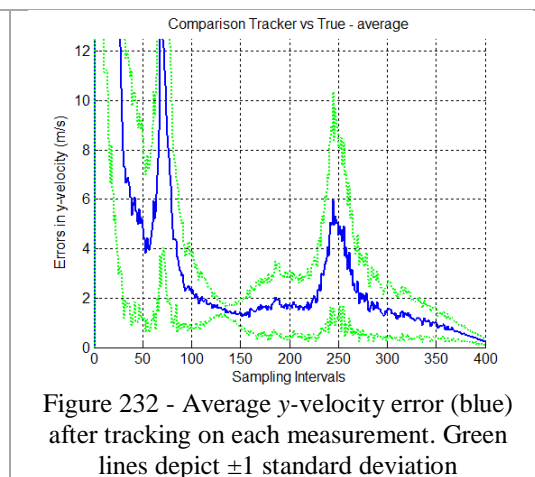
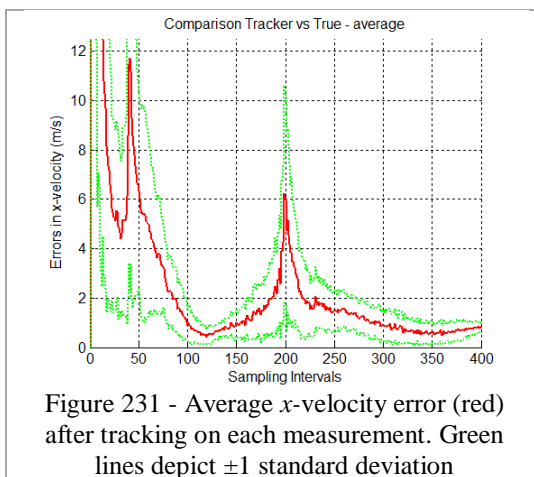
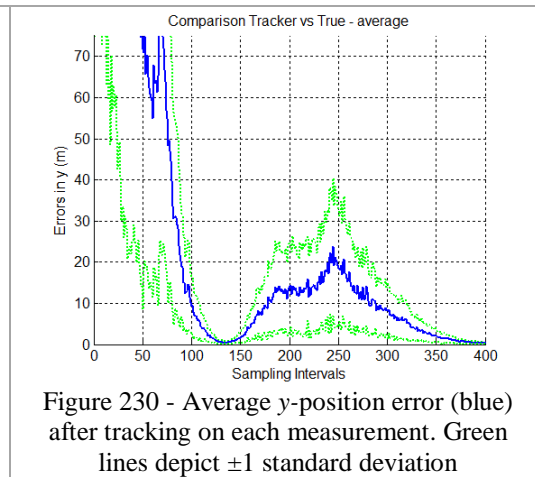
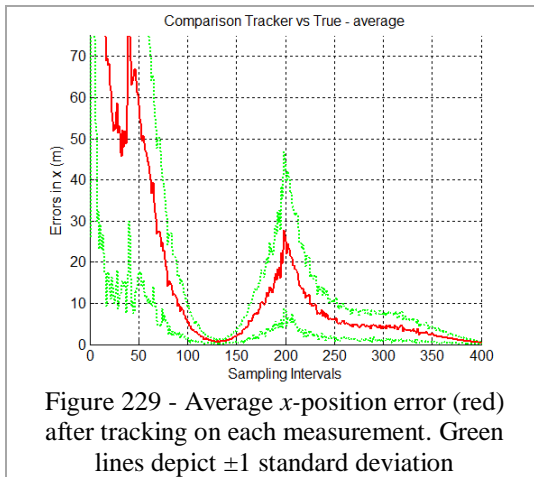
In the following scenarios, configurations using many monostatic radars are presented. In all cases, the total power is 25 kW, regardless of the number of radars.

#### 7.2.2.3.1 4 monostatic (6.25 kW each)

This scenario represents a netted monostatic geometry with 4 radars with 6.25 kW transmitter power each.



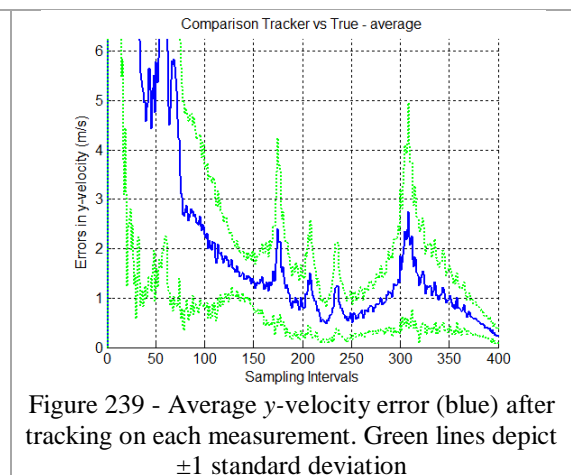
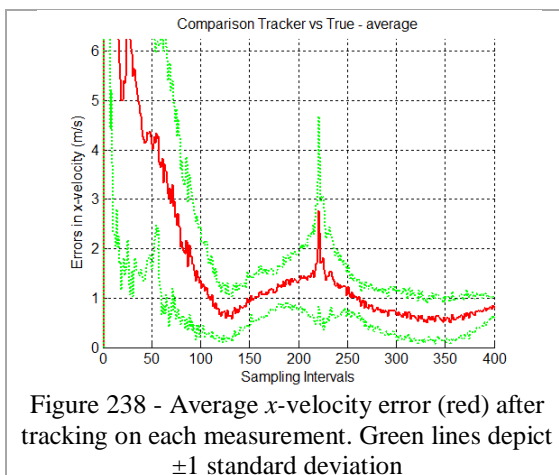
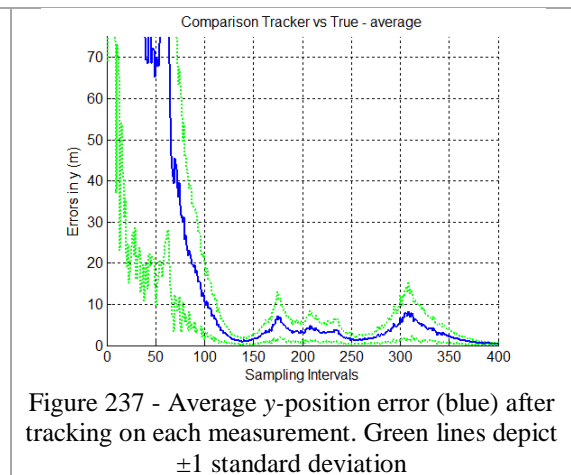
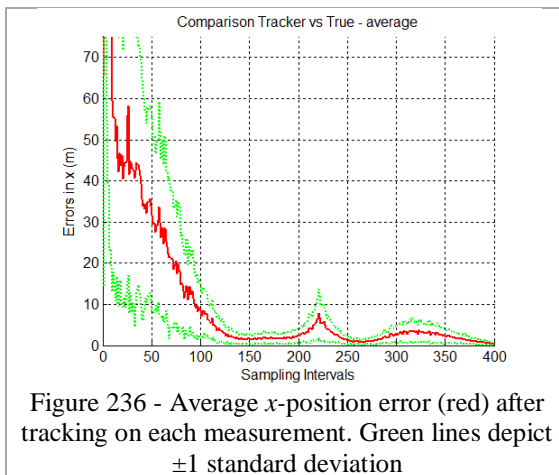
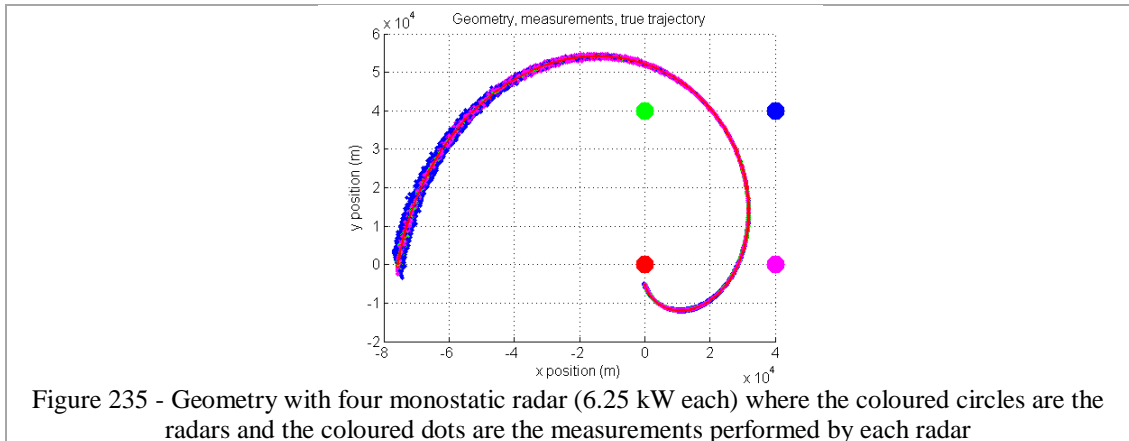
Comparing this scenario with the monostatic one in 7.2.2.1, the results here are similar although there are some peaks because now, the total power is spread and the standard deviations are different in each radar. However, it still delivers good results (especially when it is close to “green circle” radar near the measurement number 130) and has the big advantage of being more immune to attacks, because if the target destroys the aimed transmitter, the system still has 3 more transmitters (graceful degradation).

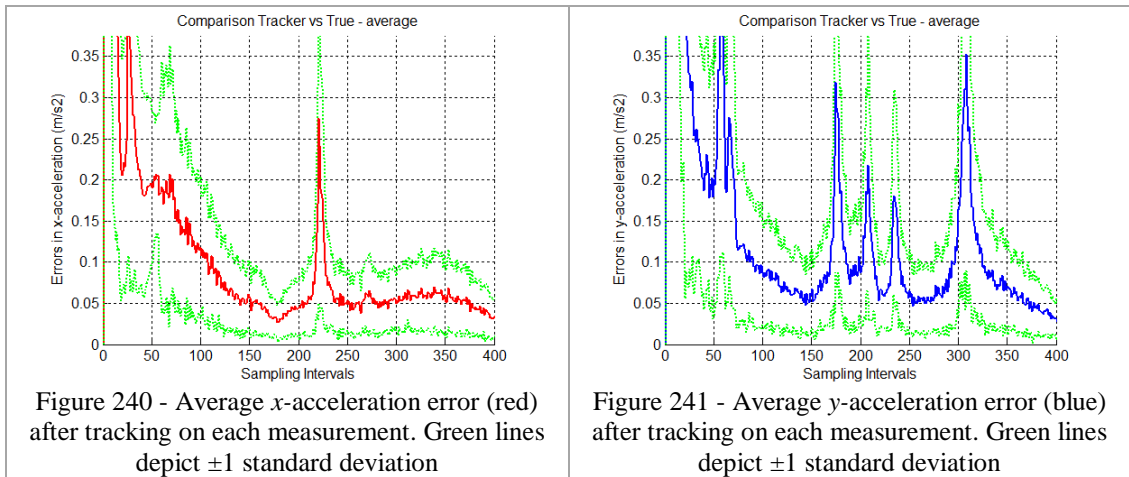


**7.2.2.3.2 4 monostatic (6.25 kW each) – closer to the target**

This scenario, if compared to the previous one, is undoubtedly better, because the radars are much closer to the target. In addition, if this geometry is compared with the monostatic radar with 25 kW in 7.2.2.1, it shows that this geometry has better results especially during the initial measurements with the position estimates

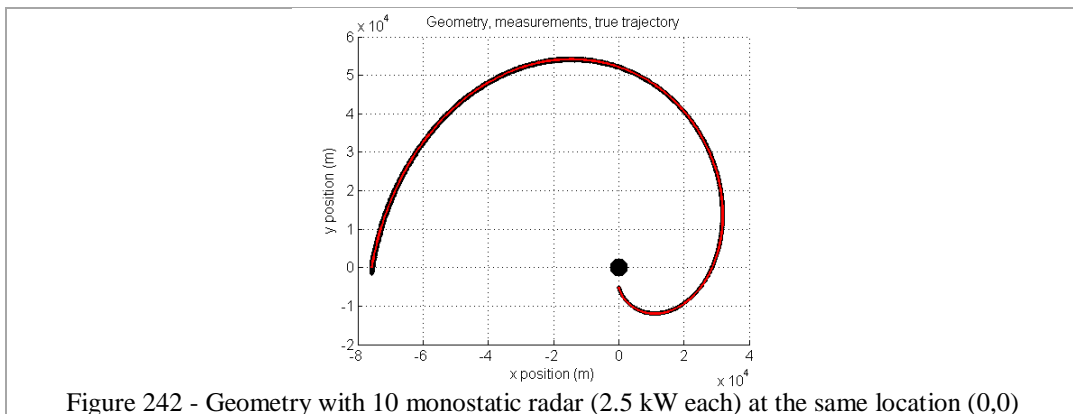
converging faster. The final result, in terms of location is overall better than the monostatic case. Nevertheless, there are some peaks in the velocity and acceleration estimates which do not change significantly the position results. Furthermore, this geometry is still more immune to attacks from enemies and consequently, the system is more resilient.

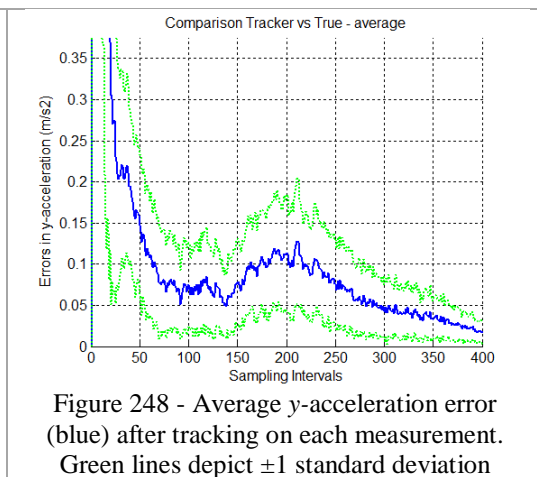
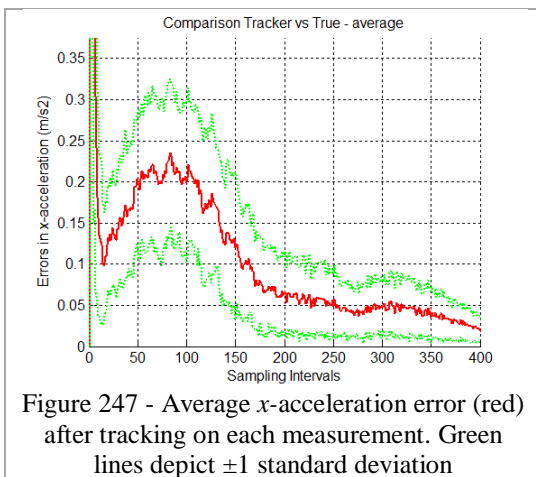
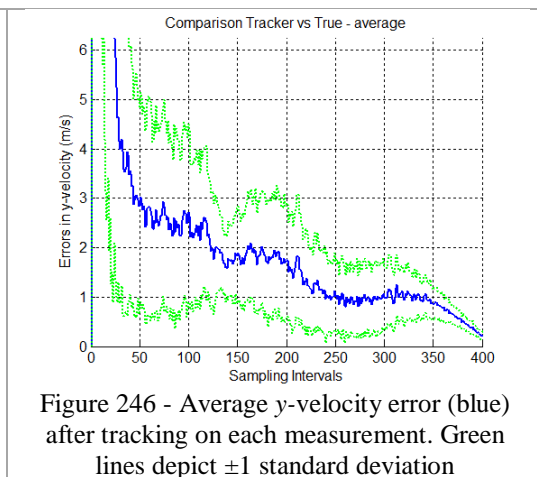
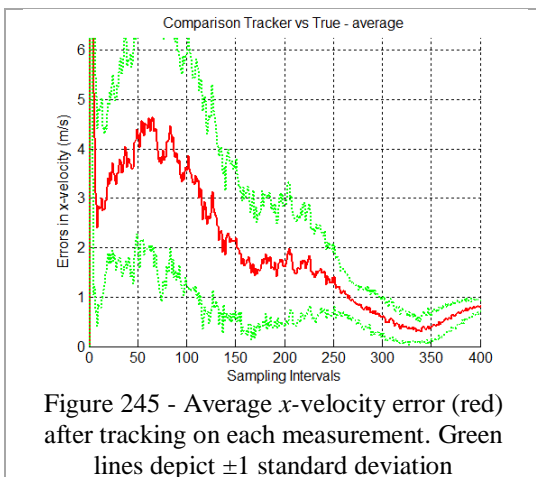
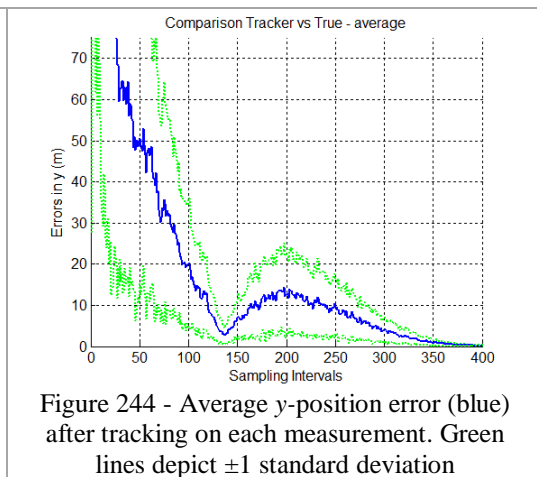
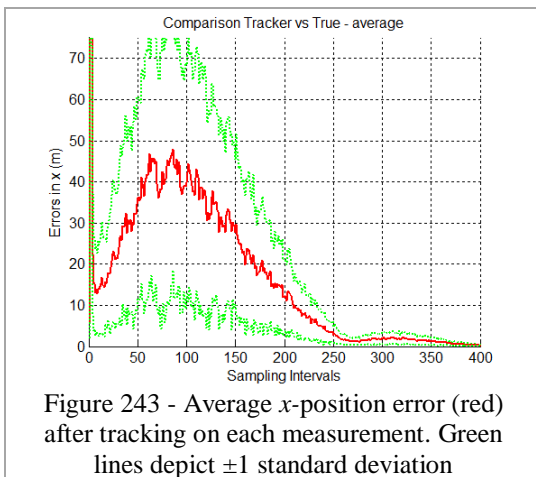




**7.2.2.3.3 10 monostatic (2.5 kW) at the same location**

This scenario, with 10 monostatic radars at the same location of 7.2.2.1 but with 10 times less power each produces a total power of 25 kW. The main idea of this scenario is to compare with the scenario where just one monostatic radar is used and show that the results are basically the same. This confirms that if it is not possible to increase the power of a transmitter, then it is possible to use many of them to achieve the desired transmitter power (as shown in 7.2.1.3.2).





**7.2.2.3.4 10 monostatic (2.5 kW) on a line**

This scenario also uses a network of monostatic radars but now they are positioned along a horizontal line following the target trajectory. In the beginning of the trajectory the radars are close to each other but the distance between them increases along the horizontal line. The difference here is that this scenario is better than the

previous one at the beginning of the trajectory but not in the middle of it. At the end of trajectory this geometry is just slightly worse than the previous one although in the previous one it takes advantage of having a very powerful transmitter close to the target.

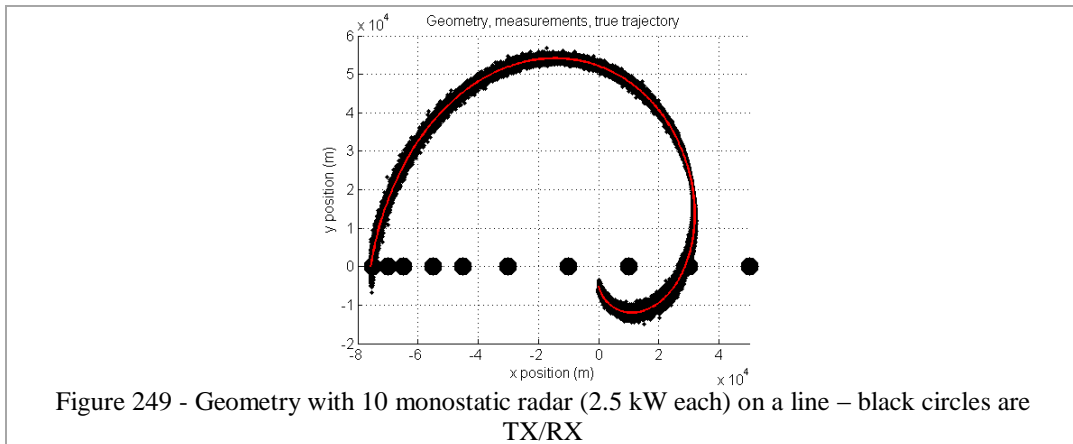


Figure 249 - Geometry with 10 monostatic radar (2.5 kW each) on a line – black circles are TX/RX

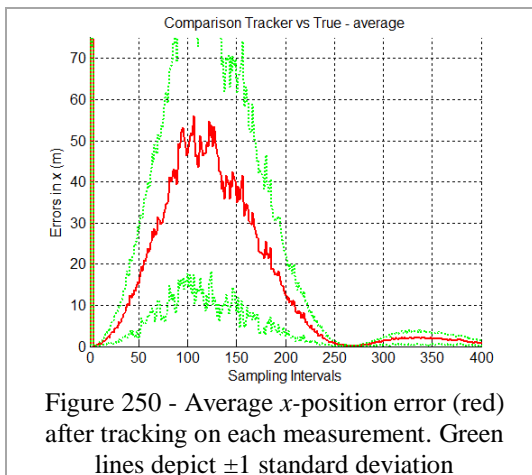


Figure 250 - Average  $x$ -position error (red) after tracking on each measurement. Green lines depict  $\pm 1$  standard deviation

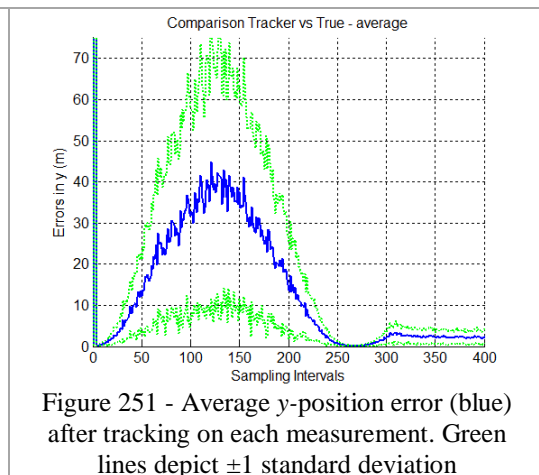


Figure 251 - Average  $y$ -position error (blue) after tracking on each measurement. Green lines depict  $\pm 1$  standard deviation

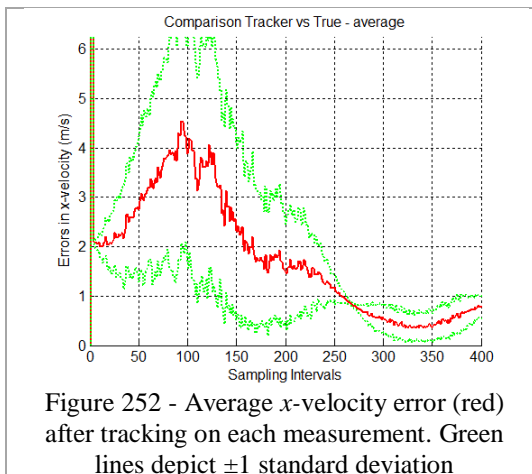


Figure 252 - Average  $x$ -velocity error (red) after tracking on each measurement. Green lines depict  $\pm 1$  standard deviation

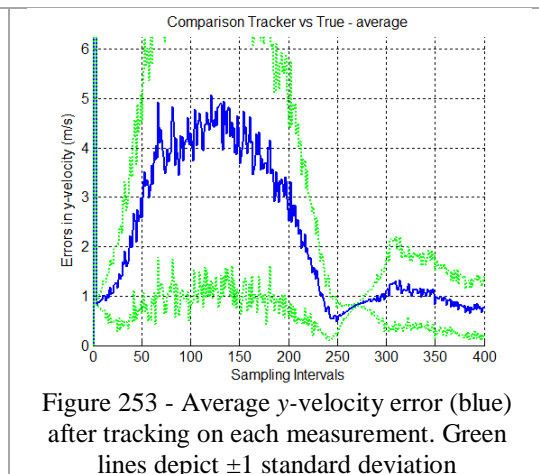
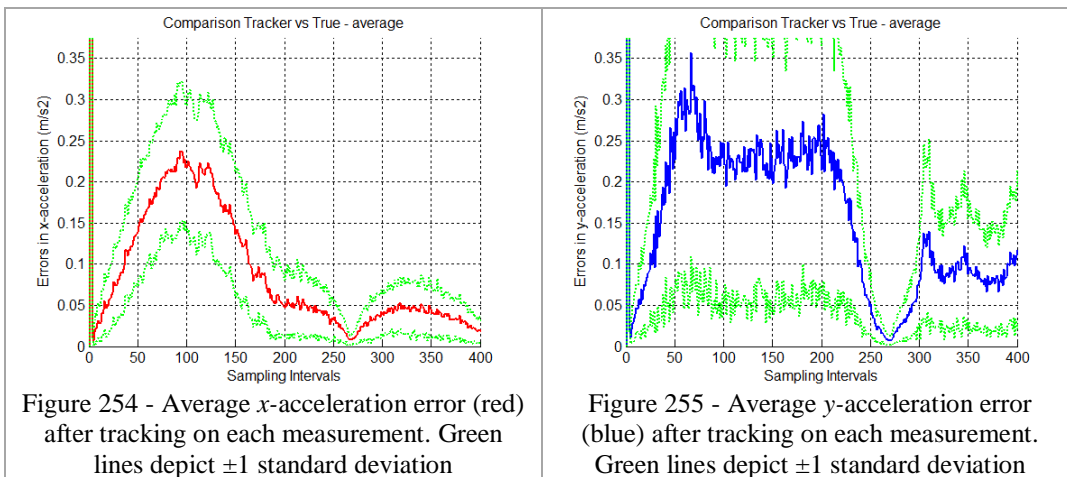


Figure 253 - Average  $y$ -velocity error (blue) after tracking on each measurement. Green lines depict  $\pm 1$  standard deviation



### 7.2.2.4 Multistatic (1 x N)

This section presents 2 different scenarios where a combination of bistatic radars result in a Multistatic Radar with 1 TX and many RXs.

#### 7.2.2.4.1 1 TX (25 kW) and 4 RXs

This geometry is comprised of 1 TX (25 kW) at (0,0) km (black circle) and 4 RXs located around the trajectory. This geometry is very similar to the one with 4 monostatic radars and is compared with it. Figure 256 depicts the geometry where all 4 RXs are in the same location as the 4 monostatic radars in 7.2.2.3.2. In fact, one pair of “bistatic” radar is working as a monostatic one because they are co-located.

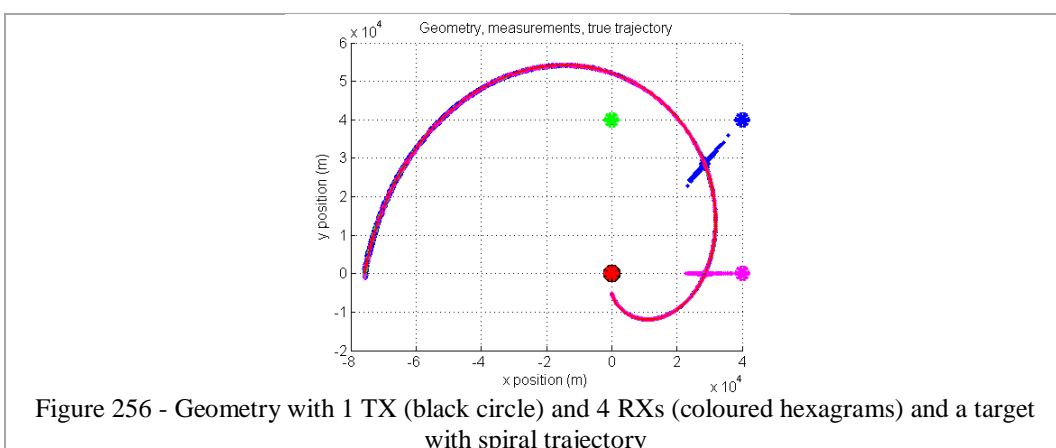


Figure 257 and Figure 258 depict the tracking results and compared with the 4 monostatic case, it shows that this one is better in the beginning of the trajectory for  $x$ -axis. The main point to be noted here, is that in the multistatic case, when the target

is getting closer to the end of the trajectory, it crosses 2 bistatic radar baselines what makes the results to be not so good, although there is a very strong “monostatic” (1 TX and 1 RX collocated) in this region (black/red pair).

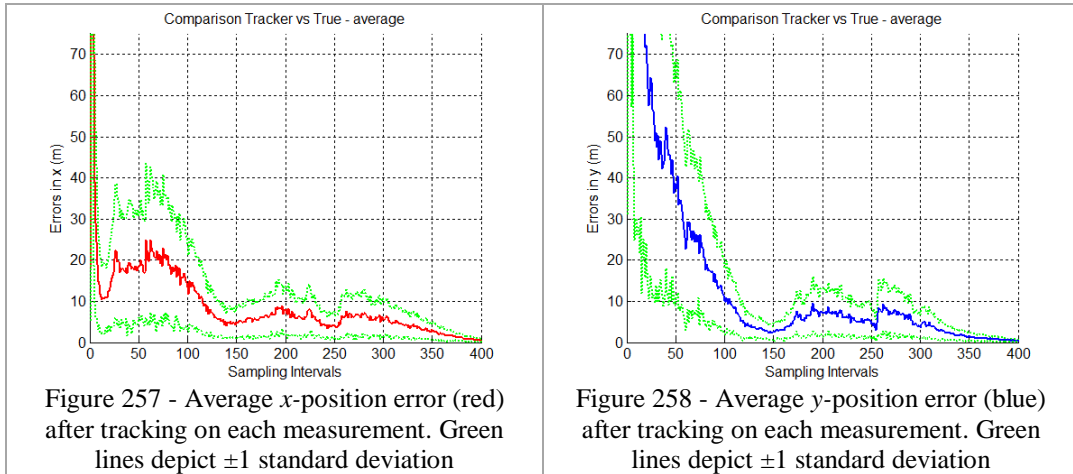


Figure 257 - Average  $x$ -position error (red) after tracking on each measurement. Green lines depict  $\pm 1$  standard deviation

Figure 258 - Average  $y$ -position error (blue) after tracking on each measurement. Green lines depict  $\pm 1$  standard deviation

Therefore, although it was expected that this geometry was better than the four 6.25 kW netted monostatic radar presented in 7.2.2.3.2, this geometry, which comprises 4 pairs of 25 kW bistatic radars, is just slightly better than the netted monostatic one.

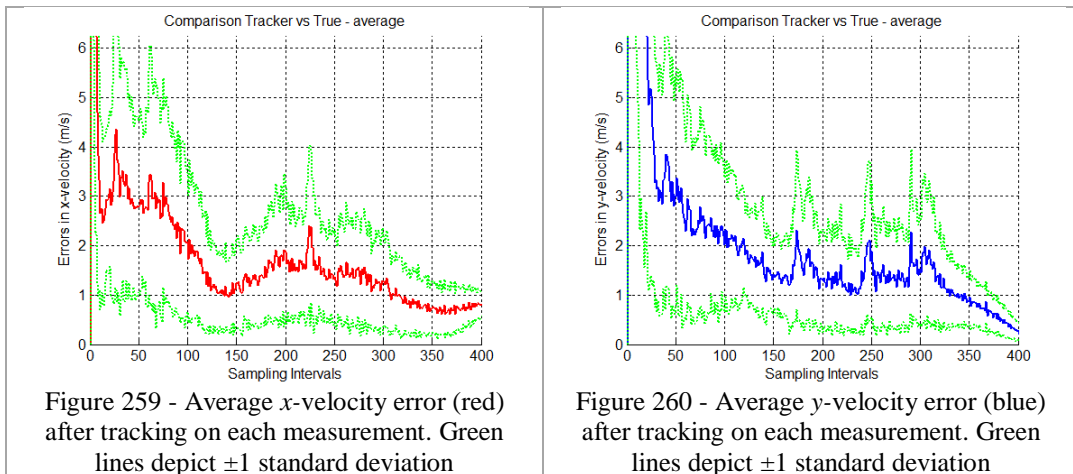
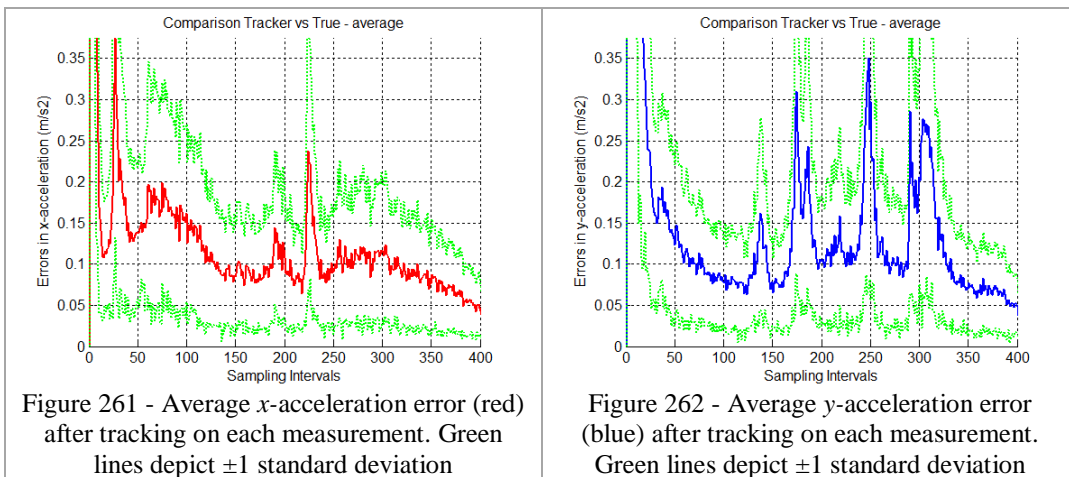


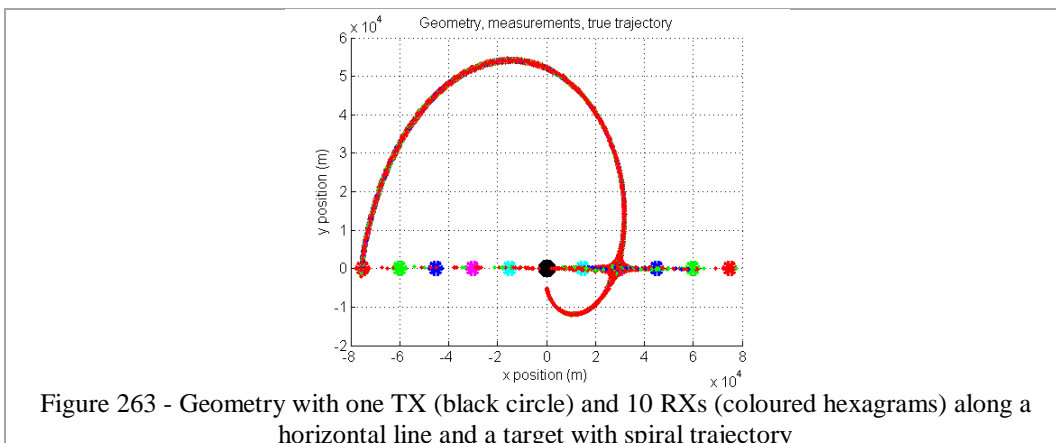
Figure 259 - Average  $x$ -velocity error (red) after tracking on each measurement. Green lines depict  $\pm 1$  standard deviation

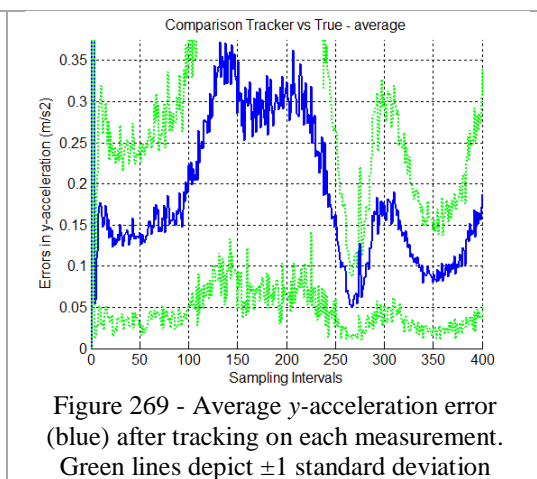
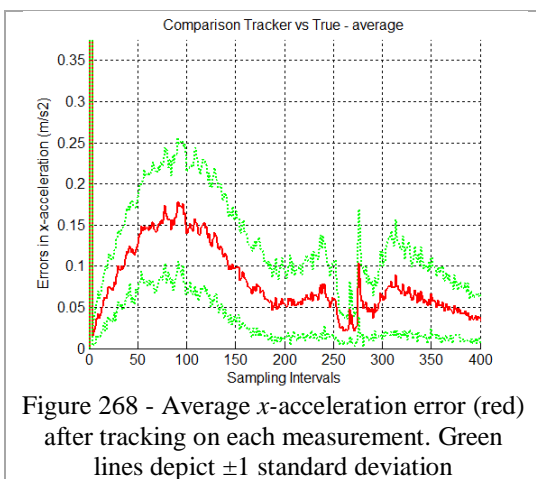
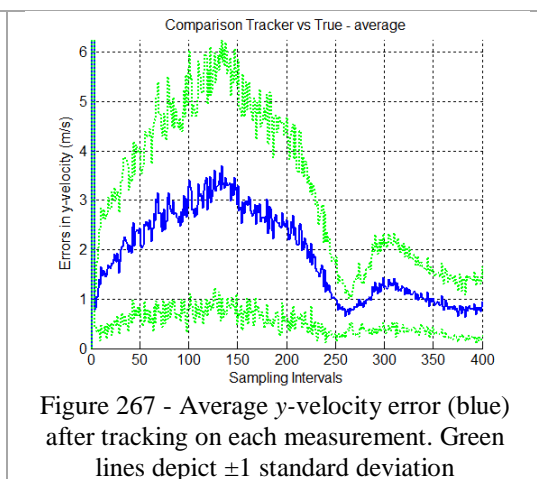
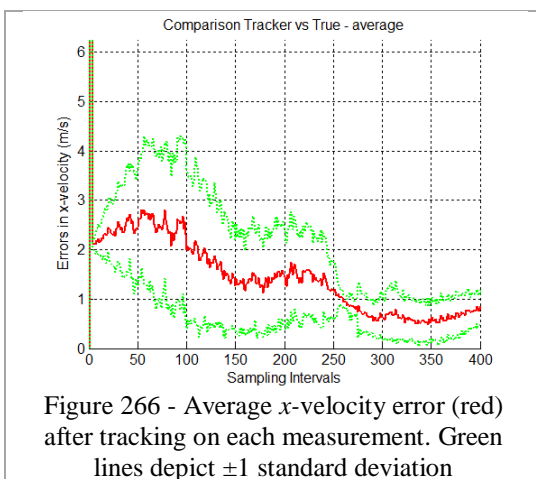
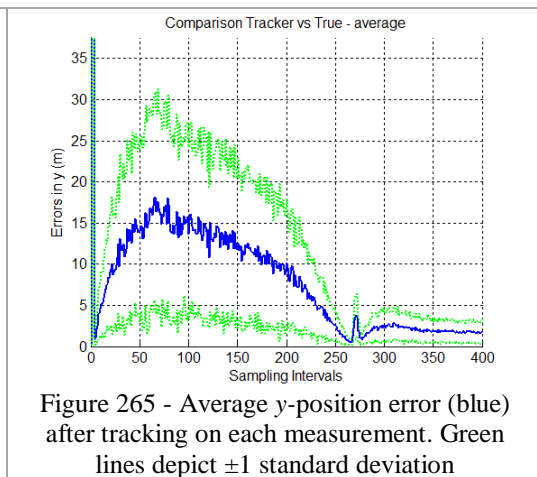
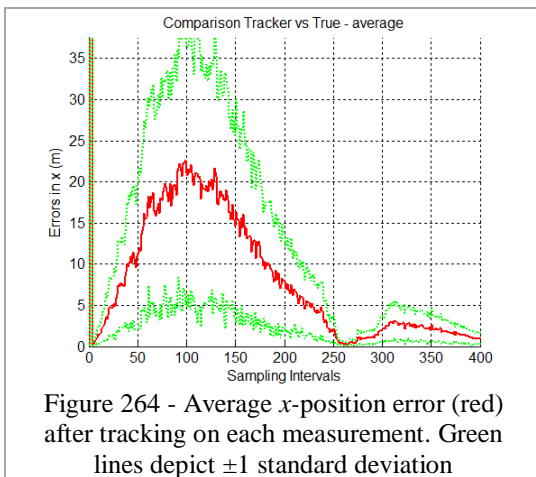
Figure 260 - Average  $y$ -velocity error (blue) after tracking on each measurement. Green lines depict  $\pm 1$  standard deviation



**7.2.2.4.2 1 TX (25 kW) and 10 RXs (on a horizontal line)**

Here, 10 pairs of 25 kW bistatic radars are put on a horizontal line. TX (25 kW) is located in the middle of this line of radars with 5 RXs to the left and 5 RXs to the right. Overall, the results presented here are better than the results in 7.2.2.3.4. However, it seems that estimates are just similar at the end of trajectory. This might be due to the fact that the target crosses 4 baselines when it is near (25,0) km.



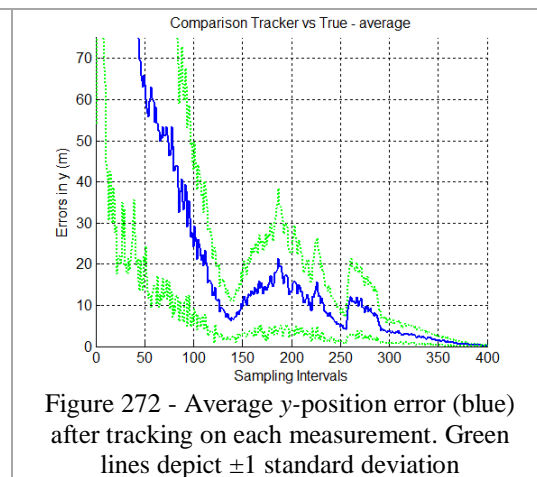
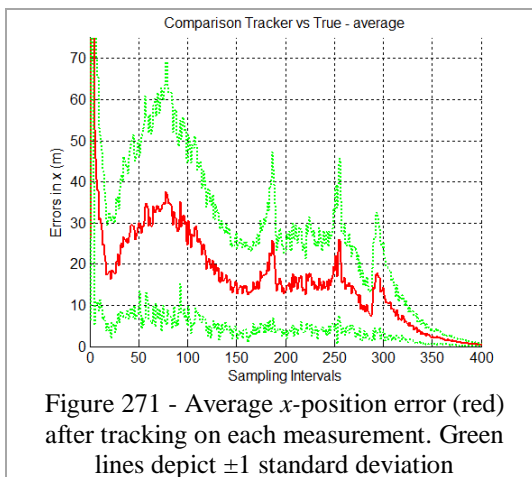
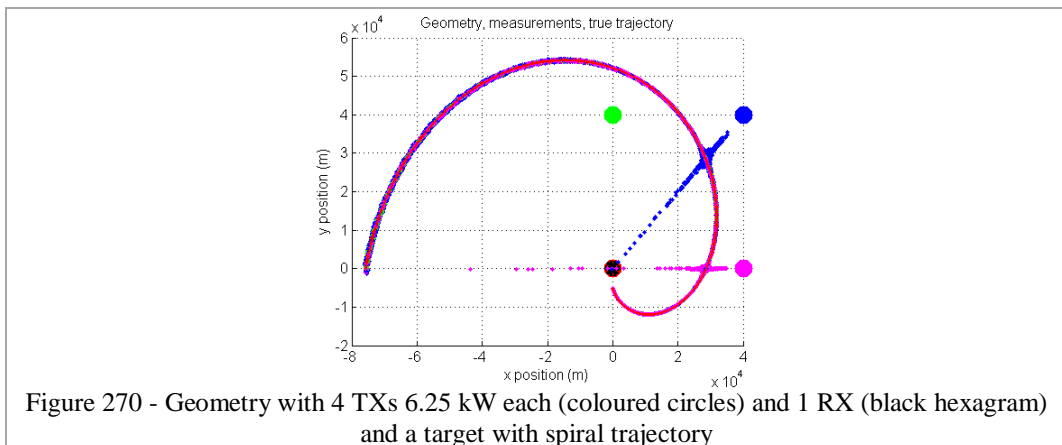


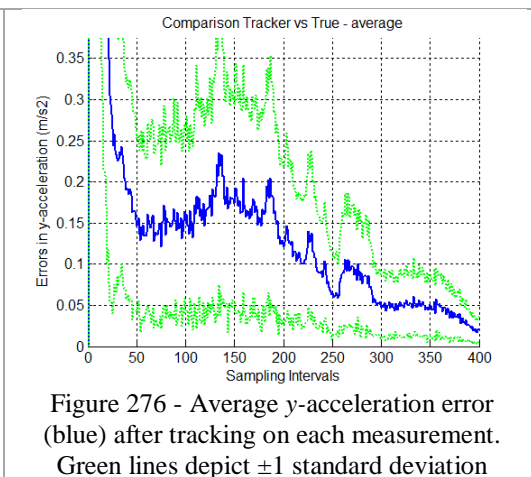
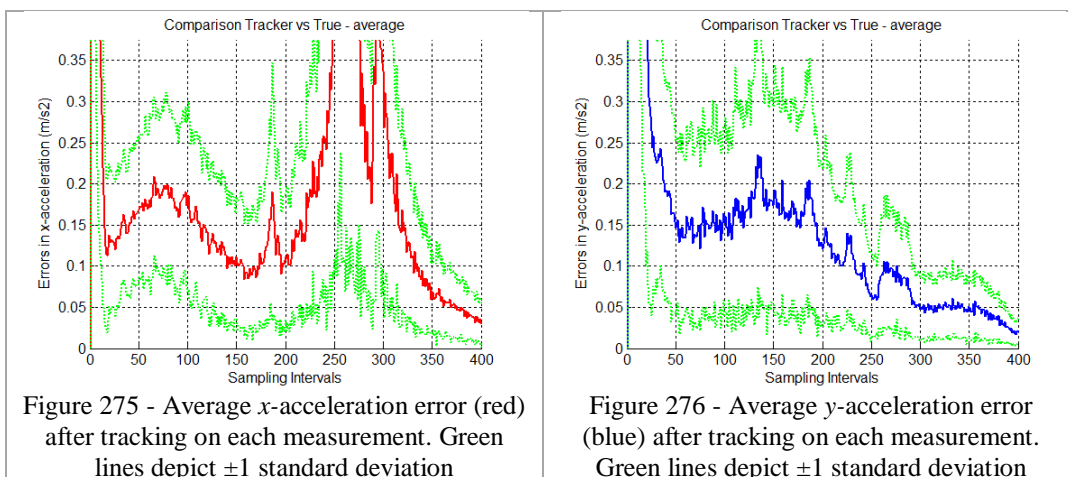
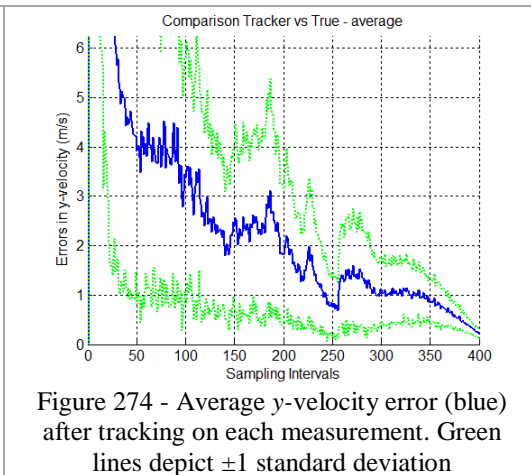
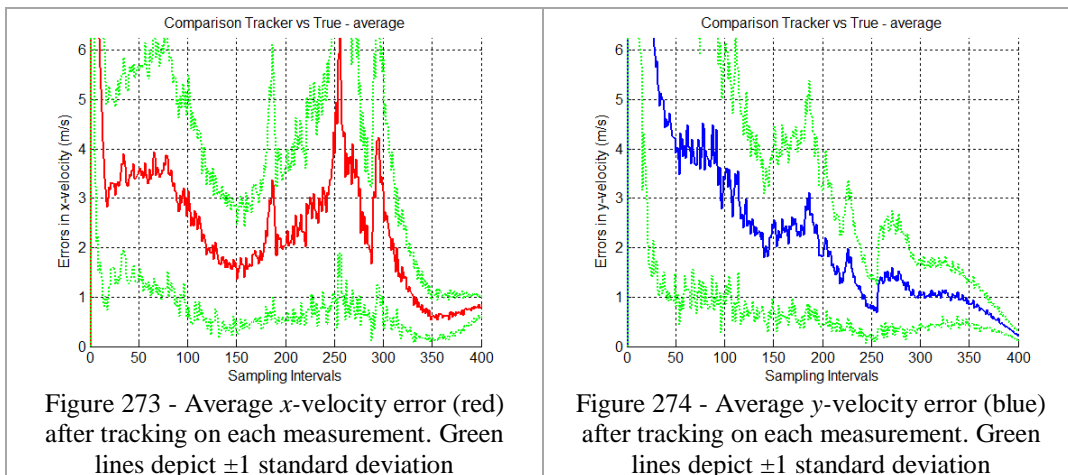
### 7.2.2.5 Multistatic (M x 1)

This section presents 2 different scenarios where a combination of bistatic radars results in a Multistatic Radar with many TXs and 1 RX.

#### 7.2.2.5.1 4 TXs (6.25 kW each) and 1 RX

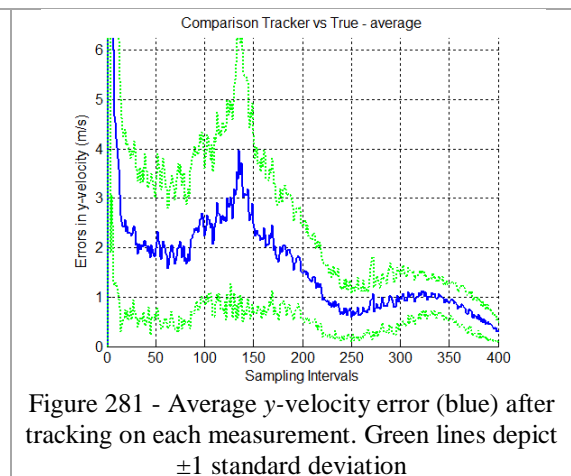
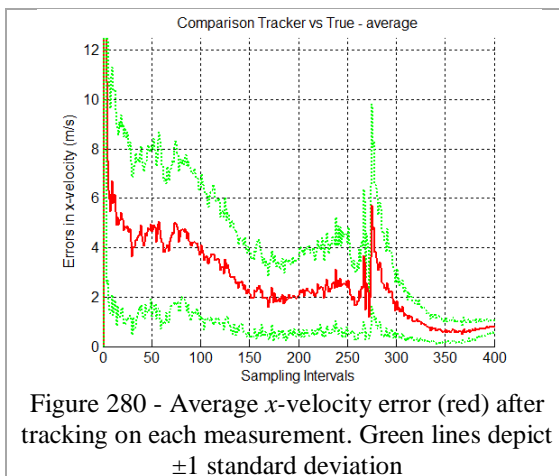
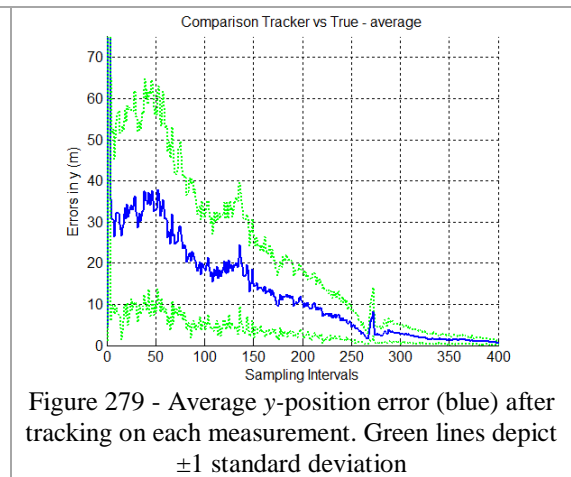
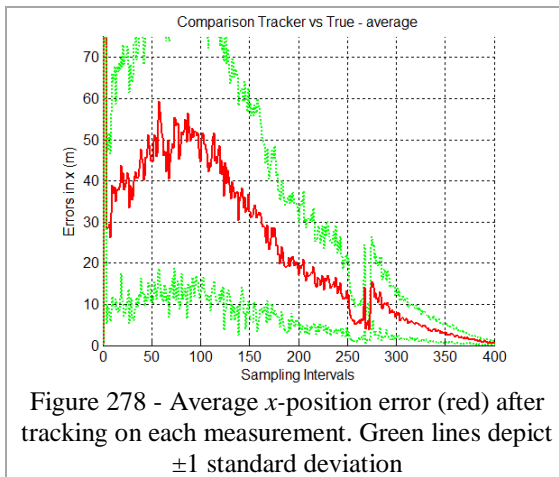
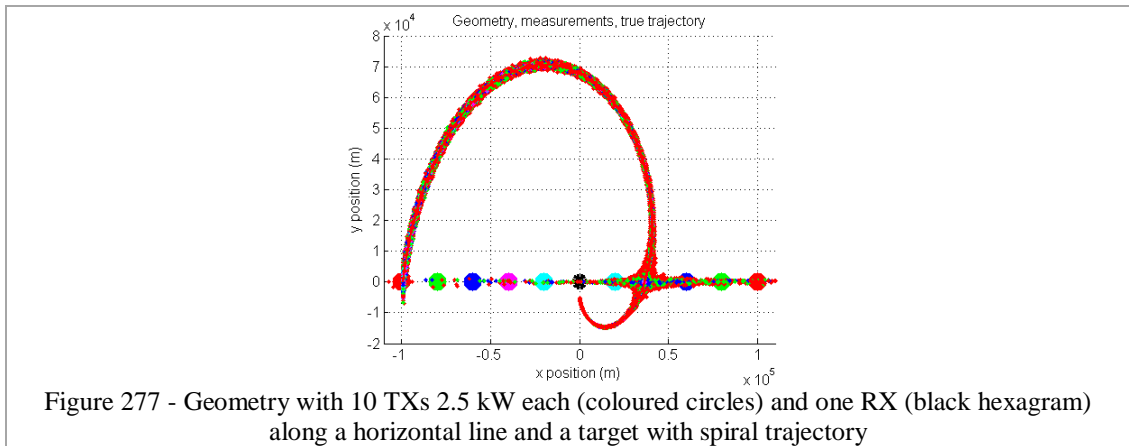
This section presents a geometry with 4 pairs of 6.25 kW bistatic radars. One of those bistatic radars is actually a monostatic one because TX and RX (red/black pair) are co-located at (0,0). This geometry is compared with the 1xN multistatic case in 7.2.2.4.1. The geometry presented here has worse results and it can be seen by comparing Figure 271 and Figure 272 with Figure 257 and Figure 258. It is an expected result because here 4 pairs of 6.25 kW bistatic radars are used instead of 4 pairs of 25 kW bistatic in 7.2.2.4.1. Nonetheless, it is always worth mentioning that this geometry could be an option if a more resilient system is desirable.

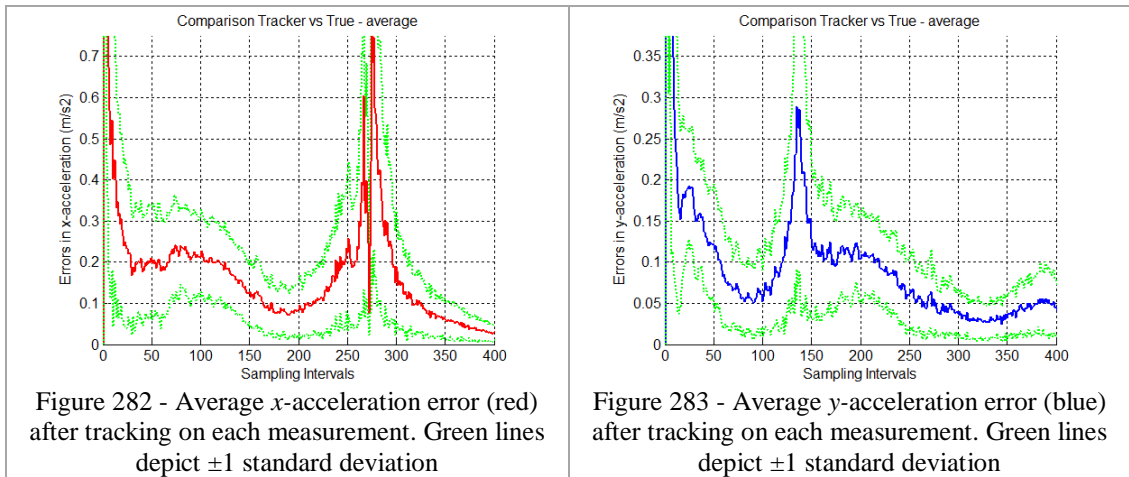




#### 7.2.2.5.2 10 TXs (2.5 kW each) and 1 RX (on a line)

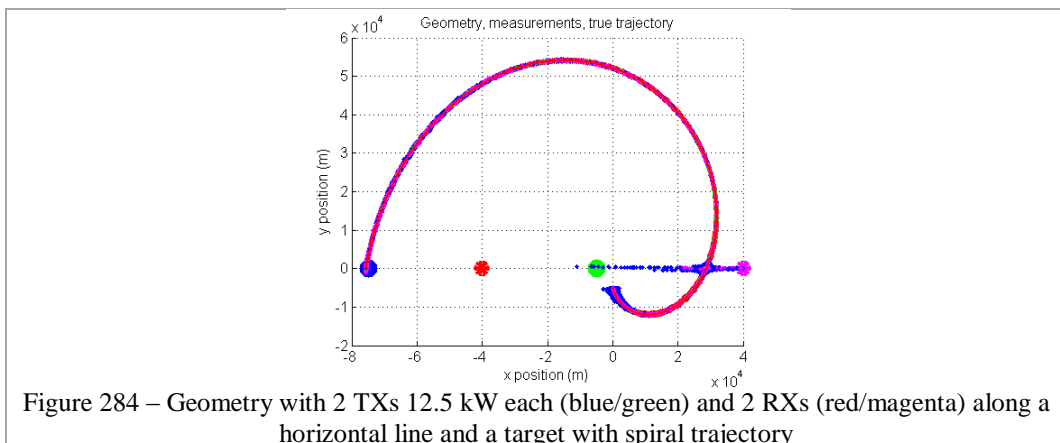
This geometry presents a configuration where 10 pairs of 2.5 kW bistatic radars are put on a horizontal line. RX is located in the middle of this line of radars with 5 TXs (2.5 kW each) to the left and 5 TXs (2.5 kW each) to the right. Overall, the results presented here are worse than the results in 7.2.2.4.2. Comparing this geometry with one in 7.2.2.3.4, the latter is better at the beginning and at the end of the trajectory.

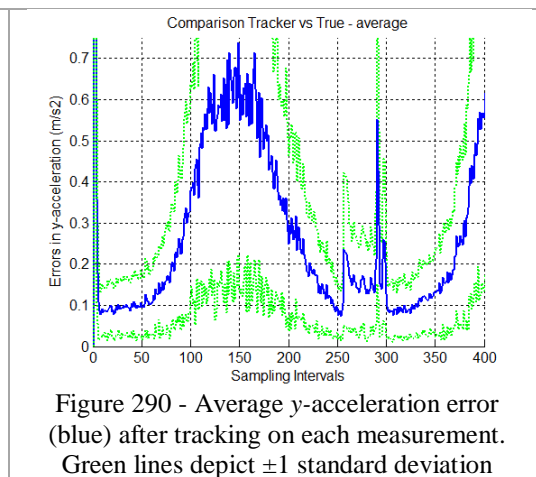
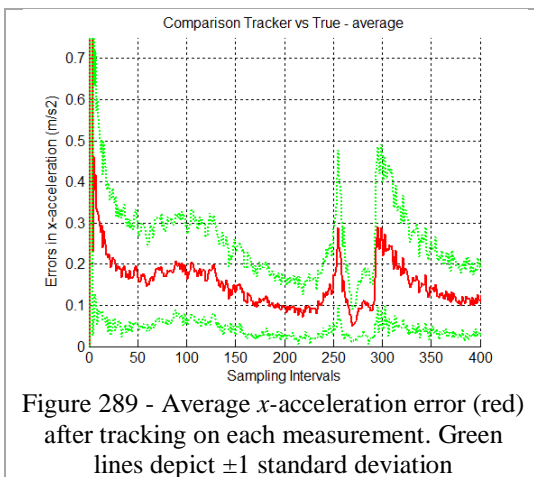
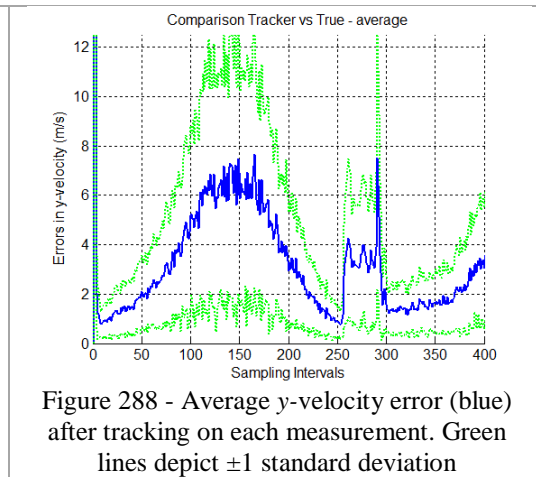
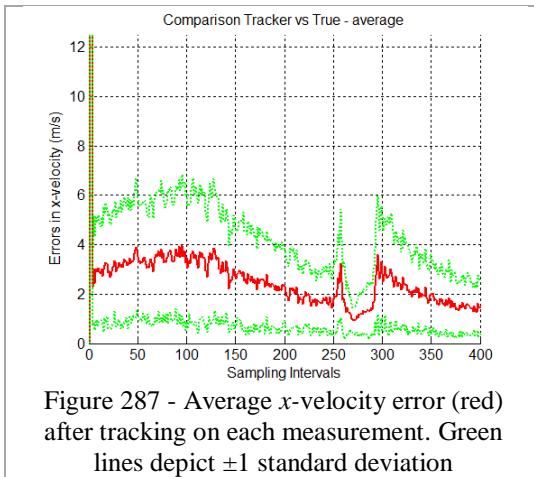
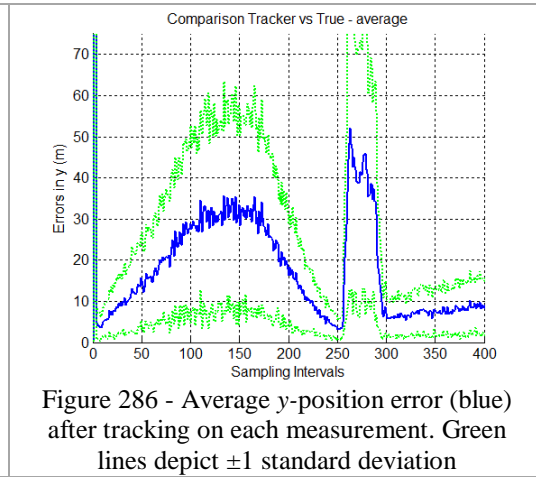
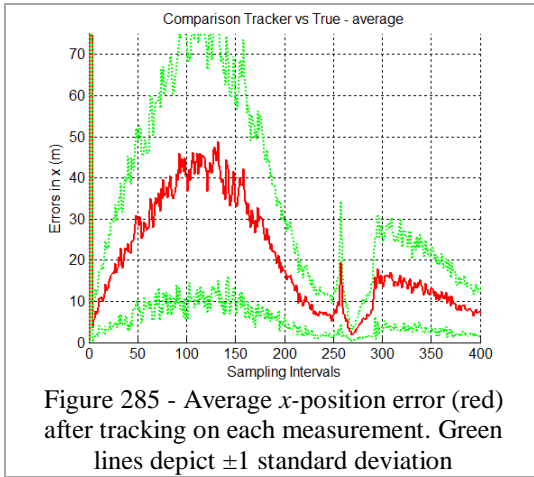




### 7.2.2.6 Multistatic (2 TXs and 2 RXs)

In this scenario, there are 2 TXs (12.5 kW) and 2 RXs, comprising 4 pairs of 12.5 kW bistatic radars. Comparing, this geometry with the one [10 TXs and 1 RX], they are very similar but this scenario is better at the beginning of the trajectory. Besides, one could decide to implement this one if it were to reduce deployment costs or to minimize synchronization problems. Note, in Figure 286, that for  $y$ -axis position, there is a peak between measurement 250 and 300 that might be because the target is crossing the baseline of the bistatic pairs (green-magenta and blue-magenta).





This scenario, if compared with the geometry (1 TX / 10 RXs) in 7.2.2.4.2, is worse. On the other hand, has one more transmitter which might be good depending on how the radar is intended to be used.

## 7.2.3 Tracking Summary Tables

### 7.2.3.1 Target 1

Table 9 summarizes the tracking position errors for  $x$  and  $y$ -axis for a target that flies with a constant velocity of 250 m/s and has an RCS of  $0.1 \text{ m}^2$ . All the geometries presented in 7.2.1 are summarized in this table.

Tables in this section present some quantitative values at certain points of the trajectory and illustrate the influence of transmitter power and geometry in the results. However, the graphics in previous sections depict a more thorough idea on how the tracking accuracy behave along the whole trajectory for different geometries.

Table 9 – Tracking Results Summary – tracking position errors during the trajectory of a target that flies on a straight line with constant velocity of 250 m/s

Geometry	Tracking Errors for position in $x$ -axis (m)				Tracking Errors for position in $y$ -axis (m)			
	$x=-40$ km	$x=-20$ km	$x=0$ km	$x=20$ km	$x=-40$ km	$x=-20$ km	$x=0$ km	$x=20$ km
(1) Monostatic (25 kW)	6	2.5	2	2	12	3	0.5	1
(2) Bistatic (25 kW) crossing	0.7	0.5	7.3	0.5	30	15	400	180
(3) Bistatic (25 kW) parallel TX-RX	18	12	10	7	22	9	2	7
(3a) Bistatic (25 kW) parallel RX-TX	9	6	10	12	14	8	2	8
(4) Netted Mono 4 TX/RX (6.25 kW)	4	2	2	1.5	5	1.5	2	1.5
(5) Netted Mono 10 TX/RX (2.5 kW) same location	6	2.5	2	2	11	3	0.5	1
(6) Netted Mono 10 TX/RX (2.5 kW) line	2.4	2.4	2	1.9	1.5	1.7	1.9	1.5
(7) Multistatic 1 TX (25 kW) and 4 RXs	1.8	1.4	1.8	1.7	4	2	1.5	1.5
(8) Multi 1 TX (25 kW) and 10 RXs line	2	1.6	1	1	2	1	0.8	0.7
(9) Multi 4 TXs (6.25 kW) and 1 RX	2.5	1.8	1.5	2.3	5.8	2.9	3.8	5

(10) Multi 10 TXs (2.5 kW) and 1 RX line	11	5	2.5	2.5	7	2.5	2	2.5
(11) Multi 2 TXs (12.5 kW) and 2 RXs	4.4	4	3.7	3.5	3	2	3	3

Similarly to Table 9, Table 10 depicts the target tracking velocity errors in  $x$  and  $y$ -axis at certain  $x$ -axis positions.

Table 10 - Tracking Results Summary – tracking velocity errors during the trajectory of a target that flies on a straight line with constant velocity of 250 m/s

Geometry	Tracking Errors for velocity in $x$ -axis (m/s)				Tracking Errors for velocity in $y$ -axis (m/s)			
	$x=-40$ km	$x=-20$ km	$x=0$ km	$x=20$ km	$x=-40$ km	$x=-20$ km	$x=0$ km	$x=20$ km
(1) Monostatic (25 kW)	0.12	0.05	0.02	0.01	0.25	0.06	0.02	0.01
(2) Bistatic (25 kW) crossing	0.05	0.04	0.5	0.04	2	2	100	38
(3) Bistatic (25 kW) parallel TX-RX	1.3	1	0.8	0.6	1.5	0.6	0.2	1
(3a) Bistatic (25 kW) parallel RX-TX	0.7	0.5	0.75	0.9	1	1.2	0.2	0.4
(4) Netted Mono 4 TX/RX (6.25 kW)	0.06	0.02	0.15	0.1	0.12	0.04	0.02	0.01
(5) Netted Mono 10 TX/RX (2.5 kW) same location	0.1	0.04	0.02	0.01	0.25	0.06	0.02	0.01
(6) Netted Mono 10 TX/RX (2.5 kW) line	0.03	0.02	0.015	0.01	0.02	0.015	0.01	0.005
(7) Multistatic 1 TX (25 kW) and 4 RXs	0.03	0.02	0.015	0.01	0.08	0.03	0.02	0.015
(8) Multi 1 TX (25 kW) and 10 RXs line	0.03	0.02	0.01	0.01	0.35	0.02	0.01	0.01
(9) Multi 4 TXs (6.25 kW) and 1 RX	0.045	0.02	0.015	0.015	0.13	0.07	0.04	0.03
(10) Multi 10 TXs (2.5 kW) and 1 RX line	0.18	0.06	0.04	0.03	0.14	0.05	0.03	0.02
(11) Multi 2 TXs (12.5 kW) and 2 RXs	0.06	0.03	0.025	0.02	0.05	0.025	0.025	0.02

### 7.2.3.2 Target 2

Target 2 is a target that flies on a spiral-like trajectory with non constant velocity and acceleration starting from (-100,0) km and going towards one transmitter of the network. Table 11, Table 12 and

Table 13 depict, respectively the tracking errors for position, velocity and acceleration for all scenarios from section 7.2.2.

Table 11 - Tracking Results Summary – tracking position errors during the trajectory of a target that flies on a spiral trajectory with non constant velocity and acceleration. The errors are depicted at certain measurement sequence number. Each measurement is performed every 2.5 seconds.

Geometry	Tracking Errors for position in x-axis (m)			Tracking Errors for position in y-axis (m)		
	At 100	At 200	At 350	At 100	At 200	At 350
(1) Monostatic (25 kW)	45	15	2	25	15	2
(2a) Bistatic (25 kW) crossing	10	2	20	20	30	15
(2b) Bistatic (25 kW)	60	50	20	10	70	20
(3a) Netted Mono 4 TX/RX (6.25 kW)	6	28	3	10	14	2
(3b) Netted Mono 4 TX/RX (6.25 kW) closer	8	3	3	10	4	3
(3c) Netted Mono 10 TX/RX (2.5 kW) same location	43	12	2	20	14	2
(3d) Netted Mono 10 TX/RX (2.5 kW) line	47	12	15	33	15	3
(4a) Multistatic 1 TX (25 kW) and 4 RXs	15	8	3	10	7	2
(4b) Multistatic 1 TX (25 kW) and 10 RXs line	23	8	3	15	10	2
(4c) Multistatic 4 TXs (6.25 kW) and 1 RX	30	13	3	26	14	2
(4d) Multistatic 10 TXs (2.5 kW) and 1 RX line	45	20	4	20	10	2
(5) Multistatic 2 TXs (12.5 kW) and 2 RXs	40	16	14	29	18	7

Table 12 - Tracking Results Summary – tracking velocity errors during the trajectory of a target that flies on a spiral trajectory with non constant velocity and acceleration. The errors are depicted at certain measurement sequence number. Each measurement is performed every 2.5 seconds.

Geometry	Tracking Errors for velocity in x-axis (m/s)			Tracking Errors for velocity in y-axis (m/s)		
	At 100	At 200	At 350	At 100	At 200	At 350
(1) Monostatic (25 kW)	4.8	2.5	0.7	3.7	2.5	0.9
(2a) Bistatic (25 kW) crossing	2.4	1.4	2.5	3	5	3
(2b) Bistatic (25 kW)	6	6	4	2	5	2.8
(3a) Netted Mono 4 TX/RX (6.25 kW)	1	6	0.8	2.2	1.8	1
(3b) Netted Mono 4 TX/RX (6.25 kW) closer	1.3	1.4	0.6	2.4	2.4	1

(3c) Netted Mono 10 TX/RX (2.5 kW) same location	3.5	1.6	0.5	2.6	1.8	0.9
(3d) Netted Mono 10 TX/RX (2.5 kW) line	4	1.5	0.5	4.2	3	1
(4a) Multistatic 1 TX (25 kW) and 4 RXs	2	1.9	0.7	2.2	1.3	0.9
(4b) Multistatic 1 TX (25 kW) and 10 RXs line	2.2	1.4	0.6	3.1	2.5	1
(4c) Multistatic 4 TXs (6.25 kW) and 1 RX	3	2.2	0.6	3.5	2	0.9
(4d) Multistatic 10 TXs (2.5 kW) and 1 RX line	4	2	0.9	2.2	1.6	1
(5) Multistatic 2 TXs (12.5 kW) and 2 RXs	3.5	2	2	5	3.4	1.8

Table 13 - Tracking Results Summary – tracking acceleration errors during the trajectory of a target that flies on a spiral trajectory with non constant velocity and acceleration. The errors are depicted at certain measurement sequence number. Each measurement is performed every 2.5 seconds.

Geometry	Tracking Errors for acceleration in x-axis ( $m/s^2$ )			Tracking Errors for acceleration in y-axis ( $m/s^2$ )		
	At 100	At 200	At 350	At 100	At 200	At 350
(1) Monostatic (25 kW)	0.23	0.17	0.08	0.18	0.19	0.07
(2a) Bistatic (25 kW) crossing	0.24	0.01	0.17	0.2	0.35	0.35
(2b) Bistatic (25 kW)	0.3	0.3	0.4	0.04	0.22	0.15
(3a) Netted Mono 4 TX/RX (6.25 kW) far	0.1	0.6	0.06	0.1	0.12	0.06
(3b) Netted Mono 4 TX/RX (6.25 kW) closer	0.12	0.05	0.06	0.09	0.1	0.07
(3c) Netted Mono 10 TX/RX (2.5 kW) same location	0.23	0.07	0.04	0.07	0.12	0.04
(3d) Netted Mono 10 TX/RX (2.5 kW) line	0.23	0.05	0.05	0.25	0.25	0.1
(4a) Multistatic 1 TX (25 kW) and 4 RXs	0.15	0.1	0.08	0.08	0.1	0.07
(4b) Multistatic 1 TX (25 kW) and 10 RXs line	0.15	0.05	0.07	0.2	0.3	0.08
(4c) Multistatic 4 TXs (6.25 kW) and 1 RX	0.18	0.11	0.07	0.17	0.13	0.05
(4d) Multistatic 10 TXs (2.5 kW) and 1 RX line	0.22	0.09	0.07	0.06	0.11	0.03
(5) Multistatic 2 TXs (12.5 kW) and 2 RXs	0.16	0.1	0.14	0.35	0.3	0.13

## 7.3 Analysis

Sections 7.1 and 7.2 present the simulations performed in several different scenarios where some parameters are varied in order to assess how the performance of the radars are affected in terms of measurements and tracking when compared with the real state of the target. Section 7.1.5 and 7.2.3 show, respectively for measurement and tracking, a summary of position errors (measurement and tracking), velocity errors (tracking) and acceleration errors (tracking) when it is applicable.

All the results in Section 7.1 are according to the model that uses the radar range equation (9). When the RCS is reduced by 20 dB (from  $10 \text{ m}^2$  to  $0.1 \text{ m}^2$ ), SNR is also reduced by 20 dB. Moreover, when the transmitter power is reduced by a factor of 4 (or 6 dB), SNR is also reduced by the same factor according to the radar equation. In scenarios where a multistatic radar is used, comparing a multistatic radar with 1 TX (25 kW) and 2 RXs against a multistatic radar with 2 TXs (12.5 kW each) and 1 RX, because of the process of fusion, it is shown that having 2 pairs of 12.5 kW bistatic radars is not necessarily worse than having 2 pairs of 25 kW bistatic radars. In some situations, for example, in Table 5, when  $x=-50 \text{ km}$  the fused measurement errors for  $x$ -position are the same (800 m) in both multistatic scenarios. The same happens for  $y$ -position when  $x=0 \text{ km}$ . And, although it is useful to compare the numbers presented in Table 5, it is easier to see the differences when comparing, for example, Figure 122 with Figure 133 or Figure 123 with Figure 134.

In section 7.2, several scenarios are presented in order to bring a better understanding about the benefits of using a multistatic radar when tracking a target, either using a network of monostatic radars or a set of bistatic radars. Again, although the tables in section 7.2.3 present quantitatively the errors in a form where it might be easy to compare different scenarios at once, the tables do not show how the numbers are changing at a certain time. Sometimes, having a better number at  $x=0$ , is worse as whole because, after that it might be increasing or changing abruptly. For example, line (2a) of Table 11 indicates that the tracking error for position in  $y$ -axis changes from 20 m at measurement number 100 to 30 m at measurement number 200. However, it does not show that between measurements number 100 and 200 (see Figure 216), there is a peak where the errors are very large (more than 150 m). Nonetheless, it is possible to see, when comparing lines (3b) and (4a) of the same table that using a netted monostatic radar with 4 radars of 6.25 KW is slightly better than using 4 pair of 25 KW bistatic radars. This is probably because, in this case, the target is crossing the baseline of a bistatic pair at a certain point of the trajectory.

Section 7.2.1 and 7.2.2 present the results when a target is flying with a constant velocity and in a spiral-like trajectory, respectively. In both cases, many different scenarios are simulated keeping the total transmitted power equal to 25 kW. One difference between those 2 situations is that the results for

position/velocity/acceleration errors are spikier in the “Target 2” scenarios. This is due to the fact that Kalman Filter has to be set for a situation where it expects a non constant behaviour of the target.

Either for target 1 (Section 7.2.1) or target 2 (Section 7.2.2), simulations show the advantages of using a combination of radar measurements to track a target. The idea of all simulations is to show that it is not easy to track a target with RCS of  $0.1 \text{ m}^2$ , which is about 100 or even more times worse than the expected target RCS of this kind of radar with 25 kW power. The radar with 25 kW is a typical radar for navigation purposes where the main targets are located no more than the horizon distance (around 25 km for ships, which may have an RCS of tens or even hundreds and thousands of square meters). For targets, like aircrafts flying at a height of 10 km, the horizon distance can be around 400 km (see Table 2), which is quite far for a radar like this to detect and track an aircraft with  $\text{RCS}=0.1 \text{ m}^2$ . For a target with such RCS flying at a distance of about 65 km, the tracking error for  $x$ -position is about 15 m (Figure 145) after some time tracking the target (about 60 seconds). This error can be as good as 1.5 m if the RCS is increased to  $10 \text{ m}^2$ . Thus, the main challenge is to obtain better results when tracking  $0.1 \text{ m}^2$  RCS targets using 25 kW radar built for navigation purposes.

Sections 7.2.1.3.2 and 7.2.2.3.3 are examples that show that combining 10 radars of 2.5 kW has equivalent results to a radar with 25 kW (or even slightly better). It means that it is possible to emulate a radar of 250 kW power, for example, just using 10 radars of 25 kW at the same location. Problems with interference or timing are not considered in this study though.

The results also show that distributing the power of the radar along the trajectory (compare Figure 171 and Figure 177, for example) makes it to converge quicker to a certain level of error, but it does not get better along the trajectory.

Scenarios where the target crosses the baseline of a bistatic radar present worse results with the filter and fusion algorithm being used. It is possible to see as well (comparing Figure 150 and Figure 151) that tracking results are better along the axis that crosses the baseline. Figure 150 shows that it has the best  $x$ -position track results

at the beginning of the track if compared with all the other geometries (see line (2) of Table 9).

Scenarios with just one TX with 25 kW can have much better results when using many receivers to make use of this power, making the system as a whole be comprised of many bistatic radars with 25 kW (Figure 185, for example). This scenario with the same total power as the monostatic case (Figure 144) is overall better when comparing the results for tracking position (Figure 145, Figure 186 and Table 9).

A scenario that keeps that same total power, spreading the power along many TXs, using only 1 RX is also simulated (Figure 195). In this case, the system comprises 10 TXs with 2.5 kW power and 1 RX. The results are worse than the 1 TX and many RXs scenario but there is the big advantage of having many TXs which makes the system more resilient to attacks against the TXs. The system can still work with some degraded performance when one or more TXs are destroyed, for example.

The same ideas of changing the geometry of a radar are applied with target 2. Figure 205 and Figure 206 show how velocity and acceleration of the target are varying according to time in a spiral-like trajectory (Figure 207).

In section 7.2.2 there are scenarios that show that there is a good improvement on the results when the radars are brought closer to the target for monostatic cases (Figure 228 and Figure 235), which is an expected result. Nevertheless, the use of 4 bistatic radars (25 kW pairs) like in Figure 256, instead of 4 monostatic 6.25 kW radars (Figure 235), does not show better results. In fact, the results are very similar, but in the first moment, it is not an expected result. The fact that the target crosses the baseline of 2 of those 4 bistatic radars, can make the system have more modest results. At the beginning of the trajectory, though, the multistatic radar performs better (comparing Figure 236 and Figure 257).

Overall, the tracking and fusion algorithm performed well and according to expected. However, there are cases where, especially for acceleration and velocity, the filter presents some peaks during the estimation of these states (see, for example Figure 232, Figure 234, Figure 237, Figure 239, Figure 240, Figure 260, Figure 261, Figure 262 and so on). The good thing is that, apparently, the position tracking results are

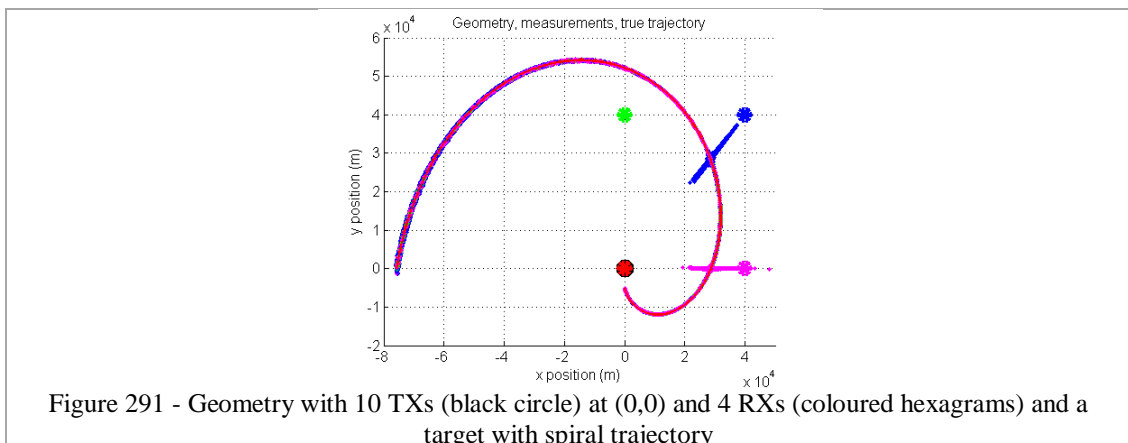
not affected. The existence of peaks seems to be related to the fusion process and how information about output from the fusion is passed to Kalman Filter.

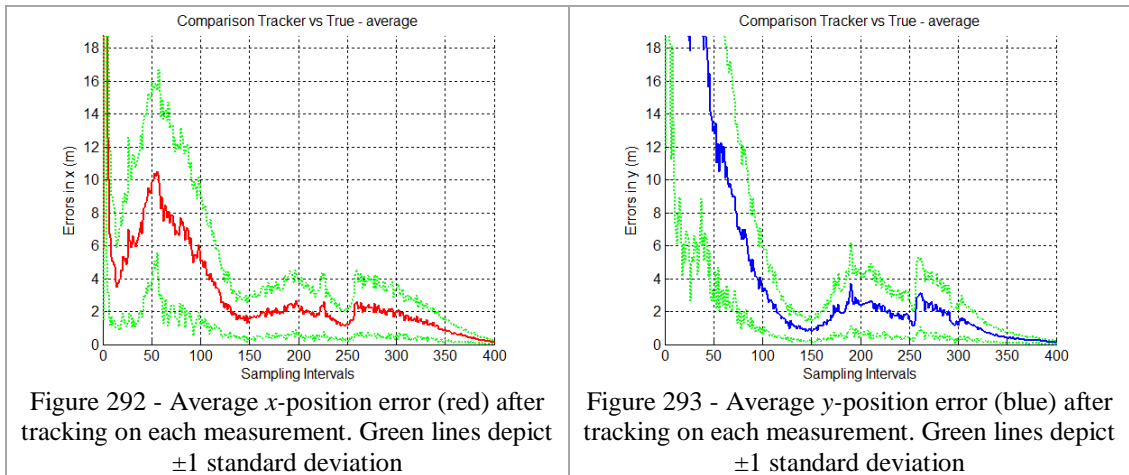
## 7.4 Examples

To summarize and to illustrate what can be done with the information from the previous sections, this section shows the same scenario as in 7.2.2.4.1. The target flies in a spiral-like trajectory and has  $RCS=0.1 \text{ m}^2$ . The main objective in this example is to improve the tracking results especially at the beginning of the trajectory (*script31.m* is used).

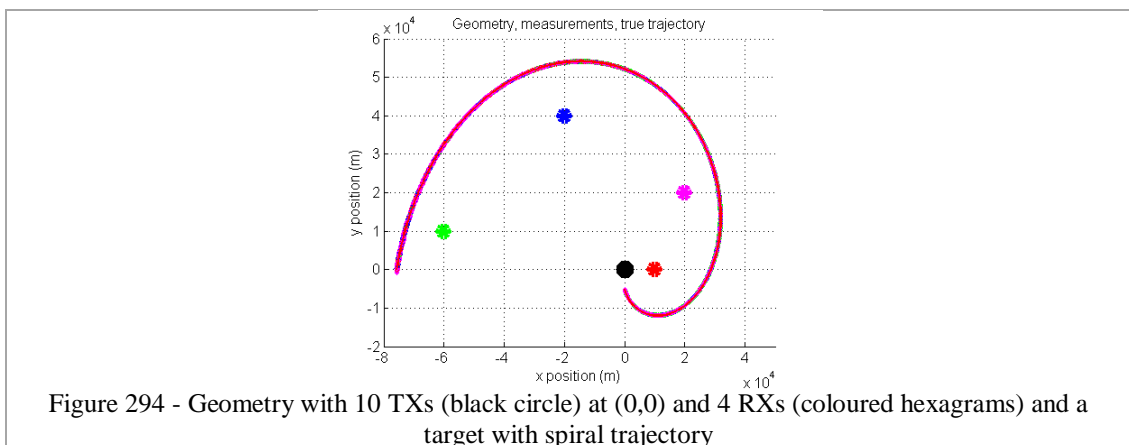
The comparison is done against Figure 257 and Figure 258.

Figure 291 depicts the same geometry but instead of using one TX of 25 kW, 10 TXs of 25 kW are used. The results are depicted in Figure 292 and Figure 293. As the total power increases by a factor of 10, SNR also increases by the same amount. And the errors, consequently (according to Equations (18) and (19)), decrease by a factor of  $\sqrt{10}$ . If it was possible to use just one TX of 250 kW, the results would be very similar.





Despite the fact that overall the errors are better, at the beginning of the trajectory, it is still not so good. Next scenario, with the same 10 TXs of 25 kW but with 3 of 4 RXs repositioned, it is possible to improve this requirement. This improvement comes by changing the position of an RX (green hexagram) to somewhere closer to the beginning of trajectory and to reposition other 2 RXs (blue and magenta hexagrams) to a place where the target would not cross the baseline of pairs of bistatic radars (see Figure 294).



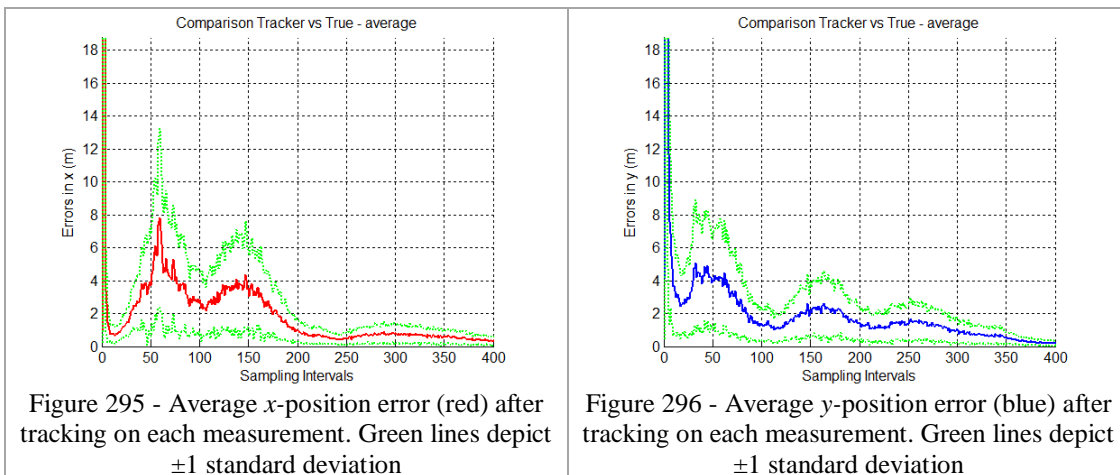


Figure 295 and Figure 296 depict the results of tracking position errors using the new geometry and, as expected, the tracking position errors are much better now. A great improvement happened especially in  $y$ -axis position accuracy as can be seen comparing Figure 296 with Figure 293.

Now, for the same scenario shown in Figure 294 but with just one TX of 250 kW (for simplicity) and 4 RXs, the measurements of the 4 bistatic pairs are not performed at the same time. Instead, they are alternated and there is one measurement done by one of the 4 bistatic pairs every 0.625 seconds ( $\frac{2.5}{4}$  seconds). As can be seen in Figure 297 and Figure 298, the average position errors have the similar magnitude although in this last scenario the errors are spikier. This is due to the fact that each pair of bistatic radar has different measurement standard deviations which affect the output of Kalman Filter.

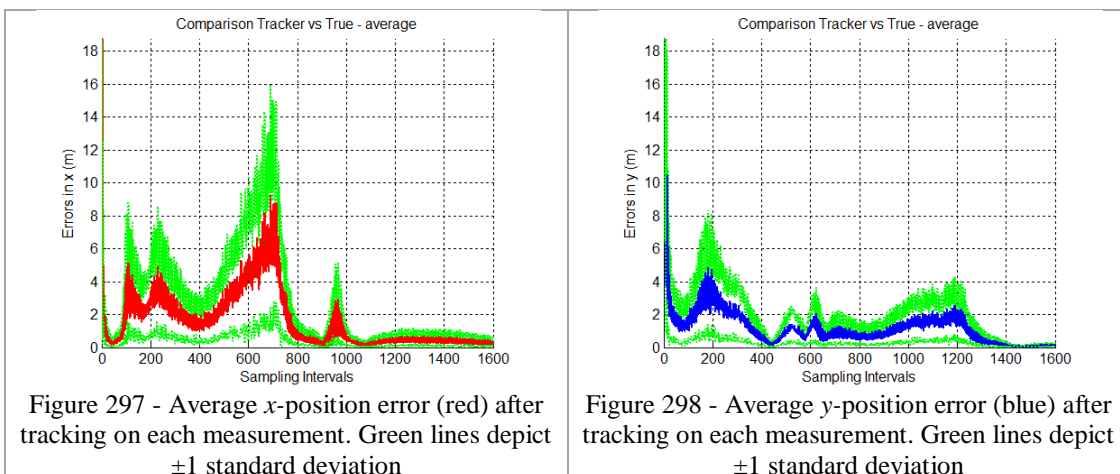
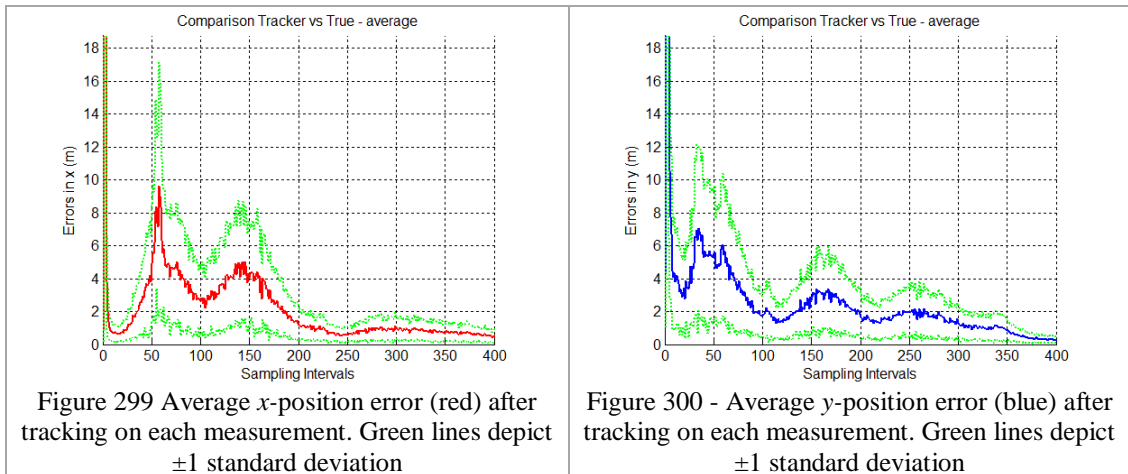
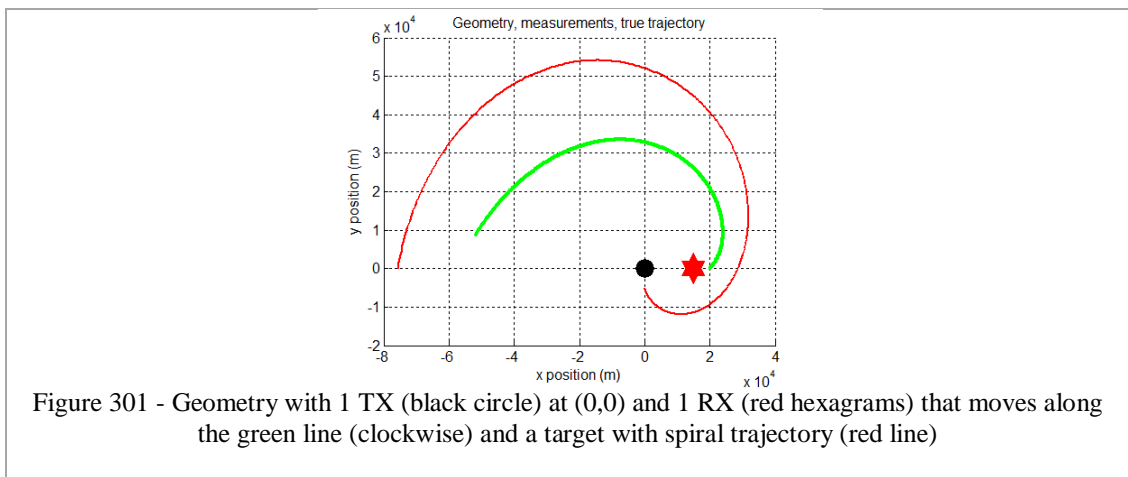


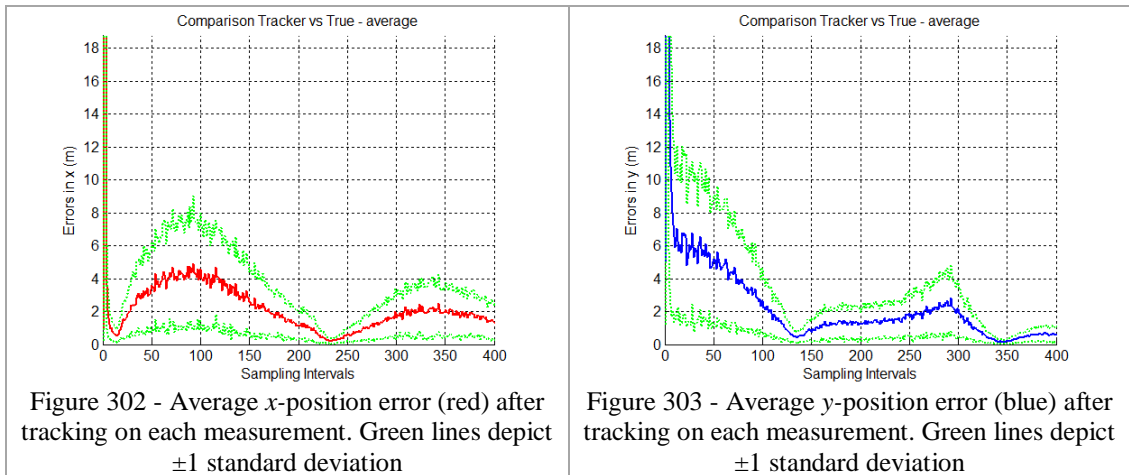
Figure 299 and Figure 300 show, for the same scenario above, how is the behaviour of the errors if all 4 bistatic pairs perform the measurement at the same time every 2.5 seconds. Again, for simplicity, it is used just one TX of 250 kW and the results are quite similar to Figure 295 and Figure 296 (where 10 TXs of 25 kW is used).



As the last example, Figure 301 represents a scenario where there is only 1 TX (250 kW for simplicity, instead of 10 TXs of 25 kW) and only 1 RX that moves along the green line trajectory (clockwise direction).



This shows what would happen if a intelligent radar decide to move one RX (or TX) following the target at a certain distance and keeping the bistatic angle at values that are smaller than 145-180 degrees.



So, with just one RX it is possible to achieve results (see Figure 302 and Figure 303) that are similar to what is obtained in the previous scenario. To perform this specific scenario (case 4 of *script31.m*), another version of class TRadar has to be used and *TRadar1.m* must substitute *TRadar.m* to perform this simulation.

## 8 Conclusions and Further Work

The first radars used in military scenarios to detect enemies were quasi-bistatic, due to the fact that by that time, it had not been developed a technology that would allow the transmitter and receiver to use the same antenna. After the development of monostatic radars, there was almost no interest in the bistatic radars subject. Apparently, this interest in bistatic and multistatic radars has been happening in cycles of 15-20 years according to [3]. However, due to the fact that monostatic radars alone have been reaching their limits in terms of performance and because of the existence of new threats, the interest in bistatic and multistatic radars, nowadays, should last longer.

In order to detect stealth targets and to be able to overcome jamming attacks by enemies, networks of radars operating either monostatically or bi/multistatically can be used. Among many things, this delivers better sensitivity, coverage and tracking accuracy.

The research reported in this thesis has investigated how much multistatic radars can be better than stand alone monostatic radars when tracking a target. Simulations with different geometries and different target trajectories have been performed in order to assess the tracking performance in each scenario. Although three simple tracking filters ( $g-h$ ,  $g-h-k$  and KF) have been programmed, only the KF has been used for the final results. Tracking performance has been analysed in terms of estimated position, velocity and acceleration accuracies. Different geometries including monostatic radar, bistatic radars with target crossing and not crossing the baseline, multistatic

radars with only 1 TX and many RXs, multistatic radars with many TXs and only 1 RX and multistatic radars with many TXs and RXs have been considered.

In terms of target state (position, velocity and acceleration) accuracy of the measurements and tracking, the simulations have shown that performance is proportional to the total power of the network transmitters. Nonetheless, depending on the configuration of the geometry, the results have not been as good as expected. It happened because the fusion algorithm is very simple and it considers the measurements from each radar of the network using weights to perform average of the measurements. While the weight is related to SNR, the algorithm considers measurements with higher SNR more important than the ones with lower SNR. In scenarios where the target crosses the baseline of a pair of bistatic radar, it has been assumed that measurements coming from the region where the bistatic angle is close to 180 degrees are not very reliable and thus their weights are reduced.

The simulations were performed with real radar characteristics because the idea was to assess if it was possible to use characteristics of navigation radars to track targets with low RCS. The research reported in this thesis has shown that it is possible to achieve a good accuracy configuring a geometry that is suitable for the requirements of a system.

Also, from the results of the simulations it is possible to understand why multistatic radars can still work with acceptable accuracy if one TX is lost or destroyed (graceful degradation). Losing one TX from a multistatic radar with 10 TXs, means that the total power of the system is reduced to 90% if all TXs are identical. If all TXs are located at the same position, the reduction in SNR would be the same as the reduction in total power. Thus, the errors increase by a factor of about 5%.

The problem of jamming attacks to TX does not affect performance of bistatic radars or multistatic radars comprised of pairs of bistatic radars. In addition, jamming attacks to a monostatic radar of a network makes the system to perform with a degraded performance and not to be completely out of service. Besides, an intelligent system could order the monostatic radar to stop emitting and become just a receiver in the network making jamming attacks less effective.

This work has presented several figures that show the tracking accuracy (for position, velocity and acceleration) of different geometries when the target is flying at certain velocity and at a certain distance from the radar. Therefore, it is possible to see how the performance of a tracker can be improved just adding another TX or RX or just deploying them into a more suitable location. Furthermore, it has shown that if the technology does not allow the system to have more powerful radars, so adding some more TXs to the network can help to improve accuracy, for example. Also, if the budget does not allow buying so many TXs, adding cheap RXs can still enhance the performance of the system.

Consequently, using more than one monostatic radar, a number of TXs and RXs and combining information from all radars of a network will allow the system to be more accurate, more resilient and maybe cheaper. However, there are some improvements that should be tackled in future research. The report herein presented has considered that the radars (nodes) of the network communicate without delays or any other problems related to communication among them. The information necessary for data fusion is 100% available for the fusion algorithms and then for the tracking algorithm. Additionally, position estimates have been considered to be known by all the nodes so that they can point their antennas to the correct region of the space. It is also considered to be performed by another software module not developed in this thesis. As a consequence, resource management software should be developed in order to make the best use of all information that herein is considered available for all algorithms whenever necessary. Another important characteristic of the simulations performed in this thesis is that all the measurements have been performed in fixed intervals of 2.5 seconds. These intervals could be variable according to the needs of the system if the system uses Electronically Steered Antennas. Again, “needs of the system” means that there is some module managing where the resources are most necessary at a certain moment. The same ideas applied for Multifunctional Radar could be applied on a radar network when it is about managing the resources of a system [22][36].

This thesis has shown that deploying a radar platform (TX and/or RX) in different locations can bring better or worse results. A resource management software can also designate a platform to move during the tracking process to a more suitable location

according to the needs of the scenario. It would be done especially, for example, when the system is prepared to launch a missile against a target and more accuracy is needed. Even the missile can be working cooperatively with some RXs nodes in order to keep track of the target during its flight even if the target is trying to jam its TX.

Also, this work has shown quantitatively that the use of navigation radars of 25 kW (aimed to track ships with RCS of tens, hundreds or thousands of square meters) and operational frequency of 9.41 GHz (X-band) working co-operatively in a network of radars makes it possible to track targets with RCS as small as  $0.1 \text{ m}^2$  flying within the surveillance area. Uncountable scenarios are possible. This thesis has focused on working with the same fusion and tracking algorithm and also the basic characteristics of the radar (operational frequency, PRF, beam width, pulse width, etc) and only varying the geometry of the radar network to assess its performance. Some future work may include more simulations changing some other variables such as pulse width to improve range resolution, measurement accuracy and tracking accuracy.

Also, from the results of the simulations it is possible to see that bistatic radars have very good performance along the axis that is crossing its baseline but not so good on the other axis. Nevertheless, this affirmative is true only when the bistatic angle is smaller than 145 degrees. This information is very useful, especially if TXs and RXs can move dynamically while tracking targets in order to have the best precision most of the time. And, although for bistatic angles around 180 degrees the accuracy of measurements and tracking are very bad, detection in this region is very high because of the effect shown in 3.3.4.1 and Figure 16. The information that a target is lying on the baseline of a bistatic radar might be important especially if another pair of bistatic radar can be used in order to find the location of the target.

Comparing the results reported in this research with the work present in [55], it seems that the latter is also a work that shows how tracking accuracy varies in different scenarios of systems of sensors. Its approach is more spatially oriented showing how the accuracy varies in the surveillance area. It uses the same idea of fixing the algorithm and assessing it against different geometries. Nonetheless, it does not show examples using bistatic radars or even a multistatic radars. Only

monostatic radars are considered. The work presented in this thesis has a different approach when presenting the results, showing for a particular target dynamics how the tracking performance varies when different geometries are used to track the target. Moreover, the work presented herein has considered that standard deviation in range and angle vary according to SNR and thus, distance to the target.

In [57], the authors present simulations where the configuration of the radar network does not change and 4 different target trajectories and 3 different tracking algorithms are assessed. The paper shows different figures to illustrate the tracking accuracy in these different situations. Once more, it is another paper that approaches the problem of tracking a target in a multistatic scenario but it does not include information about how different configurations of radars would affect the results in tracking accuracy. On the other hand, important information can be extracted from the paper, for instance, the difference in tracking accuracy for each tracking algorithm that is executed.

Some simulations are also performed in the work presented in [24]. In this case, only measurement accuracy is considered and 5 different configurations of radars are assessed by the use of “constant accuracy contours”: monostatic case, bistatic case, netted monostatic, netted bistatic (linear) and netted bistatic (triangular). Similarly to what has been done in this thesis, the total power of the systems are kept the same to make the comparisons fairer. [24] though does not go further to investigate tracking accuracy or to assess some additional geometries with more TXs, for example. From the same author, [7] presents a multistatic tracking system and makes comparisons between multistatic and netted monostatic radar systems from the tracking point of view. Contrasting these two papers [7] [24] with the work herein presented it is possible to see that this thesis, although not using the same type of graphs, goes further in the investigation of tracking performance in several different geometries of multistatic radars usually with more than 2 TXs or RXs.

Additionally, the Matlab code developed for the purpose of this thesis can be reused and straightforwardly some parameters can be changed in order to assess how performance changes. Some of the parameters than can be changed include: transmitter power, beamwidth, operating frequency, pulse width and sampling interval.

Further research can be done simulating the use of Electronically Steered Antennas, assessing scenarios with more than one target, making the platforms to move intelligently according to the scenario, using 3D geometries and making the radars to communicate among them in order to synchronize and exchange data. Parameters that are considered to be ideal by this research can be modelled in further studies, for example, clutter levels, probability of detection, probability of false alarm data link delays and missed and out-of-sequence measurements. In addition, improvements in the algorithms of fusion and tracking can be developed aiming better accuracy and reduction in the computational load according to each geometry.

Performing simulations with Electronically Steered Antennas will show, for example, how changing the sampling interval can improve tracking accuracy. The use of this kind of antenna allows the system to “look” at a certain region of the space immediately without having to wait for a complete revolution of a rotating antenna. The agility provided by this kind of antenna allows a resource management system to make the best use of the existing resources and from the ideas herein presented, the developer team of such system has an idea of where to move a platform, where to point the antenna, which sampling interval to use, how much time to be looking at a certain target and so on.

In addition, from the ideas presented in this thesis, more analysis can be done if more variables are considered. For example, considering communication links delays can affect tracking accuracy and thus delays should be quantified and demonstrated how they could affect the performance of the whole tracking system.

If the resource management system can move the nodes, it is important that the new positions are accurate. The simulations performed in this thesis have considered that the location of the platforms were very accurate without errors. Moving the platforms must be very important if the system is trying to avoid, for example, that a target lies in the region of the baseline of a bistatic radar. Or even if it is impossible, it can move some platforms in order to keep the target on the forward scatter region (where the detection is very high) of 2 or more bistatic radars in order to find the position of the target by using high detection information coming from a number of bistatic radars. The problem here is that it might be necessary to have platforms that can move at velocities similar to the target velocity.

Finally, from the work presented in this thesis, it is expected that more aspects of the scenarios can be taken into account as well as more characteristics of the radar can be varied in order to help in the development of intelligent and adaptive systems that will be able to make the best use of all resources of a radar network in order to keep track of one or more targets.

## 8.1 Summary

Summarizing, the main contribution of this thesis is to show that it is possible to use characteristics of simple and cheap navigation radars (when they are used in a multistatic configuration) to track targets located as far as 70-80 km with RCS ( $0.1 \text{ m}^2$ ) that is smaller than the RCS of targets that usually this kind of radar is designed for. In addition, the thesis has shown how several different geometries (with one or more TXs and RXs) can affect the results in tracking accuracy and also showed quantitatively the respective accuracies along trajectory of the target.

Some of the most important conclusions include:

- Using the algorithms chosen, it was better to avoid targets crossing the baseline of bistatic radars
- Adding more TXs to the system made it possible to achieve similar results if comparing to an equivalent more powerful radar
- Splitting the power of one radar into smaller radars brought similar results and depending on the geometry could also bring better results, for example, making the tracking prediction to converge faster
- Geometry is important and being able to move nodes to better locations according to the needs of the system could bring better results
- Intelligent systems are needed in order to control the network aiming for a dynamic geometry that changes according to scenario

# References

- [1] J. I. Glaser, ‘Fifty years of bistatic and multistatic radar’, *IEE Proceedings F - Communications, Radar and Signal Processing*, vol. 133, no. 7, pp. 596–603, 1986.
- [2] S. S. Swords, *Technical History of the Beginnings of Radar*, illustrated ed. Institution of Engineering and Technology, 1986.
- [3] N. J. Willis, *Bistatic Radar*, 2nd Revised ed. SciTech Publishing Inc, 2005.
- [4] G. W. Ng and K. H. Ng, ‘Sensor management-what, why and how’, *Information Fusion*, vol. 1, no. 2, pp. 67–75, 2000.
- [5] H. Durrant-Whyte, ‘A Beginner’s Guide to Decentralised Data Fusion’, *Technical Document of Australian Centre for Field Robotics, University of Sydney, Australia*, 2000.
- [6] A. Farina and S. Pardini, ‘Multiradar Tracking System Using Radial Velocity Measurements’, *IEEE Transactions on Aerospace and Electronic Systems*, vol. AES-15, no. 4, pp. 555–563, Jul. 1979.
- [7] A. Farina, ‘Multistatic Tracking and Comparison with Netted Monostatic Systems’, *Proceedings of the International Conference Radar-82, London, UK*, pp. 183–187, 1982.
- [8] A. Farina, ‘Tracking function in bistatic and multistatic radar systems’, *IEE Proceedings F - Communications, Radar and Signal Processing*, vol. 133, no. 7, pp. 630–637, 1986.
- [9] H. F. Durrant-Whyte, B. Y. . Rao, and H. Hu, ‘Toward a fully decentralized architecture for multi-sensor data fusion’, in *IEEE International Conference on Robotics and Automation*, Cincinnati, OH, USA, 1990, vol. 2, pp. 1331–1336 vol.2.
- [10] B. S. Rao and H. F. Durrant-Whyte, ‘Fully decentralised algorithm for multisensor Kalman filtering’, *IEE Proceedings D - Control Theory and Applications*, vol. 138, no. 5, pp. 413–420, Sep. 1991.
- [11] M. N. Petsios, E. G. Alivizatos, and N. K. Uzunoglu, ‘Manoeuvring target tracking using multiple bistatic range and range-rate measurements’, *Signal Processing*, vol. 87, no. 4, pp. 665–686, 2006.

- [12] A. D. Lallo, A. Farina, R. Fulconi, A. Stile, L. Timmoneri, and D. Vigilante, 'A Real Time Test Bed for 2D and 3D Multi-Radar Tracking and Data Fusion with Application to Border Control', in *CIE '06. International Conference on Radar*, Shanghai, China, 2006, pp. 1–6.
- [13] 'IEEE Standard Radar Definitions'. IEEE Standards, 2008.
- [14] H. D. Griffiths, 'Bistatic Radar - Principles And Practice', in *SBMO International Microwave Conference/Brazil*, Sao Paulo, Brazil, 1993, vol. 2, pp. 519–526.
- [15] H. D. Griffiths, 'From a different perspective: principles, practice and potential of bistatic radar', in *International Radar Conference*, Adelaide, SA, Australia, 2003, pp. 1–7.
- [16] M. I. Skolnik, *Radar Handbook, Third Edition*, 3rd ed. McGraw-Hill Professional, 2008.
- [17] K. M. Siegel, H. A. Alperin, R. R. Bonkowski, J. W. Crispin, A. L. Maffett, C. E. Schensted, and I. V. Schensted, 'Bistatic Radar Cross Sections of Surfaces of Revolution', *Journal of Applied Physics*, vol. 26, no. 3, pp. 297–305, Mar. 1955.
- [18] H. Griffiths, 'Multistatic, MIMO and networked radar: The future of radar sensors?', in *European Radar Conference (EuRAD)*, Paris, France, 2010, pp. 81–84.
- [19] C. J. Baker, 'An Introduction to Multistatic Radar', NATO/OTAN, RTO-EN-SET-133, 2009.
- [20] R. E. Kalman, 'A new approach to linear filtering and prediction problems', *Journal of basic Engineering*, vol. 82, no. 1, pp. 35–45, 1960.
- [21] G. van Keuk and S. S. Blackman, 'On phased-array radar tracking and parameter control', *IEEE Transactions on Aerospace and Electronic Systems*, vol. 29, no. 1, pp. 186–194, 1993.
- [22] S. Miranda, C. Baker, K. Woodbridge, and H. Griffiths, 'Knowledge-based resource management for multifunction radar: a look at scheduling and task prioritization', *IEEE Signal Processing Magazine*, vol. 23, no. 1, pp. 66–76, 2006.
- [23] S. Haykin, 'Cognitive radar: a way of the future', *IEEE Signal Processing Magazine*, vol. 23, no. 1, pp. 30–40, 2006.
- [24] A. Farina and E. Hanle, 'Position Accuracy in Netted Monostatic and Bistatic Radar', *IEEE Transactions on Aerospace and Electronic Systems*, vol. AES-19, no. 4, pp. 513–520, 1983.
- [25] C. J. Baker and A. L. Hume, 'Netted radar sensing', *IEEE Aerospace and Electronic Systems Magazine*, vol. 18, no. 2, pp. 3–6, 2003.
- [26] C. J. Baker and H. D. Griffiths, 'Bistatic and Multistatic Radar Sensors for Homeland Security', *Advances in sensing with security applications, 2006 - Springer*, pp. 1–22, 2006.
- [27] H. Griffiths, 'Future radar developments', *Electronics & Communication Engineering Journal*, vol. 14, no. 6, pp. 250–251, 2002.

- [28] H. D. Griffiths, 'New directions in bistatic radar', in *RADAR '08. IEEE Radar Conference*, Rome, Italy, 2008, pp. 1–6.
- [29] T. Derham, K. Woodbridge, H. Griffiths, and C. J. Baker, 'The design and development of an experimental netted radar system', in *International Radar Conference*, Adelaide, SA, Australia, 2003, pp. 293–298.
- [30] S. Doughty, K. Woodbridge, and C. Baker, 'Characterisation of a Multistatic Radar System', in *EuRAD 2006. 3rd European Radar Conference*, Manchester, UK, 2006, pp. 5–8.
- [31] I. Papoutsis, C. J. Baker, and H. D. Griffiths, 'Netted radar and the ambiguity function', in *IEEE International Radar Conference*, Arlington, VA, USA, 2005, pp. 883–888.
- [32] Y. Teng, S. Doughty, K. Woodbridge, H. Griffiths, and C. Baker, 'Netted Radar Theory and Experiments', in *IDC '07. Information, Decision and Control*, Adelaide, SA, Australia, 2007, pp. 23–28.
- [33] Y. Teng, H. D. Griffiths, C. J. Baker, and K. Woodbridge, 'Netted radar sensitivity and ambiguity', *IET Radar, Sonar & Navigation*, vol. 1, no. 6, pp. 479–486, 2007.
- [34] P. F. Sammartino, C. J. Baker, and M. Rangaswamy, 'Moving target localization with multistatic radar systems', in *RADAR '08. IEEE Radar Conference*, Rome, Italy, 2008, pp. 1–6.
- [35] A. Farina, P. Lombardo, and M. Marsella, 'Joint tracking and identification algorithms for multisensor data', *IEE Proceedings - Radar, Sonar and Navigation*, vol. 149, no. 6, pp. 271–280, 2002.
- [36] G. T. Capraro, A. Farina, H. Griffiths, and M. C. Wicks, 'Knowledge-based radar signal and data processing: a tutorial review', *IEEE Signal Processing Magazine*, vol. 23, no. 1, pp. 18–29, 2006.
- [37] P. F. Sammartino, C. J. Baker, H. D. Griffiths, and M. Rangaswamy, 'Decentralized processing in radar networks', in *IET International Conference on Radar Systems*, Edinburgh, UK, 2007, pp. 1–5.
- [38] E. G. Alivizatos, M. N. Petsios, and N. K. Uzunoglu, 'Architecture of a multistatic FMCW direction-finding radar', *Aerospace Science and Technology*, vol. 12, no. 2, pp. 169–176, 2007.
- [39] P. F. Sammartino, C. J. Baker, and M. Rangaswamy, 'Coverage in radar networks', in *ACSSC 2007. Conference Record of the Forty-First Asilomar Conference on Signals, Systems and Computers*, Pacific Grove, California, USA, 2007, pp. 197–201.
- [40] A. P. Hopf, E. J. Knapp, and D. J. McLaughlin, 'Scalable Multifunction Dense Radar Network', in *IGARSS 2008. IEEE International Geoscience and Remote Sensing Symposium*, Boston, Massachusetts, USA, 2008, vol. 4, p. IV – 1018–IV – 1021.
- [41] B. Philips, D. Westbrook, D. Pepyne, J. Brotzge, E. J. Bass, and D. Rude, 'User Evaluations of Adaptive Scanning Patterns in the CASA Spring Experiment 2007', in *IGARSS 2008. IEEE International Geoscience and Remote Sensing Symposium*, Boston, Massachusetts, USA, 2008, vol. 5, p. V – 156–V – 159.

- [42] F. Junyent and V. Chandrasekar, 'Radar network characterization', in *IGARSS 2007. IEEE International Geoscience and Remote Sensing Symposium*, Barcelona, Spain, 2007, pp. 2730–2733.
- [43] M. Zink, E. Lyons, D. Westbrook, D. Pepyne, B. Pilips, J. Kurose, and V. Chandrasekar, 'Meteorological Command & Control: Architecture and Performance Evaluation', in *IGARSS 2008. IEEE International Geoscience and Remote Sensing Symposium*, Boston, Massachusetts, USA, 2008, vol. 5, p. V – 152–V – 155.
- [44] F. Junyent and V. Chandrasekar, 'Weather Radar Network Design', in *IGARSS 2008. IEEE International Geoscience and Remote Sensing Symposium*, Boston, Massachusetts, USA, 2008, vol. 4, p. IV – 1022–IV – 1025.
- [45] V. Chandrasekar, D. McLaughlin, J. Brotzge, M. Zink, B. Philips, and Y. Wang, 'Evaluation of Distributed Collaborative Adaptive Sensing in a Four-Node Radar Network: Integrated Project 1', in *IGARSS 2008. IEEE International Geoscience and Remote Sensing Symposium*, Boston, Massachusetts, USA, 2008, vol. 5, p. V – 148–V – 151.
- [46] D. McLaughlin, E. Knapp, Y. Wang, and V. Chandrasekar, 'Distributed weather radar using X-band active arrays', *IEEE Aerospace and Electronic Systems Magazine*, vol. 24, no. 7, pp. 21–26, 2009.
- [47] J. L. Salazar, A. Hopf, R. F. Contreras, B. Philips, E. J. Knapp, D. McLaughlin, J. Brotzge, and K. Brewster, 'Coverage comparison of short range radar networks vs. conventional weather radars: Case study in the northwestern United States', in *IGARSS 2009. IEEE International Geoscience and Remote Sensing Symposium*, Cape Town, South Africa, 2009, vol. 2, p. II–964–II–967.
- [48] D. Pepyne, D. McLaughlin, D. Westbrook, E. Lyons, E. Knapp, S. Frasier, and M. Zink, 'Dense radar networks for low-flyer surveillance', in *IEEE International Conference on Technologies for Homeland Security (HST)*, Waltham, MA, USA, 2011, pp. 413–418.
- [49] 'Engineering Research Center for Collaborative Adaptive Sensing of the Atmosphere (CASA)', *Engineering Research Center for Collaborative Adaptive Sensing of the Atmosphere (CASA)*. [Online]. Available: <http://www.casa.umass.edu>. [Accessed: 16-May-2011].
- [50] E. Brookner, *Tracking and Kalman Filtering Made Easy*. Wiley-Interscience, 1998.
- [51] H. W. Thomas, G. Maignan, and J. T. Storey, 'Tracking in a multiradar environment', *Proceedings of the Institution of Electrical Engineers*, vol. 123, no. 3, pp. 191 –194, Mar. 1976.
- [52] D. Willner, C. B. Chang, and K. P. Dunn, 'Kalman filter algorithms for a multi-sensor system', in *IEEE Conference on Decision and Control including the 15th Symposium on Adaptive Processes*, Florida, USA, 1976, vol. 15, pp. 570 –574.
- [53] F. R. Castella, 'Multisensor, multisite tracking filter', *IEE Proceedings - Radar, Sonar and Navigation*, vol. 141, no. 2, pp. 75 –82, Apr. 1994.

- [54] R. Baltes and G. van Keuk, 'Tracking multiple manoeuvring targets in a network of passive radars', in *IEEE 1995 International Radar Conference*, Alexandria, VA, USA, 1995, pp. 304–309.
- [55] A. Andersson and T. R. Kronhamn, 'General tracking performance description for systems of sensors', in *Proceedings of the Fifth International Conference on Information Fusion*, Maryland, USA, 2002, vol. 1, pp. 128 – 134 vol.1.
- [56] M. K. Kalandros, L. Trailovic, L. Y. Pao, and Y. Bar-Shalom, 'Tutorial on multisensor management and fusion algorithms for target tracking', in *American Control Conference*, Boston, Massachusetts, USA, 2004, vol. 5, pp. 4734–4748 vol.5.
- [57] T. Johnsen, B. Hafskjold, and K. E. Olsen, 'Tracking and data fusion in bi-and multistatic radar: a simulation study of geometry dependent uncertainties, filter selection and their influence', in *IEEE International Radar Conference*, Arlington, VA, USA, 2005, pp. 441–446.
- [58] S. Coraluppi and C. Carthel, 'Distributed tracking in multistatic sonar', *IEEE Trans. Aerosp. Electron. Syst.*, vol. 41, no. 3, pp. 1138–1147, Jul. 2005.
- [59] S. Coraluppi, D. Grimmitt, and P. Theije, 'Benchmark Evaluation of Multistatic Trackers', in *9th International Conference on Information Fusion*, Florence, Italy, 2006, pp. 1–7.
- [60] B. La Cour, 'Bayesian Multistatic Tracking: Results on Simulated Data from the Multistatic Tracking Working Group', in *9th International Conference on Information Fusion*, Florence, Italy, 2006, pp. 1 –7.
- [61] D. Grimmitt, S. Coraluppi, B. R. La Cour, C. G. Hempel, T. Lang, P. A. . de Theije, and P. Willett, 'MSTWG multistatic tracker evaluation using simulated scenario data sets', in *11th International Conference on Information Fusion*, Cologne, Germany, 2008, pp. 1 –8.
- [62] D. Grimmitt, 'SPECSweb multistatic tracking on a truth-blind simulated scenario of the MSTWG', in *FUSION '09. 12th International Conference on Information Fusion*, Seattle, Washington, USA, 2009, pp. 1568 –1575.
- [63] M. N. Petsios, E. G. Alivizatos, and N. K. Uzunoglu, 'Solving the association problem for a multistatic range-only radar target tracker', *Signal Processing*, vol. 88, no. 9, pp. 2254–2277, 2008.
- [64] A. O. Bozdogan, G. Soysal, and M. Efe, 'Multistatic tracking using bistatic range - Range rate measurements', in *FUSION '09. 12th International Conference on Information Fusion*, Seattle, Washington, USA, 2009, pp. 2107 –2113.
- [65] D. Stromberg, 'Scheduling of track updates in phased array radars', in *IEEE National Radar Conference*, Ann Arbor, MI, USA, 1996, pp. 214–219.
- [66] J. M. Butler, A. R. Moore, and H. D. Griffiths, 'Resource Management For A Rotating Multi-function Radar', in *Radar 97 (Conf. Publ. No. 449)*, Edinburgh, UK, 1997, pp. 568–572.
- [67] W. Komorniczak and J. Pietrasinski, 'Selected problems of MFR resources management', in *FUSION 2000. Third International Conference on Information Fusion*, Paris, France, 2000, vol. 2, p. WEC1/3–WEC1/8 vol.2.

- [68] S. L. C. Miranda, C. J. Baker, K. Woodbridge, and H. D. Griffiths, 'Simulation methods for prioritising tasks and sectors of surveillance in phased array radars', *Int. Jnl. Simulation: Systems, Science and Technology*, vol. 5, no. 1–2, pp. 18–25, 2004.
- [69] S. L. C. Miranda, C. J. Baker, K. Woodbridge, and H. D. Griffiths, 'Phased array radar resource management: a comparison of scheduling algorithms', in *IEEE Radar Conference*, Philadelphia, Pennsylvania, USA, 2004, pp. 79–84.
- [70] S. L. C. Miranda, C. J. Baker, K. Woodbridge, and H. D. Griffiths, 'Comparison of scheduling algorithms for multifunction radar', *IET Radar, Sonar & Navigation*, vol. 1, no. 6, pp. 414–424, 2007.
- [71] S. Haykin, 'Cognitive radar networks', in *1st IEEE International Workshop on Computational Advances in Multi-Sensor Adaptive Processing*, Puerto Vallarta, Mexico, 2005, pp. 1–3.
- [72] F. Smits, A. Huizing, W. van Rossum, and P. Hiemstra, 'A cognitive radar network: Architecture and application to multiplatform radar management', in *EuRAD 2008. European Radar Conference*, Amsterdam, The Netherlands, 2008, pp. 312–315.
- [73] S. Haykin, A. Zia, I. Arasaratnam, and Y. Xue, 'Cognitive tracking radar', in *IEEE Radar Conference*, Washington DC, USA, 2010, pp. 1467–1470.
- [74] S. S. Blackman and R. Popoli, *Design and analysis of modern tracking systems*. Artech House Norwood, MA, 1999.

# **Appendix A - Matlab Code**

This is a CD-ROM that contains the Matlab source code used to perform the simulations reported in this thesis.